UNIVERSITY OF TWENTE.

Faculty of Electrical Engineering,

Mathematics & Computer Science

Quantification of simulated pathological synergies in stroke patients using a multisensory system based on inertial sensing and sEMG

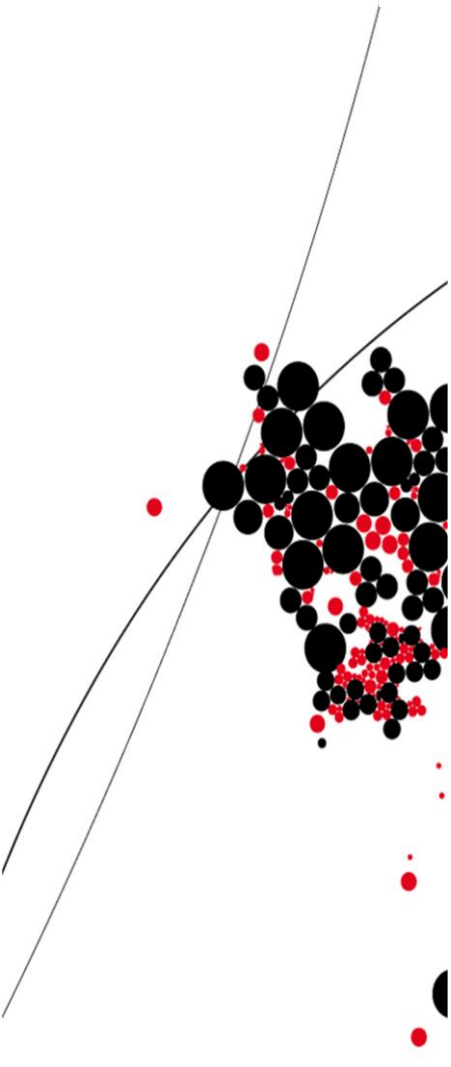

Jacques S.D. Getrouw

M.Sc. Thesis

Supervisors:
Dr. ir. B.J.F. van Beijnum
Prof. dr. ir. P. H. Veltink
Prof. dr. ir. G.J.M Krijnen
G. J. W. Wolterink M.Sc.
Anne Schwarz M.Sc.

Faculty of Electrical Engineering,
Mathematics and Computer Science
Biomedical Signals and Systems (BSS)
University of Twente
P.O. Box 217, 7500 AE Enschede
The Netherlands

ABSTRACT

Introduction. The Fugl-Meyer assessment is a valid and reliable clinical assessment for determining the stage of recovery in patients with stroke. The examiner quantifies the corresponding impairment for each item by means of a score (0, 1 or 2 per item). The lowest score is assigned when the voluntary movement task cannot be executed; the median score is assigned when the task is partly executed, while the maximum score is assigned when the task is fully executed. However, the assigned score depends on experimenter's subjective judgement and can vary depending on individual opinions. Moreover, consistent estimations of the joint angles and information concerning electromyographic (EMG) activity of the muscles are not provided by the Fugl-Meyer assessment, so that the exact underlying pathophysiological mechanisms that form the basis of limb synergies are still unclear.

Research questions. 1. What is the optimal set of sensor-to-segment calibration movements performed by the subjects?
2. Which clinically relevant insights related to stroke patients can the multisensory system provide?

Methods. Healthy subjects were instructed to perform a set of twenty-six calibration movements so that the multisensory system could estimate the joint angles during the movements. Based on the variance accounted for (VAF) and the mutual angles between pairs of calibration movements, the optimal set of calibration movements is investigated. After the calibration procedure, the subjects were instructed to perform movements within synergies, mixing synergies, and out of synergies based on the Fugl-Meyer Assessment for the upper extremity (FMA-UE). The subjects were instructed to perform these movements without the limitations caused by the flexor synergy (pathologically unaffected), and then with the limitations caused by the flexor synergy (pathologically affected). The system was tested on detecting clinically relevant differences in joint angles and muscle activities between unimpaired and simulated pathologically affected movements. These differences were statistically tested by means of the Wilcoxon signed rank test with a significance level of 5%.

Findings. Overall, the system could detect statistically significant differences in the joint angles regarding shoulder abduction, shoulder flexion, elbow flexion, and forearm pronation and/or supination. Moreover, a significant decrease in agonistic and antagonistic muscle activity during pathologically affected movements could be detected by the system. However, a significant difference in coactivation between selected muscles during pathologically unaffected and simulated pathologically affected movements could not be detected.

Conclusion: The optimal set of sensor-to-segment calibration movements include a static pose of the ulnar side of the hand, repeated forearm pronation or supination, a static pose on the left side of the thumb, a static pose of the forearm aligned in the direction of gravity with the elbow fully extended, repeated elbow flexion with the forearm pronated, repeated shoulder flexion with the elbow flexed, repeated trunk flexion, and repeated ipsilateral and contralateral trunk rotation.

The influence of the flexor synergy caused limitations in joint angles due to insufficient activity of the agonist muscles.

CONTENT

LIST OF ACRONYMS

CMRR	Common-Mode Rejection Ratio
CNS	Central Nervous System
CVA	Cerebrovascular accident
ECG	Electrocardiogram
EMG	Electromyography
FMA	Fugl-Meyer Assessment
FMA-UE	Fugl-Meyer Assessment for the Upper Extremity
FSR	Force Sensing Resistor
iHAMS	instrumented Hand Arm Measuring System
IMMU	Inertial and Magnetic Measurement Unit
IMU	Inertial Measurement Unit
MEMS	Micro Electrical Mechanical System
MUAP	Motor Unit Action Potentials
sEMG	surface Electromyography
SPSS	Statistical Package for Social Science
SRE	Smooth Rectified Electromyography
VAF	Variance Accounted For

1. INTRODUCTION

1.1 FUGL-MEYER ASSESSMENT OF STROKE

A cerebrovascular accident (CVA) or stroke is an interruption of blood flow to the brain, resulting in damaged brain tissue. The syndromes that lead to stroke can be categorized in two types: ischemic and hemorrhagic stroke. Ischemic stroke, which accounts for 80% of the stroke cases, concerns an occlusion of cerebral blood flow caused by a blood clot, resulting in tissue anoxia (Auer, 2016; Gillen, 2015). Hemorrhage stroke, which accounts for the remaining 20%, concerns blood leaking into brain tissue when a damaged or weakened blood vessel bursts. Cerebrovascular accident (CVA) survivors encounter several mechanical constraints that limit their ability to perform daily tasks and force them to develop alternative movement strategies (Mathiowetz, 2016; Sabari, 2016). Upper extremity function deficiency is a common and challenging outcome of a stroke (Carr & Shepherd, 2003; Gillen, 2015). Impairment of motor functioning and body structure include paresis, muscle weakness (decreased muscle force), dexterity, spasticity, sensory loss, and decreased postural control.

Normally, multiple different synergies are included in normal human movement. However, voluntary activity or motor control of stroke patients is accompanied with reduced capability to control the degrees of freedom of the shoulder, arm, hand and fingers independently while performing functional movements (pathological synergies) (Miller et al., 2014). The resulting abnormal movement patterns reflect muscle weaknesses, loss of inter-joint coordination, and lack of joint and muscle flexibility due to soft tissue length changes and increased muscle stiffness. Pathological synergies or abnormal joint coupling after stroke have been described (Twitchell, 1951). This empirical longitudinal work found the basis for the later construction and evaluation of the Fugl-Meyer Assessment (FMA) for assessing voluntary movement control after stroke. The researchers examined a relatively definable course from “initially nearly flaccid hemi paralysis” to a certain degree of selective motor control through the course of stroke recovery (Fugl-Meyer, 1971). Likewise, the items follow a hierarchical structure from movements within synergies (e.g. combined elbow flexion and shoulder flexion), combined synergies (e.g. combination of elbow extension and shoulder flexion) and out of synergies (e.g. combination of elbow extension and shoulder abduction) as well as an order from proximal to distal movements. Based on the execution of the hierarchically structured voluntary controlled movement tasks, a therapist quantifies the corresponding impairment for each item by means of a score (0, 1 or 2 per item). The lowest score is assigned when the voluntary movement task cannot be executed; the median score is assigned when the task is partly executed, while the maximum score is assigned when the task is fully executed. Although the assigned score depends on experimenter’s subjective judgement and can vary depending on individual opinions, the 3-graded scale of the FMA gives a good degree of reliability (Fugl-Meyer, Jääskö, Leyman, Olsson, & Steglind, 1975; van Kordelaar, van Wegen, & Kwakkel, 2012).

Although the FMA is a valid and reliable clinical assessment for determining the stage of recovery in patients with stroke, the exact underlying pathophysiological mechanisms that form the basis of limb synergies are still unclear (van Kordelaar et al., 2012). The first drawback concerns a lack of concrete and precise information of the corresponding joint angles during the motion. The second drawback of the clinical assessment is the lack of information concerning activation of the muscles. Electromyography recorded simultaneously across various muscles forms a multi-muscle EMG patterns and provides valuable insights for identifying synergies (Santello & Lang, 2015).

1.2 PROBLEM STATEMENTS AND RESEARCH QUESTIONS

This research aims at the development of a prototype multisensory system that provides a quantified analysis to describe specific physiological aspects of pathological synergies in stroke subjects. The analysis is based on a multisensory system that includes inertial sensing of movements and muscle activations. However, the multisensory system requires a sensor-to-segment calibration procedure which consists of a set of calibration movements. The sensor-to-segment calibration procedure requires careful execution by each subject so that the inertial sensing during the movements can be more accurate. Furthermore, the calibration procedure is time-consuming and should be reduced to a minimum, yet optimal, set of calibration movements.

After the sensor-to-segment calibration procedure, the multisensory system can provide optimal joint angles in correspondence with the movements performed by the subjects. The examiner can assess the movements objectively by means of the joint angles and muscle activities. However, in order to evaluate the feasibility of the multisensory system, healthy subjects are instructed to execute a selected set of movements based on the FMA-UE. The subjects are instructed to perform these movements without the limitations caused by the flexor synergy (pathologically unaffected), and then with the limitations caused by the flexor synergy (pathologically affected). The limitations caused by the flexor synergy can be described as an unintentional occurrence of elbow flexion and/or shoulder abduction during the performance of the movement. The system is tested on detecting clinically relevant differences in joint angles and muscle activities between unimpaired and simulated pathologically affected movements.

Moreover, Brunnstrom described the limitations caused by the flexor synergy as the occurrence of strong linkages between certain muscles during certain movements (Brunnstrom, 1970). The detection of significant differences in joint angles, muscle activities and strong linkages during the selected movements provides an objective quantification of the flexor synergy. The final goal of the multisensory system concerns further investigation whether relevant clinical insights regarding stroke patients can be provided.

Based on the described problem statements, the following research questions are of interest:

1. What is the optimal set of sensor-to-segment calibration movements performed by the subjects?
2. Which clinically relevant insights related to stroke patients can the multisensory system provide?
    I. Is the multisensory system able to detect significant differences in joint angles between pathologically unaffected and affected movements?
    II. Is the multisensory system able to detect significant differences in muscle activities between pathologically unaffected and affected movements?
    III. Is the multisensory system able to detect linkages between muscles caused by the flexor synergy?

1.3 REPORT STRUCTURE

This thesis is part of the EU Softpro project under work package 2, which focusses on multisensory integration regarding EMG, kinematic and kinetic sensing. The structure of the thesis consists of an introduction, theoretical background, a methodology, results and discussions, and finally conclusions and recommendations. Chapter 2 provides relevant theoretical background for understanding the development of the FMA-UE and a brief explanation regarding sEMG and inertial sensing. Chapter 3 describes the methodology. Chapter 4 presents an overview, a description and discussions of the results. Chapter 5 presents the conclusions and the recommendations.

2. THEORETICAL BACKGROUND

2.1 POST-STROKE PATHOLOGICAL SYNERGIES

Patients who suffered from lesions in certain portions of the brain exhibit motor disorders in one half of the body, referred to as hemiplegia or hemiparesis, and motor and sensory deficits appear at the contralateral body half to the brain lesion (Brunnstrom, 1970). Normal firmly linked physiological synergies become stereotyped pathological synergies consisting of a complete flexion or extension of the upper extremity (flexor or extensor synergy respectively) (Twitchell, 1951). The complete flexor synergy consists of an acute elbow flexion, a full range forearm supination, shoulder abduction to 90°, external shoulder rotation and finally retraction and/or elevation of the shoulder girdle (see Figure 2.1). The dominant component of the flexor synergy is elbow flexion (caused by the elbow flexor muscles), while shoulder abduction and external rotation of the shoulder are often weak components (Brunnstrom, 1970). The complete extensor synergy consists of a full-range elbow extension and forearm pronation, a shoulder adduction in front of the body and an internal rotation of the arm (see Figure 2.1). The dominant component is the internal rotation and the adduction in front of the body (caused by the pectoralis major muscle), while elbow extension (caused by the triceps) is in general weak and occurs afterwards. The pectoralis major muscle becomes strongly activated when voluntary elbow extension is performed.

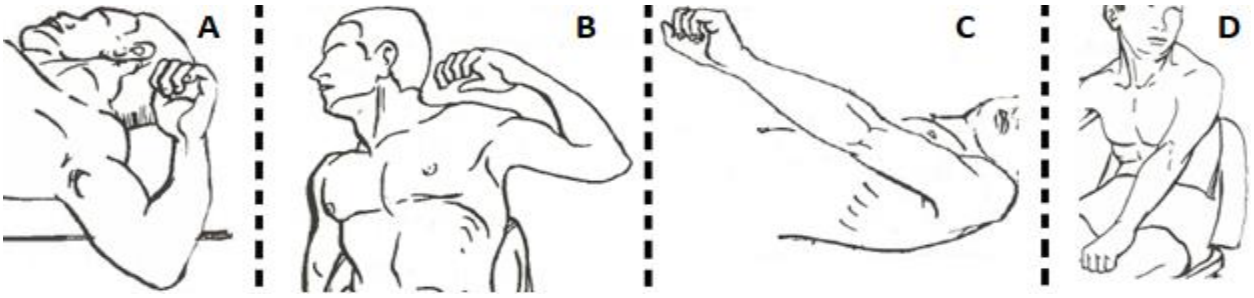

Figure 2.1: Flexor synergy of the upper limb when subject is lying (A) and sitting (B). the strongest component is elbow flexion. Extensor synergy of the upper limb when subject is lying (C) and sitting (D). the strongest component is shoulder adduction and internal rotation. Picture is taken and modified from (Brunnstrom, 1970).

2.1.1 GENERAL COURSE OF STROKE RECOVERY: TWITCHELL AND BRUNNSTROM

A series of special events regarding the recovery process of stroke were observed and described by Twitchell and Brunnstrom (Brunnstrom, 1970; Fugl-Meyer et al., 1975). Although great variation was found in the recovery process, the restoration of motor function in the hemiplegia patients followed a general pattern in which certain phenomena were remarkable during distinct stages or phases of the process. The main events during the recovery process observed by Brunnstrom are similar to the observations of Twitchell and are summarized as follows (Brunnstrom, 1970):

1. Immediately after the onset of hemiplegia, the affected limbs were completely flaccid and felt heavy when moved passively with little or no muscular resistance to movement.
2. As the patients began to recover, spasticity began to develop, first in the wrist and finger flexors, and then in the flexors and adductors of the upper limb, and any attempt of voluntary movement resulted in

some of the components of the limb synergies, e.g. components of the flexor or extensor synergy of the upper arm.

3. After some time, spasticity increased further and became severe resulting in abnormally stiff and tight muscles. In this stage of recovery, the patients gained voluntary control of joint movements within the synergies. However, full range of voluntary movements within the synergies did not necessarily develop.
4. In the fourth stage of recovery, spasticity started to decrease and some movement combinations that are not directly within the flexor or extensor synergy could be performed gradually.
5. As the patients recovered further and spasticity declined further, more motor control was regained and more difficult volitional movements out of the synergies or with little involvement of the synergies could be performed. In this stage of recovery, the basic limb synergies (flexor and extensor synergy) lost their influence and voluntary movements was performed in a controlled manner.
6. Finally, spasticity was completely absent (when passive movements were performed), individual joint movements could be performed, and coordination approached normal. However, some interference could be observed on the affected side when active movements with increasing speed were performed.

2.1.2 CLINICAL EVALUATION STROKE RECOVERY

In order to develop a clinical evaluation form for the neuromuscular progress of patients with hemiplegia, the condition of the portions of the central nervous system (CNS) responsible for the regulation of motor performance must be considered. An assessment of the degree of recovery of the CNS can be developed by instructing patients to perform movements that correspond with gradually increasing finer neuromuscular control (Brunnstrom, 1970). A suitable procedure for the evaluation of the recovery progress of hemiplegia patients is based on a "typical" recovery course, so that an indication of the extent of recovery concerning the CNS can be provided. Moreover, such procedure must be brief and easy to execute by patients, so that fatigue and loss of time can be prevented. Furthermore, the clinical evaluation must be objective and standardized.

The Fugl-Meyer scale, which is based on the observation of recovery stages of motor function by Twitchell and Brunnstrom is the most widely-used quantitative measure of motor recovery post stroke (Brunnstrom, 1970; Raghavan, 2015; Twitchell, 1951). The assessment consists of an ordinal-scale which includes three grades, with 0 as the minimum grade and 2 as the maximum grade (Twitchell, 1951).

Moreover, based on the observations of Twitchell and Brunnstrom the recovery stages 1 to 3 concern the period following the beginning of hemiplegia when the originally flaccid condition (stage 1) comes to an end and hyperactivity of the tendons (spasticity) begins to develop (stage 2), and then reaches its peak (stage 3). The phenomena in these stages indicate the gradual appearance and influence of the limb synergies on motor performance, and therapeutic procedures in these stages are designed to promote voluntary control of the limb synergies (Brunnstrom, 1970). Hence the first part of the Fugl-Meyer assessment for the upper extremity (FMA-UE) concerns the assessment of reflex activity and the assessment of volitional movements within the limb synergies (Fugl-Meyer et al., 1975). Thus, the volitional movements contain all the components of either the flexor synergy or the extensor synergy, which means that total influence of the basic limb synergy on the movement is allowed.

Furthermore, the fourth recovery stage concerns the phase in which spasticity begins to decline and synergy dominance over motor acts decreases. The performance of voluntary movement increases gradually, and the patients start to learn several movement combinations that deviate from the standard limb

synergies. Moreover, in this stage therapeutic procedures aim to increase the motor function performance such that voluntary impulses are reinforced to overcome the still existing, although diminishing, linkage between certain components of each synergy (Brunnstrom, 1970). The FMA-UE for patients in this stage assesses volitional movements that can be performed when certain components of the flexor synergy and extensor synergy are combined, e.g. forward arm-raising with the elbow extended (Brunnstrom, 1970; Fugl-Meyer et al., 1975). In case the flexor synergy influences cannot be overcome, the patients attempt to flex the shoulder, but partial shoulder abduction occurs, and the elbow cannot be kept extended. In case the influence of the extensor synergy cannot be overcome, the patients extend the elbow, but elevation of the arm is hindered (due to the contraction of the pectoralis major muscle, which is linked with the triceps). The goal of this movement is to check whether the patients can perform the movement without the (unintentional) influence of some of the components of the flexor and extensor synergy. In other words, some degree of control for mixing some components of the synergies is required.

The patients in the fifth stage experience further decrease of spasticity and further increase of voluntary motor function performance such that more difficult movement combinations can be performed. The FMA-UE for patients in this stage assesses volitional (therapeutic) movements that can be performed when a higher degree of control for mixing components of the synergies is reached, e.g. 90° shoulder abduction with the elbow extended and the forearm pronated. If patients in an earlier stage attempt to abduct the shoulder, the elbow tends to flex due to the strong linkage between the flexor muscles of the elbow and the abductor muscles of the shoulder. The goal of this movements is to check whether the patients can control the mixing of synergies such that two components of the extensor synergy (elbow extension and forearm pronation) associated with two components of the flexor synergy (shoulder girdle retraction and shoulder abduction). In order to investigate further whether individual joint movements of the wrist can be performed, the patients are instructed to perform a repeated dorsiflexion and volar (palmar) flexion of the wrist with the forearm pronated, the elbow extended, and the shoulder slightly flexed and abducted. Prior to this stage of recovery, the flexor synergy and the extensor synergy are accompanied by wrist flexion or wrist extension respectively. In case the influence of synergies is declined sufficiently, the elbow can be kept extended and the forearm can be kept pronated when the wrist is flexed.

Patients in the sixth stage of recovery can perform individual joint movements of the shoulder, elbow, forearm and wrist in a normal or almost normal way, which means that synergy influence has disappeared or at least cannot be easily demonstrated and resistance to passive movement (spasticity) has vanished. However, recovery of the hand, i.e. grasp usually lags behind the rest of the limb (Brunnstrom, 1970). The rehabilitation concerning the grasp aims at full recovery of the grip when grasping a cylindrical and spherical object. Moreover, independent flexion and extension of the fingers are also investigated (Fugl-Meyer et al., 1975).

2.2 INERTIAL MEASUREMENT UNITS

An Inertial Measurement Unit (IMU) is an electronic device that contains an accelerometer and a gyroscope for determining 3D kinematics. Micro Electrical Mechanical System (MEMS) technology has opened many possibilities for motion analysis using inertial sensing due to the significant reduction in size, cost and power consumption (Kortier, 2018; Roetenberg, Slycke, & Veltink, 2007). A state-of-the-art IMU contains a tri-axial accelerometer, a tri-axial gyroscope, and a tri-axial magnetometer henceforth referred to as an Inertial and Magnetic Measurement Unit (IMMU). A gyroscope measures the angular velocity of the sensor, i.e. the rate of change of the sensor's orientation. An accelerometer measures the external specific

force acting on a mass in the sensor, which consists of both the sensor's acceleration and the earth's gravity directly proportional to the mass. Magnetometers measure the local magnetic field which consist of the earth's magnetic field and any magnetic field induced by a magnetic source such as electrical currents in conductors or passive ferromagnetic material (Kortier, 2018).

Since IMUs are used for navigation of human movement, an explanation of three different coordinate frames is necessary (see Figure 2.2). The sensor frame is the coordinate frame of the moving IMU aligned to the casing with the origin located at the centre of the accelerometer triad (Kok, Hol, & Schön, 2017; Kortier, 2018). The inertial recordings are expressed in this coordinate frame. The global navigation frame (also called global frame) is a local frame for navigation purposes at an arbitrary static position and orientation on earth. In most applications this frame is stationary with respect to the earth. The segment frame is the coordinate frame of the (human) body part at which the IMU is mounted. This frame can be either defined based on the recommendations of the International Society of Biomechanics (Wu et al., 2005) or self-defined.

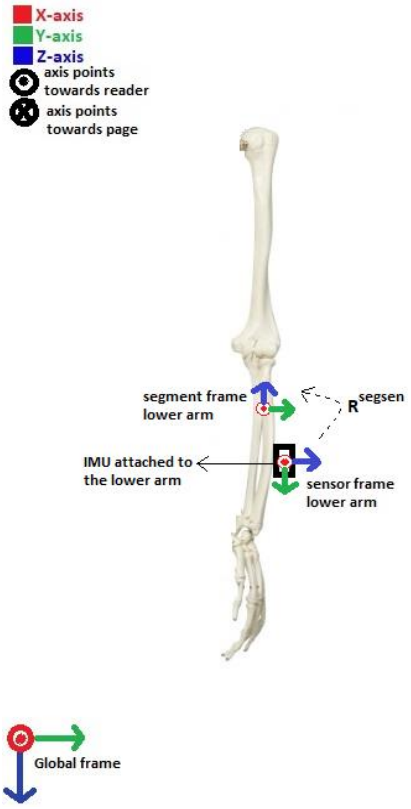

Figure 2.2: An example of the sensor frame, the segment frame and the global frame. The rotation matrix R^{segsen} converts orientations expressed in sensor frame to orientations expressed in segment frame.

2.3 ELECTROMYOGRAPHY

Electromyography (EMG) is an experimental technique concerned with the development, recording and analysis of electrical signals associated with the contraction of muscles (Peter, 2005). In order to measure and record myoelectric signals, electrodes can be applied to the skin surface where the muscles are located or invasively in the muscles of interest. EMG recorded using surface electrodes is called surface EMG

(sEMG), while EMG recorded using indwelling electrodes is called intramuscular EMG (Winter, 2009). Surface electrodes are mostly used in studies regarding prosthesis control, ergonomics and movement analysis due to their non-invasive character (Merletti, Parker, & Parker, 2004).

The neural control of muscular contraction can be described by the smallest functional unit called a motor unit (Peter, 2005). A motor unit consists of the cell body and dendrites of a motor neuron, the terminal branches of its axon, and all cylindrical cells containing the contractile units of the muscle that are innervated by it called muscle fibres (see). Each motor neuron has axon terminals on the membrane of several muscle fibres called sarcolemma. These axon terminals form the neuromuscular junctions called motor endplates (Pavelka & Roth, 2010; Peter, 2005). The contraction of a muscle is initiated by impulses (action potentials) generated by the neurons of several motor units and sent to the motor endplates via the axons. These action potentials, called motor unit action potentials (MUAPs) are then spread along the sarcolemma in both directions and inside the muscle fibres through a tubular system resulting in an excitation that leads to a contraction of the muscle (Peter, 2005; Reaz, Hussain, & Mohd-Yasin, 2006). Moreover, muscle fibres of one motor unit are distributed throughout the muscle and contract maximally when activated. The strength of the muscle contraction depends on the number of motor units that are activated simultaneously, the frequency of stimulation of individual motor units and the size of the motor units activated.

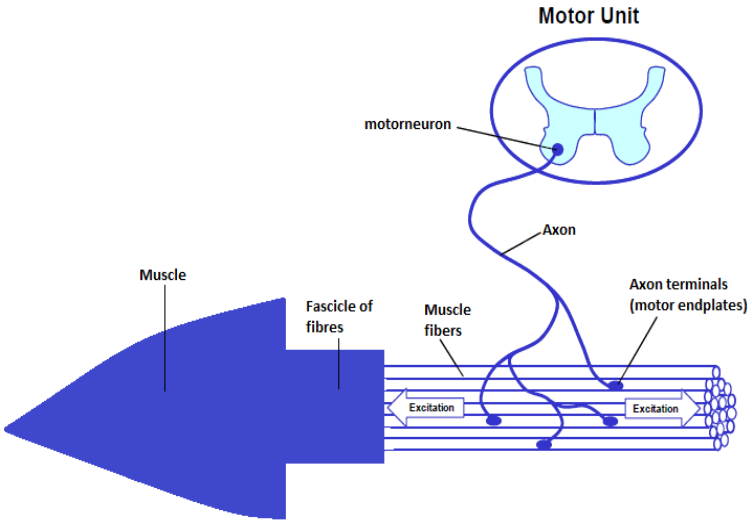

Figure 2.3: The motor unit. The picture is taken from (Peter, 2005) and modified.

An EMG signal, recorded with a biological amplifier of certain specifications, is the summation of m.u.a.ps and should be undistorted and free of noise or artefacts (Peter, 2005). The MUAPs are the action potentials of the active motor units during the movement (Reaz et al., 2006). Moreover, an undistorted EMG is amplified linearly over the range of the amplifier and recording system, and a noise free EMG is not contaminated with the electromagnetic fields generated by power lines (hum) and movement artefacts caused by mechanical alterations due to loose electrodes at the skin interface or loose leads on the wires (Reaz et al., 2006; Sinderby, Grassino, Friberg, & Lindstrom, 1997; Winter, 2009). The most important specifications of a suitable EMG amplifier are the gain of the amplifier, the input impedance, the frequency response and the common-mode rejection ratio (CMRR) (Winter, 2009).

The amplitudes of EMG signals recorded with surface electrodes are generally low and can range between -5 mV to + 5mV (Reaz et al., 2006; Webster & Clark, 1995; Winter, 2009). The amplifier is required to increase the amplitude of the weak EMG signal while maintaining high fidelity so that it can be further processed, recorded or displayed (Webster & Clark, 1995). The gain of the amplifier is defined as the ratio of the output voltage to the input voltage and should be adjustable between 100 and 10000 (Winter, 2009). Moreover, in case the amplification of the EMG signal occurs in several stages, the first stage, called preamplifier, must have low noise since its output will be amplified through the remaining stages of the amplifier. The preamplifier often has a relatively low gain (e.g. 10 or 20) and is for safety reasons either electrically isolated from the rest of the amplifier stages or is located near the electrodes (Webster & Clark, 1995). Furthermore, the input impedance of the pre-amplifier must be at least 1 MΩ in order to prevent attenuation and distortion of the recorded EMG signals (Peter, 2005; Webster & Clark, 1995; Winter, 2009). The frequency response is an important property to consider in the amplifier. The amplifier must amplify the biopotential such that the frequency spectrum is without attenuation (Webster & Clark, 1995). A recommended range for surface EMG is 10-1000 Hz (Winter, 2009). The last important specification of a proper EMG amplifier is the CMRR. The CMRR provides information on the extent to which common signal components in bipolar EMG signals are attenuated (Webster & Clark, 1995). Moreover, bipolar electrode configuration makes use of a differential amplifier, which subtracts the potential at one electrode from that at the other and then amplifies the difference resulting in a suppression of unwanted common signals. These unwanted common mode signals can be caused by power sources, fluorescent lighting, electromagnetic devices or from other muscles (crosstalk) (Staudenmann, Roeleveld, Stegeman, & Van Dieën, 2010; Winter, 2009).

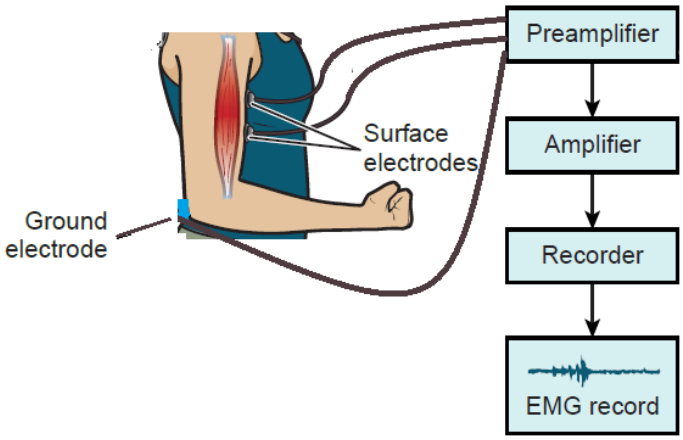

Figure 2.4: Basic working principle of the EMG amplifier.
The picture is taken from (Houglum & Bertoti, 2011) and modified.

3. METHODOLOGY

An overview and corresponding workflow of the multisensory system are presented in this chapter. The EMG processing to linear envelopes and the determination of the muscle activities are first described. Secondly, a description of the inertial system is provided. The inertial processing consists of sensor calibration procedure, a strapdown integration algorithm, and a sensor-to-segment conversion in order to determine joint angles. Thirdly, the synchronization and data selection algorithms are described. Lastly, a description of the experimental protocol is given. Moreover, the signal processing algorithms are implemented offline. The sequences of the offline processing are in accordance with Figure 3.1.3.

3.1 INSTRUMENTED HAND ARM MEASURING SYSTEM

The instrumented Hand Arm Measuring System (iHAMS) consists of two measurements systems: a 24 channel Porti system (bipolar input channels) developed by Twente Medical Systems international b.v. (Twente Medical Systems international (TMSi)) and an inertial measurement system. The Porti system is used for measuring muscle activity at a sampling frequency of 2048 Hz. This system has a digital trigger input which can be used for synchronization with the inertial system.

The inertial measurement system contains two strings of IMUs: a string consisting of IMUs for the forearm, the upper arm, the shoulder, and the sternum; and a string consisting of IMUs for the hand and the distal phalanxes of the index finger, the middle finger and the thumb. Each IMU (MPU-9150) contains a 3D gyroscope, a 3D accelerometer and a 3D magnetometer. The IMUs on the distal phalanxes of the index and middle finger and thumb also consist of force sensing resistors (FSRs) to measure the interaction force with the environment (see Figure 3.1.1). The bus-master collects and packages the data from the IMU-strings and then sends it to a personal computer for further processing. Moreover, the bus-master contains an unsigned 16-bit sample counter and an external voltage supply of 5 V to the IMU-strings. When the bus-master is connected to the Porti system via the sync cable, it generates a synchronization signal which is sampled at a frequency of 2048 Hz by the Porti. The design of the inertial system is based on earlier designed instrumentation for measurement of hand and finger movements (Kortier, 2018). An overview of the connection regarding the iHAMS and a personal computer is given in Figure 3.1.2.

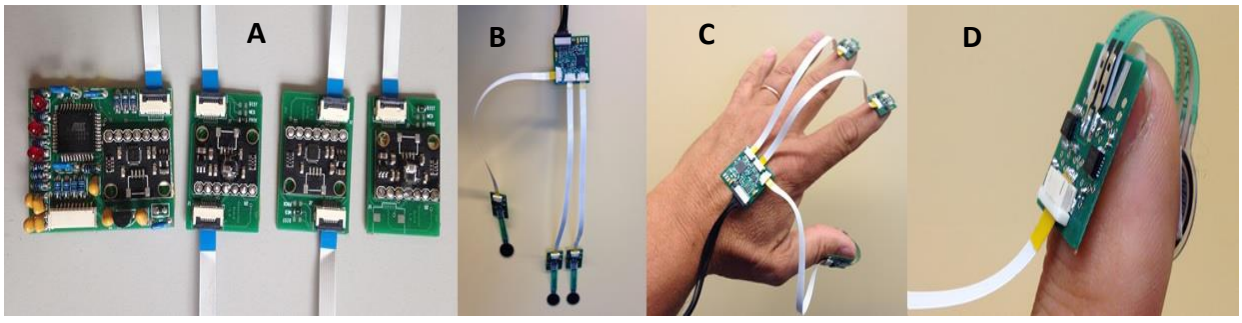

Figure 3.1.1: Set of IMUs for the forearm, upper arm, shoulder and sternum (A). IMU-set for the hand and the distal phalanxes of the thumb, index finger and middle finger with connected FSRs (B). Demonstration how the hand IMU-set can be applied (C). Zoomed-in picture of the thumb-IMU (D).

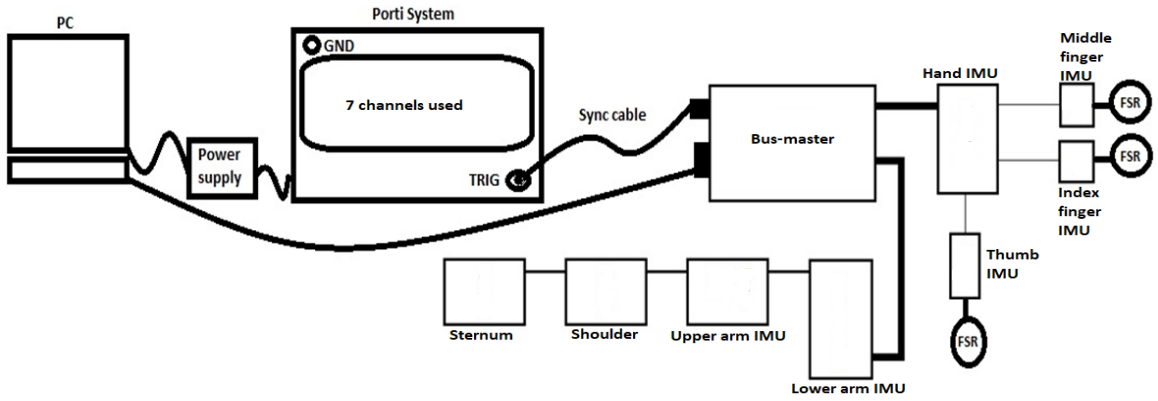

Figure 3.1.2: Connection of the iHAMS with the PC. The two inertial strings are connected via a bus-master. The bus-master is connected to the USB port of the PC and to the digital trigger input of the Porti system via a sync cable. The Porti system is connected to its power supply and a USB port of the PC.

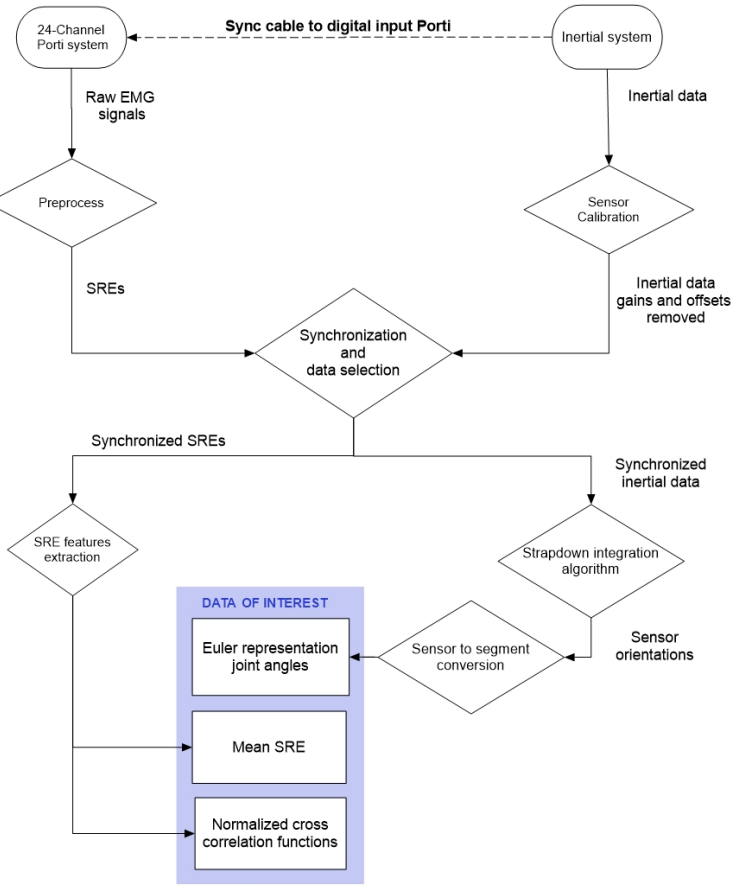

Figure 3.1.3: Flow chart of the offline processing. Firstly, raw EMG signals are pre-processed to linear envelopes. Secondly, the compensation of the offsets and gains regarding the accelerometer and gyroscope recordings is implemented. The compensation is developed during the sensor calibration procedure. Thirdly, the linear envelopes and the inertial data within each trial are synchronized and the synchronized data that corresponds with the movements is selected. Finally, averaged interaction forces, joint angles, average values of the envelopes and normalized cross-correlation coefficients are determined.

3.1.1 PORTI EMG MEASUREMENT SYSTEM AND EMG PROCESSING

Muscle activity is measured with a bipolar input Porti-system at a sample rate of 2048 Hz with a MATLAB driver and interface provided by TMSi. The electrode cables are shielded with the average of the 'plus' and 'minus' electrode signal (true active signal shielding) so that cable movement artefacts and powerline interference (50/60 Hz) are reduced to a minimum (Twente Medical Systems international (TMSi)). The data acquired from the Porti system contains a 2048 Hz sync signal (for synchronization with the inertial system) and electromyography (EMG) of the biceps, triceps (lateral head and long head), deltoideus (anterior and medial) and wrist muscles are recorded (see Table 3.1.1). The electrode pairs are placed in accordance to the SENIAM (Surface Electromyography for the Non-Invasive Assessment of Muscles) recommendations, demonstrated in Figure 3.1.4 (Freriks & Hermens, 2000). Moreover, the optimal electrode position for recording activity of the ECR during wrist extension can be identified by means of the forearm length and a marked line starting from the lateral epicondyle of the humerus to the radial and ulnar styloid processes (Ghapanchizadeh, Ahmad, & Ishak, 2015). The optimal position of the extensor carpi radialis is at 89 % of the forearm length. The optimal electrode position for recording activity of the ECR during wrist extension can be identified by means of the forearm length and a marked line starting from the lateral epicondyle of the humerus to the radial and ulnar styloid processes. The optimal position of the extensor carpi radialis is at 89 % of the forearm length. The electrode placement regarding the FCR and the ECR is illustrated in Figure 3.1.5

In addition, the reference electrode is placed at the elbow and silver/silver chloride electrocardiogram (ECG) electrodes of the type COVIDIEN^{TM} are used for recording muscle activity. An illustration of the iHAMS can be seen in Figure 3.1.6.

Table 3.1.1: Bipolar channels of the Porti EMG system connected to corresponding muscle.

Bipolar Channel	Muscles
1	Biceps brachii
2	Triceps lateral head
3	Triceps long head
4	Deltoideus medial
5	Deltoideus anterior
6	Flexor carpi radialis
7	Extensor carpi radialis

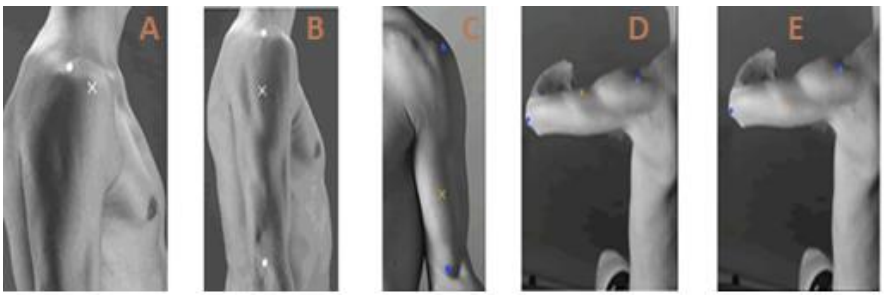

Figure 3.1.4: Electrode placement on the deltoideus anterior (A), deltoideus Medial (B), biceps brachii (C), triceps lateral head (D) and triceps long head (E). The small cross indicates the location at which the electrode pair is placed, and the small dots are used as guidance for finding the recommended location. The locations are recommended according to the SENIAM standards. The picture is taken from (Freriks & Hermens, 2000).

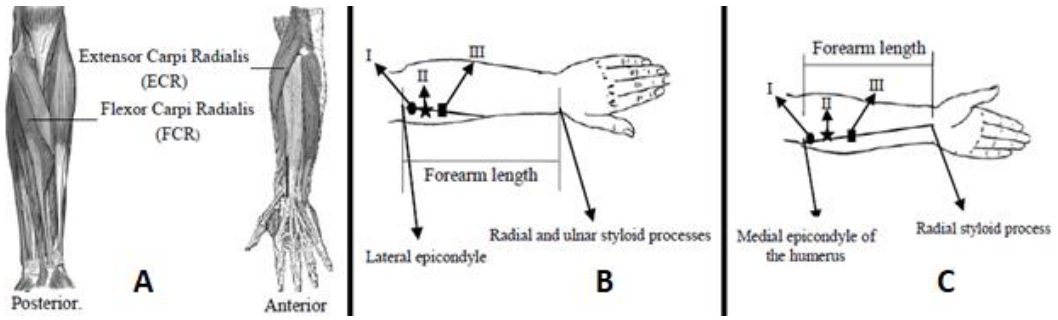

Figure 3.1.5: Posterior and anterior side of the left forearm (A), possible electrode positions of the ECR (B), and possible electrode positions of the FCR (C). The optimal position of the ECR and FCR are at 89% respectively 90% distance of the forearm length. The picture is taken from (Ghapanchizadeh et al., 2015).

Figure 3.1.6: iHAMS containing a 24 bipolar channel Port-system of which 7 are used and the inertial system. Each blue cover contains an IMU.

EMG pre-processing.

The EMG signals are high pass filtered using a second order recursive Butterworth filter with a cut off frequency of 30 Hz. The cut-off frequency of the high pass filtering process of the EMG signals is chosen to be 30 Hz because the EMG recordings at the deltoideus muscles (medial and anterior) are contaminated by the electrocardiogram (ECG) and most of ECG's spectral power is located below 30 Hz (Willigenburg, Daffertshofer, Kingma, & Van Dieën, 2012). Although the EMG signals of the rest of the muscles are not contaminated by the ECG, pre-processing the EMG signals of all muscles in a similar way is important to maintain the phase relationship between the EMG profiles (Prince, Winter, Stergiou, & Walt, 1994).

The high pass filtered EMGs are then notched using a second order recursive Butterworth filter at band frequency of 49.5 Hz until 50.5 Hz for eliminating possible powerline interference, then rectified and smoothed using a second order recursive low pass Butterworth filter with a cut off frequency of 6 Hz (Peter,

2005; Winter, 2009). The above steps describe the (offline) pre-processing of the raw EMG signals to smooth rectified EMG (SRE) signals (see Figure 3.1.3).

SRE features extraction

The mean of the SRE curve gives a good indication of the contraction level of the corresponding muscle (Winter, 2009). For a duration starting from the onset detection of the movement till the offset detection of the movement, T, the mean of the SRE of a muscle is determined as follows:

$$\mu_{SRE} = \frac{1}{T}\int_0^T SRE.dt \qquad Eq.3.1$$

Moreover, cross-correlation analyses evaluate how well a given signal is correlated with another signal over past, present, and future points in time (lags). The cross-correlation of two signals (time series) results in a series of correlation values as a function of the lags (phase shift, τ). The normalized cross-correlation normalizes the series so that the autocorrelations at zero lag is equal to 1 (Orfanidis, 1988). The normalized cross-correlation can be determined by the MATLAB-function "xcorr" and the formula for the cross-correlation between two signals $x(t)$ and $y(t)$ is as follows (Winter, 2009).

$$R_{xy}(\tau) = \frac{\frac{1}{T}\int_0^T x(t)y(t+\tau)dt}{\sqrt{R_{xx}(0)R_{yy}(0)}} \qquad Eq.3.2$$

Where, the numerator is the mean of the product of signal $x(t)$ and a phase shifted $y(t)$, and the denominator is the square root of the product of the autocorrelations of the signals. The denominator normalizes the correlations to be dimensionless from -1 to +1. The two-time series $x(t)$ and $y(t)$ must have zero mean. The autocorrelation of a signal $x(t)$ is as follows (Winter, 2009)

$$R_{xx}(\tau) = \frac{\frac{1}{T}\int_0^T x(t)x(t+\tau)dt}{R_{xx}(0)} \qquad Eq.3.3$$

Where, τ is the phase shift, and $R_{xx}(0)$, which is the mean square of $x(t)$, is the maximum value of $R_{xx}(\tau)$. Furthermore, $x(t)$ has zero mean. Cross-correlations are used to measure the delay between physiological signals. Since the raw EMG signals at the biceps, triceps (lateral head and long head), deltoideus (anterior and medial) and wrist muscles are pre-processed to SREs in a similar way, the phase relationship between the EMG profiles is maintained (Prince et al., 1994). Cross-correlations can also be as a measure for synergistic and coactivation of EMG profiles (Winter, 2009). A normalized correlation close to +1 indicates that the two signals are acting together in phase, while a normalized correlation close to -1 indicates that one signal is at a maximum while the other at a minimum. A peak positive value at $\tau = 0$ indicates that the two muscles are being activated and deactivated simultaneously (Nelson-Wong, Gregory, Winter, & Callaghan, 2008; Prince et al., 1994). Before determining the cross-correlations between the muscles, the mean value of each corresponding SRE is first subtracted from the SRE, so that the signal becomes zero mean.

3.1.2 INERTIAL MEASUREMENT SYSTEM AND PROCESSING

Before the inertial system can be used, a sensor calibration procedure is required. The sensor calibration procedure is necessary for determining the offsets and gains of the accelerometers and gyroscopes. The offsets and gains are caused by non-zero biases, inaccurate scaling and sensor axis misalignments (Lötters, Schipper, Veltink, Olthuis, & Bergveld, 1998; Tedaldi, Pretto, & Menegatti, 2014). During the sensor calibration, the IMUs are taped to the inside of a metal block (Figure 3.1.7) that is rotated around three

different axes and placed in three different static positions. During each rotation, the gain of the 3D gyroscope of each sensor is determined as follows:

$$k = \frac{2\pi}{\int(\omega - \omega_b).dt} \qquad Eq.3.4$$

Where ω is the angular velocity of the rotation among each corresponding axis when the block lays on a side and ω_b is the non-zero bias. However, before determining the gains, the non-zero biases of the gyroscopes are determined approximately 1 second prior to the rotation. Prior to the rotation, the block is in a static position and the gyroscope bias is determined by the baseline mean. The 3D biases are then subtracted from the 3D gyroscope recordings. Moreover, the biases and misalignments of the accelerometers are determined during each static position (Tedaldi et al., 2014). In a static position, the norm of the accelerometer recordings is equal to the magnitude of gravity ($9.81^{m}/_{s}$) plus an offset that includes biases and misalignments.

An algorithm for determining offsets and misalignments of the IMUs as described above existed already in the inertial measurements system. However, the algorithm switched the direction of the accelerations inconsistently, and the norms of the accelerometer recordings during static positions are not equal to the magnitude of gravity. Moreover, the offsets of the gyroscope recording are not completely compensated. Therefore, the directions are manually changed in a consistent manner, and the offsets and gains are further compensated (see Figure 3.1.8). After this procedure, the values of the gains and offset are stored and compensated. Moreover, based on the output of the calibration procedure (see Figure 3.1.8) an indication of the sensor frames can be provided when the sensors are placed on a table. (see Figure 3.1.9).

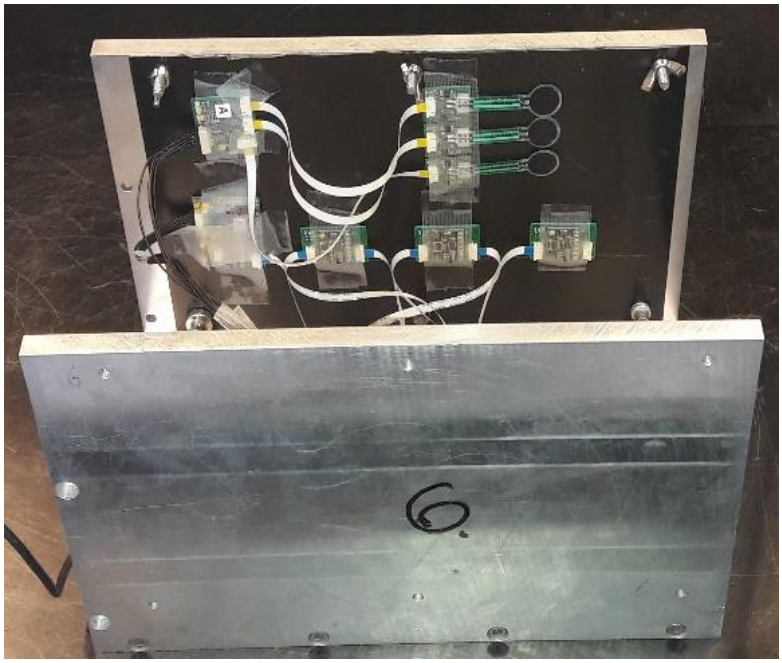

Figure 3.1.7: Aluminium block with the IMUs taped to the inside. The IMUs of the index finger, the middle finger, the thumb and the hand have the same heading direction, while the IMUs on the lower arm, the upper arm, the shoulder and the sternum have the opposite heading.

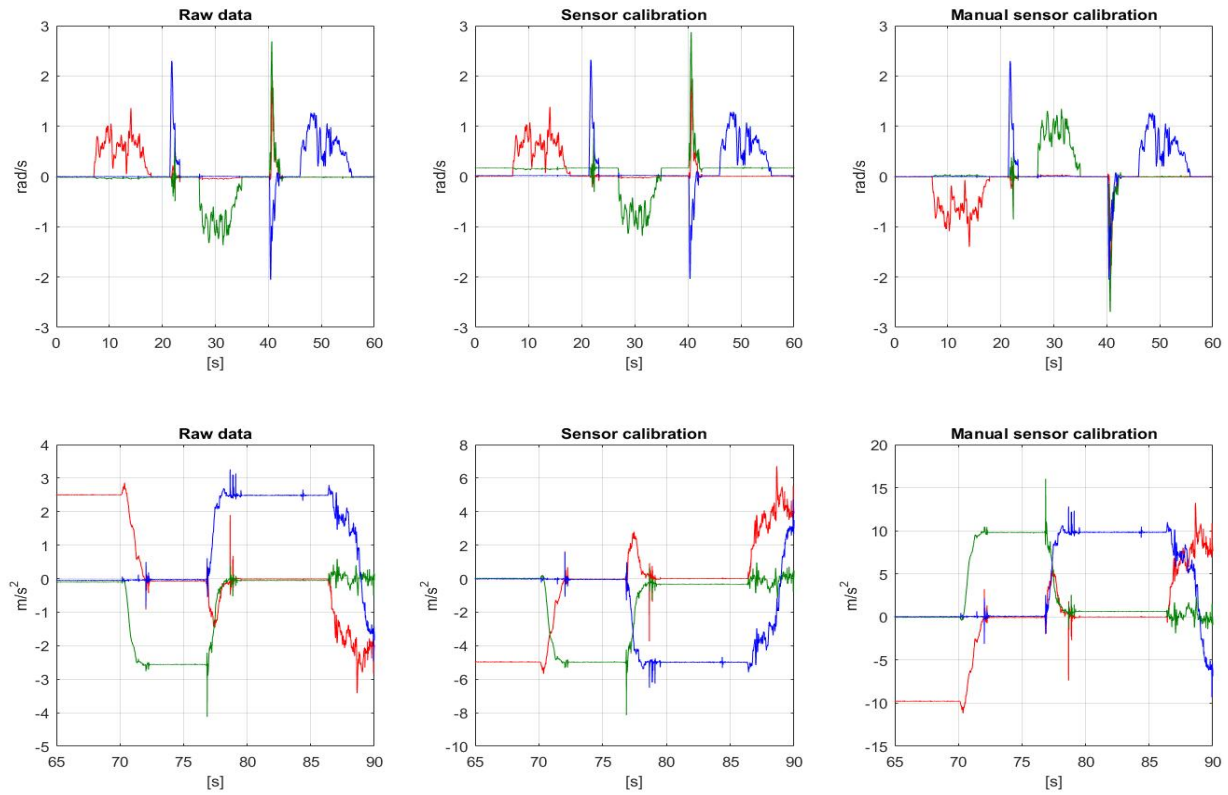

Figure 3.1.8: An example of the angular velocities (top row) and accelerations (bottom row) of the IMU of the index finger during the three rotations and three different static positions.

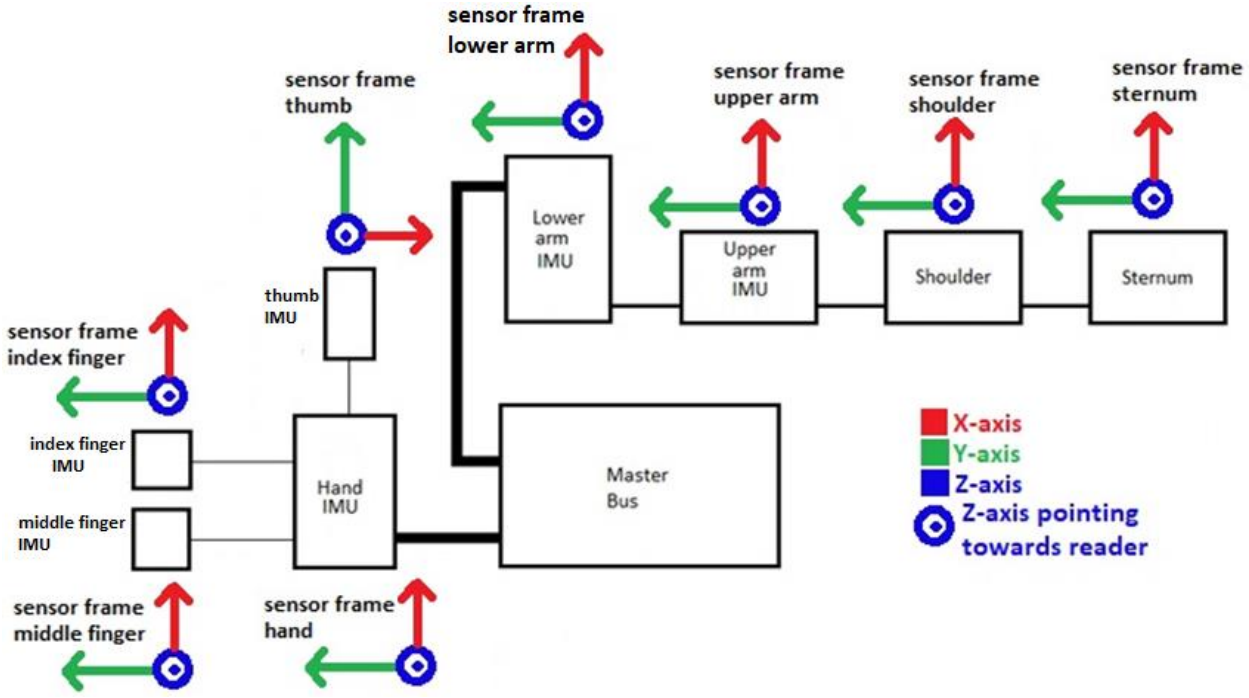

Figure 3.1.9: Top view of the inertial measurement system and the orientation of the sensor coordinate frame of the IMUs.

3.1.2.1 STRAPDOWN INTEGRATION ALGORITHM

The strapdown integration algorithm uses as input angular velocities and accelerations expressed in the sensor frame. Moreover, the algorithm is based on two procedures. The first procedure concerns the estimation of the initial orientation of each IMU attached on corresponding segment at the beginning of the movement. The second procedure concerns a numerical integration in order to estimate the rest of the orientations of each IMU until the end of the movement.

3.1.2.1.1 ESTIMATION INITIAL SENSOR ORIENTATION

During the resting position, the acceleration of each inertial sensor represents the inclination. For example, consider the IMU on the lower arm (see Figure 3.1.10). Shortly before the onset of the movement is detected, the inclination is determined by normalizing the mean of the acceleration recordings as follows.

$$\bar{a}_y^{sen} = \left[\hat{a}_y^{sen} \,/\, \left\|\hat{a}_y^{sen}\right\|_2\right]^T \qquad Eq.3.5$$

Where, $\hat{a}_y^{sen} \epsilon \mathbb{R}^{1\times 3}$ is the mean of the 3D acceleration recordings shortly before the onset of the movement. The columns of $\hat{a}_y^{sen}$ represent the mean value of the recordings in the x-, y-, and z-direction. $\left\|\hat{a}_y^{sen}\right\|_2 \epsilon\, \mathbb{R}^{1\times 1}$ is the norm of $\hat{a}_y^{sen}$, and $\bar{a}_y^{sen} \epsilon \mathbb{R}^{3\times 1}$ is then the corresponding unit vector in the y-direction of the sensor frame. The superscript, T, indicates the transpose. If the IMU on the lower arm is aligned in the direction of the gravity (inclination is then 0°), then the unit vector $\bar{a}_y^{sen}$ is equal to $[0\ 1\ 0]^T$. However, the inclination is not equal to 0° since muscles are bulky and the acceleration recordings during the resting position are accompanied with movement artefacts and measurement noise.

The unit vector in the z-direction of the sensor frame can be determined by assuming that the IMU is perfectly aligned in the direction of gravity. The x-direction of the sensor frame an inclination of 0°, the heading, is then $[1\ 0\ 0]^T$ and the z-direction of the sensor can be determined by means of the cross-product as follows

$$\bar{a}_z^{sen} = \frac{\left([1\ 0\ 0]^T \times \bar{a}_y^{sen}\right)}{\left\|[1\ 0\ 0]^T \times \bar{a}_y^{sen}\right\|_2} \qquad Eq.3.6$$

Where, the numerator is the cross-product of the unit vector in x-, and the y direction of the sensor frame, and the denominator is the norm of the vector resulting from the corresponding cross-product. Since this unit vector is determined by assuming that the inclination is 0°, an error-correction must be considered.

Moreover, the unit vector in the x-direction expressed in sensor frame is determined by means of the cross-product of $\bar{a}_y^{sen}$ and $\bar{a}_z^{sen}$ respectively as follows

$$\bar{a}_x^{sen} = \frac{\left(\bar{a}_y^{sen} \times \bar{a}_z^{sen}\right)}{\left\|\bar{a}_y^{sen} \times \bar{a}_z^{sen}\right\|_2} \qquad Eq.3.7$$

Where, the numerator is the cross-product of the unit vector in y-, and the z direction of the sensor frame, and the denominator is the norm of the vector resulting from the corresponding cross-product. In order to correct for the assumption that the inclination is 0°, the unit vector in the z-direction of the sensor frame, $\bar{a}_z^{sen}$, is recalculated as follows

$$(\bar{a}_z^{sen})^* = \frac{\left(\bar{a}_x^{sen} \times \bar{a}_y^{sen}\right)}{\left\|\bar{a}_x^{sen} \times \bar{a}_y^{sen}\right\|_2} \qquad Eq.3.8$$

The initial sensor frame (for the lower arm in this example), also known as the initial orientation expressed in sensor frame $R_{init}^{sen} \epsilon \mathbb{R}^{3\times3}$, is constructed as follows:

$$R_{init}^{sen} = \left[\bar{a}_x^{sen} \;\; \bar{a}_y^{sen} \;\; (\bar{a}_z^{sen})^*\right] \qquad Eq.3.9$$

The initial orientations of the IMUs mounted on the rest of the segments is constructed in similar manner.

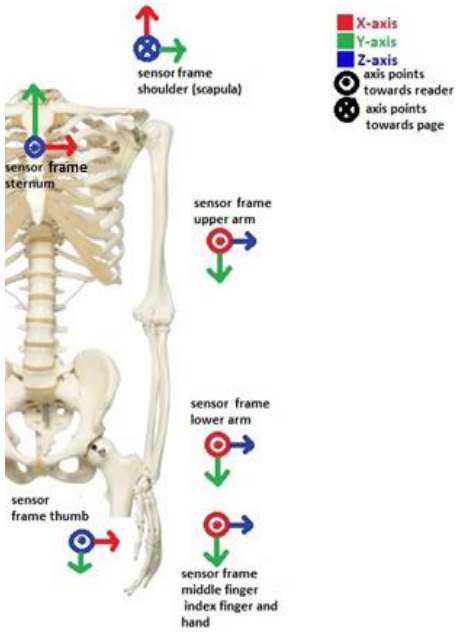

Figure 3.1.10: A (rough) indication of the sensor frame of each IMU when the inertial system is attached to the segments (IMUs not shown, IMUs sensor frames are shown instead). The indication is based on the output of the sensor calibration

3.1.2.1.2 NUMERICAL INTEGRATION ALGORITHM

The angular velocities recordings during the selected Fugl-Meyer movements are integrated to orientations expressed in sensor frame by solving the differential equation in a strapdown navigation algorithm as follows (Bortz, 1971; Schepers, Koopman, & Veltink, 2007; Titterton, Weston, & Weston, 2004; Weenk, Van Beijnum, Baten, Hermens, & Veltink, 2013).

$$\dot{R}_i^{sen} = R_{i-1}^{sen} \, \widetilde{\omega}_i^{sen} \qquad Eq.3.10$$

Where, $\dot{R}_i^{sen}$ is the rate of the sensor frame at current iteration time step $(i = 2,3,\dots,N)$. R_{i-1}^{sen} is the sensor frame at previous iteration time step. For the first iteration time step $(i = 2)$, R_{i-1}^{sen} is the initial orientation determined by means of the acceleration recordings (see previous paragraph). $\widetilde{\omega}_i^{sen}$ is the skew of the 3D angular velocity expressed in sensor frame (in x-,y, and z-direction) at the current iteration time step which can be determined as follows:

$$\widetilde{\omega}_i^{sen} = \begin{bmatrix} 0 & -\omega_z & \omega_y \\ \omega_z & 0 & -\omega_x \\ -\omega_y & \omega_x & 0 \end{bmatrix}_i \qquad Eq.3.11$$

Where ω_x , ω_y , and ω_z are angular velocity recordings in the x-, y, and z-direction respectively. The solution of the differential equation (see equation 3.10) can be determined as follows

$$R_i^{sen} = R_{i-1}^{sen} + T\dot{R}_i^{sen} \qquad Eq.3.12$$

Where, T is the sample period (0.005 seconds). Since the initial sensor frame is known, R_i^{sen} represents the orientation expressed in sensor frame at the current iteration time step during the movement.

3.1.2.2 SENSOR-TO-SEGMENT CONVERSION ALGORITHM

The orientations expressed in the sensor frame need to be converted to orientations expressed in segment frame. A sensor-to-segment calibration procedure which is performed prior to the performance of the selected set of the FMA-UE is required in order to obtain the sensor-to-segment orientation, R^{segsen} (Kortier, 2018). The orientations expressed in sensor frame are converted to segment frame as follows

$$R_j^{seg} = R_j^{sen} R^{segsen} \qquad Eq.3.13$$

Where $j = 1,2, \dots, N$, are the iteration time steps during the performance of the selected set of the FMA-UE. R_j^{sen} is the orientation expressed in sensor frame at iteration time step j and R_j^{seg} is the orientation expressed in segment frame at iteration time step j. R^{segsen} is a fixed rotation matrix that converts sensor orientations to corresponding segment orientations. After the orientations are expressed in segment frame, corresponding joint angles can be determined.

Sensor-to-segment calibration procedure

The sensor-to-segment calibration procedure is necessary to convert kinematic data expressed in sensor frame to kinematic data expressed in segment frame. Thus, a mapping from sensor frames to the corresponding segment frames is required. The mapping is achieved by the multiplication with the corresponding sensor-to-segment rotation matrix (see Eq. 3.13). In order to construct the sensor-to-segment rotation matrix that corresponds with a certain segment, proper calibration movements are required. The subjects are instructed to perform a total of twenty-six calibration movements in order to investigate which movement combinations are optimal to calibrate each corresponding segment (see Table 3.1.2 and Appendix A). Moreover, each calibration movement defines a certain anatomical axis. The anatomical axes of the different segments are defined as illustrated in Figure 3.1.11.

During the performance of static calibration movements, the accelerometer recordings of the corresponding segment(s) are of interest, while during dynamic calibration movements, the gyroscope recordings of the corresponding segment(s) are of interest. Each set of measurement recordings corresponding to a calibration movement is processed by means of the least squares regression curve fitting method (Bonnet, Bassompierre, Godin, Lesecq, & Barraud, 2009). In order to provide a clear conception regarding the construction of the sensor-to-segment rotation matrix, the calibration movements of the upper arm are considered:

1. The first calibration movement of the upper arm concerns an alignment of the upper arm with the direction of gravity so that the inclination of the sensor can be determined (see Table 3.1.2, calibration movement 15). This static pose is held for several seconds and defines the anatomical axis of the upper arm in the z-direction (see Figure 3.1.11), which is determined by normalizing the linear curve fit obtained by least squares regression fitting of the corresponding accelerometer recordings as follows

$$\bar{Z}_{acc}^{upper} = \frac{\overleftarrow{\mathrm{acc}}_{upper}^{sen}}{\left\| \overleftarrow{\mathrm{acc}}_{upper}^{sen} \right\|_2} \qquad Eq.3.14$$

   Where, $\bar{Z}_{acc}^{upper}$ is the anatomical vector in the z-direction of the upper arm expressed in sensor frame and $\left\| \overleftarrow{\mathrm{acc}}_{upper}^{sen} \right\|_2$ is the norm of the least squares regression fit through the accelerometer recordings.

Similarly, the anatomical vectors in the y- and x-direction of the upper arm, $\overline{\mathrm{Y}}_{acc}^{upper}$ respectively $\overline{\mathrm{X}}_{acc}^{upper}$, are determined on corresponding static calibration poses (see Table 3.1.2, Calibration movement 16 and 17 respectively).

2. The next calibration movement considered is repeated abduction of the shoulder while the elbow is kept in a 90° flexion pose (see table, calibration movement 18). Moreover, this calibration movement defines the anatomical axis of the upper arm in the x-direction (see Figure 3.1.11), which is determined by normalizing the linear curve fit obtained by least squares regression fitting of the corresponding gyroscope recordings as follows

$$\overline{\mathrm{X}}_{gyr}^{upper} = \frac{\overleftarrow{\mathrm{gyr}}_{upper}^{sen}}{\left\|\overleftarrow{\mathrm{gyr}}_{upper}^{sen}\right\|_2} \qquad Eq.3.15$$

Where, $\overline{\mathrm{X}}_{gyr}^{upper}$ is the anatomical vector in the x-direction of the upper arm based on gyroscope recordings and $\left\|\overleftarrow{\mathrm{gyr}}_{upper}^{sen}\right\|_2$ is the norm of the least squares regression fit through the gyroscope recordings. Similarly, the anatomical vectors in the y- and z-direction of the upper arm, $\overline{\mathrm{Y}}_{gyr}^{upper}$ respectively $\overline{\mathrm{Z}}_{gyr}^{upper}$, are determined based on the corresponding calibration movements (Table 3.1.2, Calibration movement 19 and 20 respectively).

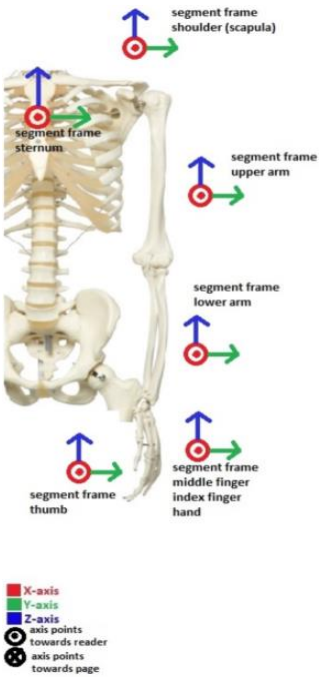

Figure 3.1.11: self-defined segment frame.

3. The calibration movements result in six anatomical vectors, three constructed by means of acceleration recordings and three by means of gyroscope recordings. However, the two most optimal vectors are required for constructing the sensor-to-segment rotation matrix. The selection of the two most optimal vectors is based on two indicators: the variance accounted for (VAF) and the mutual angle. The variance accounted for indicates the quality of the linear regression and can be determined as follows

$$VAF_{gyr} = 1 - \frac{RMSe\left(\overleftarrow{\mathrm{gyr}}_{upper}^{sen}\right)}{RMS\left(\overleftarrow{\mathrm{gyr}}_{upper}^{sen}\right)} \; or \; VAF_{acc} = 1 - \frac{RMSe\left(\overleftarrow{\mathrm{acc}}_{upper}^{sen}\right)}{RMS\left(\overleftarrow{\mathrm{acc}}_{upper}^{sen}\right)} \qquad Eq.3.16$$

Where, the numerator is the root mean square error of the linear least squares regression fit of the gyroscope recordings during one calibration movement. The numerator is the standard deviation of the residuals of the regression fit. The denominator is the root mean square of the regression fit. Moreover, a value of the VAF close to one indicates that the calibration movement is well performed. The two vectors with the highest VAF and mutual angle closest to 90° are then selected.

The sensor-to-segment rotation matrix can be determined as follows. Assume that the anatomical vectors $\overline{\mathrm{X}}_{gyr}^{upper}$ and $\overline{\mathrm{Y}}_{acc}^{upper}$ have the highest VAF values and a mutual angle closest to 90° compared to the rest of the pairs. Furthermore, assume that $\overline{\mathrm{X}}_{gyr}^{upper}$ has the highest VAF. The sensor-to-segment rotation matrix is determined as follows (Luinge, Veltink, & Baten, 2007):

$$R_{upper}^{segsen} = \left[\overline{\mathrm{X}}_{gyr}^{upper} \ \left(\left(\overline{\mathrm{X}}_{gyr}^{upper} \times \overline{\mathrm{Y}}_{acc}^{upper}\right) \times \overline{\mathrm{X}}_{gyr}^{upper}\right) \left(\overline{\mathrm{X}}_{gyr}^{upper} \times \overline{\mathrm{Y}}_{acc}^{upper}\right)\right] \quad Eq.3.17$$

In case $\overline{\mathrm{Y}}_{acc}^{upper}$ has the highest VAF, the sensor-to-segment rotation matrix is determined as follows:

$$R_{upper}^{segsen} = \left[\left(\overline{\mathrm{Y}}_{acc}^{upper} \times \left(\overline{\mathrm{X}}_{gyr}^{upper} \times \overline{\mathrm{Y}}_{acc}^{upper}\right)\right) \ \overline{\mathrm{Y}}_{acc}^{upper} \left(\overline{\mathrm{X}}_{gyr}^{upper} \times \overline{\mathrm{Y}}_{acc}^{upper}\right)\right] \quad Eq.3.18$$

Table 3.1.2: Description of 26 calibration movements for sensor-to-segment calibration. The subject is seated while performing calibration movements 1 to 20 but standing while performing the last six movements.

Calibration #	***Description***
1	Middle and index finger flat for several seconds
2	Three times flexion and extension of the middle and index finger
3	Thumb flat for several seconds
4	Three times flexion and extension of the thumb
5	Palmar side of the hand flat on a table or flat object for several seconds
6	Ulnar side of the hand on a box or table in a static pose for several seconds
7	Static pose on the left side of the thumb
8	Three times flexion and extension of the wrist
9	Three times pronation and supination of the forearm
10	Three times elbow flexion and extension with the hand in mid position of pronation and supination
11	Three times elbow flexion with the forearm pronated
12	Static pose of the forearm aligned in the direction of gravity with the elbow fully extended (inclination)
13	Static pose of the forearm in mid position of pronation and supination with the elbow 90° flexed
14	Static pose of the forearm fully pronated with the elbow 90° flexed
15	Static pose of the upper arm aligned with gravity*
16	Static pose of the upper arm while the elbow is 90° flexed and the shoulder 90° abducted
17	Static pose of the upper arm while the elbow and shoulder are 90° flexed
18	Three times shoulder abduction with the elbow 90° flexed
19	Three times shoulder flexion with the elbow 90° flexed
20	Three times shoulder internal and external rotation with the shoulder and elbow kept in 90° flexed pose
21	Subject in neutral pose (N-pose)
22	Static pose standing trunk flexion (90°)
23	Static pose standing trunk lateral flexion (approximately 35°, left side)
24	Three times trunk flexion
25	Three times trunk ipsilateral and contralateral rotation
26	Three-time lateral trunk rotation

** Calibration movement twelve and fifteen are identical regarding the calibration of the upper arm.*

3.1.2.2.1 DETERMINING JOINT ANGLES

The orientations expressed in segment frame regarding the lower arm, upper arm, sternum, and the hand are of interest for determining joint angles such as, elbow flexion, shoulder flexion, shoulder abduction, wrist flexion and extension. In order to determine the joint angles, segment orientations are determined with respect to the sternum, and then with respect to each other. For example, orientations expressed in segment frame regarding the hand, upper arm and forearm relative to the sternum are determined as follows

$$R_j^{SU} = \left(R_j^S\right)' R_j^U$$
$$R_j^{SL} = \left(R_j^S\right)' R_j^L$$
$$R_j^{SH} = \left(R_j^S\right)' R_j^H \qquad Eq.3.19$$

Where $j = 1,2,\dots,N$, are the iteration time steps during the performance of the selected set of the FMA-UE. R_j^U, R_j^L, R_j^H are the orientations at iteration step j, expressed in segment frame regarding the upper arm, the lower arm and the hand respectively. $\left(R_j^S\right)'$ is the transpose of the orientations at iteration step j, expressed in segment frame regarding the sternum. R_j^{SU}, $R_j^{SL}$and R_j^{SH} are the orientations expressed in segment frame regarding the upper arm, the lower arm respectively the hand with respect to the sternum.
Joint angles at the elbow such as: elbow flexion, forearm supination and forearm pronation, and joint angles at the wrist, such as: wrist flexion and wrist extension, can be extracted from the following orientations

$$R_j^{SUL} = \left(R_j^{SU}\right)' R_j^{SL}$$
$$R_j^{SLH} = \left(R_j^{SL}\right)' R_j^H \qquad Eq.3.20$$

Where R_j^{SUL} is the orientation at iteration step j, expressed in segment frame regarding the lower arm relative to the upper arm with respect to the sternum. R_j^{SLH} is the orientation at iteration step j, expressed in segment frame regarding the hand relative to the lower arm with respect to the sternum.

3.1.2.2.2 CONVERSION ROTATION MATRIX TO EULER ANGLES

The transformation from one orientation frame at an iteration time step to another at the next iteration time step can be performed by three successive rotations about different axes (Titterton et al., 2004). Many sequences of rotation were introduced by the Swiss mathematician, Leonhard Euler (1707-1783), but the most commonly used in biomechanics is the Cardan sequence (Winter, 2009). The Cardan sequence concerns a rotation α around the X-axis, a rotation β around the Y-axis, and a rotation γ around the Z-axis. The following rotation matrix describes such a rotation sequence as follows

$$R_{XYZ}(\alpha,\beta,\gamma) = ROT\left(\hat{Z},\gamma\right)\ ROT\left(\hat{Y},\beta\right)\ ROT\left(\hat{X},\alpha\right)$$
$$= \begin{bmatrix} c\gamma & s\gamma & 0 \\ -s\gamma & c\gamma & 0 \\ 0 & 0 & 1 \end{bmatrix} \begin{bmatrix} c\beta & 0 & -s\beta \\ 0 & 1 & 0 \\ s\beta & 0 & c\beta \end{bmatrix} \begin{bmatrix} 1 & 0 & 0 \\ 0 & c\alpha & s\alpha \\ 0 & -s\alpha & c\alpha \end{bmatrix}$$
$$= \begin{bmatrix} c\gamma c\beta & c\gamma s\beta s\alpha + c\alpha s\gamma & s\alpha s\gamma - c\alpha s\beta c\gamma \\ -s\gamma c\beta & c\alpha c\gamma - s\alpha s\beta s\gamma & s\alpha c\gamma + c\alpha s\beta s\gamma \\ s\beta & -c\beta s\alpha & c\beta c\alpha \end{bmatrix} \qquad Eq.3.21$$

Where $c\alpha = cos\alpha$ and $s\alpha = sin\alpha$, etc. $\hat{X}$, $\hat{Y}$, and $\hat{Z}$ are the unit vectors $[1\ 0\ 0]'$, $[0\ 1\ 0]'$and $[0\ 0\ 1]'$ respectively. Moreover, all the successive rotations take place about an axis in the fixed known reference frame (Craig, 2009), in this case the initial orientation frame. The solution for extracting X-Y-Z Euler/Cardan angles from a rotation matrix can be done as follows (Craig, 2009).

Given:

$$R_{XYZ}(\alpha,\beta,\gamma) = \begin{bmatrix} r_{11} & r_{12} & r_{13} \\ r_{21} & r_{22} & r_{23} \\ r_{31} & r_{32} & r_{33} \end{bmatrix}$$

Then the Euler/Cardan angles can be determined as follows:

$$\alpha = -Atan2(r_{32}, r_{33})$$
$$\beta = Atan2\left(r_{31}, \sqrt{{r_{11}}^2 + {r_{21}}^2}\right)$$
$$\gamma = Atan2(r_{21}, r_{11}) \qquad Eq.3.22$$

Where, $Atan2$ is a two-argument arc tangent function. The angles extracted from the Euler/Cardan technique are sequence dependent, which means that angles calculated for a X-Y-Z sequence can differ significantly from angles calculated for a Z-Y-X sequence (Crawford, Yamaguchi, & Dickman, 1999). In case the sequence is anti-cyclic, i.e. Z-Y-X, then the cyclic sequence (X-Y-Z) can be determined as follows (Woltring, 1991)

$$R_{XYZ}(\alpha,\beta,\gamma) = \left(R_{ZYX}(-\gamma,-\beta,-\alpha)\right)' \qquad Eq.3.23$$

Moreover, since the bias in the gyroscope is not compensated, the Euler/Cardan representation of the joint angles is contaminated with drift. This drift is due to the integration process of the angular velocity with nonzero bias to orientations. An example of drift compensation is illustrated in Figure 3.1.12. The drift compensation is based on the assumption that the initial and final orientation of each corresponding segment are identical, and that the initial and final joint angles are zero.

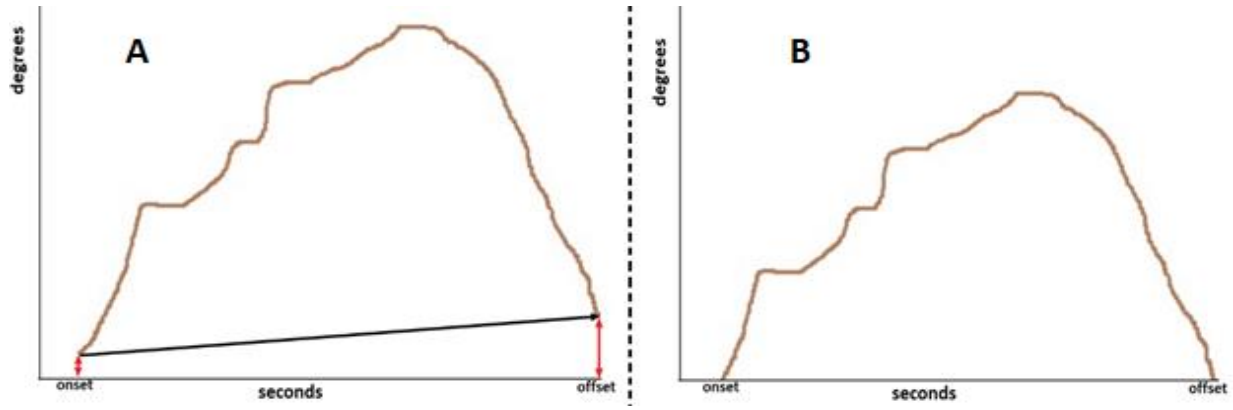

Figure 3.1.12: The orientations (brown curve) contaminated with a linear drift (black arrow) are depicted in A. The red arrows indicate the integration off the non-zero bias. During the onset and offset of the movement, these biases are identified and modelled linearly which result in a trend (black arrow). Detrending of the orientations is achieved when subtracting the orientations from the linear trend (B).

3.1.3 SYNCHRONIZATION AND DATA SELECTION

The synchronization algorithm uses SREs, inertial data (angular velocities and accelerations) and force data as inputs. The Porti system and the inertial system are synchronized by means of the sync signal and the sample counter. The sample counter is a 100 Hz unsigned 16-bit integer value that increases one sample each time a new acquisition of data from the gyroscopes, accelerometers, and magnetometers is finished. Moreover, the sync signal is provided by the inertial system and send to the trigger input of the Porti via the sync cable (see Figure 3.1.2). Each time when the reset sample is activated, a lower peak and a gap can

be noticed in the sample counter and the sync signal respectively (see Figure 3.1.13 and Figure 3.1.14). However, the first gap in the sync signal corresponds with the activation of the inertial system (automatic reset), while the rest of the noticeable gaps are caused by the reset button in the interface. Resetting via the interface-button is done at the beginning and end of each trial and the corresponding lower peaks and gaps are selected and used for offline synchronization (see Figure 3.1.14).

The synchronized data per trial contains SRE of muscles, angular velocities, accelerations and interaction force of the distal phalanxes of the index-, middle-finger and thumb. The SRE data is downsampled from 2048 Hz to the gyroscope sampling rate of 200 Hz, while accelerations and interaction forces are upsampled from 100 Hz to the gyroscope sampling frequency of 200 Hz. The resampling procedure is performed in MATLAB by means of the function “resample”. The resample-options are chosen such that the data is linearly interpolated to an intermediate uniform grid with sample rate equal to 200 Hz.

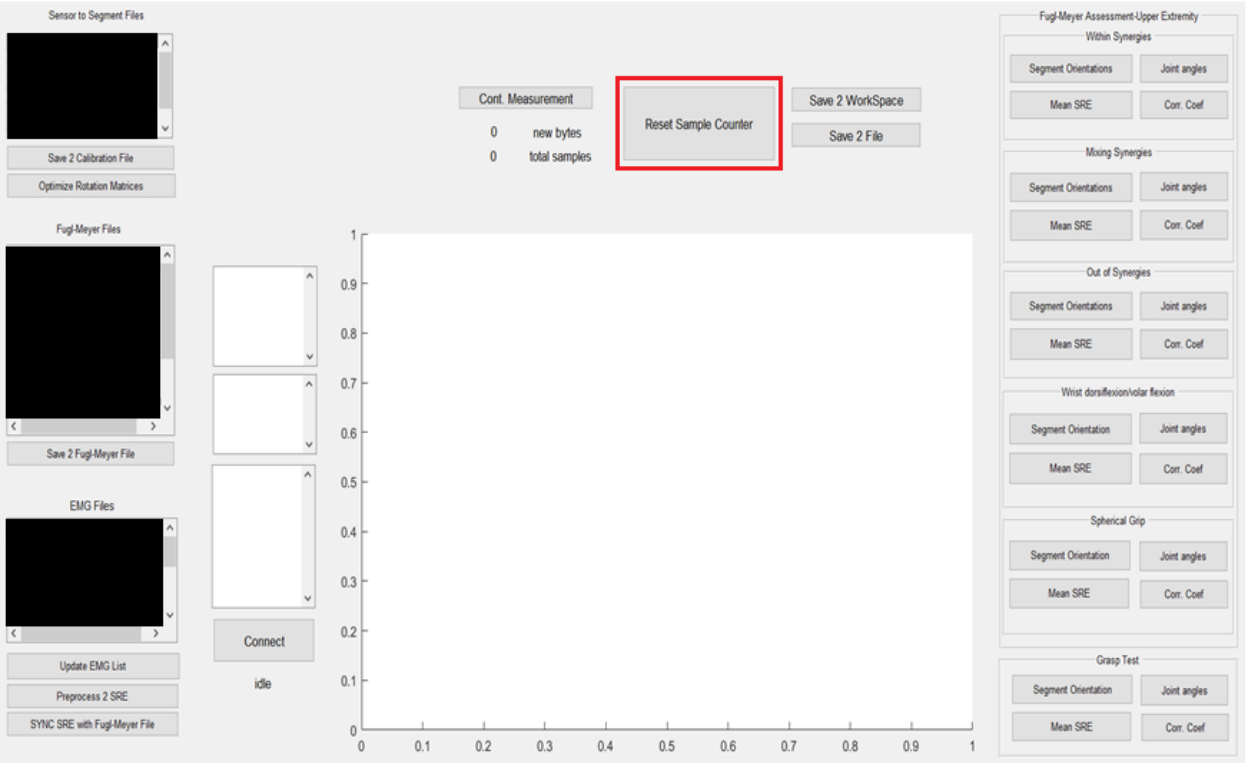

Figure 3.1.13: The interface of the system. The ‘Reset Sample Counter’ button is pressed during the beginning and end of each trial. Each time this button is pressed, a gap and a lower peak is noticed in the sync signal and the sample counter respectively.

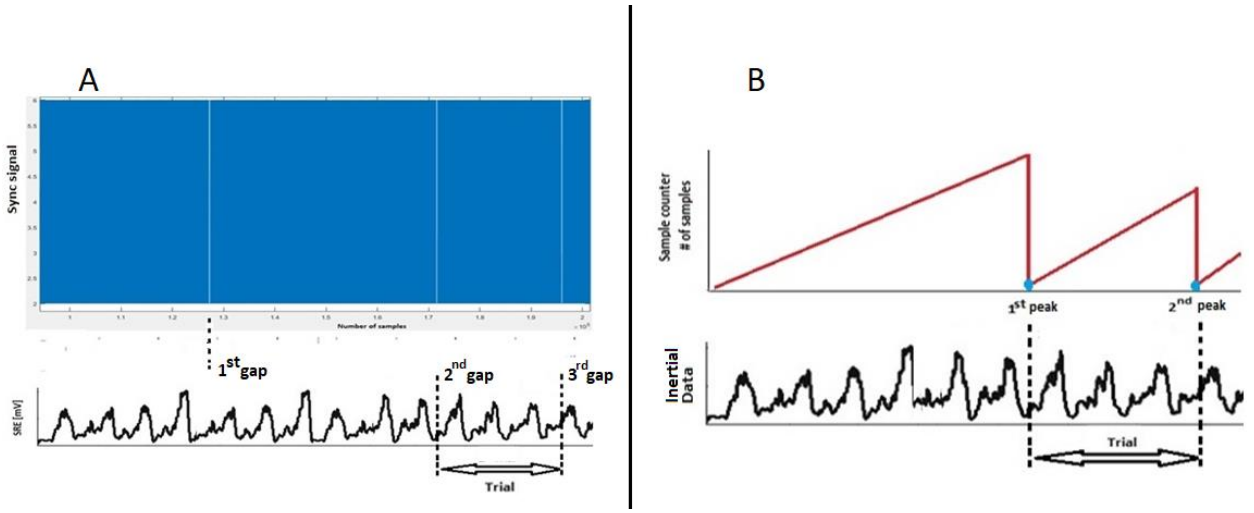

Figure 3.1.14: The synchronization procedure of the iHAMS. The data that corresponds with the trials is selected by means of the gaps and lower peaks of the sync signal and the sample counter respectively. SRE data of the muscles is synchronized with inertial data.

Data selection

Furthermore, during each trial, the subjects are instructed prior and after performing a movement of the FMA-UE to keep the corresponding upper limb in a resting posture with the elbow fully extended. Thus, within each trial, the actual onset and offset of the movement have yet to be determined. Angular velocity is used to determine the onset and offset of each movement performed within each trial. Movement detection from inertial sensors is in general easier compared to EMG, but EMG can detect movement onset earlier than the actual movement (Wentink, Schut, Prinsen, Rietman, & Veltink, 2014). However, during a limb movement several muscles are involved, and EMG onset and offset detection can result in various onsets and offsets for the corresponding muscles involved. Since a notable detection of the entire movement is of interest, determining movement onsets and offsets based on inertial sensors is more favourable. The onset and offset of the movements are detected by means of the modulus of the 3D angular velocity (Wentink et al., 2014). The modulus is determined and intersected with its mean value. By means of this intersection, two identification points are determined (see Figure 3.1.15). The first identification point is used to determine the onset, while the second is used to determine the offset. In order to determine the onset, the modulus starting from the first identification point down to the beginning of the trial is selected and sample wise analysed at which moment a certain threshold value is not exceeded. The offset of the movement is determined in a similar way, but then the analysis starts at the second identification point down to the end of the trial. The threshold value is based on the baseline mean plus two times the standard deviation. This was the lowest threshold that did not detect any movements during the resting period regarding the sensors on the arm and the shoulder. This onset-offset-detection algorithm is used to select the proper data which correspond with the movement during each trial. The data selection consists of SREs, angular velocities, accelerations and force data. The data is further processed as described by the overview and previous paragraphs (see Figure 3.1.3). An example of the data selection is illustrated in Figure 3.1.16.

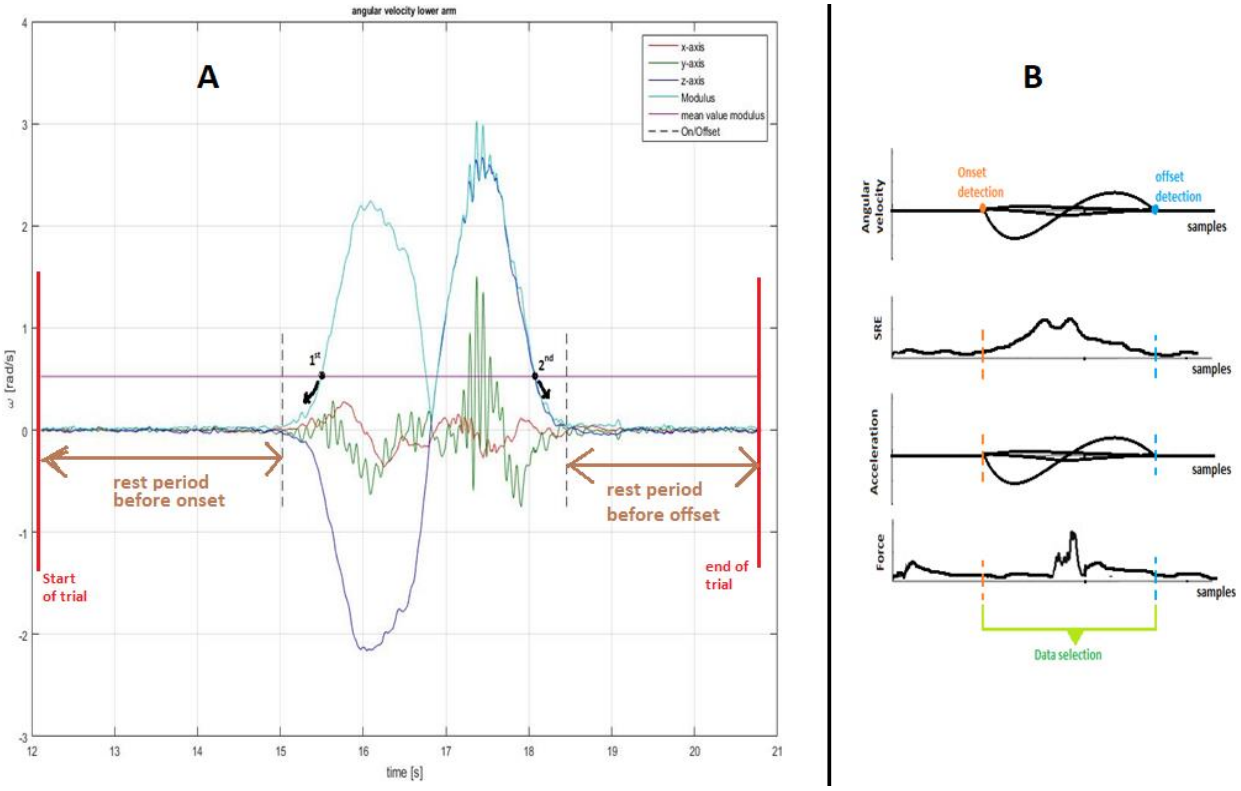

Figure 3.1.15: The onset-offset-detection algorithm (A). The data that corresponds with the movement is then selected since all signals have a sampling frequency of 200 Hz (B).

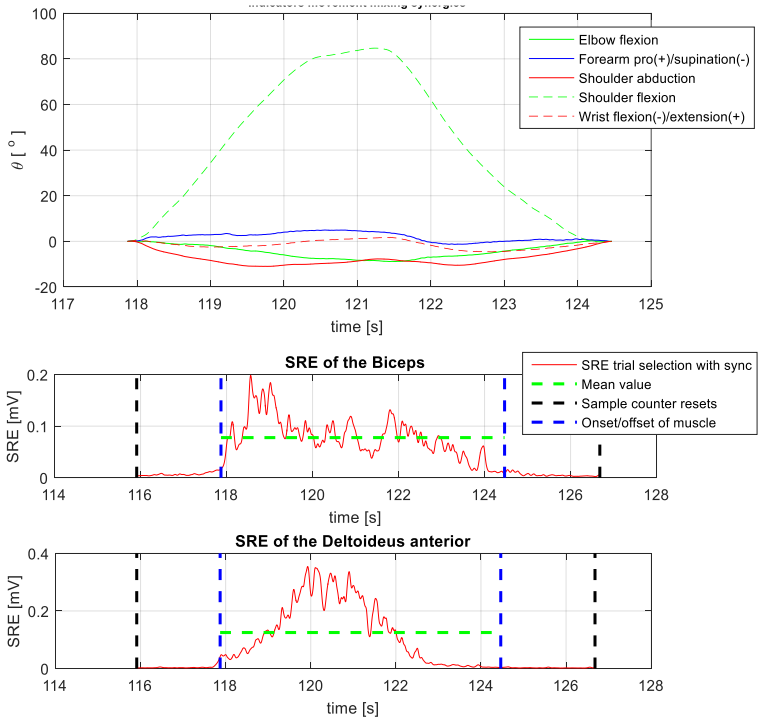

Figure 3.1.16: An example of synchronized joint angles, biceps and deltoideus anterior linear envelopes during shoulder flexion.

3.2 EXPERIMENTAL PROTOCOL

The study concerns a cross-sectional experimental design, in which eight healthy subjects between the age of 25 and 65 years old performed, first sensor-to-segment calibration movements, and then volitional (left) upper extremity movements based on a selected set of items regarding the FMA-UE and one arbitrary grasp test with a cylindrical object. The group of subjects included 7 men and 1 woman. The study was approved by the ethics committee at the university of Twente. The set of movements that is investigated consists of 5 items of the FMA-UE and 1 grasp test. The tasks of the FMA-UE are selected to examine movements within synergies, movements combining synergies, and movements out of synergies, as well as relevant proximal and distal hand functions. Moreover, distal movements regarding repeated dorsiflexion and volar flexion of the wrist in elbow extension, and the spherical grasp are investigated. In the first instance, each subject is requested to perform the task such that the maximum score of the FMA-UE can be assigned. Then, each subject is requested to simulate the movement with pathological synergies. All movements are repeated three times.

3.2.1 SELECTED SET OF MOVEMENTS

The set of movements performed by the healthy subjects is as follows:

1. The flexor synergy. This movement is performed within the synergies.
2. Shoulder flexion 90°. This movement can be performed by mixing the flexor and extensor synergy.
3. Shoulder abduction 90°. This movement is performed out of the synergies.
4. Repeated wrist dorsi flexion and volar flexion.
5. Spherical hand grip.
6. Cylindrical grasp test.

Movements within synergies: the flexor synergy (FMA-UE item A2)
The seated subject is asked to raise his/her hand to the ipsilateral ear with the forearm fully supinated. The shoulder should be abducted at least 90°. The joint angles of interest are shoulder abduction, elbow flexion, and forearm supination. Moreover, the mean values of the SRE at the biceps, triceps and deltoideus muscles, and the cross-correlations between these muscles are determined in order to detect differences between pathologically unaffected and simulated pathologically affected movements.

Table 3.2.1: Inertial indicators of the flexor synergy (FMA-UE item A2).

Kinematics	Unaffected	Affected
Shoulder abduction	≥ 90°	<90°
Elbow flexion	≥90°	<90°
Forearm supination	≈90°	<90°

Movements mixing synergies: shoulder flexion (FMA-UE item A3)
The seated subject is instructed to flex the shoulder from 0° to 90° while the elbow is kept completely extended. The joint angles of interest are shoulder abduction, elbow flexion, and shoulder flexion. Furthermore, the mean values of the SRE at the biceps, triceps and deltoideus muscles, and the cross-

correlations between these muscles are determined in order to detect differences between pathologically unaffected and simulated pathologically affected movements.

Table 3.2.2: Inertial indicators of the movement mixing synergies (FMA-UE item A3).

Kinematics	Unaffected	Affected
Shoulder abduction	0°	>0°
Elbow flexion	0°	>0°
Shoulder flexion	≈90°	<90°

Movements out of synergies: shoulder abduction (FMA-UE item A3)

The seated subject is instructed to abduct the shoulder from 0° to 90° while the elbow is kept completely extended. The joint angles of interest are shoulder abduction, elbow flexion, and forearm pronation. Furthermore, the mean values of the SRE at the biceps, triceps and deltoideus muscles, and the cross-correlations between these muscles are determined in order to detect differences between pathologically unaffected and simulated pathologically affected movements.

Table 3.2.3: Inertial indicators of the movement combining synergies (FMA-UE item A4).

Kinematics	Unaffected	Affected
Shoulder abduction	≈ 90°	<90°
Elbow flexion	0°	>0°
Forearm supination	0°	>0°

Repeated wrist dorsi flexion and volar flexion (FMA-UE item B)

The seated subject is instructed to perform repeated smooth alternating movements with the wrist from maximum dorsiflexion (wrist extension) to maximum palmar flexion (wrist flexion) while the elbow is completely extended and the shoulder at 30° flexed. Thus, wrist flexion and extension, elbow flexion, and shoulder flexion are the joint angles of interest. Furthermore, the mean values of the SRE at the biceps, triceps, deltoideus anterior, and the extensor and flexor carpi radialis are determined. Moreover, the cross-correlations between these muscles are determined in order to detect differences between pathologically unaffected and simulated pathologically affected movements.

Table 3.2.4: Inertial indicators repeated wrist dorsiflexion/volar flexion (FMA-UE item B).

Kinematics	Unaffected	Affected
Wrist dorsi/volar flexion	− 45°, 45°	>-45°, <45°
Elbow flexion	0°	>0°
Shoulder flexion	30°	≠30°

Spherical hand grip (FMA-UE item C)

The seated subject is instructed to flex the elbow 90° (with 0° shoulder flexion and abduction) and to keep this pose. The experimenter places a tennis ball in the hand palm of the subject, who is instructed to grasp

the ball. The subject is instructed to maintain the grasp as the experimenter attempts to pull the ball out with a slight tug so that the subject's grip against resistance can be examined. Moreover, as a variation, some of the subjects are instructed to hold the wrist in flexion or extension while grasping the ball, so that the grasp can be examined when the wrist flexor or extensor muscles are shortened. Wrist flexion and extension and elbow flexion are the joint angles of interest. Furthermore, the mean values of the SRE at the biceps, triceps, deltoideus muscles, extensor and flexor carpi radialis, and the cross-correlations between these muscles are determined in order to detect differences between pathologically unaffected and simulated pathologically affected movements. Moreover, the mean values of the output of the force sensors during interaction with the object are determined for detecting differences as well.

Table 3.2.5: Inertial indicators spherical hand grip (FMA-UE item C).

Kinematics	**Unaffected**	**Affected**
Wrist flexion/extension	$-45°$,0°, 45°	No grip
Elbow flexion	90°	$\neq 90°$

Cylindrical grasp test (not part of FMA-UE)

The seated subject is instructed to grasp, lift vertically, place and then release a cylindrical object to a desired location. Since the object must be lifted vertically, shoulder abduction is expected to be minimum. The joint angles of interest are shoulder abduction and wrist flexion or extension. Furthermore, the mean values of the SRE at the biceps, triceps, deltoideus muscles, extensor and flexor carpi radialis, and the cross-correlations between these muscles are determined in order to detect differences between pathologically unaffected and simulated pathologically affected movements. Moreover, the mean values of the output of the force sensors during interaction with the object are determined for detecting differences as well.

Table 3.2.6: Inertial indicators cylindrical grasp test.

Kinematics	**Unaffected**	**Affected**
Shoulder abduction	0°	>0°
Wrist flexion/extension	0°	>0°

3.2.2 STATISTICAL TEST

In order to investigate whether the measurement system can detect differences between the pathologically unaffected and pathologically affected inertial indicators, the Wilcoxon signed rank test for nonparametric paired data will be performed in SPSS (Statistical Package for Social Science) version 25. This statistical test is suitable because of the relatively low sample size (8 subjects), which cannot be modelled by means of a normal distribution, and because of the dependency between the paired measurements. The Wilcoxon signed rank test investigates the hypothesis whether the median difference between pathologically unaffected and affected movements is zero (McCrum-Gardner, 2008). The hypothesis is tested based on a 5% significance level ($\alpha = 0.05$), which means that there is some risk of at most 5% for rejecting the null hypothesis while it is true (error of the first kind). The null hypothesis states that there is no significant difference between the median pairs regarding the pathologically unaffected and affected movements, while the alternative hypothesis states that there is a significant difference.

4. RESULTS

The results regarding the sensor-to-segment calibration procedure are firstly described and an example concerning the transformation of joint angles expressed in sensor frame to joint angles expressed in segment frame is provided. Furthermore, the optimal set of calibration movements is investigated. Secondly, joint angles, mean muscle activities and cross-correlations regarding movements within synergies, mixing synergies, and out of synergies are presented and analysed. Moreover, due to time limitations, the results regarding the remaining movements could not be analysed due to time limitations. However, the analysis of these three movements provides sufficient understanding of pathological synergies.

4.1 SENSOR-TO-SEGMENT CALIBRATION PROCEDURE

The sensor-to-segment calibration of each sensor is based on a set of static poses and dynamic movements. However, each sensor requires merely two optimal sensor-to-segment calibration movements. Figure 4.1.1 demonstrates the selection procedure of these two optimal movements for the sensor attached to the lower arm. In this case, the subject repeatedly pronated and supinated the lower arm (calibration movement nine). Then, the subject repeatedly flexed the elbow (calibration movement ten). The description of each calibration movement can be read from Table 3.1.2. The remaining movements regarding the lower arm are described in Figure 4.1.1. The variance accounted for (VAF) is determined based on $Eq.3.16$ and the two movements with relatively the highest VAF and mutual angle closest to 90° are selected. The two optimal sensor-to-segment calibration movements in this case are repeated pronation and supination of the forearm and static pose with the elbow flexed and the forearm pronated. The corresponding mutual angle is 93° (see Figure 4.1.1).

Moreover, these calibration movements are defined as the z-axis respectively the y-axis of the lower arm. The x-axis is determined by means of the cross-product, and in order to construct the rotation matrix that converts the sensor orientations at the lower arm to segment orientations (R^{segsen}), the y-axis is recalculated since its VAF (0.1688) is lower than the VAF of the z-axis (0.1843). The recalculation of the y-axis is determined by means of the cross-product of x-axis and the z-axis. The conversion of orientations expressed in sensor frame to orientations expressed in segment frame regarding the lower arm can be seen in Figure 4.1.2. The subject was instructed to flex the shoulder approximately 90° with the elbow completely extended. In sensor frame, this movement is performed around the z-axis, while in segment frame the y-axis is defined as the flexion axis. The y-axis of the lower arm is in this case around 80° (see Figure 4.1.2). The orientations expressed in segment frame and the calculated joint angles are not errorless. The quality of the sensor-to-segment conversion regarding each segment is based on the two selected axes with highest VAF and mutual angle closest to 90°. These two selected axes can differ for each segment, which will introduce an error in the calculated joint angles. Furthermore, since the sensor drift is a non-zero bias, multiplication by the sensor-to-segment rotation matrix will cause additional drift that can vary for each segment. Lastly, drift compensation is linearly implemented and includes not only the bias-factor, but also the difference between the initial and final orientation during the movement, which can be different for each segment.

	Description
Calib #9	Repeated forearm pronation/supination
Calib #10	Repeated elbow flexion (forearm in midposition)
Calib #11	Repeated elbow flexion (forearm pronated)
Calib #12	Static pose forearm aligned with gravity
Calib #13	Static pose elbow flexed with forearm in midposition
Calib #14	Static pose elbow flexed with forearm pronated

	VAF_lower arm x_acc	VAF_lower arm y_acc	VAF_lower arm z_acc	VAF_lower arm x_gyr	VAF_lower arm y_gyr	VAF_lower arm z_gyr
Calib #9	NA	NA	NA	NA	NA	0.1843
Calib #10	NA	NA	NA	NA	-0.0563	NA
Calib #11	NA	NA	NA	0.0732	NA	NA
Calib #12	NA	NA	0.1582	NA	NA	NA
Calib #13	0.1826	NA	NA	NA	NA	NA
Calib #14	NA	0.1688	NA	NA	NA	NA

	Lower arm x_acc	Lower arm y_acc	Lower arm z_acc	Lower arm x_gyr	Lower arm y_gyr	Lower arm z_gyr	VAF
Lower arm x_acc	0	X	X	X	X	X	0.1826
Lower arm y_acc	52.2698	0	X	X	X	X	0.1688
Lower arm z_acc	67.9423	75.9001	0	X	X	X	0.1582
Lower arm x_gyr	66.1139	117.2683	85.2442	0	X	X	0.0732
Lower arm y_gyr	74.3518	22.0838	82.9386	139.3023	0	X	-0.0563
Lower arm z_gyr	82.1078	93.4534	18.0937	80.7641	97.6733	0	0.1843

Figure 4.1.1: Description of the calibration movements regarding the lower arm. Based on the variance accounted for (VAF), the best six movements are pre-selected (middle), so that the optimal two movements can be determined as a final selection based on their mutual angle (bottom). In this case, the sensor-to-segment calibration procedure regarding the lower arm is optimal when the subject repeatedly pronated and supinated the lower arm (calibration #9) and when the subject kept the elbow flexed for several seconds with the forearm pronated (calibration #14).

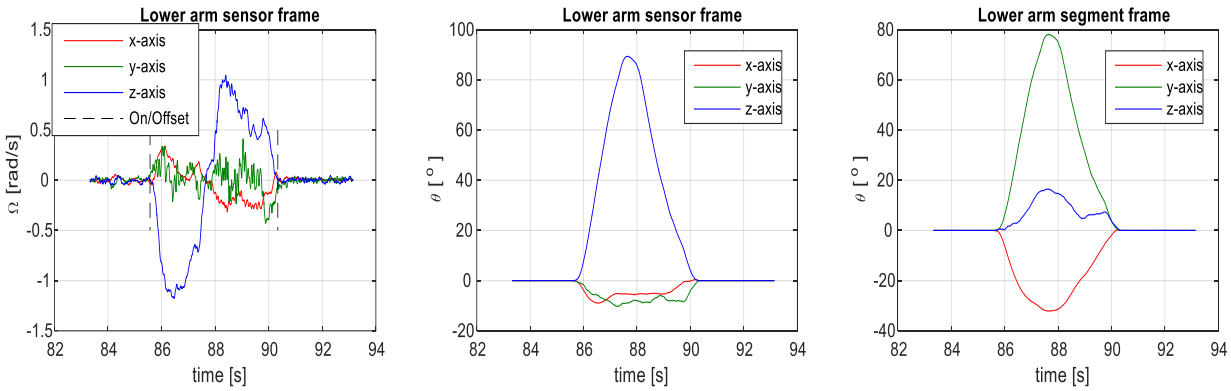

Figure 4.1.2: Angular velocity of the lower arm expressed in sensor frame during shoulder flexion (left). Orientations expressed in sensor frame by means of strapdown integration (middle). Finally, orientations expressed in segment frame of the lower arm by means of the sensor-to-segment rotation matrix (right).

In order to calibrate all the sensors attached to the segments, twenty-six sensor-to-segment calibration movements are performed by each of the eight subjects. The sensor-to segment calibration procedure is therefore time-consuming and must be optimized by minimizing the number of movements based on their VAF value and mutual angle.

Moreover, the top three pairs of sensor-to-segment calibration movements for each sensor performed by each subject are listed in Appendix A. The top two calibration movements performed by most subjects are listed in Table 4.1.1. Based on Table 4.1.1, the top two combinations for the calibrating the middle finger are calibration movements six and nine, and calibration movements twelve and thirteen. All four combinations regarding the index and middle finger are performed optimally by three subjects. Regarding the thumb, eight subjects performed the combination consisting of calibration movements seven and twelve optimal, while seven subjects performed the combination consisting of calibration movements three and four optimal. The result concerning the rest of the subjects can be read in Table 4.1.1. The total amount of calibration movements is then reduced from twenty-six movements to fifteen movements.

Finally, the last selection of sensor-to-segment calibration movement combinations is chosen such that the total amount of calibration movements is minimal (see highlighted combinations in Table 4.1.1). The selection of fifteen movements is then further reduced to a total of eight calibration movements. The first calibration movement is a static pose of the ulnar side of the hand on a box or table (calibration movement six). The purpose of this movement is to calibrate the index finger, the middle finger, and the hand partly. The second calibration movement is a repeated pronation (or supination) of the forearm in order to finalize the calibration of the index and middle finger (calibration movement nine). The third calibration movement is a static pose on the left side of the thumb on a box or table (calibration movement seven). This calibration movement is suitable for the thumb. The fourth calibration movement is a static pose of the forearm aligned in the direction of gravity with the elbow fully extended (calibration movement twelve). This static movement can be used to calibrate the hand, the lower arm, the upper arm, and the movement can be used to finalize the calibration procedure of the thumb. The fifth calibration movement is a repeated elbow flexion with the forearm pronated (calibration movement eleven). This calibration movement is suitable for finalizing the calibration process of the hand and the lower arm. The sixth calibration movement is a repeated shoulder flexion with the elbow 90° flexed (calibration movement nineteen). This calibration movement is used to complete the calibration procedure of the upper arm. The final calibration movements are a repeated trunk flexion and a repeated ipsilateral and contralateral trunk rotation (calibration movement twenty-four respectively twenty-five). These calibration movements are used to calibrate the shoulder and the sternum. The total amount of calibration movements is then further reduced to eight movements instead of fifteen.

The drawback however concerns the number of subjects that performed the selected calibration movements optimally. For example, based on the final selection (highlighted in Table 4.1.1), 37.5% of the total amount of subjects used the combination consisting of calibration movements six and nine to calibrate the index finger optimally, while the rest of the subjects used different combinations. In case the combination consisting of calibration movements nine and thirteen is included in the selection for calibrating the index finger, the number of subjects increases to 75% (six out of eight subjects). Thus, reducing the amount of calibration movements reduces the time consumption, but can influence the optimization since each subject performs the calibration movements differently. An exception concerns the calibration movements of the thumb. Notice that all eight subjects performed the combination consisting of calibration movements seven and twelve optimally. In this case, the combination consisting of calibration movements three and four might be excluded. Besides the individual execution of the calibration

movements by each subject, difference in sensor placement on the segments plays an important role. Since the segments of each subject have their own unique shape, the placement of the sensors on the segments of each subject is different. This makes a general statement concerning the optimal set of calibration movements challenging. Overall, by including all combinations of calibration movements presented in Table 4.1.1, the possibility of selecting optimal calibration movements per subject is not excluded. Moreover, the influence of the sample size on the selection of calibration movements should be further investigated.

Table 4.1.1: Optimal calibration movements performed by the eight subjects. The selection is chosen based on the number of subjects that performed the calibration movements optimal. For example, all eight subjects (100%) performed the combination consisting of calibration number seven and calibration number twelve optimal during the thumb calibration procedure. In order to choose a minimum set of calibration movements, a final selection is highlighted, resulting in the most optimal and least time-consuming set of calibration movements.

OPTIMAL CALIBRATION MOVEMENTS				
Segment	***Calibration #***	***Number of subjects***	***Total number of subjects***	***Median angle* (°)**
Index	6;9	3 out of 8 (37.5%)	6 out of 8 (75%)	92
	9;13	3 out of 8 (37.5%)		89
Middle	6;9	3 out of 8 (37.5%)	6 out of 8 (75%)	89
	12;13	3 out of 8 (37.5%)		88
Thumb	7;12	8 out of 8 (100%)	8 out of 8 (100%)	86
	3;4	7 out of 8 (87.5%)		88
Hand	10;12	5 out of 8 (62.5%)	7 out of 8 (87.5%)	90
	6;12	4 out of 8 (50%)		90
Lower	9;14	6 out of 8 (75%)	7 out of 8 (87.5%)	91
	11;12	4 out of 8 (50%)		88
Upper	18;19	4 out of 8 (50%)	8 out of 8 (100%)	90
	15*;19	4 out of 8 (50%)		88
Shoulder	21;24	3 out of 8 (37.5%)	7 out of 8 (87.5%)	89
	24;25	5 out of 8 (62.5%)		88
Sternum	21;24	6 out of 8 (75%)	8 out of 8 (100%)	90
	24;25	5 out of 8 (62.5%)		90

** Calibration movement twelve and fifteen are identical regarding the calibration of the upper arm.*

4.2 VOLITIONAL MOVEMENTS WITHIN SYNERGIES: FLEXOR SYNERGY

The items to be scored when the subjects performed the flexor synergy are shoulder abduction, elbow flexion, and forearm pronation/supination. Based on the FMA-UE the subjects should abduct the shoulder at least 90°. The joint angles of the eight subjects during the performance of the flexor synergy are presented. Detailed figures of all individual subjects can be found in Appendix B. the joint angles as function of the time regarding the first subject during the first trial is taken as an example and depicted in Figure 4.2.1. Furthermore, the averaged muscle activity and the synergistic profiles are presented and discussed.

4.2.1 INERTIAL INDICATORS FLEXOR SYNERGY

According to the results, most subjects flexed the elbow around 90° or higher, and most subjects except the third subject (see Appendix B), abducted the shoulder greater than 90°. Most likely, this subject unintentionally did not abduct the shoulder completely. During the second and third trial, however, the

abduction is greater than 90°. Moreover, the 3rd and 5th subject performed forearm pronation instead of supination (see Appendix B). Since the Fugl-Meyer assessment focusses especially on the minimum abduction angle and since the difference between pathologically unaffected and affected movements is of interest, the maximum forearm pronation or supination angle is considered. Lastly, consider the pathologically unaffected elbow flexion performed by the sixth subject (see Figure 4.2.2). the maximum angle of the elbow flexion is greater than 180°. This introduced a singularity problem in the software, which could be solved by adding 360° to the angle. Overall, the subjects simulated the pathologically synergies such that the affected movements have less shoulder abduction and less elbow flexion.

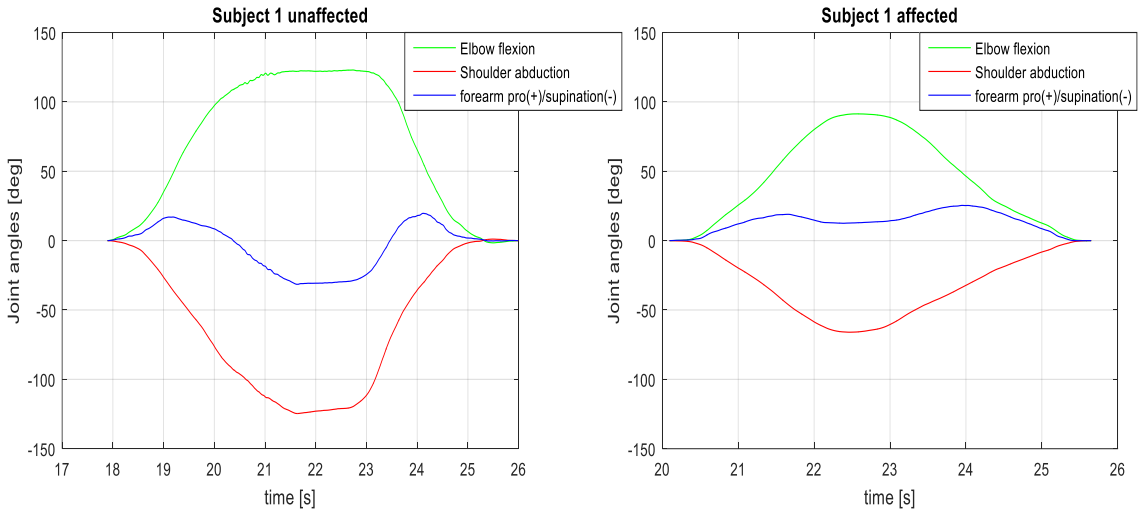

Figure 4.2.1: Joint angles of the first subject during the first trial regarding the flexor synergy.

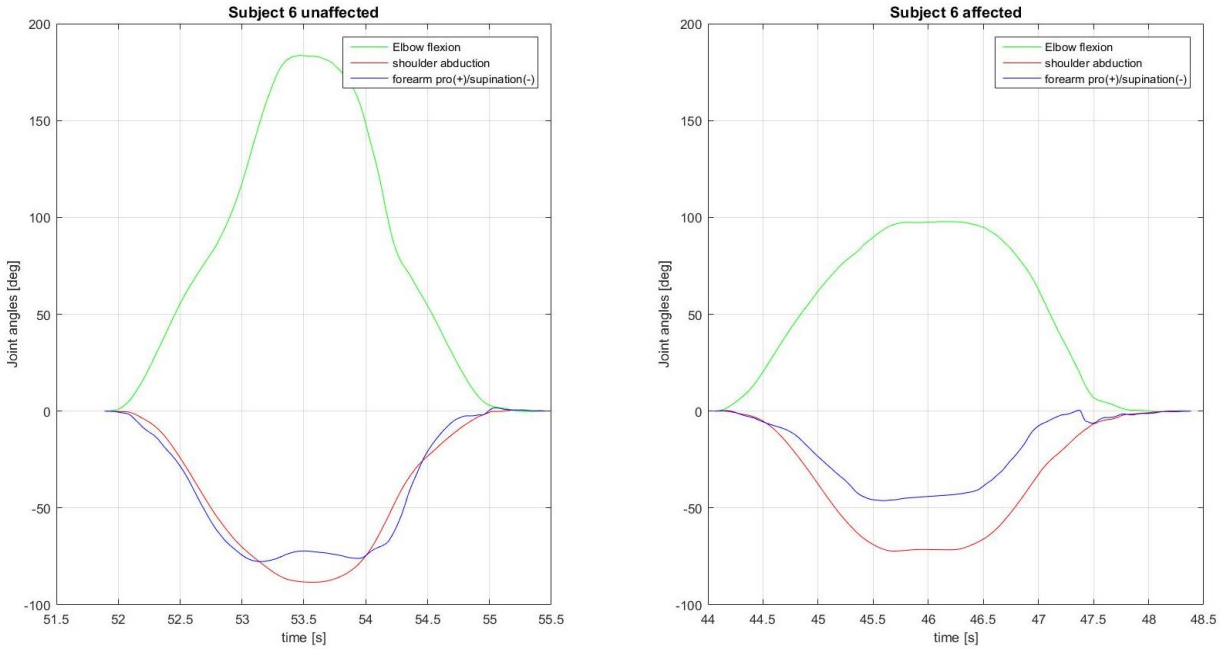

Figure 4.2.2: Joint angles of the sixth subject during the third trial regarding the flexor synergy. The system calculates an elbow flexion greater than 180°.

Moreover, the subjects were instructed to perform the movement three times, so that the peak values of the joint angles can be recorded and averaged over the three trials. The maximum of the absolute values regarding shoulder abduction, elbow flexion and forearm pronation or supination along with corresponding standard deviation are presented in Figure 4.2.3. The results regarding the Wilcoxon signed rank test are presented in Table 4.2.1. According to the results, the p-value regarding shoulder abduction and elbow flexion is 1.2%, which is smaller than the 5% significance level. Therefore, the null hypothesis is rejected. Thus, there is a significant difference between the median pairs regarding the pathologically unaffected and affected shoulder abduction and elbow flexion.

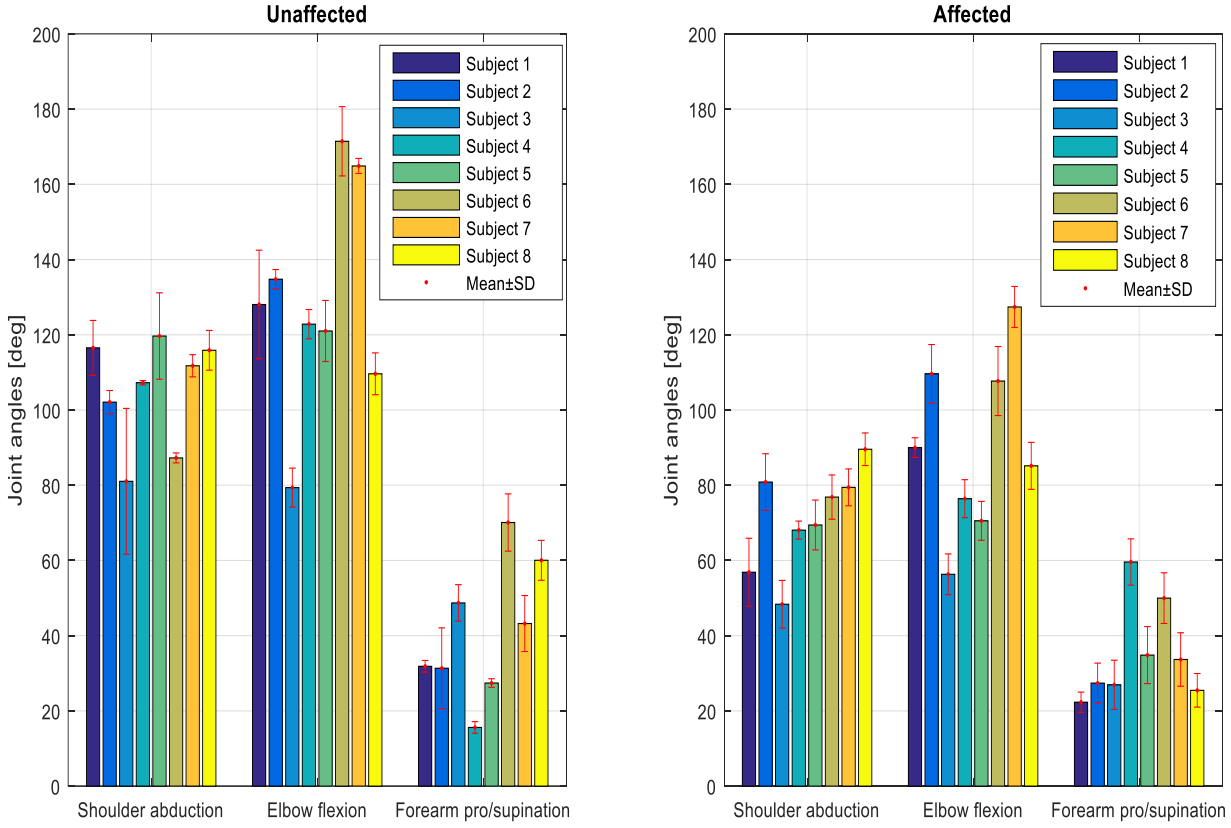

Figure 4.2.3: Joint angles averaged over the three trials presented with corresponding standard deviation. Subjects performed movements first pathologically unaffected and then with mimicked pathological synergies.

Table 4.2.1: Results of the Wilcoxon signed rank test. The joint angles of interest are shoulder abduction (SA), elbow flexion (EF), and forearm pronation or supination (FPS). The data is presented as the median and corresponding interquartile range (IQR). The IQR can be used to divide the corresponding data set into quartiles or to construct a box plot. The last column listed the p-values of the test based on a 5% significance level. Values except the p-values are expressed in degrees.

Kinematics	**Unaffected**		**Affected**		**Difference**		
	Median (deg)	**[IQR] (deg)**	**Median (deg)**	**[IQR] (deg)**	**Median (deg)**	**[IQR] (deg)**	**P**
SA	110	[91,116]	73	[60,81]	33	[22,48]	0.012
EF	125	[112,157]	88	[72,109]	38	[25,50]	0.012
FPS	38	[28,57]	31	[26,46]	10	[-5,21]	0.263

4.2.2 MEAN SRE AND MUSCLE ACTIVITY

The mean value of each envelope is determined and is used as an indicator of the level of activity of each muscle during the movement. However, since one of the interesting indicators based on inertial data concern supination of the forearm, activity of the FCR and ECR can be excluded for further analysis. FCR and ECR are muscles that contribute mostly to wrist flexion and wrist extension respectively. Moreover, the second and third trial have similar results (see Appendix B). The three trials result in three mean values of the SRE of each muscle. These three mean values of each muscle are averaged and presented with corresponding standard deviation (see Figure 4.2.4 unaffected). Furthermore, the subject also performed the flexor synergy with simulated pathological synergies. Similarly, the three mean values of the linear envelope of each muscle are averaged and presented with corresponding standard deviation (see Figure 4.2.4 affected). Overall, the pathologically unaffected movements required more muscle activity of this subject compared to the pathologically affected movements (see Figure 4.2.4, and Table 4.2.2).

The muscle activity during pathologically unaffected and affected movement for all subjects is depicted in Figure 4.2.5. The Wilcoxon signed rank test is used to investigate whether the median difference in muscle activity between the pathologically unaffected and pathologically affected flexor synergy is significant. The results of the statistical test can be seen in Table 4.2.3. The P-values regarding the muscles of interest are smaller than the 5% significant level. The activity of the biceps, triceps lateral head, triceps long head, the deltoideus medial and the deltoideus anterior is significantly higher during the pathologically unaffected flexor synergy compared to the pathologically affected flexor synergy.

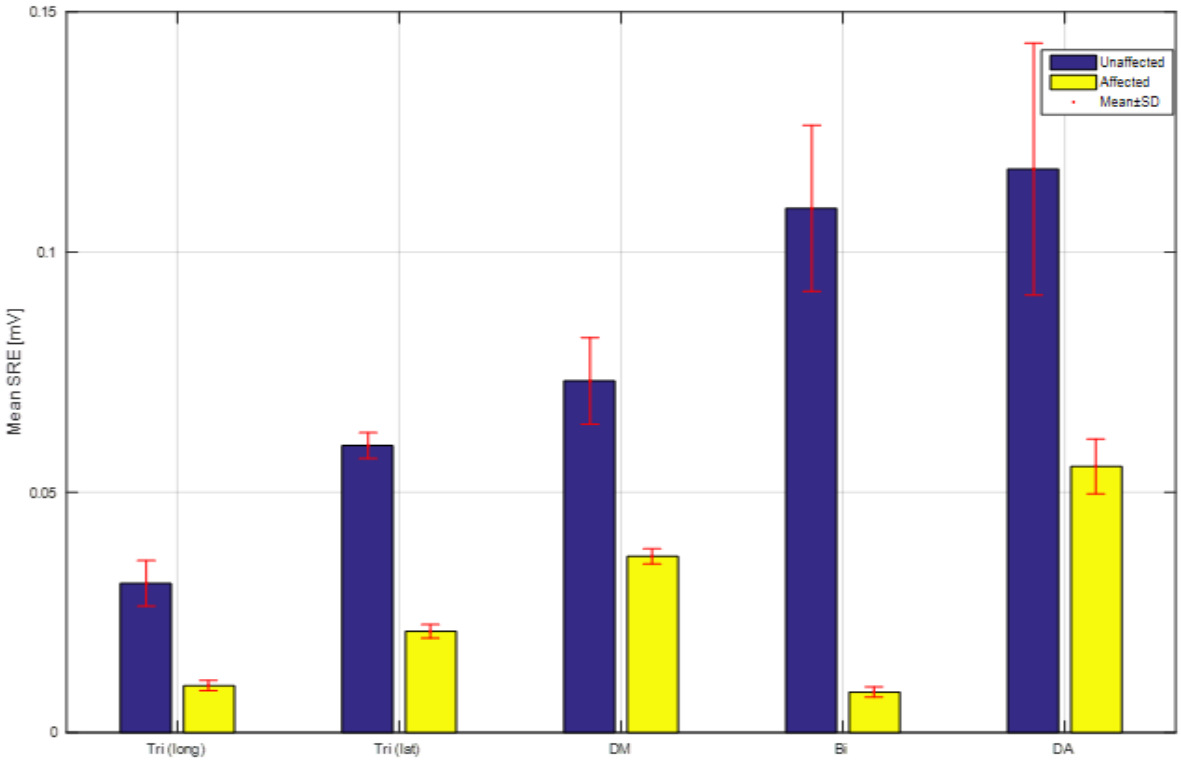

Figure 4.2.4: Averaged mean values and corresponding standard deviations of the envelopes of the triceps long head, the triceps lateral head, the deltoideus medial, the biceps, and the deltoideus anterior respectively. The averaged mean values of the pathologically unaffected movements are presented as blue bars, while the averaged mean values of the affected movements are presented as yellow bars.

Table 4.2.2: Mean values of the SREs during the first, the second and the third trial of pathologically unaffected and affected movements. These mean values are then averaged and presented with corresponding standard deviation for pathologically unaffected (blue) and affected (yellow) movements. Muscles of interest are biceps, lateral head triceps, long head triceps, deltoideus medial and deltoideus anterior respectively.

	MEAN SRE (mV)							
	Pathologically unaffected				Pathologically affected			
Muscles	**Trial 1**	**Trial 2**	**Trial 3**	**Mean(SD)**	**Trial 1**	**Trail2**	**Trial 3**	**Mean(SD)**
Bi	0.09	0.11	0.13	**0.11(0.02)**	0.01	0.01	0.01	**0.01(0.01)**
Tri (lat)	0.06	0.06	0.06	**0.06(0.00)**	0.02	0.02	0.02	**0.02 (0.00)**
Tri (long)	0.03	0.03	0.04	**0.03(0.00)**	0.01	0.01	0.01	**0.01(0.00)**
DM	0.08	0.08	0.06	**0.07(0.01)**	0.04	0.04	0.04	**0.04(0.00)**
DA	0.13	0.13	0.09	**0.12(0.03)**	0.06	0.05	0.05	**0.06(0.01)**

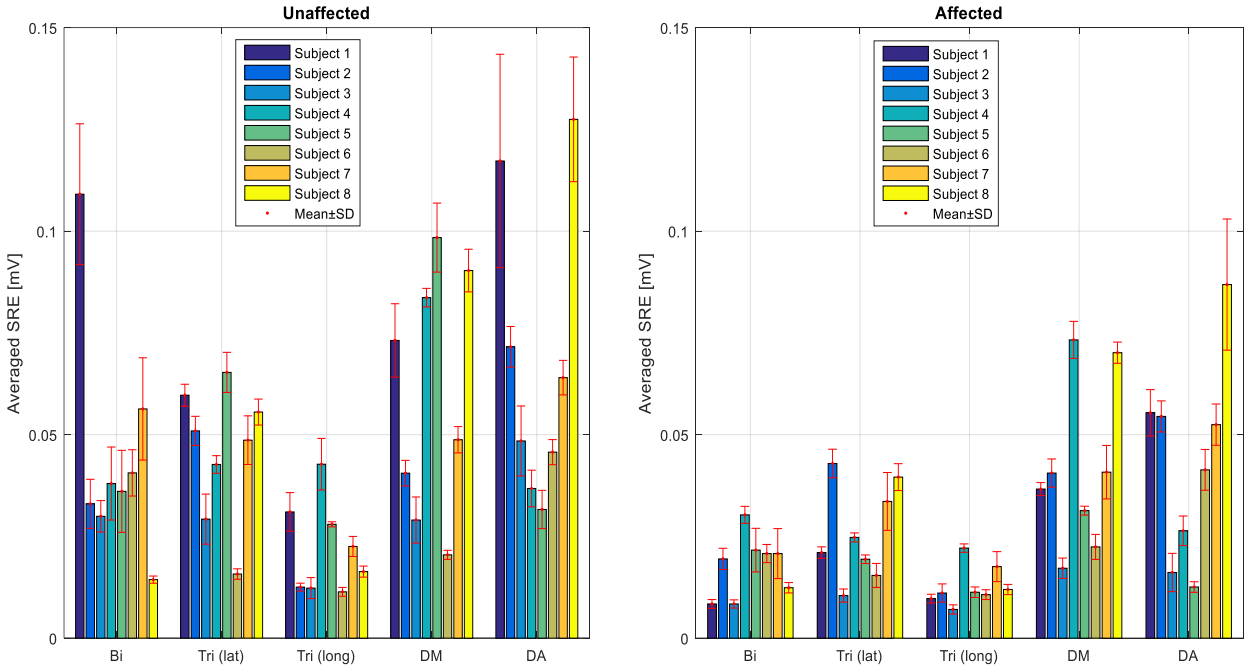

Figure 4.2.5: Muscle activity averaged over the three pathologically unaffected trials (left) and affected trials (right). The averaged muscle activity of the biceps, lateral head triceps, long head triceps, deltoideus medial and deltoideus anterior respectively for all subjects is of interest.

Table 4.2.3: Results of the Wilcoxon signed rank test. The data is presented as the median and corresponding interquartile range (IQR). The IQR can be used to divide the corresponding data set into quartiles or to construct a box plot. Muscles of interest are biceps, lateral head triceps, long head triceps, deltoideus medial and deltoideus anterior respectively. The last column listed the p-values of the test based on a 5% significance level. Values except the p-values are expressed in millivolts.

Muscle activity	**Unaffected**		**Affected**		**Difference**		
	Median (mV)	**[IQR] (mV)**	**Median (mV)**	**[IQR] (mV)**	**Median (mV)**	**[IQR] (mV)**	**P**
Bi	0.03	[0.03,0.05]	0.02	[0.00,0.02]	0.01	[0.00,0.03]	0.012
Tri (lat)	0.04	[0.03,0.05]	0.02	[0.01,0.03]	0.01	[0.00,0.03]	0.012
Tri (long)	0.01	[0.01,0.03]	0.01	[0.01,0.01]	0.00	[0.00,0.01]	0.012
DM	0.06	[0.03,0.08]	0.03	[0.02,0.06]	0.01	[0.00,0.03]	0.036
DA	0.05	[0.03,0.10]	0.04	[0.01,0.05]	0.01	[0.01,0.03]	0.012

4.2.3 SYNERGISTIC AND COACTIVATION SRE PATTERNS

Synergistic and coactivation patterns of the movements can be developed using the cross-correlation function (CCF) between the linear envelopes of the EMGs (see Figure 4.2.6). The maximum cross-correlations and corresponding time lags during the three trials are averaged and presented in Table 4.2.4 through Table 4.2.7. The patterns of the rest of the subjects are presented in Appendix D. Although the synergistic pattern of each subject is unique, the pathologically affected flexor synergy consists of a strong linkage between the elbow flexor muscles and the forearm supinator muscles (Brunnstrom, 1970). Therefore, elbow flexion and forearm supination tend to occur together. Since the activity of the forearm supinator muscle is not recorded and since the flexor synergy also consists of shoulder abduction, the search for a linkage between the shoulder abductors and elbow flexors is of interest (see Table 4.2.8). Furthermore, according to the Wilcoxon signed rank test displayed in Table 4.2.9, a significant difference in cross-correlations between the pathologically unaffected and affected flexor synergies performed by the subjects could not be detected, since the p-value (32.7%) is greater than the 5% significant level. Thus, overall, the subjects performed the pathologically unaffected flexor synergy and the simulated affected flexor synergy such that there is no significant difference in coactivation between the biceps brachii and the deltoideus medial.

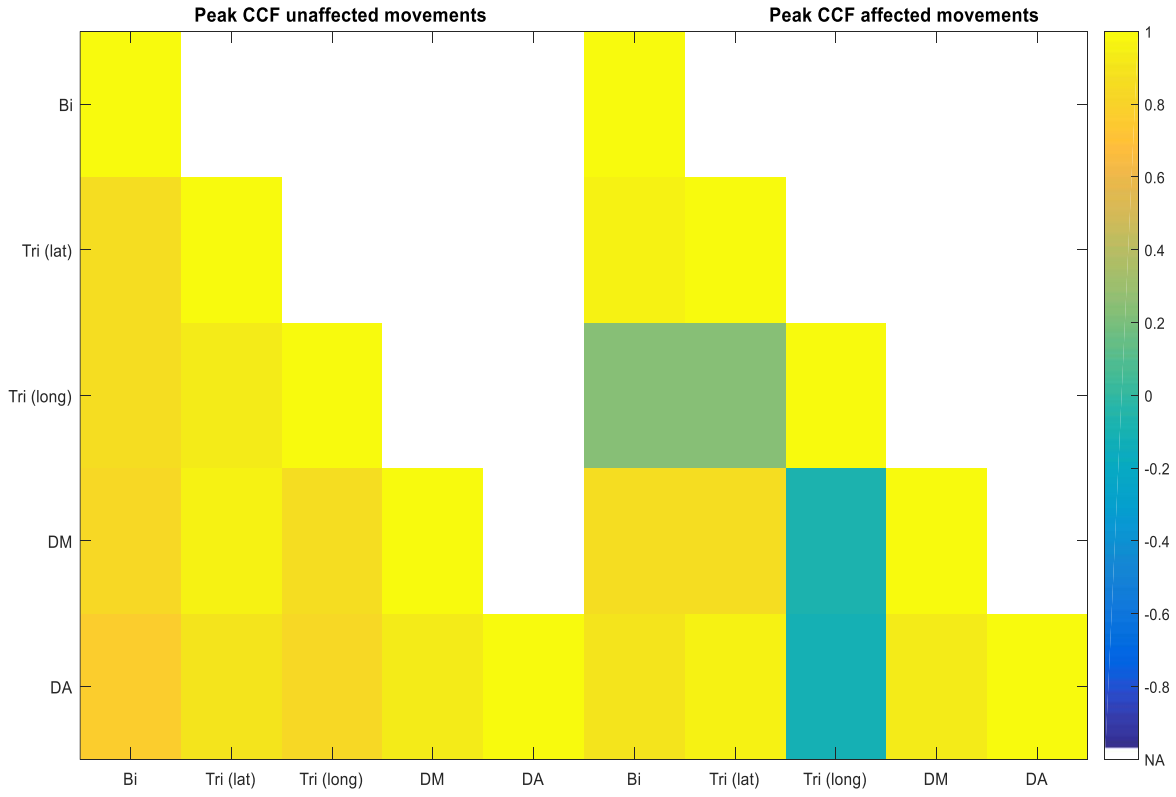

Figure 4.2.6: The maximum peaks of the cross-correlation functions between the muscle-pairs for pathologically unaffected (left) and affected (right) movement during the first trial performed by the first subject.

Table 4.2.4: The averaged peak values and standard deviations of the cross-correlation functions between the muscle-pairs regarding pathologically unaffected movements performed by the first subject. Muscles of interest are biceps, lateral head triceps, long head triceps, deltoideus medial and deltoideus anterior respectively. These values are the maximum Pearson correlations coefficients.

MEAN(SD) PEAK CCF UNAFFECTED MOVEMENTS					
Muscles	**Bi**	***Tri (lat)***	***Tri (long)***	**DM**	**DA**
Bi	1.00(0.00)				
Tri (lat)	0.85(0.00)	1.00(0.00)			
Tri (long)	0.85(0.01)	0.92(0.02)	1.00(0.00)		
DM	0.81(0.03)	0.95(0.02)	0.87(0.04)	1.00(0.00)	
DA	0.77(0.06)	0.90(0.04)	0.83(0.04)	0.93(0.02)	1.00(0.00)

Table 4.2.5: The corresponding time lags (expressed in seconds) between the muscle-pairs for pathologically unaffected movements performed by the first subject. Muscles of interest are biceps, lateral head triceps, long head triceps, deltoideus medial and deltoideus anterior respectively.

MEAN(SD) TIME LAG CCF UNAFFECTED MOVEMENTS [s]					
Muscles	**Bi**	***Tri (lat)***	***Tri (long)***	**DM**	**DA**
Bi	0.00(0.00)				
Tri (lat)	0.79(0.13)	0.00(0.00)			
Tri (long)	0.45(0.21)	-0.01(0.02)	0.00(0.00)		
DM	0.84(0.14)	0.01(0.01)	0.18(0.09)	0.00(0.00)	
DA	1.11(0.13)	0.00(0.00)	0.24(0.12)	-0.01(0.01)	0.00(0.00)

Table 4.2.6: The averaged peak values and standard deviations of the cross-correlation functions between the muscle-pairs regarding pathologically affected movements performed by the first subject. Muscles of interest are biceps, lateral head triceps, long head triceps, deltoideus medial and deltoideus anterior respectively. These values are the maximum Pearson correlations coefficients.

MEAN(SD) PEAK CCF AFFECTED MOVEMENTS					
Muscles	**Bi**	***Tri (lat)***	***Tri (long)***	**DM**	**DA**
Bi	1.00(0.00)				
Tri (lat)	0.94(0.01)	1.00(0.00)			
Tri (long)	0.24(0.68)	0.23(0.70)	1.00(0.00)		
DM	0.86(0.01)	0.86(0.04)	-0.09(0.61)	1.00(0.00)	
DA	0.90(0.02)	0.94(0.01)	-0.11(0.64)	0.91(0.02)	1.00(0.00)

Table 4.2.7: The corresponding time lags (expressed in seconds) between the muscle-pairs for pathologically affected movements performed by the first subject. Muscles of interest are biceps, lateral head triceps, long head triceps, deltoideus medial and deltoideus anterior respectively.

MEAN(SD) TIME LAG CCF AFFECTED MOVEMENTS [s]					
Muscles	**Bi**	***Tri (lat)***	***Tri (long)***	**DM**	**DA**
Bi	0.00(0.00)				
Tri (lat)	0.00(0.00)	0.00(0.00)			
Tri (long)	-0.38(1.03)	-0.51(0.90)	0.00(0.00)		
DM	0.07(0.09)	0.00(0.00)	-0.27(1.75)	0.00(0.00)	
DA	0.01(0.01)	0.00(0.00)	1.01(0.93)	0.00(0.00)	0.00(0.00)

Table 4.2.8: Maximum averaged Pearson correlation coefficients and corresponding averaged time lags regarding the pathologically unaffected and affected flexor synergy performed by all the eight subjects. The muscle-pair of interest is formed by the biceps brachii and the deltoideus medial.

	BICEPS — DELTOIDEUS MEDIAL			
	Maximum averaged Pearson correlation (SD)		Corresponding Time lag (s)	
	Unaffected	Affected	Unaffected	Affected
Subject 1	0.81(0.03)	0.86(0.01)	0.83(0.14)	0.07(0.09)
Subject 2	0.66(0.03)	0.84(0.04)	0.30(0.22)	0.03(0.03)
Subject 3	0.88(0.06)	0.81(0.02)	0.07(0.04)	0.01(0.01)
Subject 4	0.70(0.04)	0.71(0.09)	1.00(0.19)	0.04(0.08)
Subject 5	0.82(0.11)	0.86(0.03)	0.37(0.36)	0.02(0.05)
Subject 6	0.65(0.05)	0.83(0.01)	0.35(0.09)	0.08(0.11)
Subject 7	0.88(0.04)	0.89(0.06)	-0.02(0.02)	0.00(0.00)
Subject 8	0.93(0.02)	0.85(0.09)	0.00(0.00)	0.08(0.07)

Table 4.2.9: Results of the Wilcoxon signed rank test. The data is presented as the median and corresponding interquartile range (IQR) regarding the cross-correlation coefficients and corresponding time lags. The IQR can be used to divide the corresponding data set into quartiles or to construct a box plot. The muscle pair of interest is the biceps and the deltoideus medial. The last column listed the p-values of the test based on a 5% significance level. The time lags are expressed in seconds.

	Unaffected		Affected		Difference		
	Median	[IQR]	Median	[IQR]	Median	[IQR]	P
$R_{\mathrm{Bi-DM}}$	0.81	[0.67,0.88]	0.85	[0.82,0.86]	-0.03	[-0.14,0.04]	0.327
$\tau_{\mathrm{Bi-DM}}$ (s)	0.32	[0.02,0.72]	0.04	[0.01,0.08]	0.26	[0.00,0.36]	0.05

4.3 VOLITIONAL MOVEMENTS MIXING SYNERGIES: SHOULDER FLEXION

The items to be scored when the subjects performed the movement by combining the synergies are shoulder abduction, shoulder flexion, and elbow flexion. Based on the FMA-UE the subjects should flex the shoulder at least 90° while the elbow is completely extended. The joint angles of the eight subjects during the performance of the flexor synergy are depicted in Appendix E and are mostly similar to Figure 4.3.1. Furthermore, the averaged muscle activity and the synergistic profiles are presented and discussed.

4.3.1 INERTIAL INDICATORS MOVEMENT MIXING SYNERGIES

The eight subjects were instructed to perform the movement three times, so that the peak values of the joint angles can be recorded and averaged over the three trials. The maximum of the absolute values regarding shoulder abduction, elbow flexion and shoulder flexion along with corresponding standard deviation are presented in Figure 4.3.2. The results concerning the Wilcoxon signed rank test are shown in Table 4.3.1. According to the results, there is a significant difference between the median pairs regarding the pathologically unaffected and affected shoulder abduction, elbow flexion and shoulder flexion.

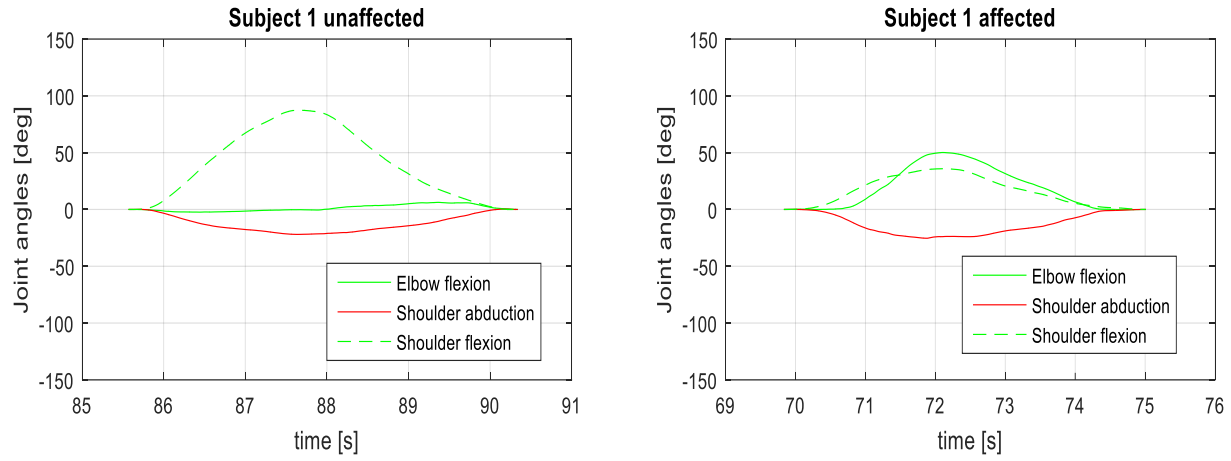

Figure 4.3.1: Joint angles of the first subject during the first trial regarding the 90° shoulder flexion with the elbow at 0° (left) and then with the elbow flexed (right).

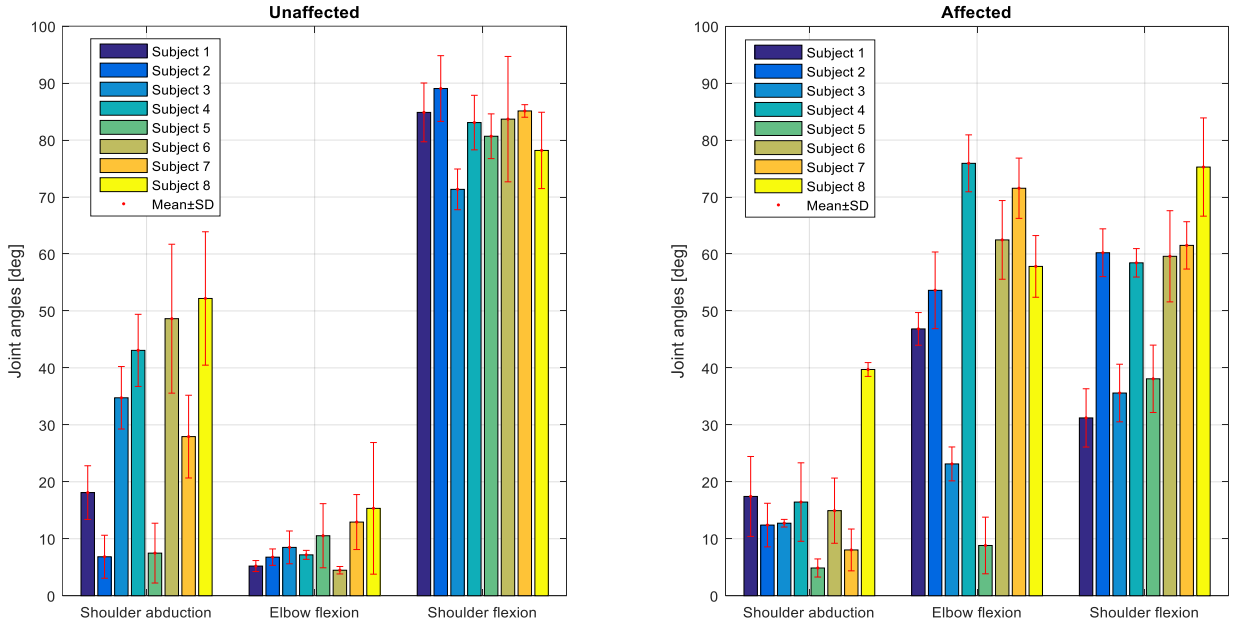

Figure 4.3.2: Joint angles averaged over the three trials presented with corresponding standard deviation. Subjects performed shoulder flexions first pathologically unaffected and then with mimicked pathological synergies.

Table 4.3.1: Results of the Wilcoxon signed rank test. The joint angles of interest are shoulder abduction (SA), elbow flexion (EF), and shoulder flexion (Mansfield & Neumann). The data is presented as the median and corresponding interquartile range (IQR). The IQR can be used to divide the corresponding data set into quartiles or to construct a box plot. The last column listed the p-values of the test based on a 5% significance level. Values except the p-values are expressed in degrees.

kinematics	**Unaffected**		**Affected**		**Difference**		
	Median (deg)	**[IQR] (deg)**	**Median (deg)**	**[IQR] (deg)**	**Median (deg)**	**[IQR] (deg)**	**P**
SA	31	[10,47]	14	[9,17]	16	[1,25]	0.036
EF	8	[6,12]	56	[29,69]	-45	[-58,-21]	0.017
SF	83	[79,85]	59	[36,61]	27	[23,41]	0.012

4.3.2 MEAN SRE AND MUSCLE ACTIVITY

The mean value of each envelope is determined and is used as an indicator of the level of activity of each muscle during the movement. Activity of the FCR and ECR can be excluded for further analysis since wrist flexion and wrist extension are not assessed by the FMA-UE during shoulder flexion. The averaged muscle activities with corresponding standard deviations during the three trials performed by each subject are presented in Figure 4.3.3.

The Wilcoxon signed rank test is used to investigate whether the median difference in muscle activity between the pathologically unaffected and pathologically affected shoulder flexion is zero. The results of the statistical test can be seen in Table 4.3.2. According to the results, muscle activity regarding the triceps lateral head and long head, deltoideus medial, and deltoideus anterior decreased significantly when the subjects performed shoulder flexion with pathologically affected synergies ($p = 0.012$). Biceps brachii activity, however, decreased insignificantly when the subjects performed shoulder flexion with pathologically affected synergies ($p = 0.208$).

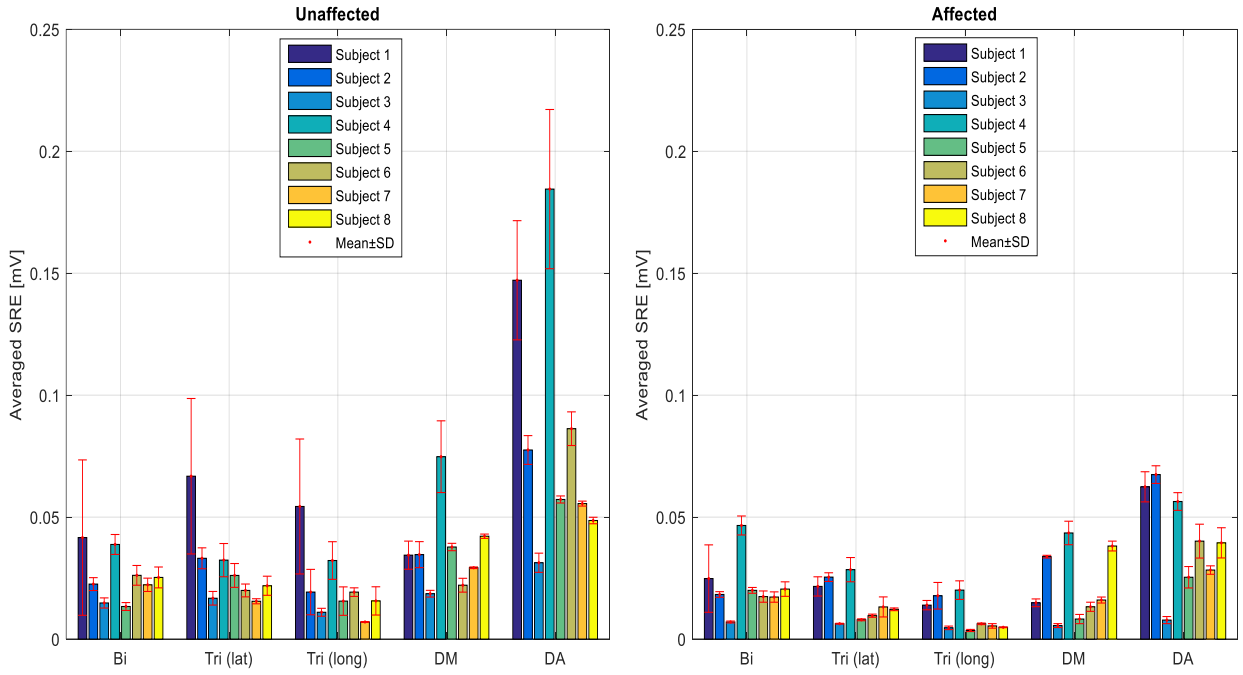

Figure 4.3.3: Muscle activity averaged over the three pathologically unaffected trials (left) and affected trials (right). The averaged muscle activity of the biceps, lateral head triceps, long head triceps, deltoideus medial and deltoideus anterior respectively for all subjects is of interest.

Table 4.3.2: Results of the Wilcoxon signed rank test. The data is presented as the median and corresponding interquartile range (IQR). The IQR can be used to divide the corresponding data set into quartiles or to construct a box plot. Muscles of interest are biceps, lateral head triceps, long head triceps, deltoideus medial and deltoideus anterior respectively. The last column listed the p-values of the test based on a 5% significance level. Values except the p-values are expressed in millivolts.

Muscle activity	**Unaffected**		**Affected**		**Difference**		
	Median (mV)	**[IQR] (mV)**	**Median (mV)**	**[IQR] (mV)**	**Median (mV)**	**[IQR] (mV)**	**P**
Bi	0.02	[0.01,0.03]	0.01	[0.01,0.02]	0.00	[0.00,0.00]	0.208
Tri (lat)	0.02	[0.01,0.03]	0.01	[0.00,0.02]	0.01	[0.00,0.01]	0.012
Tri (long)	0.01	[0.01,0.02]	0.00	[0.00,0.01]	0.01	[0.00,0.01]	0.012
DM	0.03	[0.02,0.04]	0.01	[0.00,0.03]	0.01	[0.00,0.02]	0.012
DA	0.06	[0.05,0.13]	0.03	[0.02,0.06]	0.02	[0.01,0.07]	0.012

4.3.3 SYNERGISTIC AND COACTIVATION SRE PATTERNS

The synergistic coactivation patterns of the subjects regarding the pathologically unaffected and affected shoulder flexion is presented in Appendix C. In case stroke survivors cannot overcome the influence of the flexor synergy during shoulder flexion, the elbow cannot be kept fully extended and the arm tends to move into partial shoulder abduction (Brunnstrom, 1970). The search for linkages between the shoulder flexors, shoulder abductors and elbow flexors are of interest (see Appendix C). The Wilcoxon signed rank test is used to investigate whether the pathologically unaffected shoulder flexions differ significantly from the affected shoulder flexions performed by the subjects. In this case, the cross-correlations and corresponding time lags between the biceps brachii, deltoideus medial and deltoideus anterior during the pathologically unaffected and affected shoulder flexions are investigated and shown in Table 4.3.3. According to the results, a significant difference in cross-correlations and corresponding time lags between the muscle pairs could not be detected (all p-values greater than or equal to 0.05).

Table 4.3.3: Results of the Wilcoxon signed rank test. The data is presented as the median and corresponding interquartile range (IQR) regarding the cross-correlation coefficients and corresponding time lags. The IQR can be used to divide the corresponding data set into quartiles or to construct a box plot. The muscle pair of interest are the biceps and the deltoideus medial, the biceps and the deltoideus anterior, and the deltoideus medial and deltoideus anterior. The last column listed the p-values of the test based on a 5% significance level. The time lags are expressed in seconds.

	Unaffected		**Affected**		**Difference**		
	Median	**[IQR]**	**Median**	**[IQR]**	**Median**	**[IQR]**	**P**
$R_{\mathrm{Bi-DM}}$	0.78	[0.69,0.86]	0.75	[0.64,0.81]	0.26	[0.00,0.66]	0.263
$R_{\mathrm{Bi-DA}}$	0.83	[0.73,0.93]	0.81	[0.74,0.83]	0.05	[-0.05,0.10]	0.327
$R_{\mathrm{DM-DA}}$	0.91	[0.83,0.94]	0.91	[0.74,0.92]	0.00	[-0.06,0.14]	0.779
$\tau_{\mathrm{Bi-DM}}$ (s)	0.01	[-0.01,0.03]	0.00	[-0.08,0.23]	0.00	[-0.22,0.17]	0.726
$\tau_{\mathrm{Bi-DA}}$ (s)	0.00	[-0.27,0.08]	-0.06	[-0.17,0.01]	0.01	[-0.24,0.21]	0.779
$\tau_{\mathrm{DM-DA}}$ (s)	0.00	[-0.01,0.01]	0.01	[-0.01,0.02]	-0.00	[-0.02,0.12]	0.624

4.4 VOLITIONAL MOVEMENTS OUT OF SYNERGIES: SHOULDER ABDUCTION

The items to be scored when the subjects performed the movement with little or no influence of the synergies are shoulder abduction, elbow flexion, and forearm pronation/supination. Based on the FMA-UE the subjects should abduct the shoulder at least 90° while the elbow is completely extended, and the forearm in mid-position of pronation and supination. The joint angles of each subject during the first trial are presented as well as muscle activity and synergistic profiles. The joint angles of the eight subjects during the performance of the movement are depicted in Appendix D and are mostly similar to Figure 4.4.1. Furthermore, the averaged muscle activity and the synergistic profiles are presented and discussed.

4.4.1 INERTIAL INDICATORS MOVEMENT OUT OF SYNERGIES

The eight subjects were instructed to perform the movement three times, so that the peak values of the joint angles can be recorded and averaged over the three trials. The maximum of the absolute values regarding shoulder abduction, elbow flexion and forearm pronation along with corresponding standard deviation are presented in Figure 4.4.2. The results concerning the Wilcoxon signed rank test are shown in Table 4.4.1. According to the results, there is a significant difference between the median pairs regarding the pathologically unaffected and affected shoulder abduction, elbow flexion and forearm pronation/supination.

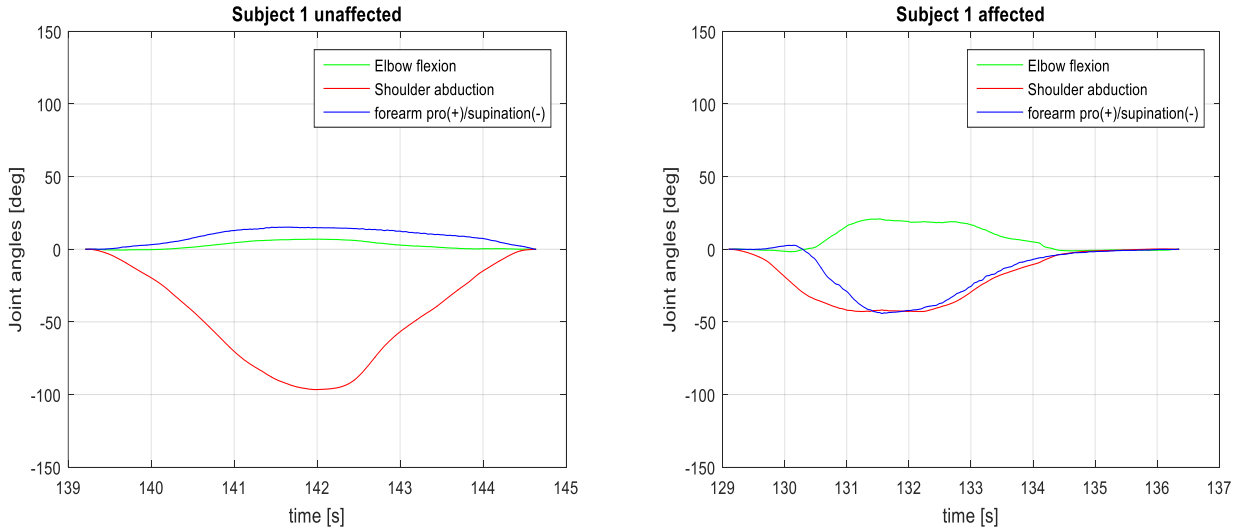

Figure 4.4.1: Joint angles of the first subject during the first trial regarding the 90° shoulder abduction with the elbow at 0° and the forearm pronated (left). Then performed pathologically affected (right).

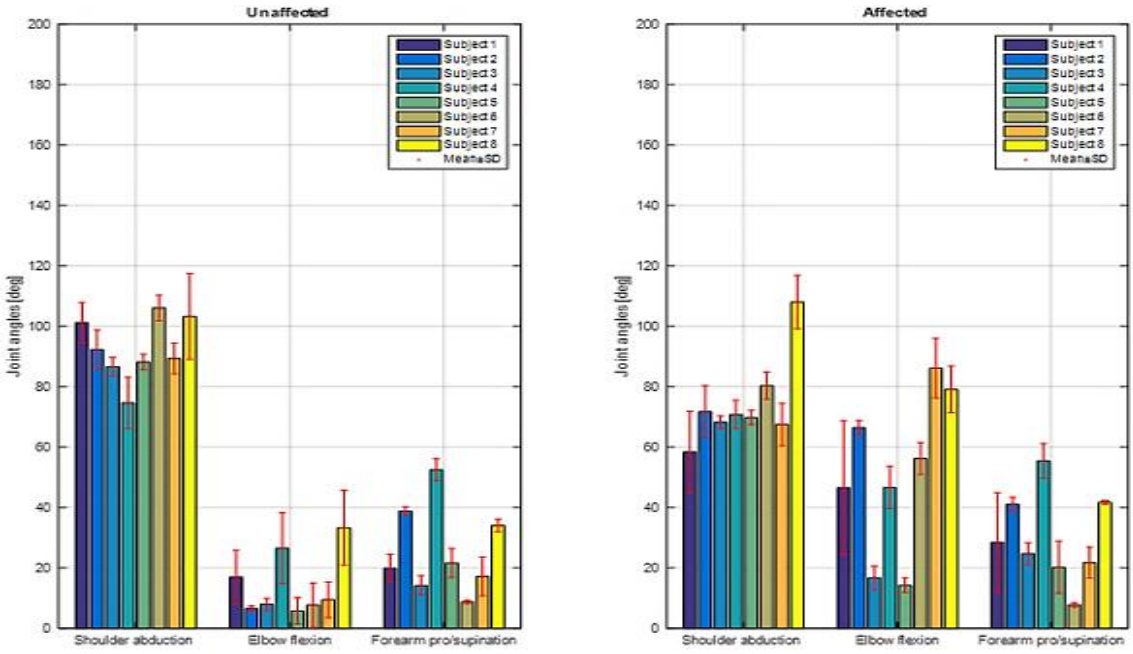

Figure 4.4.2: Joint angles averaged over the three trials presented with corresponding standard deviation. Subjects performed shoulder abduction first pathologically unaffected and then with mimicked pathological synergies.

Table 4.4.1: Results of the Wilcoxon signed rank test. The joint angles of interest are shoulder abduction (SA), elbow flexion (EF), and forearm pronation or supination (FPS). The data is presented as the median and corresponding interquartile range (IQR). The IQR can be used to divide the corresponding data set into quartiles or to construct a box plot. The last column listed the p-values of the test based on a 5% significance level. Values except the p-values are expressed in degrees.

Kinematics	**Unaffected**		**Affected**		**Difference**		
	Median (deg)	**[IQR] (deg)**	**Median (deg)**	**[IQR] (deg)**	**Median (deg)**	**[IQR] (deg)**	P
SA	91	[87,103]	70	[68,78]	20	[7,25]	0.025
EF	9	[7,24]	51	[24,76]	-38	[-57,-12]	0.012
FPS	21	[15,38]	27	[21,42]	-4	[-8,0]	0.036

4.4.2 MEAN SRE AND MUSCLE ACTIVITY

The mean value of each envelope is determined and is used as an indicator of the level of activity of each muscle during the movement. Activity of the FCR and ECR can be excluded for further analysis since wrist flexion and wrist extension are not assessed by the FMA-UE during shoulder abduction. The averaged muscle activities with corresponding standard deviations during the three trials performed by each subject are presented in Figure 4.4.3.

The Wilcoxon signed rank test is used to investigate whether the median difference in muscle activity between the pathologically unaffected and pathologically affected shoulder flexion is zero. The results of the statistical test can be seen in Table 4.4.2. According to the results, muscle activity regarding the biceps brachii, the triceps lateral head and long head, the deltoideus medial, and the deltoideus anterior

decreased significantly when the subjects performed shoulder abduction with pathologically affected synergies ($p = 0.012$).

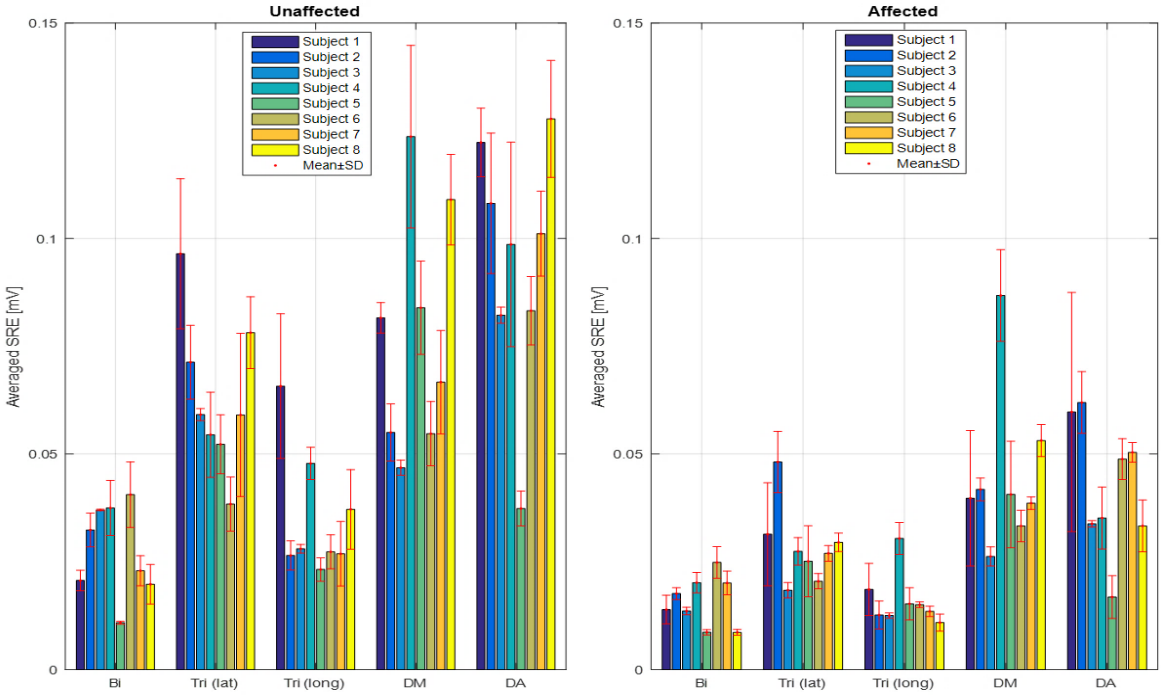

Figure 4.4.3: Muscle activity averaged over the three pathologically unaffected trials (left) and affected trials (right). The averaged muscle activity of the biceps, lateral head triceps, long head triceps, deltoideus medial and deltoideus anterior respectively for all subjects is of interest.

Table 4.4.2: Results of the Wilcoxon signed rank test. The data is presented as the median and corresponding interquartile range (IQR). The IQR can be used to divide the corresponding data set into quartiles or to construct a box plot. Muscles of interest are biceps, lateral head triceps, long head triceps, deltoideus medial and deltoideus anterior respectively. The last column listed the p-values of the test based on a 5% significance level. Values except the p-values are expressed in millivolts.

Muscle activity	**Unaffected**		**Affected**		**Difference**		
	Median (mV)	**[IQR] (mV)**	**Median (mV)**	**[IQR] (mV)**	**Median (mV)**	**[IQR] (mV)**	**P**
Bi	0.02	[0.02,0.03]	0.01	[0.00,0.02]	0.01	[0.00,0.01]	0.012
Tri (lat)	0.05	[0.05,0.07]	0.02	[0.02,0.03]	0.02	[0.02,0.04]	0.012
Tri (long)	0.02	[0.02,0.04]	0.01	[0.01,0.01]	0.01	[0.01,0.02]	0.012
DM	0.07	[0.05,0.10]	0.04	[0.03,0.05]	0.03	[0.02,0.04]	0.012
DA	0.09	[0.08,0.11]	0.04	[0.03,0.05]	0.04	[0.03,0.06]	0.012

4.4.3 SYNERGISTIC AND COACTIVATION SRE PATTERNS

The synergistic coactivation patterns of the subjects regarding the pathologically unaffected and affected shoulder abduction is presented in Appendix D. In case stroke survivors cannot overcome the influence of the flexor synergy during shoulder abduction, the elbow cannot be kept fully extended and the elbow tends to flex as a result of the strong linkage between the elbow flexors and the shoulder abduction muscles

(Brunnstrom, 1970). According to Brunnstrom, stroke patients can execute shoulder abduction with the elbow fully extended successfully when elbow extension and forearm pronation associate with shoulder girdle retraction and shoulder abduction. Therefore, the search for linkages between the shoulder abductors, elbow flexors, and elbow extensors are of interest. In order to investigate whether elbow flexion and shoulder abduction are associated, the cross-correlations and corresponding time lags between the biceps brachii and the deltoideus medial are determined. Moreover, in order to investigate whether elbow extension and shoulder abduction are associated, the cross-correlations and corresponding time lags between the triceps lateral head and deltoideus medial is determined as well as the cross-correlations and corresponding time lags between the triceps long head and the deltoideus medial (see Appendix D).

The Wilcoxon signed rank test is used to investigate whether the pathologically unaffected shoulder abductions differ significantly from the affected shoulder abductions performed by the subjects. In this case, the cross-correlations and corresponding time lags between the biceps brachii, deltoideus medial triceps lateral head, and triceps long head during the pathologically unaffected and affected shoulder flexions are investigated and shown in Table 4.4.3. According to the results, a significant difference in cross-correlations and corresponding time lags between the biceps and the deltoideus medial, and between the triceps long head and deltoideus medial could not be detected (p-values greater than or equal to 0.05). Regarding the cross-correlations between the triceps lateral head and the deltoideus medial, a significant difference could be detected ($p = 0.036$). However, a significant difference in corresponding time lags regarding the latter muscle pair could not be detected.

Table 4.4.3: Results of the Wilcoxon signed rank test. The data is presented as the median and corresponding interquartile range (IQR) regarding the cross-correlation coefficient and corresponding time lag. The IQR can be used to divide the corresponding data set into quartiles or to construct a box plot. The muscle pair of interest are the biceps and the deltoideus medial, the triceps lateral head and the deltoideus medial, and the triceps long head and the deltoideus medial. The last column listed the p-values of the test based on a 5% significance level. The time lags are expressed in seconds.

	Unaffected		**Affected**		**Difference**		
	Median	**[IQR]**	**Median**	**[IQR]**	**Median**	**[IQR]**	**P**
$R_{\mathrm{Bi-DM}}$	0.91	[0.64,0.94]	0.84	[0.78,0.89]	0.02	[-0.14,0.11]	0.674
$R_{\mathrm{Tri(lat)-DM}}$	0.94	[0.83,0.95]	0.86	[0.77,0.88]	0.06	[0.03,0.10]	0.036
$R_{\mathrm{Tri(long)-DM}}$	0.91	[0.70,0.94]	0.69	[0.50,0.89]	0.12	[-0.03,0.39]	0.161
$\tau_{\mathrm{Bi-DM}}$ (s)	0.02	[0.00,0.17]	0.02s	[0.01,0.03]	-0.00	[-0.02,0.14]	0.735
$\tau_{\mathrm{Tri(lat)-DM}}$ (s)	0.01	[0.00,0.11]	0.06s	[0.00,0.28]	-0.00	[-0.06,0.06]	0.889
$\tau_{\mathrm{Tri(long)-DM}}$ (s)	-0.01	[-0.05,0.03]	0.00s	[0.00,0.21]	-0.00	[-0.05,0.03]	0.726

5. DISCUSSION

The results regarding the movements within synergies, mixing synergies and out of synergies are first separately discussed. Then, the results regarding the three movements are generally considered such that an overall observation can be discussed.

5.1 VOLITIONAL MOVEMENTS WITHIN SYNERGIES: FLEXOR SYNERGY

According to the FMA-UE a score of zero is assigned when the subject is not able to perform the flexor synergy at all (Fugl-Meyer et al., 1975). A score of one is assigned when the subject performs the flexor synergy partly, which means that the movement is performed with restrictions in the corresponding joint angles. A maximum score of two is assigned when the subject performed the movement faultless. A faultless flexor synergy consists of a fully supinated forearm, a fully flexed elbow and a shoulder abducted at least (theoretically) 90°. The minimum value regarding the shoulder abduction during the pathologically unaffected flexor synergy, performed by the third subject, is 81° (see Figure 4.2.3). This value, however, is a practical value since the sensor-to-segment calibration procedure and the drift compensation are not errorless. The minimum angle of elbow flexion, performed by the third subject, is 79°. A full elbow flexion has a roughly estimated practical value between 135° to 145° (Morrey, Chao, & Hui, 1979). On the other hand, the sixth and seventh subject performed the elbow flexion unpractically high (see Figure 4.2.3). The system detects joint angles, but obviously the influence of the sensor-to-segment conversion and drift compensation cannot be excluded. The FMA-UE does not explicitly indicate a fully supinated forearm by means of a value. Normally, a fully supinated and pronated forearm are 85° respectively 75° (Mansfield & Neumann, 2009). Moreover, a fully flexed elbow increases the maximum angle of supination (Shaaban, Pereira, Williams, & Lees, 2008). However, the subjects performed the forearm pro/supination less than 75° or 85°. The third and fifth subject performed forearm pronation instead of supination (see appendix B). The possibility that the instructions given by the examiner were not abundantly clear is not ruled out. However, during the performance of the movements it was observed that most subjects found the flexor synergy challenging to perform with the forearm fully supinated.

The system could detect a difference between the pathologically unaffected and affected flexor synergy performed by each subject. Overall, the pathologically affected flexor synergy is performed such that a significant reduction of 30% in shoulder abduction and elbow flexion could be detected. A significant difference in forearm pronation or supination could not be detected (see Table 4.2.1). Some subjects performed the pathologically synergy such that forearm supination angle increased, while others performed the movement such that the supination angle decreased. Furthermore, according to Table 4.2.3, the system detected a significant reduction in muscle activity regarding the biceps, triceps lateral head, triceps long head, the deltoideus medial and the deltoideus anterior during the performance of the pathologically affected flexor synergy. Like expected, the reduction in shoulder abduction caused a reduction in activity from the deltoideus medial and deltoideus anterior, and the reduction in elbow flexion caused a reduction in activity from the biceps brachii.

Finally, the system could not detect a significant difference in coactivation between the biceps and the deltoideus medial regarding the pathologically unaffected flexor synergy and the simulated affected flexor synergy (see Table 4.2.9). According to Table 4.2.8, the second and the sixth subject performed the unaffected flexor synergy such that the cross-correlation between the biceps and the deltoideus medial is relatively low. Moreover, the fourth subject performed the pathologically unaffected and affected flexor

synergy such that in both cases the cross-correlation is relatively low. Overall, most subjects performed the pathologically unaffected as well as the pathologically affected flexor synergy such that the biceps and deltoideus medial activate and deactivate in phase with an insignificant difference ($p = 0.05$) in time lag of 0.26 seconds (see Table 4.2.9).

5.2 VOLITIONAL MOVEMENTS MIXING SYNERGIES: SHOULDER FLEXION

According to the FMA-UE a score of zero is assigned when the subject performs the 90° shoulder flexion such that at the start of the motion elbow flexion and/or shoulder abduction occurs (Fugl-Meyer et al., 1975). A score of one is assigned when elbow flexion and/or shoulder abduction occurs in a later phase. A score of two is assigned if the elbow is fully extended throughout the total required range of motion. The minimum angle of the pathologically unaffected shoulder flexion is approximately 71° (see Figure 4.3.2 performed by the third subject), while the maximum angle is 89° (performed by the second subject). The angles regarding the elbow flexion during the pathologically unaffected movement range from 5° to 15°, while the shoulder abduction angles range from 7° to 52°. Abduction angles greater than 40° are relatively high but are not necessarily the influence of the flexor synergy since the subjects were instructed to perform the shoulder flexion without the pathological synergies. The relatively high abduction angles could be due to individual's physique, and the uncompensated errors of the sensor-to-segment calibration procedure and/or drift compensation. Moreover, an elbow flexion of approximately 7° during the pathologically affected shoulder flexion is relatively low (see Figure 4.3.2, the fifth subject). Besides the influence of the sensor-to-segment conversion and drift compensation, the possibility that the subject focussed on restricted shoulder flexion and neglected elbow flexion is not excluded.

The system could detect significant differences between the pathologically unaffected and affected shoulder flexion performed by each subject. The median difference between pathologically unaffected and affected shoulder flexion regarding the abduction angle is a significant reduction of 52% (see Table 4.3.1). Contrary to the FMA-UE, most subjects performed the pathologically affected shoulder flexion with significantly less shoulder abduction compared to the pathologically unaffected scenario. However, the subjects were instructed to mimic the pathologically affected movements such shoulder flexion is restricted, and elbow flexion is emphasized. Moreover, a significant increase in elbow flexion and a significant decrease in shoulder flexion during the pathologically affected movement could be detected. The significant increase in elbow flexion, however, does not necessarily correspond with an increase in the biceps brachii, since the system could not detect a significant difference in biceps activity (see Table 4.3.2). The insignificant difference in biceps brachii activity could be due to the multiple muscles involved during elbow flexion. The muscles involved during elbow flexion are the brachialis, the biceps brachii, and the brachioradialis. According to Staudenmann et al., the brachialis contributes mostly to elbow flexion, which indicates that there could be a significant difference in brachialis activity instead of the biceps brachii (Staudenmann & Taube, 2015). However, the activity of the brachialis is not recorded. Furthermore, according to Sakurai et al., biceps activity has little dependence on elbow flexion when flexion torques are produced around the shoulder (Sakurai, Ozaki, Tomita, Nishimoto, & Tamai, 1998). Moreover, biceps brachii activity also depends on the forearm pronation/supination angle. According to several studies, the biceps brachii is more active when the forearm is supinated compared to a pronated forearm (Lehman, 2005; Staudenmann & Taube, 2015). The dependency between the biceps brachii activity and the forearm angle is relevant since the subjects were instructed to perform the movements with the forearm in mid-position of pronation and supination. Above findings could be an explanation regarding the insignificant

difference in biceps activity during shoulder flexion with the elbow fully extended and shoulder flexion with the elbow flexed.

The significant decrease in triceps (lateral and long head) activity could be related to the significant increase in elbow flexion, since the biceps and the triceps muscles have an agonist respectively antagonist relationship during elbow flexion (Gowland, deBruin, Basmajian, Plews, & Burcea, 1992). Furthermore, the significant decrease in shoulder abduction and shoulder flexion could be related with the significant decrease in deltoideus medial activity and deltoideus anterior activity respectively.

The system could not detect a significant difference in coactivation between the biceps and the deltoideus medial regarding the pathologically unaffected shoulder flexion and the affected shoulder flexion (see Table 4.3.3). A significant difference in coactivation between the biceps and the deltoideus medial could also not be detected. Similarly, a significant difference in coactivation between the deltoideus medial and the deltoideus anterior could not be detected. According to the results, most subjects performed the pathologically unaffected and affected shoulder flexion such that the deltoideus medial and deltoideus anterior have the highest correlation coefficient. The biceps and deltoideus anterior have the second highest correlation coefficient, while the biceps and the deltoideus medial have the lowest correlation coefficient. Based on the results the two muscle pairs: deltoideus medial and deltoideus anterior; and the biceps and deltoideus anterior are activated and deactivated in phase, while the biceps and deltoideus medial are not correlated during shoulder flexion. Furthermore, the insignificant difference in coactivation between the biceps and the deltoideus medial could point out that the pathologically affected shoulder flexion is simulated. Lastly, the measurement system could not detect a significant difference in the corresponding time lags as well (see Table 4.3.3).

5.3 VOLITIONAL MOVEMENTS OUT OF SYNERGIES: SHOULDER ABDUCTION

According to the FMA-UE a score of zero is assigned when the subject performs the 90° shoulder abduction such that at the start of the motion elbow flexion and/or forearm pronation/supination occurs (Fugl-Meyer et al., 1975). A score of one is assigned when elbow flexion and/or forearm pronation/supination occurs in a later phase. A score of two is assigned if the elbow is fully extended throughout the total required range of motion without any forearm pronation or supination. The minimum angle of the pathologically unaffected movements regarding shoulder flexion is approximately 75° (see Figure 4.4.2 performed by the third subject), while the maximum angle is 103° (performed by the eighth subject). The angles regarding the elbow flexion during the pathologically unaffected movement range from 6° to 33°, while the unaffected forearm pronation/supination angles range from 9° to 52°. The unaffected forearm pronation/supination angles greater than 30° are relatively high but are not necessarily the synergy influence since the subjects were instructed to perform the shoulder abduction without the pathological synergies. The relatively high forearm pronation/supination angles could be due to individual's performance, and the uncompensated errors of the sensor-to-segment calibration procedure and/or drift compensation. Moreover, an elbow flexion of less than 20° during the pathologically affected shoulder flexion is relatively low (see Figure 4.4.2, the third and the fifth subject). Besides the influence of the sensor-to-segment conversion and drift compensation, the possibility that the third and fifth subject focussed on restricted shoulder abduction and neglected elbow flexion is not excluded.

The system could detect significant differences between the pathologically unaffected and affected shoulder abduction performed by each subject. The median difference between pathologically unaffected and affected shoulder abduction angles is a significant reduction of 22% (see Table 4.4.1). Furthermore, a

significant increase in elbow flexion and forearm pronation/supination during the pathologically affected movement could be detected. In contrast to the function of the biceps brachii as one of the elbow flexors, a significant decrease in activity could be detected during pathologically affected shoulder abduction (see Table 4.4.2). However, the biceps brachii activity is more active when the forearm is supinated (Sakurai et al., 1998). Therefore, the significant decrease in biceps brachii activity could be related to the significant increase in the forearm pronation angle.

The significant decrease in triceps (lateral and long head) activity could be related to the significant increase in elbow flexion, since the biceps and the triceps muscles have an agonist respectively antagonist relationship during elbow flexion (Gowland et al., 1992). Furthermore, the significant decrease in shoulder abduction could be related with the significant decrease in deltoideus medial activity and deltoideus anterior activity respectively.

The system could not detect a significant difference in coactivation between the biceps and the deltoideus medial regarding the pathologically unaffected shoulder abduction and the affected shoulder abduction (see Table 4.4.3). A significant difference in coactivation between the triceps long head and the deltoideus medial could also not be detected. However, a significant difference in coactivation between the triceps lateral head and the deltoideus medial could be detected. According to the results, most subjects performed the pathologically unaffected and affected shoulder abduction such that the triceps lateral head and the deltoideus medial have the highest correlation coefficient. The biceps and deltoideus anterior have the second highest correlation coefficient, while the triceps long head and the deltoideus medial have the lowest correlation coefficient especially during pathologically affected shoulder abduction. Coactivation of the biceps muscle and the deltoideus medial during pathologically unaffected and affected shoulder abduction could confirm the suggestion of Sakurai et al. regarding the function of the biceps muscle as a possible shoulder abductor (Sakurai et al., 1998). Lastly, the measurement system could not detect a significant difference in the corresponding time lags as well (see Table 4.4.3).

5.4 OVERALL OBSERVATION

Considering the results of the three movements, the system detected limitations in joint angles and corresponding significant decreases in the activity of the selected set of agonist muscles during pathologically affected movements. The detection of the limitations in joint angles and corresponding decrease in agonistic muscle activity is in accordance with the findings of Gowland et al., who noticed that the activity of the set of agonist muscles in the patients who could not perform the tasks was significantly lower than in those who were able to perform the tasks (Gowland et al., 1992). Furthermore, Gowland showed that inadequate recruitment of the agonist muscles, and not abnormal co-contraction of the agonist and antagonist muscles, caused the restriction in arm movement tasks. In this experiment with healthy subjects, antagonistic muscle activity significantly decreased during movements within synergies (triceps lateral and long head) and movements out of synergies (biceps brachii), while during movements combining synergies (biceps brachii) an insignificant difference was detected. Comparable to the findings of Gowland, a significant increase in antagonistic muscle activity during pathologically affected movements could not be detected. However, Gowland could not find a significant difference in antagonistic muscle activity of the patients who were unable to perform the movements successfully compared to patients who could perform the movements successfully. In this study, the significant decrease in the antagonist muscle activity during movements within synergies (triceps lateral and long head) and movements out of synergies (bices brachii) could indicate that the influence of the flexor synergy is mimicked.

Furthermore, cross-correlations and corresponding time lags between selected muscles during movements within synergies, movements combining synergies and movements out of synergies were determined in order to detect (strong) linkages between muscles. According to the results, a significant difference between pathologically unaffected and affected movements was detected only during movements out of synergies regarding the cross-correlation between the triceps lateral head and deltoideus medial. The overall insignificant difference in cross-correlations and corresponding time lags between pathologically unaffected and affected movements could indicate that the pathologically affected movements were simulated.

Finally, due to the influence of variable distances of recording electrodes from active tissue the mean value of the linear envelope muscle activity cannot be used for direct comparisons without some form of normalization. In healthy subjects the muscle activity can be normalized by means of the ratio of the linear envelope to the maximum voluntary contraction (MVC) of the corresponding muscle. In stroke patients, however, the MVC is influenced by paresis and becomes meaningless (Gowland et al., 1992). In this study, normalization of muscle activity could be excluded since the healthy subjects performed the pathologically unaffected and affected movements with the left upper extremity.

6. CONCLUSIONS AND RECOMMENDATIONS

What is the optimal set of sensor-to-segment calibration movements performed by the subjects?
The optimal set of sensor-to-segment calibration movements consist of eight movements. The movements include a static pose of the ulnar side of the hand, repeated forearm pronation or supination, a static pose on the left side of the thumb, a static pose of the forearm aligned in the direction of gravity with the elbow fully extended, repeated elbow flexion with the forearm pronated, repeated shoulder flexion with the elbow flexed, repeated trunk flexion, and repeated ipsilateral and contralateral trunk rotation.

Which clinically relevant insights related to stroke patients can the multisensory system provide?
The influence of the flexor synergy caused limitations in joint angles due to insufficient activity of the agonist muscles. Furthermore, the significant decrease in antagonistic muscle activity and the insignificant difference in muscle coactivation could indicate that the influence of the flexor synergy was simulated.

Overall, the system could detect significant differences in the joint angles regarding shoulder abduction, shoulder flexion, elbow flexion, and forearm pronation and/or supination. Moreover, a significant decrease in agonistic and antagonistic muscle activity during pathologically affected movements could be detected by the system. However, a significant difference in coactivation between selected muscles during pathologically unaffected and affected movements could not be detected. Furthermore, the significant decrease in antagonistic muscle activity and the insignificant difference in muscle coactivation could indicate that the influence of the flexor synergy was simulated.

Recommendations

The optimized set of sensor-to-segment calibration movements is based on the performance of the subjects. The influence of the sample size on the selection of the calibration movements should be further investigated.

The system can be used to quantify the influence of the flexor synergy based on the recorded joint angles during the pathologically unaffected and affected movements. However, the system determines joint angles by means of a strapdown-integration algorithm which compensates errors related to drift linearly. Since the sensor drift has a non-linear behaviour, the joint angles are not optimally calculated. According to Kieliba et al., an algorithm based on Magdwick filtering can be used for an optimal estimation of joint angles (Kieliba et al., 2018).

Additional differences in muscle activities and coactivations provide the examiner of valuable insights for identifying strong linkages between muscles. However, the influence of the elbow flexion angle on the biceps brachii activity was not clear, due to the influence of the forearm pronation and/or supination angle. Since the brachialis contributes mostly to elbow flexion, additional recording of the brachialis activity can provide more insights. Moreover, based on the selected set of muscle activities, detection of the flexor synergy was emphasized. Additional recording of the forearm pronator and supinator muscles, and the pectoralis major provides the possibility to investigate the flexor and extensor synergies thoroughly.

Furthermore, the cut-off frequency of the high pass filtering process of the EMG signals was 30 Hz because the EMG recordings at the deltoideus muscles were contaminated by the QRS-complexes of the electrocardiogram (ECG). However, a cut-off frequency of 30 Hz does not preserve the spectral content of the linear envelopes completely. Willingenburg et al. proposed several algorithms which include reference

ECG recordings such that the QRS complexes can be removed from the EMG recordings while the frequency spectral is preserved (Willigenburg et al., 2012).

Finally, differences in coactivation between muscles during pathologically unaffected and affected movements could not be detected. However, healthy subjects were instructed to simulate the pathological synergies. The detection of pathological synergies should be tested further in stroke patients. Since stroke patients must perform the movements with the unaffected and the affected upper limb, some form of muscle activity normalization must be performed. Suitable normalization procedures should be further investigated since the use of MVCs is influenced by paresis.

REFERENCES

Auer, R. N. (2016). Histopathology of Brain Tissue Response to Stroke and Injury. In *Stroke (Sixth Edition)* (pp. 47-59): Elsevier.

Bonnet, S., Bassompierre, C., Godin, C., Lesecq, S., & Barraud, A. (2009). Calibration methods for inertial and magnetic sensors. *Sensors and Actuators A: Physical, 156*(2), 302-311.

Bortz, J. E. (1971). A new mathematical formulation for strapdown inertial navigation. *IEEE transactions on aerospace and electronic systems*(1), 61-66.

Brunnstrom, S. (1970). Movement therapy in hemiplegia. *A neurophysiological approach*, 113-122.

Carr, J. H., & Shepherd, R. B. (2003). *Stroke rehabilitation: guidelines for exercise and training to optimize motor skill*: Butterworth-Heinemann Medical.

Cohen, L. A. (1953). Localization of stretch reflex. *Journal of Neurophysiology, 16*(3), 272-285.

Craig, J. J. (2009). *Introduction to robotics: mechanics and control, 3/E*: Pearson Education India.

Crawford, N. R., Yamaguchi, G. T., & Dickman, C. A. (1999). A new technique for determining 3-D joint angles: the tilt/twist method. *Clinical Biomechanics, 14*(3), 153-165.

Ellis, M. D., Schut, I., & Dewald, J. P. (2017). Flexion synergy overshadows flexor spasticity during reaching in chronic moderate to severe hemiparetic stroke. *Clinical Neurophysiology, 128*(7), 1308-1314.

Freriks, B., & Hermens, H. (2000). *European recommendations for surface electromyography: results of the SENIAM project*: Roessingh Research and Development.

Fugl-Meyer, A. R. (1971). Effects of respiratory muscle paralysis in tetraplegic and paraplegic patients. *Scandinavian journal of rehabilitation medicine, 3*(4), 141-150.

Fugl-Meyer, A. R., Jääskö, L., Leyman, I., Olsson, S., & Steglind, S. (1975). The post-stroke hemiplegic patient. 1. a method for evaluation of physical performance. *Scandinavian journal of rehabilitation medicine, 7*(1), 13-31.

Ghapanchizadeh, H., Ahmad, S. A., & Ishak, A. J. (2015). *Recommended surface EMG electrode position for wrist extension and flexion.* Paper presented at the Biomedical Engineering & Sciences (ISSBES), 2015 IEEE Student Symposium in.

Ghez, C., & Shinoda, Y. (1978). Spinal mechanisms of the functional stretch reflex. *Experimental brain research, 32*(1), 55-68.

Gillen, G. (2015). *Stroke rehabilitation: a function-based approach*: Elsevier Health Sciences.

Gowland, C., deBruin, H., Basmajian, J. V., Plews, N., & Burcea, I. (1992). Agonist and antagonist activity during voluntary upper-limb movement in patients with stroke. *Physical therapy, 72*(9), 624-633.

Jones, G. M., & Watt, D. (1971). Observations on the control of stepping and hopping movements in man. *The Journal of Physiology, 219*(3), 709-727.

Kortier, H. G. (2018). Assessment of hand kinematics and interactions with the environment.

Lehman, G. J. (2005). The influence of grip width and forearm pronation/supination on upper-body myoelectric activity during the flat bench press. *The Journal of Strength & Conditioning Research, 19*(3), 587-591.

Luinge, H. J., Veltink, P. H., & Baten, C. T. (2007). Ambulatory measurement of arm orientation. *Journal of biomechanics, 40*(1), 78-85.

Mansfield, P. J., & Neumann, D. A. (2009). *Essentials of kinesiology for the physical therapist assistant*: Mosby Elsevier.

Mathiowetz, V. (2016). Task-oriented approach to stroke rehabilitation. In *Stroke Rehabilitation (Fourth Edition)* (pp. 59-78): Elsevier.

McCrum-Gardner, E. (2008). Which is the correct statistical test to use? *British Journal of Oral and Maxillofacial Surgery, 46*(1), 38-41.

Miller, L. C., Thompson, C. K., Negro, F., Heckman, C., Farina, D., & Dewald, J. P. (2014). *High-density surface EMG decomposition allows for recording of motor unit discharge from proximal and distal flexion synergy muscles simultaneously in individuals with stroke.* Paper presented at the Engineering in Medicine and Biology Society (EMBC), 2014 36th Annual International Conference of the IEEE.

Morrey, B., Chao, E., & Hui, F. (1979). Biomechanical study of the elbow following excision of the radial head. *The Journal of bone and joint surgery. American volume, 61*(1), 63-68.

Nelson-Wong, E., Gregory, D. E., Winter, D. A., & Callaghan, J. P. (2008). Gluteus medius muscle activation patterns as a predictor of low back pain during standing. *Clinical Biomechanics, 23*(5), 545-553.

Orfanidis, S. J. (1988). *Optimum signal processing: an introduction*: Macmillan publishing company.

Peter, K. (2005). ABC of EMG, A Practical Introduction to Kinesiological Electromyography‖ version 1.0, Noraxon Inc. In: USA.

Prince, F., Winter, D., Stergiou, P., & Walt, S. (1994). Anticipatory control of upper body balance during human locomotion. *Gait & posture, 2*(1), 19-25.

Raghavan, P. (2015). Upper limb motor impairment after stroke. *Physical Medicine and Rehabilitation Clinics, 26*(4), 599-610.

Sabari, J. S. (2016). Activity-Based Intervention in Stroke Rehabilitation. In *Stroke Rehabilitation (Fourth Edition)* (pp. 79-95): Elsevier.

Sakurai, G., Ozaki, J., Tomita, Y., Nishimoto, K., & Tamai, S. (1998). Electromyographic analysis of shoulder joint function of the biceps brachii muscle during isometric contraction. *Clinical Orthopaedics and Related Research (1976-2007), 354*, 123-131.

Santello, M., & Lang, C. E. (2015). Are movement disorders and sensorimotor injuries pathologic synergies? When normal multi-joint movement synergies become pathologic. *Frontiers in human neuroscience, 8*, 1050.

Schepers, H. M., Koopman, H. F., & Veltink, P. H. (2007). Ambulatory assessment of ankle and foot dynamics. *IEEE Transactions on Biomedical Engineering, 54*(5), 895-902.

Shaaban, H., Pereira, C., Williams, R., & Lees, V. (2008). The effect of elbow position on the range of supination and pronation of the forearm. *Journal of Hand Surgery (European Volume), 33*(1), 3-8.

Staudenmann, D., & Taube, W. (2015). Brachialis muscle activity can be assessed with surface electromyography. *Journal of electromyography and kinesiology, 25*(2), 199-204.

Tedaldi, D., Pretto, A., & Menegatti, E. (2014). *A robust and easy to implement method for IMU calibration without external equipments.* Paper presented at the 2014 IEEE International Conference on Robotics and Automation (ICRA).

Thibaut, A., Chatelle, C., Ziegler, E., Bruno, M.-A., Laureys, S., & Gosseries, O. (2013). Spasticity after stroke: physiology, assessment and treatment. *Brain injury, 27*(10), 1093-1105.

Titterton, D., Weston, J. L., & Weston, J. (2004). *Strapdown inertial navigation technology* (Vol. 17): IET.

Twente Medical Systems international (Twente Medical Systems international (TMSi)). Great Science, Astounding Signals. Retrieved from https://www.tmsi.com/

Twitchell, T. E. (1951). The restoration of motor function following hemiplegia in man. *Brain, 74*(4), 443-480.

van Kordelaar, J., van Wegen, E. E., & Kwakkel, G. (2012). Unraveling the interaction between pathological upper limb synergies and compensatory trunk movements during reach-to-grasp after stroke: a cross-sectional study. *Experimental brain research, 221*(3), 251-262.

Weenk, D., Van Beijnum, B.-J. F., Baten, C. T., Hermens, H. J., & Veltink, P. H. (2013). Automatic identification of inertial sensor placement on human body segments during walking. *Journal of neuroengineering and rehabilitation, 10*(1), 31.

Wentink, E., Schut, V., Prinsen, E., Rietman, J., & Veltink, P. (2014). Detection of the onset of gait initiation using kinematic sensors and EMG in transfemoral amputees. *Gait & posture, 39*(1), 391-396.

Willigenburg, N. W., Daffertshofer, A., Kingma, I., & Van Dieën, J. H. (2012). Removing ECG contamination from EMG recordings: A comparison of ICA-based and other filtering procedures. *Journal of electromyography and kinesiology, 22*(3), 485-493.

Winter, D. A. (2009). *Biomechanics and motor control of human movement*: John Wiley & Sons.

Woltring, H. J. (1991). Representation and calculation of 3-D joint movement. *Human Movement Science, 10*(5), 603-616.

APPENDIX A SENSOR-TO-SEGMENT CALIBRATION MOVEMENTS

Table A.1: Description of 26 calibration movements for sensor-to-segment calibration. The subject is seated while performing calibration movements one till 20 but standing while performing the last six movements.

Calibration #	*Description*	*Illustration*
1	Middle and index finger flat for several seconds	Figure A.1
2	Three times flexion and extension of the middle and index finger	Figure A.1
3	Thumb flat for several seconds	Figure A.2
4	Three times flexion and extension of the thumb	Figure A.2
5	Palmar side of the hand flat on a table or flat object for several seconds	Figure A.3
6	Ulnar side of the hand on a box or table in a static pose for several seconds	Figure A.3
7	Static pose on the left side of the thumb	Figure A.3
8	Three times flexion and extension of the wrist	Figure A.4
9	Three times pronation and supination of the forearm	Figure A.4
10	Three times elbow flexion and extension with the hand in mid position of pronation and supination	Figure A.5
11	Three times elbow flexion with the forearm pronated	Figure A.5
12	Static pose of the forearm aligned in the direction of gravity with the elbow fully extended (inclination)	Figure A.5
13	Static pose of the forearm in mid position of pronation and supination with the elbow 90° flexed	Figure A.5
14	Static pose of the forearm fully pronated with the elbow 90° flexed	Figure A.6
15	Static pose of the upper arm aligned with gravity while the elbow 90° flexed (inclination). Subject might adduct the shoulder for better alignment	Figure A.7
16	Static pose of the upper arm while the elbow is 90° flexed and the shoulder 90° abducted	Figure A.7
17	Static pose of the upper arm while the elbow and shoulder are 90° flexed	Figure A.7
18	Three times shoulder abduction and adduction with the elbow 90° flexed	Figure A.8
19	Three times shoulder flexion with the elbow 90° flexed	Figure A.8
20	Three times shoulder internal and external rotation with the shoulder and elbow kept in 90° flexed pose	Figure A.8
21	Subject in neutral pose (N-pose)	Figure A.9
22	Static pose standing trunk flexion (90°)	Figure A.9
23	Static pose standing trunk lateral flexion (approximately 35°, left side)	Figure A.9
24	Three times trunk flexion	Figure A.10
25	Three times trunk ipsilateral and contralateral rotation	Figure A.10
26	Three-time lateral trunk rotation	Figure A.10

Table A.2: First part of list with calibration movements and the corresponding defined segment axis. The segments are middle- and index finger, thumb, hand, lower- and upper arm, shoulder and sternum.

Calibration #	$\bar{X}_{acc}$	$\bar{Y}_{acc}$	$\bar{Z}_{acc}$	$\bar{X}_{gyr}$	$\bar{Y}_{gyr}$	$\bar{Z}_{gyr}$
1		**Middle Index**				
2				**Middle Index**		
3	**Thumb**					
4					**Thumb**	
5		**Middle Index Hand**				

Table A.3: Second part of list with calibration movements and the corresponding defined segment axis. The segments are middle- and index finger, thumb, hand, lower- and upper arm, shoulder and sternum. The minus sign indicates that the vector is in opposite direction based on the defined segment frame.

Calibration #	$\bar{X}_{acc}$	$\bar{Y}_{acc}$	$\bar{Z}_{acc}$	$\bar{X}_{gyr}$	$\bar{Y}_{gyr}$	$\bar{Z}_{gyr}$
6	Middle Index Hand					
7		Thumb (-)				
8				Middle Index Hand		
9						Middle Index Hand
10					Middle Index Hand Lower	
11				Middle Index Hand Lower		
12			Middle Index Thumb Hand Lower			
13	Middle Index Hand Lower					
14		Middle Index Hand Lower				
15			Upper			
16		Upper				
17	Upper					
18				Upper		
19					Upper	
20						Upper
21			Shoulder Sternum			
22	Shoulder Sternum (-)					
23		Shoulder Sternum (-)				
24					Shoulder Sternum	
25						Shoulder Sternum
26				Shoulder Sternum		

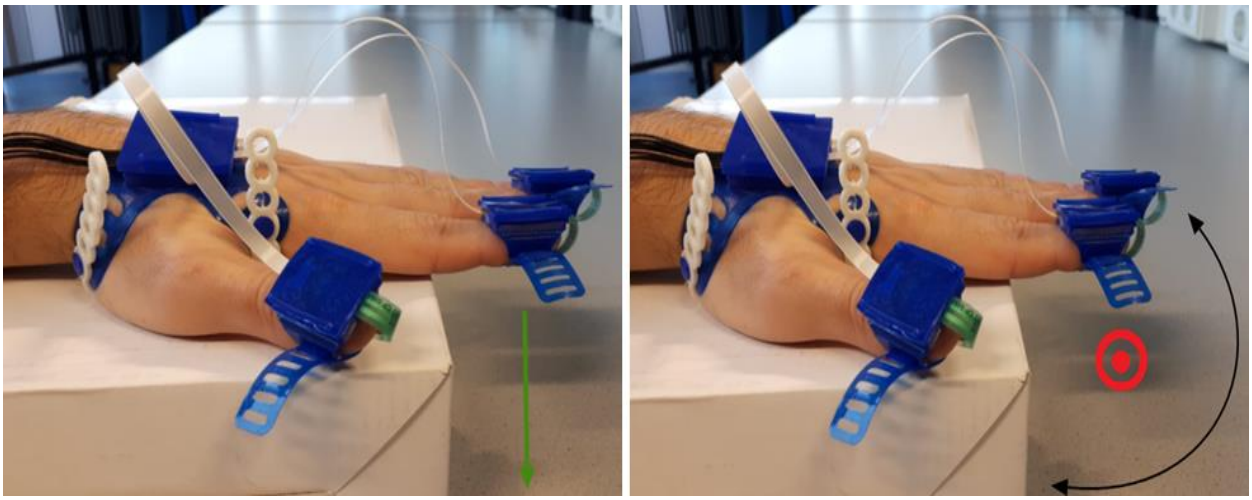

Figure A.1: On the left side, middle- and index finger flat for several seconds (static pose). The unit vectors of the segments are determined by means of least squares regression fitting and normalization of the acceleration recordings. Each unit vector is defined as the y-axis of corresponding segment. The direction of the unit vectors is based on the defined segment frame and is roughly in the direction of the green arrow. On the right side, three times flexion and extension of the middle-and index finger. The unit vectors are determined by means of the gyroscope recordings. Each unit vector is defined as the x-axis of corresponding segment. The direction of the unit vectors is based on the defined segment frame and is roughly in the direction of the red dot (red dot means that the direction of the unit vectors is towards the reader).

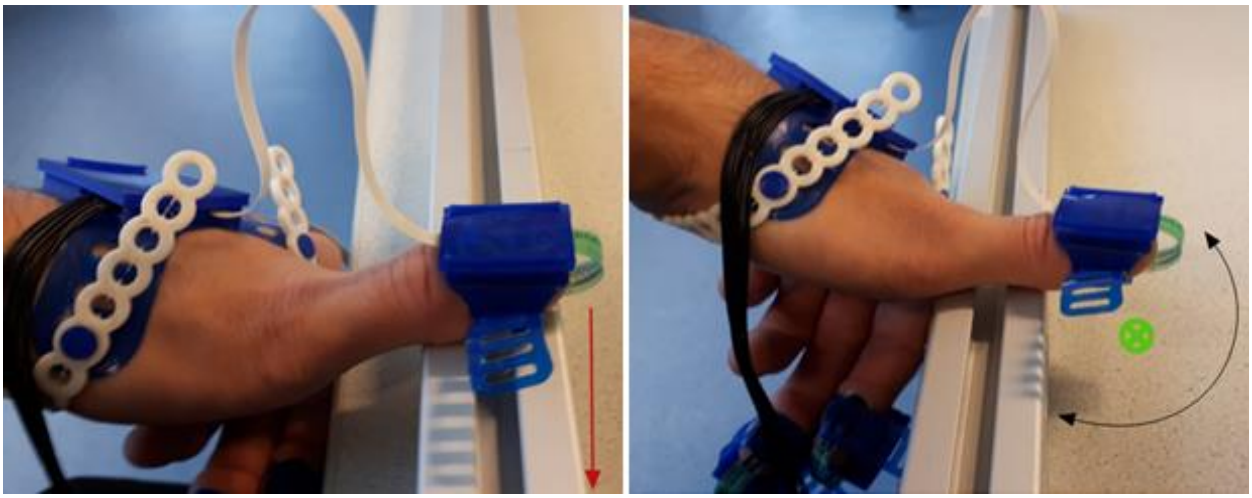

Figure A.2: On the left side, thumb flat for several seconds (static pose). The unit vector of the thumb is determined by means of least squares regression fitting and normalization of the acceleration recordings. The unit vector is defined as the x-axis of the thumb, with its direction based on the defined segment frame, which is roughly in the direction of the red arrow. On the right side, three times flexion and extension of the thumb. The unit vector is determined by means of the gyroscope recordings. The unit vector is defined as the y-axis of the thumb. The direction of the unit vector is based on the defined segment frame and is roughly in the direction of the green cross in the circle (green cross means that the arrow goes into the page).

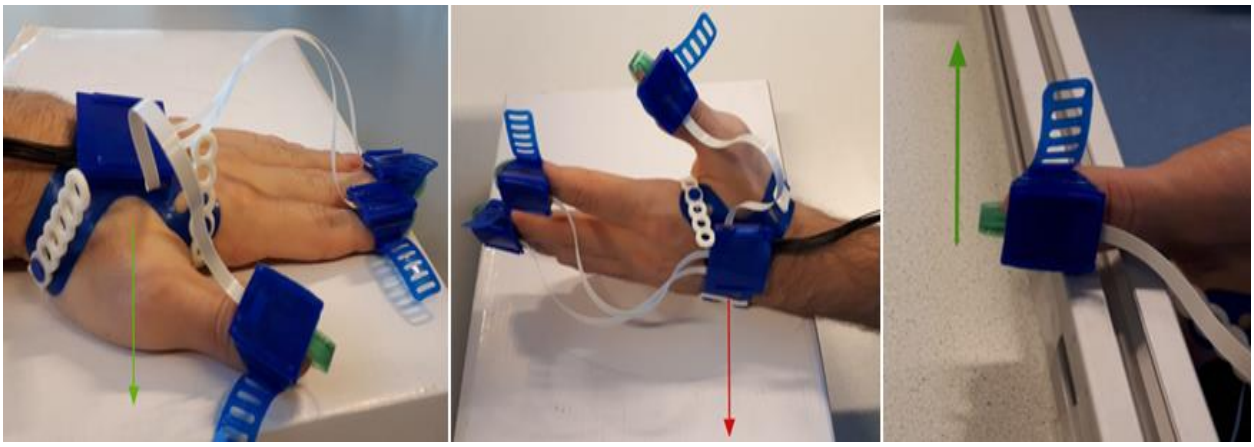

Figure A.3: On the left side, hand, middle- and index finger flat for several seconds (static pose). The unit vectors of the segments are determined by means of least squares regression fitting and normalization of the acceleration recordings. Each unit vector is defined as the y-axis of corresponding segment. The direction of the unit vectors is based on the defined segment frame and is roughly in the direction of the green arrow. In the middle, ulnar side of the hand flat on a box for several seconds (static pose). The unit vectors are determined by means of acceleration recordings at the hand, middle- and index finger. Each unit vector is defined as the x-axis of corresponding segment. The direction of the unit vectors is based on the defined segment frame and is roughly in the direction of the red arrow. On the right side, thumb sideways flat for several seconds (static pose). The unit vector is defined as the x-axis of the thumb, with its direction based on the defined segment frame, which is roughly in the direction of the green arrow. Notice that the defined direction is opposite of the direction of gravity.

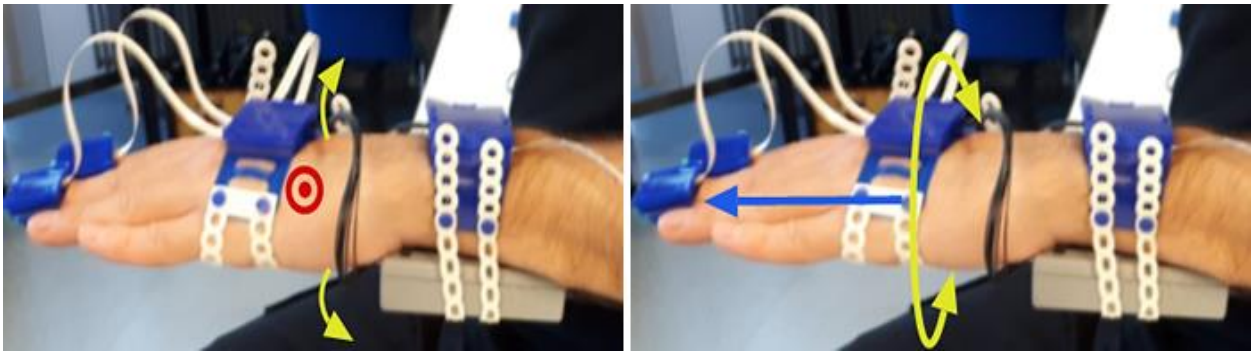

Figure A.4: On the left side, three times flexion and extension of the wrist. The unit vectors are determined by means of least squares regression fitting and normalization of the gyroscope recordings at the hand, middle- and index finger. Each unit vector is defined as the x-axis of corresponding segment. The direction of the unit vectors is based on the defined segment frame and is roughly in the direction of the red dot (red dot means that the direction of the unit vectors is towards the reader). On the right side, three times pronation and supination of the forearm. The unit vectors are determined by means of the gyroscope recordings at the forearm, the hand, the middle- and index finger. Each unit vector is defined as the z-axis of corresponding segment. The direction of the unit vectors is based on the defined segment frame and is roughly in the direction of the blue arrow.

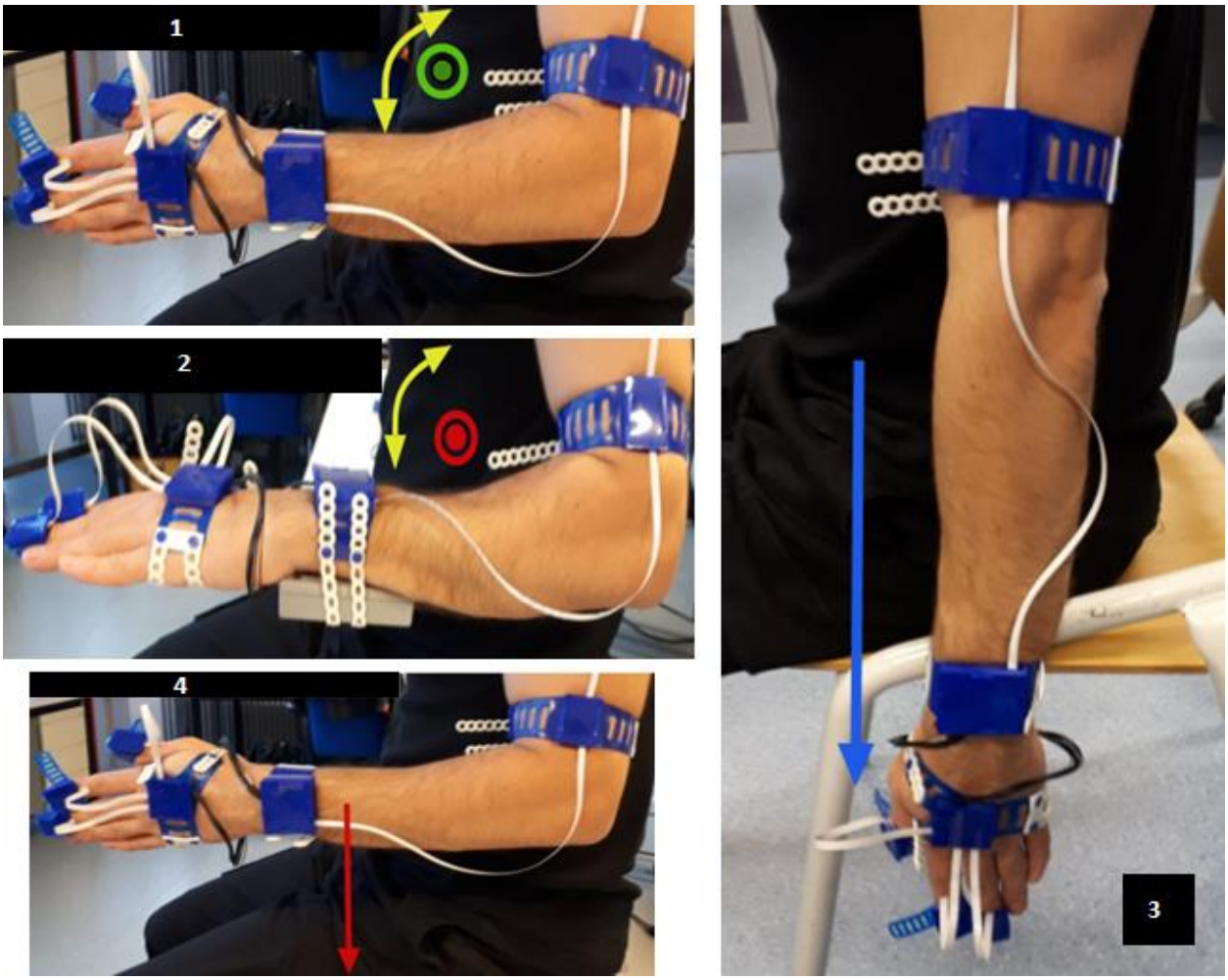

Figure A.5: Number one, three times elbow flexion and extension with the hand in mid position of pronation and supination. The unit vectors are determined by means of least squares regression fitting and normalization of the gyroscope recordings at the lower arm, the hand, middle- and index finger. Each unit vector is defined as the y-axis of corresponding segment. The direction of the unit vectors is based on the defined segment frame and is roughly in the direction of the green dot (green dot means that the direction of the unit vectors is towards the reader). Number two, three times elbow flexion and extension with the forearm pronated. The unit vectors are determined by means the gyroscope recordings at the lower arm, the hand, middle- and index finger. Each unit vector is defined as the x-axis of corresponding segment. The direction of the unit vectors is based on the defined segment frame and is roughly in the direction of the red dot. Number three, static pose of the forearm aligned in the direction of gravity with the elbow fully extended for several seconds. The unit vector of the upper arm, the forearm, the hand, the thumb, the middle- and index finger is determined by means of acceleration recordings. Each unit vector is defined as the z-axis of corresponding segment. The direction of the unit vectors is based on the defined segment frame and is roughly in the direction of the blue arrow. Number four, static pose of the forearm in mid-position of pronation and supination with the elbow kept in 90° flexion. The unit vector of the forearm, the hand, the middle- and index finger is determined by means of acceleration recordings. Each unit vector is defined as the x-axis of corresponding segment. The direction of the unit vectors is based on the defined segment frame and is roughly in the direction of the red arrow. Moreover, the unit vector of the upper arm could also be determined, but additional shoulder adduction might be necessary for better alignment with the direction of gravity. Therefore, the unit vector of the upper arm is calibrated separately.

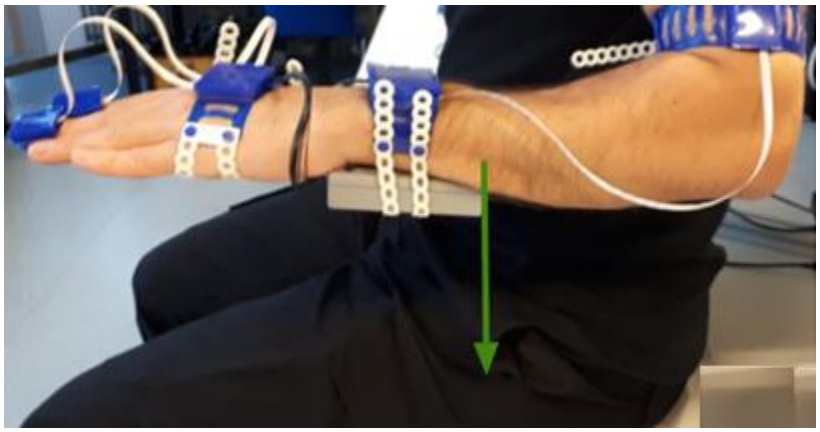

Figure A.6: static pose of the forearm fully pronated, and the elbow kept in 90° flexion. The unit vectors are determined by means of least squares regression fitting and normalization of the acceleration recordings at the forearm, the hand, the middle- and index finger. Each unit vector is defined as the y-axis of corresponding segment. The direction of the unit vectors is based on the defined segment frame and is roughly in the direction of the green arrow. Moreover, the unit vector of the upper arm could also be determined, but additional shoulder adduction might be necessary for better alignment with the direction of gravity. Therefore, the unit vector of the upper arm is calibrated separately.

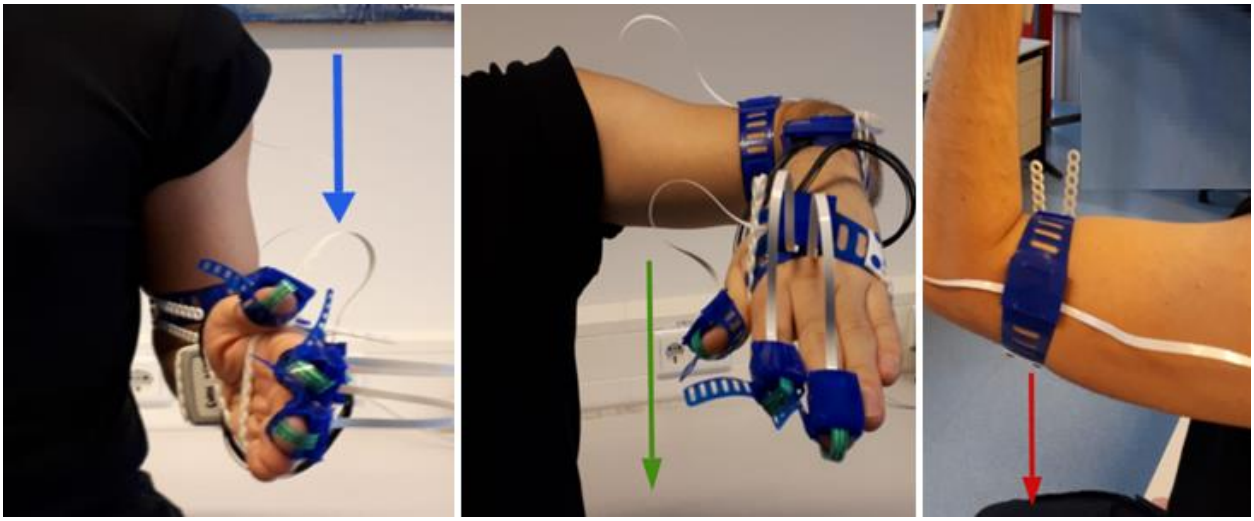

Figure A.7: From left to right: Static pose of the upper arm aligned with gravity while the elbow 90° flexed (inclination). Subject might adduct the shoulder for better alignment; Static pose of the upper arm while the elbow is 90° flexed and the shoulder 90° abducted; and Static pose of the upper arm while the elbow and shoulder are 90° flexed. During each movement the unit vector is determined by means of least squares regression fitting and normalization of the acceleration recordings at the upper arm. During the calibration movement depicted at the left side, the unit vector is defined as the z-axis of the upper arm, while during the calibrations depicted in the middle and the right side, the unit vector is defined as the y-axis respectively x-axis of the upper arm. The direction of the upper arm unit vector is in accordance with the defined segment frame and is roughly in the direction of the blue, green and red arrow during corresponding calibration movement.

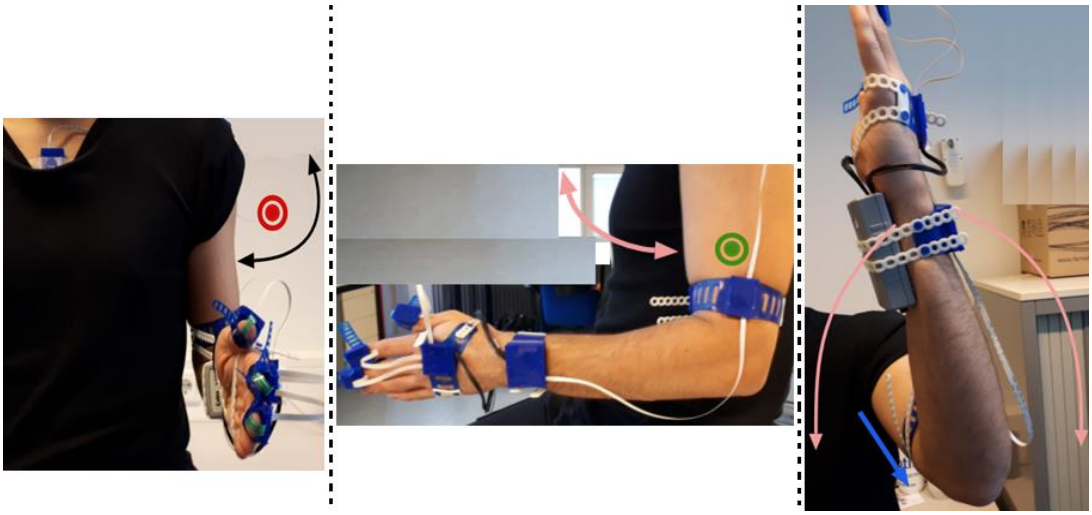

Figure A.8: From left to right: Three times shoulder abduction and adduction with the elbow 90° flexed; Three times shoulder flexion and extension with the elbow 90° flexed; and Three times shoulder internal and external rotation with the shoulder and elbow kept in 90° flexed pose. During each movement the unit vector is determined by means of least squares regression fitting and normalization of the gyroscope recordings at the upper arm. During the calibration movement depicted at the left side, the unit vector is defined as the x-axis of the upper arm, while during the calibrations depicted in the middle and the right side, the unit vector is defined as the y-axis respectively z-axis of the upper arm. The direction of the upper arm unit vector is in accordance with the defined segment frame and is roughly in the direction of the red dot, the green dot and blue arrow during corresponding calibration movement. A dot means that the direction of the unit vectors is towards the reader

Figure A.9: From left to right: Subject in neutral pose (N-pose); Static pose standing trunk flexion (90°); and Static pose standing trunk lateral flexion (approximately 35°, left side). During each movement the unit vector is determined by means of least squares regression fitting and normalization of the acceleration recordings at the shoulder and sternum. During the calibration movement depicted at the left side, each unit vector is defined as the z-axis of the corresponding segment (shoulder or sternum), while during the calibrations depicted in the middle and the right side, each unit vector is defined as the x-axis respectively y-axis of the corresponding segment. The direction of the unit vectors is in accordance with the defined segment frame and is roughly in the direction of the blue, red and green arrow during corresponding calibration movement.

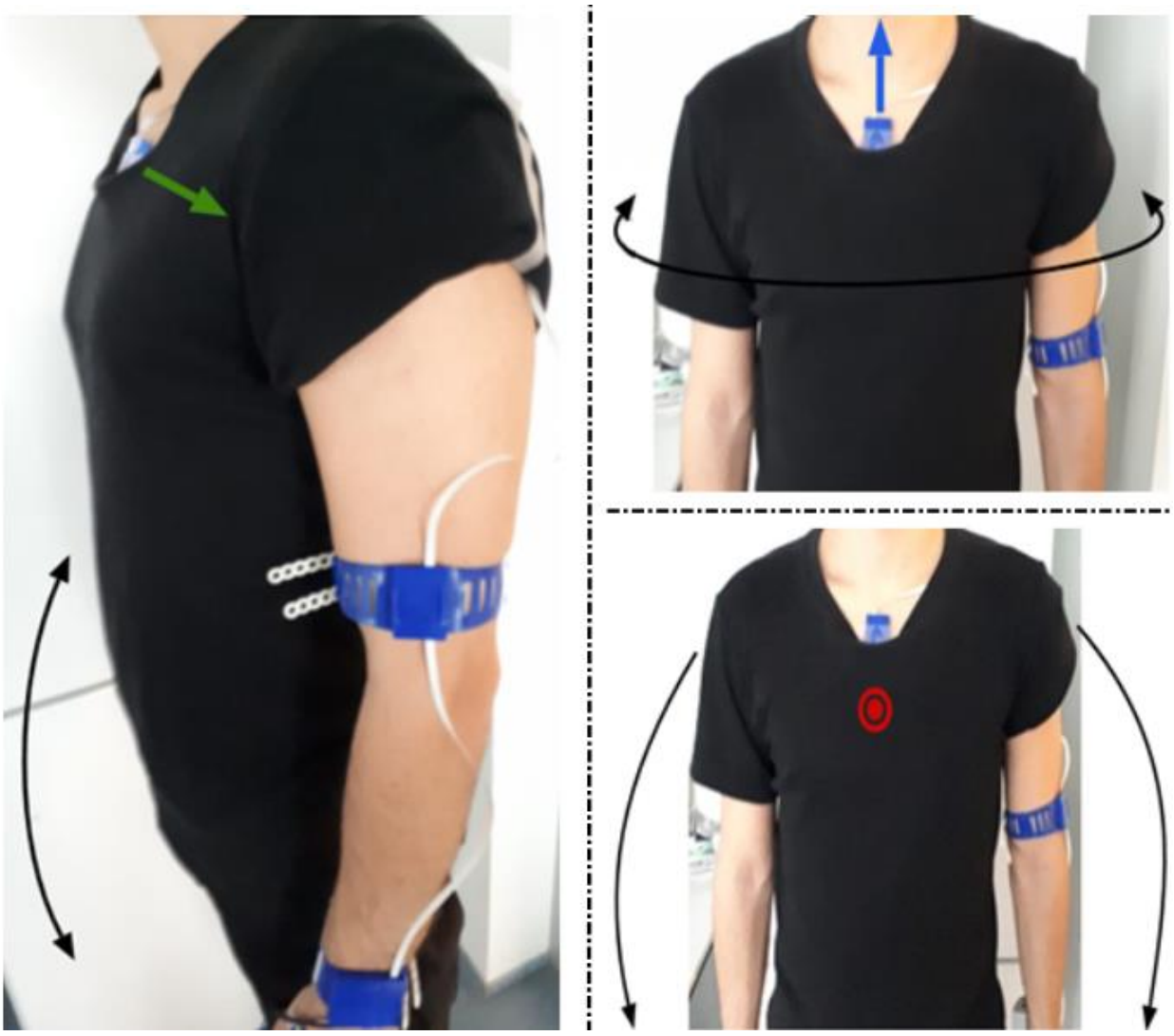

Figure A.10Three times trunk flexion and extension (left); Three times trunk ipsilateral and contralateral rotation (top right); Three-time lateral trunk rotation (bottom right). During each movement the unit vector is determined by means of least squares regression fitting and normalization of the gyroscope recordings at the shoulder and sternum. During the calibration movement depicted at the left side, each unit vector is defined as the y-axis of the corresponding segment (shoulder or sternum), while during the calibrations depicted in the top right and the bottom right, each unit vector is defined as the z-axis respectively x-axis of the corresponding segment. The direction of the unit vectors is in accordance with the defined segment frame and is roughly in the direction of the green arrow, blue arrow and red dot during corresponding calibration movement. A dot means that the direction of the unit vectors is towards the reader

	Description
Calib #1	Middle and index finger flat for several seconds
Calib #2	Repeated flexion of the index and middle finger
Calib #5	Palmar side of the hand flat
Calib #6	Ulnar side of the hand flat
Calib #8	Repeated wrist flexion/extension
Calib #9	Repeated forearm pronation/supination
Calib #10	Repeated elbow flexion (forearm in midposition)
Calib #11	Repeated elbow flexion (forearm pronated)
Calib #12	Static pose forearm aligned with gravity
Calib #13	Static pose elbow flexed with forearm in midposition
Calib #14	Static pose elbow flexed with forearm pronated

	VAF_index x_acc	VAF_index y_acc	VAF_index z_acc	VAF_index x_gyr	VAF_index y_gyr	VAF_index z_gyr
Calib #1	NA	0.1722	NA	NA	NA	NA
Calib #2	NA	NA	NA	0.1329	NA	NA
Calib #5	NA	0.1937	NA	NA	NA	NA
Calib #6	0.1828	NA	NA	NA	NA	NA
Calib #8	NA	NA	NA	0.2410	NA	NA
Calib #9	NA	NA	NA	NA	NA	0.1496
Calib #10	NA	NA	NA	NA	-0.0300	NA
Calib #11	NA	NA	NA	0.1319	NA	NA
Calib #12	NA	NA	0.1573	NA	NA	NA
Calib #13	0.1849	NA	NA	NA	NA	NA
Calib #14	NA	0.1703	NA	NA	NA	NA

	Index finger x_acc	Index finger y_acc	Index finger z_acc	Index finger x_gyr	Index finger y_gyr	Index finger z_gyr	VAF
Index finger x_acc	0	X	X	X	X	X	0.1849
Index finger y_acc	74.0068	0	X	X	X	X	0.1937
Index finger z_acc	88.5883	93.3181	0	X	X	X	0.1573
Index finger x_gyr	19.2372	89.9500	76.6930	0	X	X	0.2410
Index finger y_gyr	78.5531	7.5105	99.5259	95.4702	0	X	-0.0300
Index finger z_gyr	90.4067	80.0994	14.3948	82.4938	85.8996	0	0.1496

Figure A.11: Description of the calibration movements regarding the index finger (Miller et al.). Based on the variance accounted for (VAF), the best six movements are pre-selected (middle), so that the optimal two movements can be determined as a final selection based on their mutual angle (bottom). In this case, the sensor-to-segment calibration procedure regarding the index finger is optimal when the subject placed the palmar side of the hand flat on a table (calibration #5) and when the wrist was flexed and extended repeatedly (calibration #8).

	Description
Calib #1	Middle and index finger flat for several seconds
Calib #2	Repeated flexion of the index and middle finger
Calib #5	Palmar side of the hand flat
Calib #6	Ulnar side of the hand flat
Calib #8	Repeated wrist flexion/extension
Calib #9	Repeated forearm pronation/supination
Calib #10	Repeated elbow flexion (forearm in midposition)
Calib #11	Repeated elbow flexion (forearm pronated)
Calib #12	Static pose forearm aligned with gravity
Calib #13	Static pose elbow flexed with forearm in midposition
Calib #14	Static pose elbow flexed with forearm pronated

	VAF_middle x_acc	VAF_middle y_acc	VAF_middle z_acc	VAF_middle x_gyr	VAF_middle y_gyr	VAF_middle z_gyr
Calib #1	NA	0.1701	NA	NA	NA	NA
Calib #2	NA	NA	NA	0.1138	NA	NA
Calib #5	NA	0.1915	NA	NA	NA	NA
Calib #6	0.1809	NA	NA	NA	NA	NA
Calib #8	NA	NA	NA	0.2620	NA	NA
Calib #9	NA	NA	NA	NA	NA	0.1485
Calib #10	NA	NA	NA	NA	-0.0230	NA
Calib #11	NA	NA	NA	0.0803	NA	NA
Calib #12	NA	NA	0.1567	NA	NA	NA
Calib #13	0.1832	NA	NA	NA	NA	NA
Calib #14	NA	0.1673	NA	NA	NA	NA

	Middle finger x_acc	Middle finger y_acc	Middle finger z_acc	Middle finger x_gyr	Middle finger y_gyr	Middle finger z_gyr	VAF
Middle finger x_acc	0	X	X	X	X	X	0.1832
Middle finger y_acc	76.6952	0	X	X	X	X	0.1915
Middle finger z_acc	89.1767	103.8060	0	X	X	X	0.1567
Middle finger x_gyr	18.6699	95.0413	81.3489	0	X	X	0.2620
Middle finger y_gyr	76.3588	0.3652	103.9230	94.7142	0	X	-0.0230
Middle finger z_gyr	87.4511	83.4806	20.5597	86.0477	83.6166	0	0.1485

Figure A.12: Description of the calibration movements regarding the middle finger (Miller et al.). Based on the variance accounted for (VAF), the best six movements are pre-selected (middle), so that the optimal two movements can be determined as a final selection based on their mutual angle (bottom). In this case, the sensor-to-segment calibration procedure regarding the middle finger is optimal when the subject kept the forearm aligned in the direction of gravity for several seconds (calibration #12) and when the subject kept the elbow flexed for several seconds with the forearm in the mid position of pronation and supination (calibration #13).

	Description
Calib #3	Thumb flat
Calib #4	Repeated thumb flexion
Calib #7	Thumb sideways in static pose on table
Calib #12	Static pose forearm aligned with gravity

	VAF_thumb x_acc	VAF_thumb y_acc	VAF_thumb z_acc	VAF_thumb y_gyr
Calib #3	0.1859	NA	NA	NA
Calib #4	NA	NA	NA	0.1291
Calib #7	NA	0.1878	NA	NA
Calib #12	NA	NA	0.1677	NA

	Thumb x_acc	Thumb y_acc	Thumb z_acc	Thumb y_gyr	VAF
Thumb x_acc	0	X	X	X	0.1859
Thumb y_acc	82.9635	0	X	X	0.1878
Thumb z_acc	63.6481	80.9638	0	X	0.1677
Thumb y_gyr	86.1736	7.4420	76.3228	0	0.1291

Figure A.13: Description of the calibration movements regarding the thumb (Miller et al.). Based on the variance accounted for (VAF), the best four movements are pre-selected (middle), so that the optimal two movements can be determined as a final selection based on their mutual angle (bottom). In this case, the sensor-to-segment calibration procedure regarding the thumb is optimal when the subject placed the thumb flat on a table (calibration #3) and when thumb was flexed repeatedly (calibration #4).

	Description
Calib #5	Palmar side of the hand flat
Calib #6	Ulnar side of the hand flat
Calib #8	Repeated wrist flexion/extension
Calib #9	Repeated forearm pronation/supination
Calib #10	Repeated elbow flexion (forearm in midposition)
Calib #11	Repeated elbow flexion (forearm pronated)
Calib #12	Static pose forearm aligned with gravity
Calib #13	Static pose elbow flexed with forearm in midposition
Calib #14	Static pose elbow flexed with forearm pronated

	VAF_hand x_acc	VAF_hand y_acc	VAF_hand z_acc	VAF_hand x_gyr	VAF_hand y_gyr	VAF_hand z_gyr
Calib #5	NA	0.1923	NA	NA	NA	NA
Calib #6	0.1846	NA	NA	NA	NA	NA
Calib #8	NA	NA	NA	0.2500	NA	NA
Calib #9	NA	NA	NA	NA	NA	0.1490
Calib #10	NA	NA	NA	NA	-0.0229	NA
Calib #11	NA	NA	NA	0.1435	NA	NA
Calib #12	NA	NA	0.1597	NA	NA	NA
Calib #13	0.1870	NA	NA	NA	NA	NA
Calib #14	NA	0.1691	NA	NA	NA	NA

	Hand x_acc	Hand y_acc	Hand z_acc	Hand x_gyr	Hand y_gyr	Hand z_gyr	VAF
Hand x_acc	0	X	X	X	X	X	0.1870
Hand y_acc	76.9668	0	X	X	X	X	0.1923
Hand z_acc	87.0120	65.7034	0	X	X	X	0.1597
Hand x_gyr	19.5403	85.5613	74.3761	0	X	X	0.2500
Hand y_gyr	82.9998	13.8279	78.1170	94.9104	0	X	-0.0229
Hand z_gyr	90.3336	73.0239	7.5086	75.9372	85.1991	0	0.1490

Figure A.14: Description of the calibration movements regarding the hand (Miller et al.). Based on the variance accounted for (VAF), the best six movements are pre-selected (middle), so that the optimal two movements can be determined as a final selection based on their mutual angle (bottom). In this case, the sensor-to-segment calibration procedure regarding the hand is optimal when the subject repeatedly pronated and supinated the forearm (calibration #9) and when the subject kept the elbow flexed for several seconds with the forearm in the mid position of pronation and supination (calibration #13).

	Description
Calib #12	Static pose forearm aligned with gravity
Calib #15	Static pose upper arm aligned with gravity with the elbow flexed. Subject might adduct the shoulder for better alignment
Calib #16	Static pose of the upper arm with the shoulder abduction and elbow flexed
Calib #17	Static pose of the upper arm with shoulder and elbow flexed
Calib #18	Repeated shoulder abduction with elbow flexed
Calib #19	Repeated shoulder flexion with elbow flexed
Calib #20	Repeated shoulder internal and external rotation with shoulder and elbow flexed (90 deg static)

	VAF_upper arm x_acc	VAF_upper arm y_acc	VAF_upper arm z_acc	VAF_upper arm x_gyr	VAF_upper arm y_gyr	VAF_upper arm z_gyr
Calib #12	NA	NA	0.1586	NA	NA	NA
Calib #15	NA	NA	0.1867	NA	NA	NA
Calib #16	NA	0.1814	NA	NA	NA	NA
Calib #17	0.1836	NA	NA	NA	NA	NA
Calib #18	NA	NA	NA	-1.8399	NA	NA
Calib #19	NA	NA	NA	NA	-1.0153	NA
Calib #20	NA	NA	NA	NA	NA	-6.0652

	Upper arm x_acc	Upper arm y_acc	Upper arm z_acc	Upper arm x_gyr	Upper arm y_gyr	Upper arm z_gyr	VAF
Upper arm x_acc	0	X	X	X	X	X	0.1836
Upper arm y_acc	67.6853	0	X	X	X	X	0.1814
Upper arm z_acc	72.5964	72.7478	0	X	X	X	0.1867
Upper arm x_gyr	22.4634	75.5393	94.9902	0	X	X	-1.8399
Upper arm y_gyr	92.0919	24.4834	81.1215	97.4855	0	X	-1.0153
Upper arm z_gyr	74.6824	80.0558	7.3185	96.6827	87.9815	0	-6.0652

Figure A.15: Description of the calibration movements regarding the upper arm (Miller et al.). Based on the variance accounted for (VAF), the best six movements are pre-selected (middle), so that the optimal two movements can be determined as a final selection based on their mutual angle (bottom). In this case, the sensor-to-segment calibration procedure regarding the upper arm is optimal when the subject kept the upper arm in a static pose with the shoulder abducted and the elbow flexed (calibration #17), and when the subject repeatedly flexed the shoulder with the elbow kept in a flexed position (calibration #19).

	Description
Calib #21	Subject in neutral pose (N-pose)
Calib #22	Static pose trunk flexion 90 deg
Calib #23	Static pose trunk lateral flexion
Calib #24	Repeated trunk flexion
Calib #25	Repeated trunk contralateral rotation
Calib #26	Repeated lateral trunk rotation

	VAF_shoulder x_acc	VAF_shoulder y_acc	VAF_shoulder z_acc	VAF_shoulder x_gyr	VAF_shoulder y_gyr	VAF_shoulder z_gyr
Calib #21	NA	NA	0.1746	NA	NA	NA
Calib #22	0.1680	NA	NA	NA	NA	NA
Calib #23	NA	0.1829	NA	NA	NA	NA
Calib #24	NA	NA	NA	NA	-5.4836	NA
Calib #25	NA	NA	NA	NA	NA	-3.5667
Calib #26	NA	NA	NA	-6.2487	NA	NA

	Shoulder x_acc	Shoulder y_acc	Shoulder z_acc	Shoulder x_gyr	Shoulder y_gyr	Shoulder z_gyr	VAF
Shoulder x_acc	0	X	X	X	X	X	0.1680
Shoulder y_acc	92.3249	0	X	X	X	X	0.1829
Shoulder z_acc	101.9031	56.5713	0	X	X	X	0.1746
Shoulder x_gyr	4.8870	96.2171	106.5133	0	X	X	-6.2487
Shoulder y_gyr	89.5996	32.0623	88.3697	91.3449	0	X	-5.4836
Shoulder z_gyr	99.7129	52.2610	4.6820	104.4313	84.1901	0	-3.5667

Figure A.16: Description of the calibration movements regarding the shoulder (Miller et al.). Based on the variance accounted for (VAF), the best six movements are pre-selected (middle), so that the optimal two movements can be determined as a final selection based on their mutual angle (bottom). In this case, the sensor-to-segment calibration procedure regarding the shoulder is optimal when the subject flexed the trunk and kept this pose for several seconds (calibration #22), and when the subject repeatedly flexed the trunk (calibration #24).

	Description
Calib #21	Subject in neutral pose (N-pose)
Calib #22	Static pose trunk flexion 90 deg
Calib #23	Static pose trunk lateral flexion
Calib #24	Repeated trunk flexion
Calib #25	Repeated trunk contralateral rotation
Calib #26	Repeated lateral trunk rotation

	VAF_sternum x_acc	VAF_sternum y_acc	VAF_sternum z_acc	VAF_sternum x_gyr	VAF_sternum y_gyr	VAF_sternum z_gyr
Calib #21	NA	NA	0.1688	NA	NA	NA
Calib #22	0.1675	NA	NA	NA	NA	NA
Calib #23	NA	0.1817	NA	NA	NA	NA
Calib #24	NA	NA	NA	NA	-5.6137	NA
Calib #25	NA	NA	NA	NA	NA	-3.4378
Calib #26	NA	NA	NA	-6.2799	NA	NA

	Sternum x_acc	Sternum y_acc	Sternum z_acc	Sternum x_gyr	Sternum y_gyr	Sternum z_gyr	VAF
Sternum x_acc	0	X	X	X	X	X	0.1675
Sternum y_acc	95.3620	0	X	X	X	X	0.1817
Sternum z_acc	100.7719	53.2272	0	X	X	X	0.1688
Sternum x_gyr	3.0594	93.0448	97.7866	0	X	X	-6.2799
Sternum y_gyr	90.7332	35.7464	88.9310	90.0107	0	X	-5.6137
Sternum z_gyr	103.4212	50.7070	3.7450	100.4076	86.2737	0	-3.4378

Figure A.17: Description of the calibration movements regarding the sternum (Miller et al.). Based on the variance accounted for (VAF), the best six movements are pre-selected (middle), so that the optimal two movements can be determined as a final selection based on their mutual angle (bottom). In this case, the sensor-to-segment calibration procedure regarding the sternum is optimal when the subject repeatedly flexed the trunk (calibration #24), and when the subject repeatedly performed a lateral trunk rotation (calibration #26).

APPENDIX B MOVEMENT WITHIN SYNERGIES

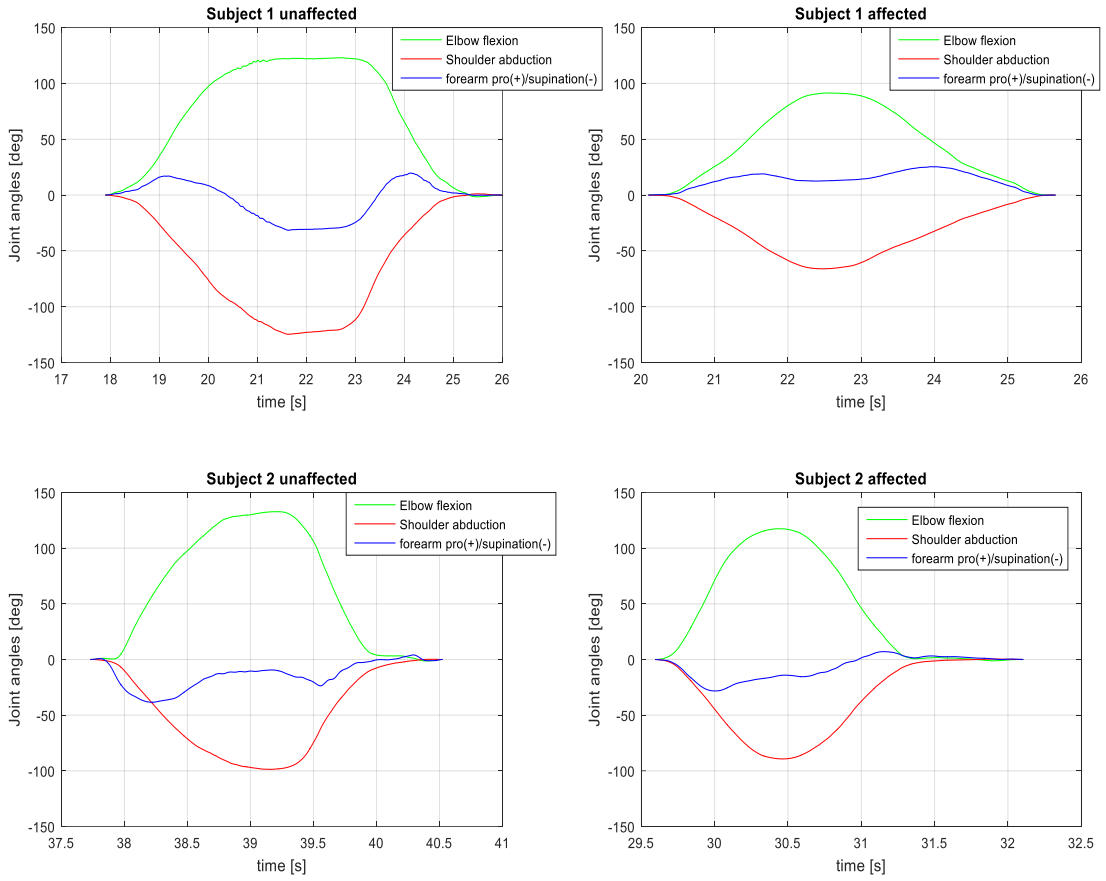

Joint angles of the first and second subject during the first trial regarding the flexor synergy.

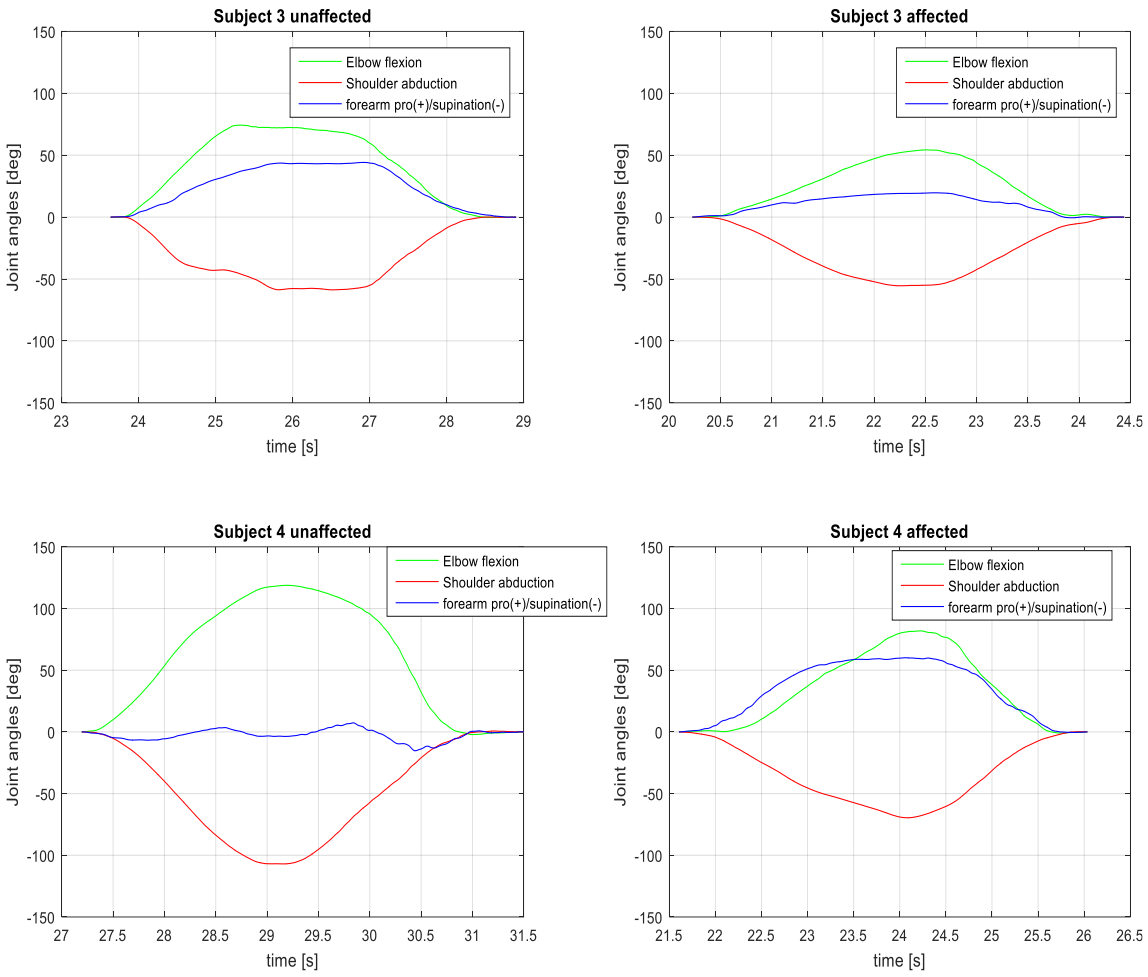

Joint angles of the third and fourth subject during the first trial regarding the flexor synergy.

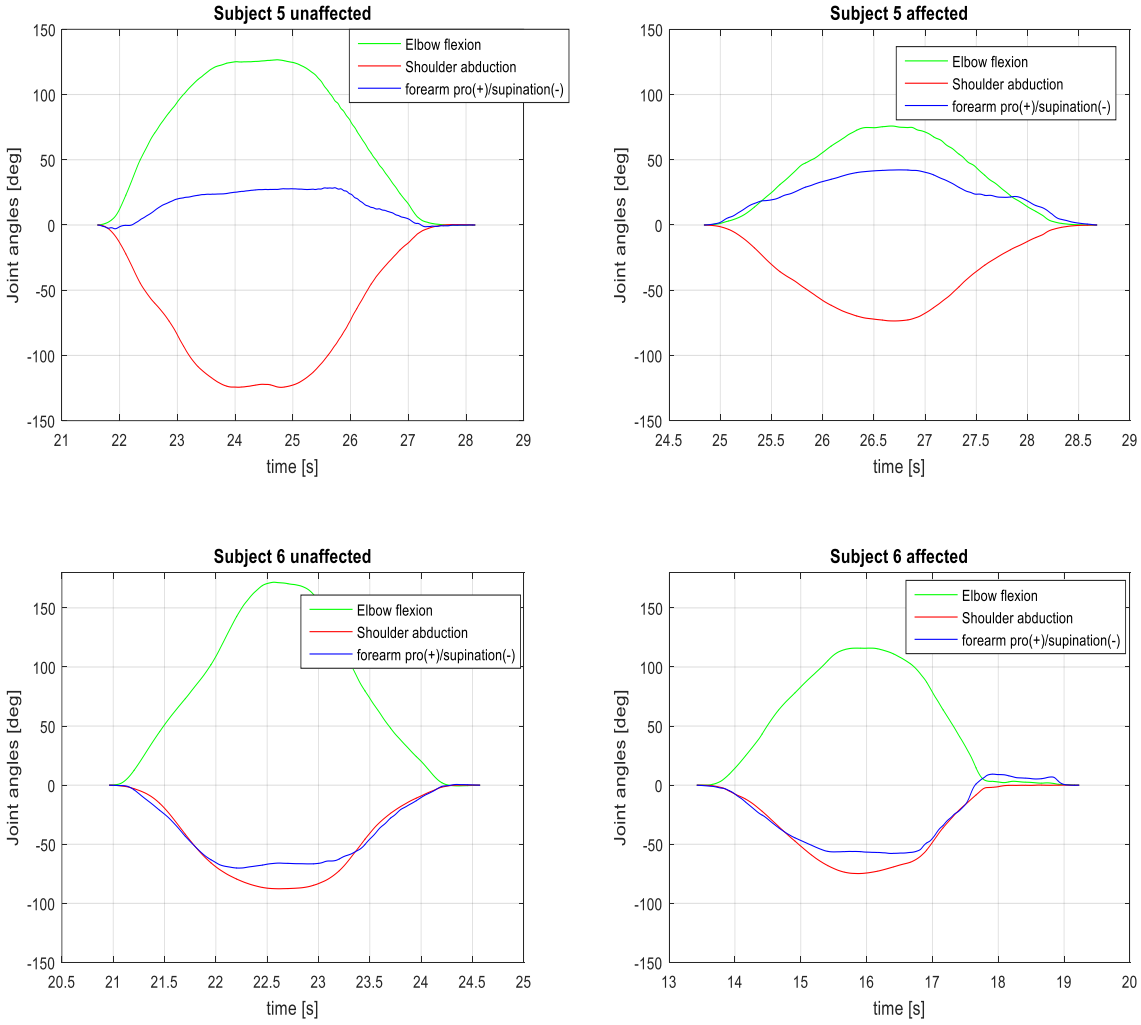

Joint angles of the fifth and sixth subject during the first trial regarding the flexor synergy.

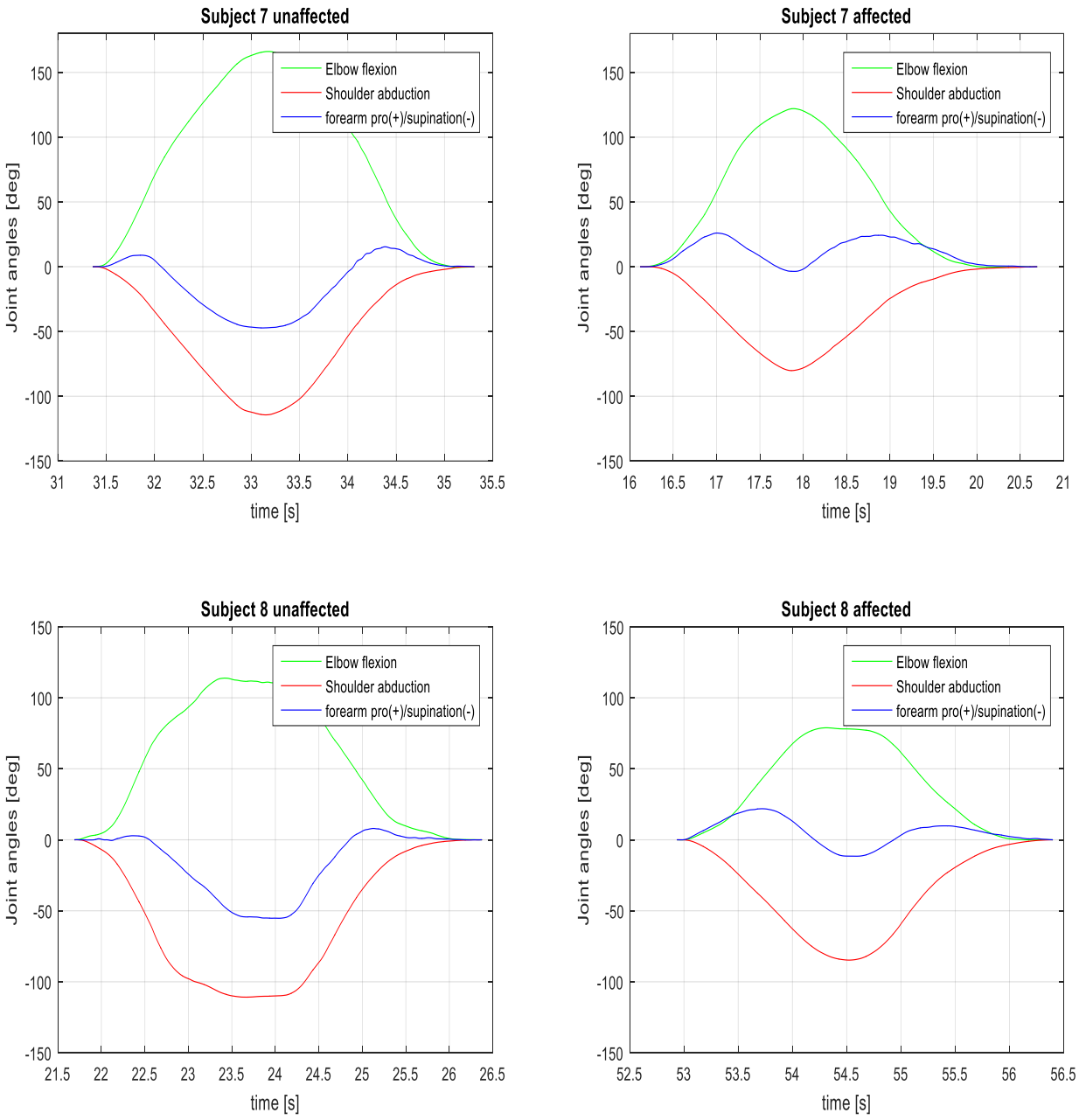

Joint angles of the seventh and eighth subject during the first trial regarding the flexor synergy.

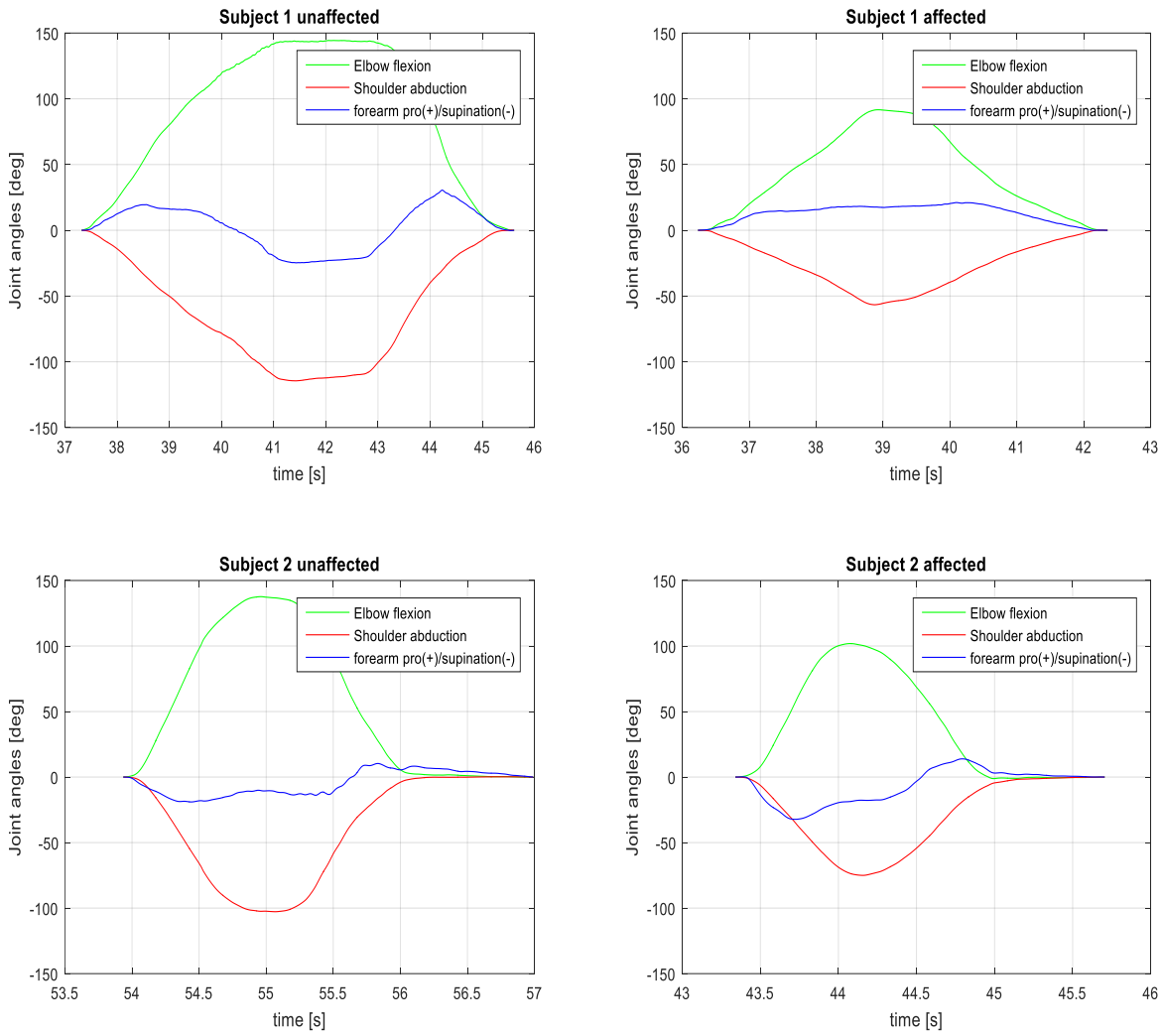

Joint angles of the first and second subject during the second trial regarding the flexor synergy.

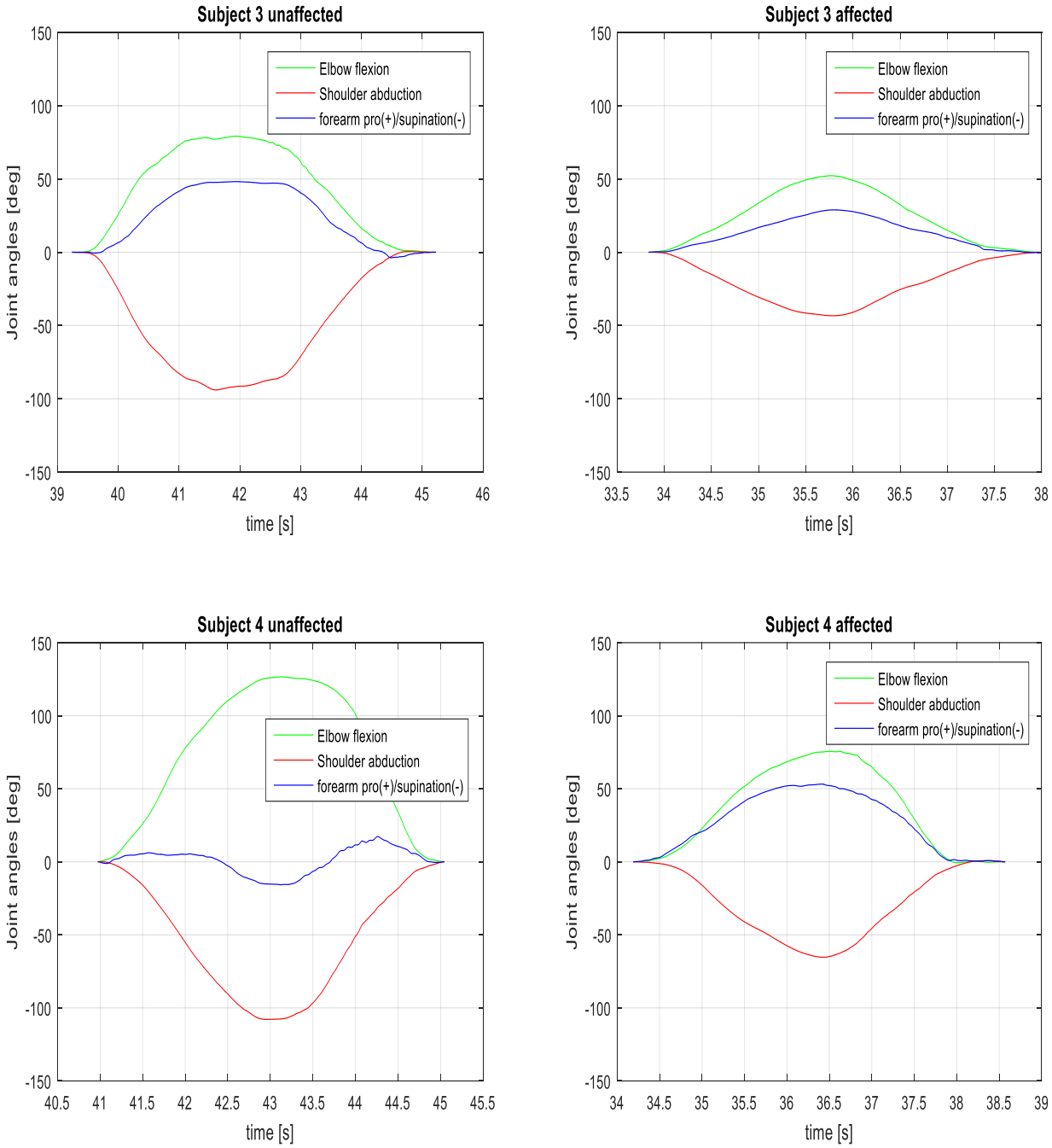

Joint angles of the third and fourth subject during the second trial regarding the flexor synergy.

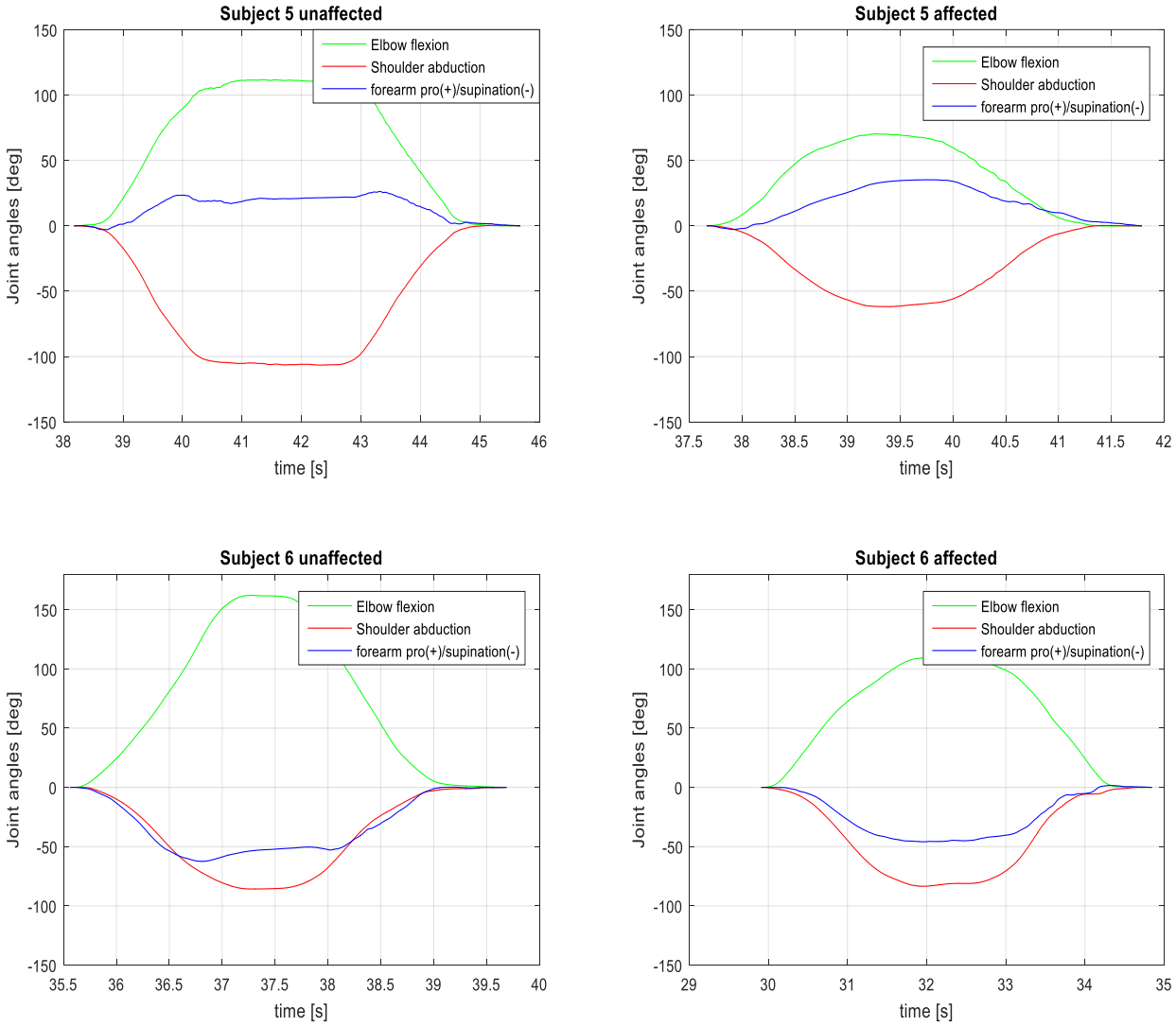

Joint angles of the fifth and sixth subject during the second trial regarding the flexor synergy.

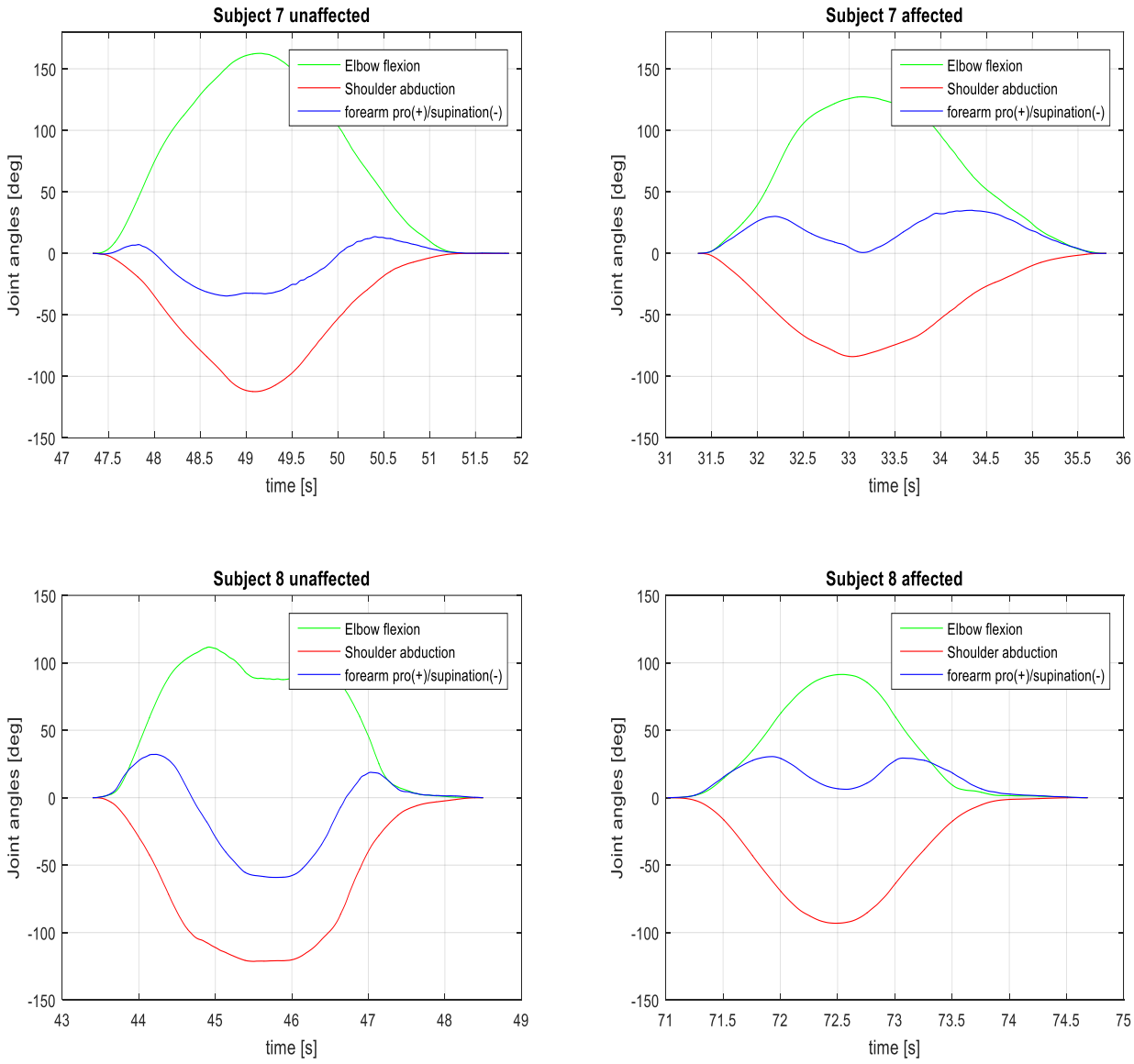

Joint angles of the seventh and eighth subject during the second trial regarding the flexor synergy.

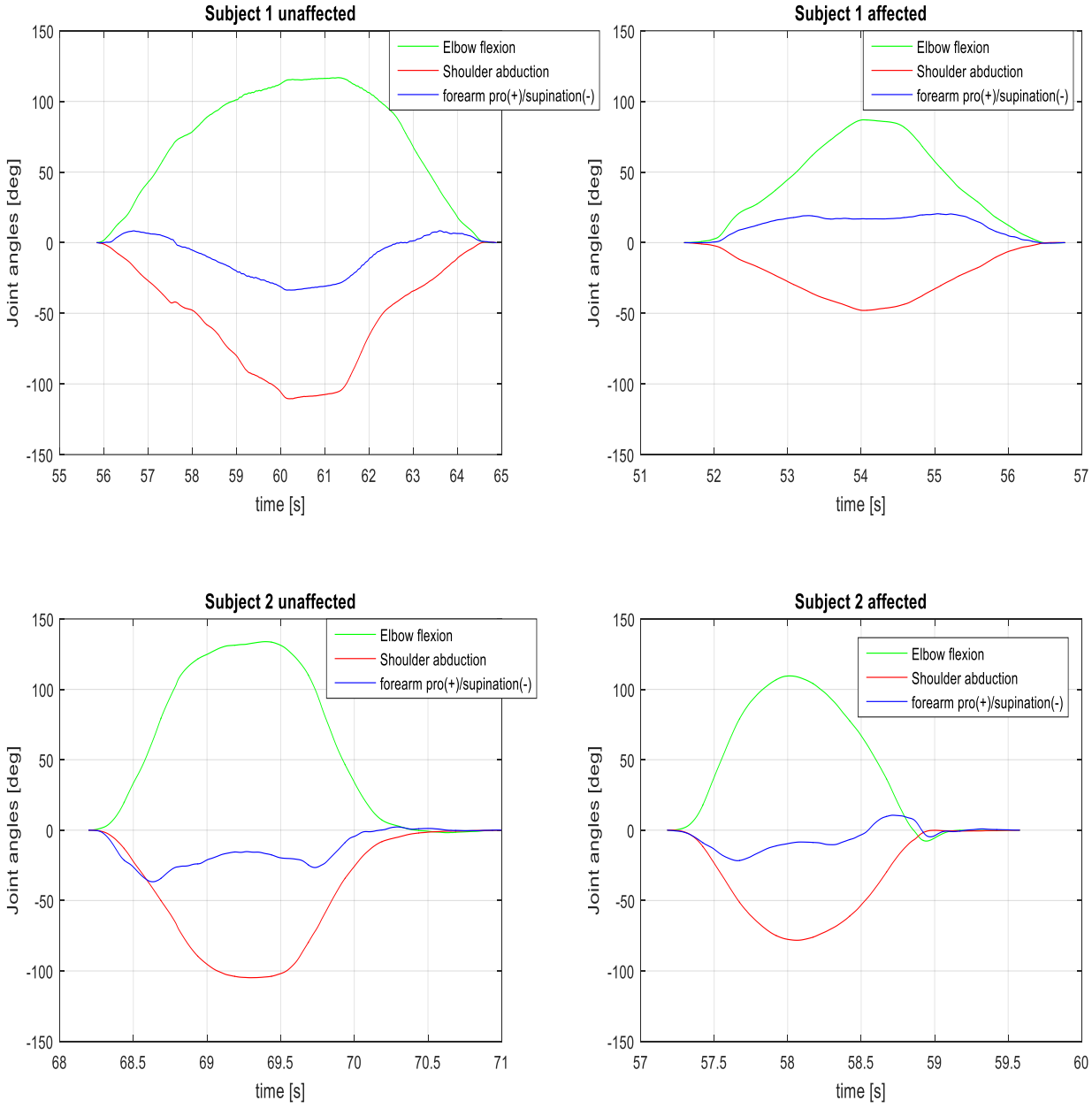

Joint angles of the first and second subject during the third trial regarding the flexor synergy.

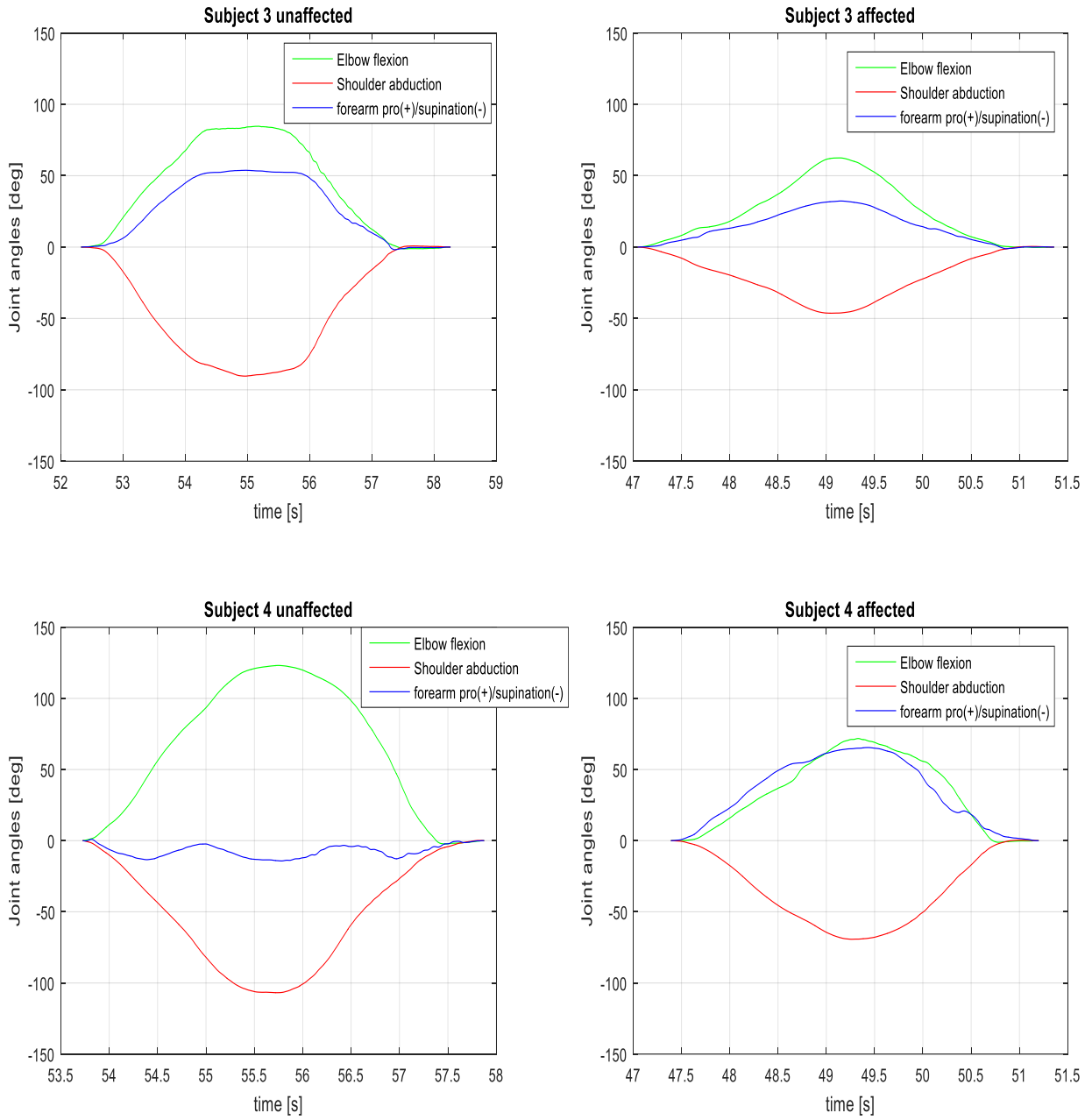

Joint angles of the third and fourth subject during the third trial regarding the flexor synergy.

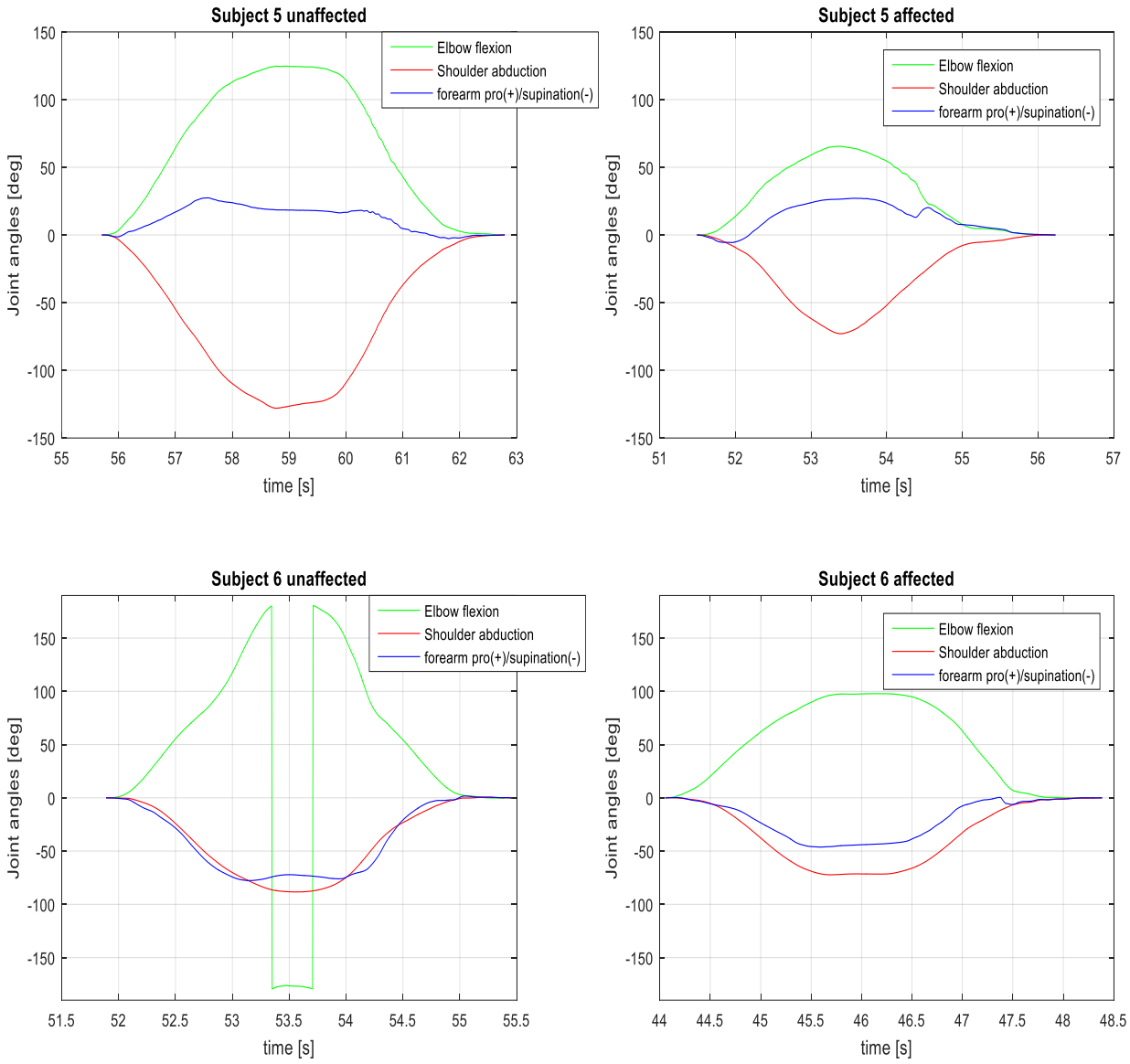

Joint angles of the fifth and sixth subject during the third trial regarding the flexor synergy.

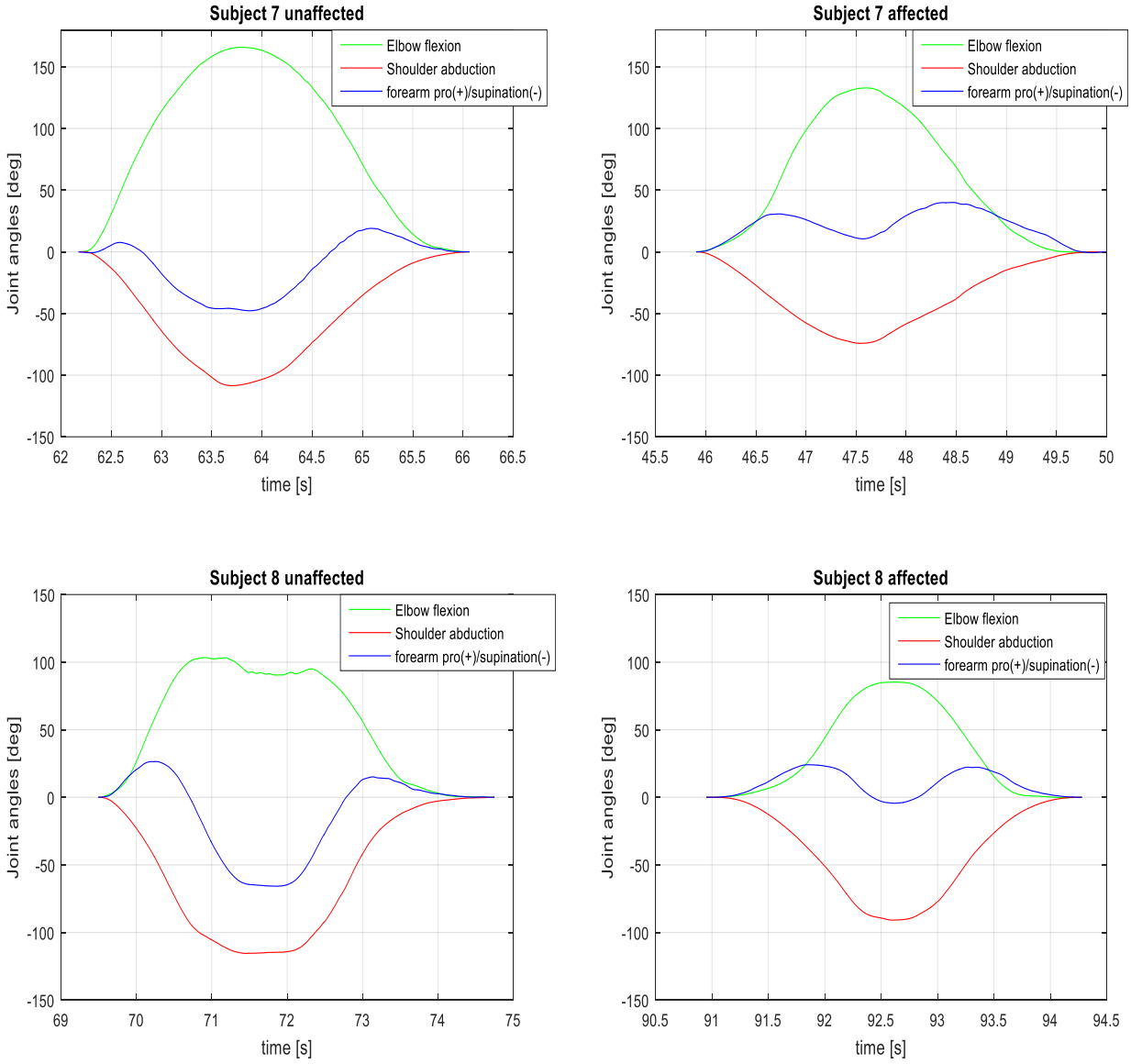

Joint angles of the seventh and eighth subject during the third trial regarding the flexor synergy.

Biceps, triceps lateral head and triceps long head activity averaged over the three trials are tabled with corresponding standard deviation (SD) regarding pathologically unaffected and mimicked pathologically affected movements for all subjects. Values are expressed in millivolt.

	MUSCLE ACTIVITY (SD) [mV]					
	Bi		Tri (lat)		Tri (long)	
	Unaffected	Affected	Unaffected	Affected	Unaffected	Affected
Subject 1	0.1091(0.0173)	0.0084(0.0011)	0.0597(0.0027)	0.0210(0.0014)	0.0310(0.0047)	0.0097(0.0011)
Subject 2	0.0330(0.0060)	0.0195(0.0026)	0.0509(0.0036)	0.0429(0.0035)	0.0125(0.0010)	0.0111(0.0022)
Subject 3	0.0299(0.0039)	0.0084(0.0010)	0.0292(0.0062)	0.0105(0.0016)	0.0123(0.0026)	0.0071(0.0011)
Subject 4	0.0380(0.0090)	0.0303(0.0021)	0.0427(0.0022)	0.0248(0.0011)	0.0427(0.0063)	0.0221(0.0010)
Subject 5	0.0361(0.0101)	0.0216(0.0054)	0.0653(0.0049)	0.0194(0.0011)	0.0280(0.0006)	0.0113(0.0013)
Subject 6	0.0406(0.0057)	0.0208(0.0022)	0.0158(0.0013)	0.0154(0.0030)	0.0114(0.0011)	0.0107(0.0012)
Subject 7	0.0563(0.0126)	0.0208(0.0061)	0.0487(0.0060)	0.0336(0.0071)	0.0225(0.0032)	0.0176(0.0037)
Subject 8	0.0144(0.0009)	0.0124(0.0013)	0.0556(0.0032)	0.0396(0.0033)	0.0164(0.0052)	0.0120(0.0013)

Deltoideus medial and deltoideus anterior activity averaged over the three trials are tabled with corresponding standard deviation (SD) regarding pathologically unaffected and mimicked pathologically affected movements for all subjects. Values are expressed in millivolt.

	MUSCLE ACTIVITY (SD) [mV]			
	DM		DA	
	Unaffected	**Affected**	**Unaffected**	**Affected**
Subject 1	0.0731(0.0090)	0.0366(0.0016)	0.1172(0.0262)	0.0554(0.0057)
Subject 2	0.0405(0.0031)	0.0406(0.0035)	0.0716(0.0050)	0.0545(0.0038)
Subject 3	0.0290(0.0057)	0.0172(0.0025)	0.0485(0.0086)	0.0161(0.0047)
Subject 4	0.0837(0.0023)	0.0733(0.0046)	0.0368(0.0045)	0.0264(0.0036)
Subject 5	0.0984(0.0085)	0.0313(0.0011)	0.0316(0.0047)	0.0126(0.0013)
Subject 6	0.0205(0.0011)	0.0224(0.0031)	0.0457(0.0031)	0.0414(0.0050)
Subject 7	0.0487(0.0032)	0.0408(0.0066)	0.0640(0.0042)	0.0525(0.0051)
Subject 8	0.0903(0.0052)	0.0701(0.0026)	0.1275(0.0153)	0.0869(0.0161)

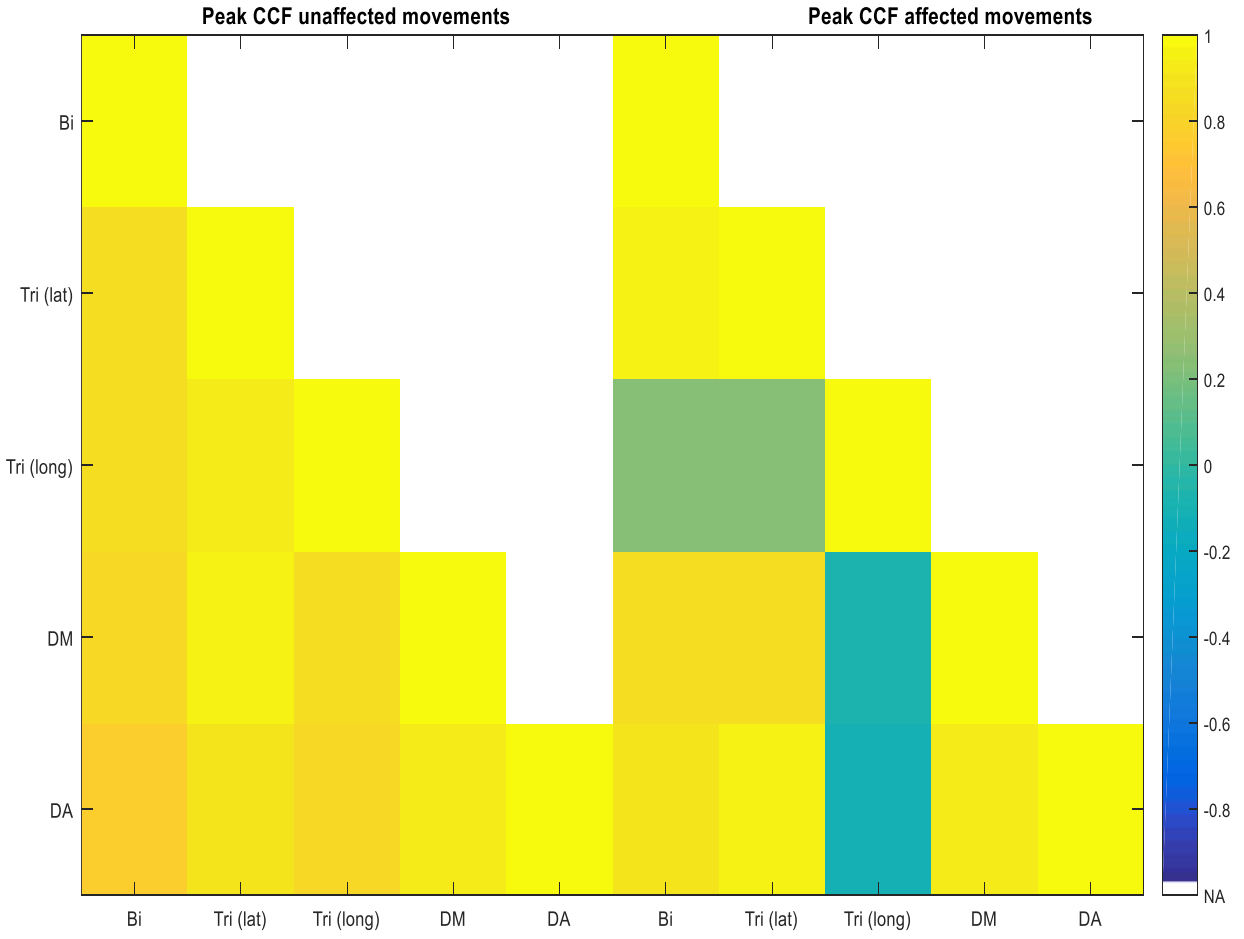

The averaged peak of each cross-correlation function (CCF) between the muscle-pairs for pathologically unaffected (left) and affected (right) movements respectively. Movements performed by the first subject.

The averaged peak values of each cross-correlation function (CCF) between the muscle-pairs for pathologically unaffected movements performed by the first subject. Muscles of interest are biceps, lateral head triceps, long head triceps, deltoideus medial and deltoideus anterior respectively. These values are the maximum Pearson correlations of the CCF.

MEAN(SD) PEAK CCF UNAFFECTED MOVEMENTS					
Muscles	**Bi**	***Tri (lat)***	***Tri (long)***	**DM**	**DA**
Bi	1(0)				
Tri (lat)	0.8463(0.0036)	1(0)			
Tri (long)	0.8468(0.0084)	0.9228(0.0219)	1(0)		
DM	0.8132(0.0307)	0.9454(0.0219)	0.8698(0.0357)	1(0)	
DA	0.7724(0.0571)	0.9040(0.0400)	0.8347(0.0379)	0.9284(0.0212)	1(0)

The corresponding time lags between the muscle-pairs for pathologically unaffected movements performed by the first subject. Muscles of interest are biceps, lateral head triceps, long head triceps, deltoideus medial and deltoideus anterior respectively.

MEAN(SD) TIME LAG CCF UNAFFECTED MOVEMENTS [s]					
Muscles	**Bi**	***Tri (lat)***	***Tri (long)***	**DM**	**DA**
Bi	0(0)				
Tri (lat)	0.7933(0.1334)	0(0)			
Tri (long)	0.4517(0.2100)	-0.0133(0.0176)	0(0)		
DM	0.8383(0.1371)	0.0067(0.0115)	0.1767(0.085)	0(0)	
DA	1.1067(0.1290)	0.0017(0.0029)	0.2483(0.1211)	-0.0050(0.0087)	0(0)

The averaged peak values of each cross-correlation function (CCF) between the muscle-pairs for pathologically affected movements performed by the first subject. Muscles of interest are biceps, lateral head triceps, long head triceps, deltoideus medial and deltoideus anterior respectively. These values are the maximum Pearson correlations of the CCF.

MEAN(SD) PEAK CCF AFFECTED MOVEMENTS					
Muscles	**Bi**	***Tri (lat)***	***Tri (long)***	**DM**	**DA**
Bi	1(0)				
Tri (lat)	0.941(0.0143)	1(0)			
Tri (long)	0.2424(0.6837)	0.2284(0.6982)	1(0)		
DM	0.8602(0.012)	0.8637(0.0362)	-0.0931(0.6057)	1(0)	
DA	0.8984(0.0196)	0.9431(0.0106)	-0.1123(0.6445)	0.9090(0.0241)	1(0)

The corresponding time lags between the muscle-pairs for pathologically affected movements performed by the first subject. Muscles of interest are biceps, lateral head triceps, long head triceps, deltoideus medial and deltoideus anterior respectively.

MEAN(SD) TIME LAG CCF AFFECTED MOVEMENTS [s]					
Muscles	**Bi**	***Tri (lat)***	***Tri (long)***	**DM**	**DA**
Bi	0(0)				
Tri (lat)	0.0017(0.0029)	0(0)			
Tri (long)	-0.38(1.0281)	-0.5133(0.9021)	0(0)		
DM	0.0683(0.0861)	0(0)	-0.2700(1.7455)	0(0)	
DA	0.0083(0.0104)	0(0)	1.0117(0.9326)	0(0)	0(0)

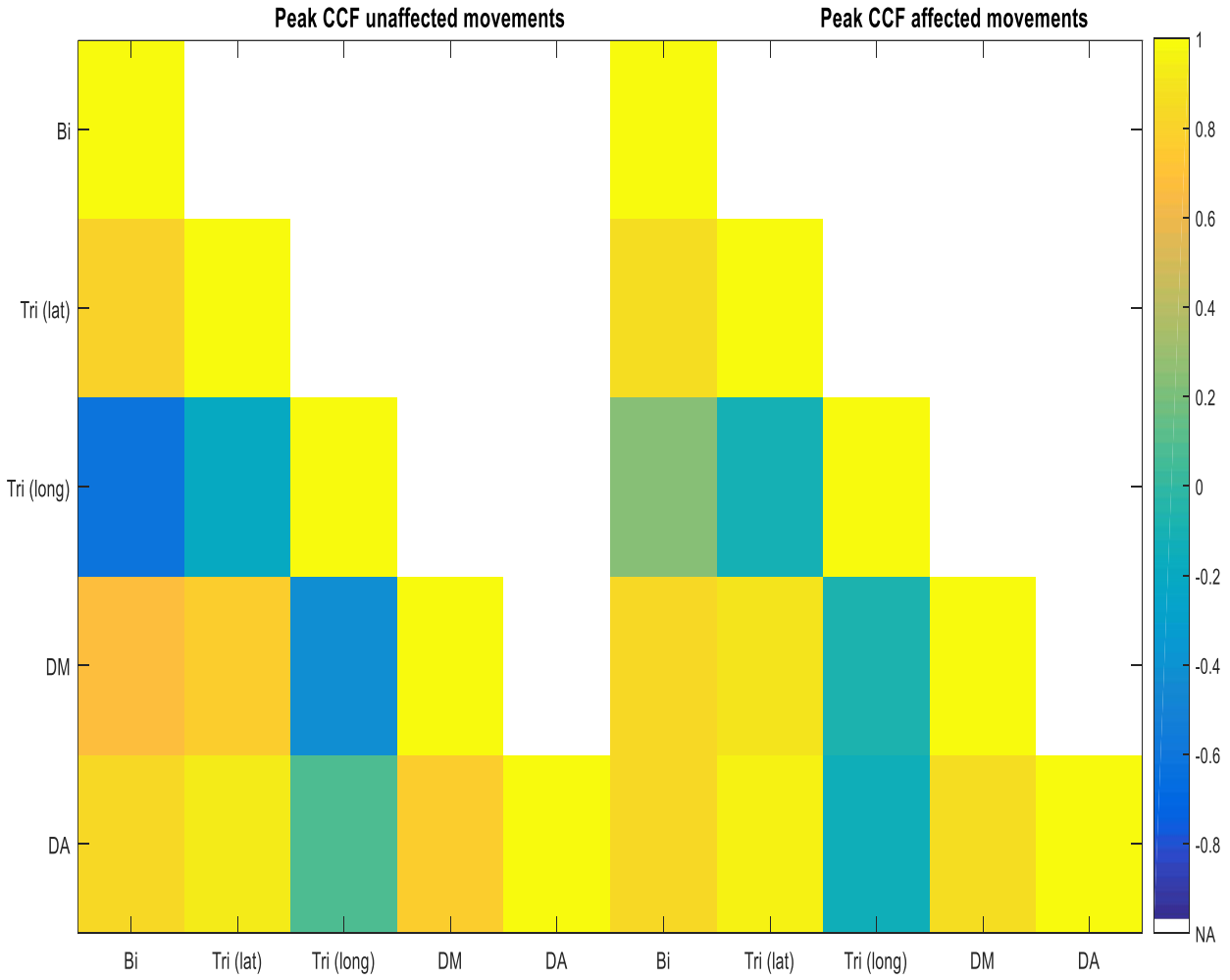

The averaged peak of each cross-correlation function (CCF) between the muscle-pairs for pathologically unaffected (left) and affected (right) movements respectively. Movements performed by the second subject.

The averaged peak values of each cross-correlation function (CCF) between the muscle-pairs for pathologically unaffected movements performed by the second subject. Muscles of interest are biceps, lateral head triceps, long head triceps, deltoideus medial and deltoideus anterior respectively. These values are the maximum Pearson correlations of the CCF.

MEAN(SD) PEAK CCF UNAFFECTED MOVEMENTS					
Muscles	**Bi**	***Tri (lat)***	***Tri (long)***	**DM**	**DA**
Bi	1(0)				
Tri (lat)	0.795(0.0574)	1(0)			
Tri (long)	-0.6198(0.0593)	-0.2077(0.4425)	1(0)		
DM	0.6636(0.0329)	0.7806(0.0495)	-0.4299(0.0114)	1(0)	
DA	0.8185(0.0589)	0.9135(0.0113)	0.0642(0.4788)	0.7578(0.0082)	1(0)

The corresponding time lags between the muscle-pairs for pathologically unaffected movements performed by the fist subject. Muscles of interest are biceps, lateral head triceps, long head triceps, deltoideus medial and deltoideus anterior respectively.

MEAN(SD) TIME LAG CCF UNAFFECTED MOVEMENTS [s]					
Muscles	**Bi**	***Tri (lat)***	***Tri (long)***	**DM**	**DA**
Bi	0(0)				
Tri (lat)	0(0.005)	0(0)			
Tri (long)	-0.6017(0.1333)	-1.1267(0.6516)	0(0)		
DM	0.2967(0.2248)	0.1017(0.0791)	0.675(0.8162)	0(0)	
DA	-0.005(0.0132)	0(0)	1.225(0.4232)	-0.0767(0.0981)	0(0)

The averaged peak values of each cross-correlation function (CCF) between the muscle-pairs for pathologically affected movements performed by the second subject. Muscles of interest are biceps, lateral head triceps, long head triceps, deltoideus medial and deltoideus anterior respectively. These values are the maximum Pearson correlations of the CCF.

MEAN(SD) PEAK CCF AFFECTED MOVEMENTS					
Muscles	**Bi**	***Tri (lat)***	***Tri (long)***	**DM**	**DA**
Bi	1(0)				
Tri (lat)	0.8673(0.0511)	1(0)			
Tri (long)	0.223(0.7323)	-0.0972(0.6659)	1(0)		
DM	0.8424(0.0439)	0.8792(0.0336)	-0.0701(0.6638)	1(0)	
DA	0.8203(0.0365)	0.9577(0.0212)	-0.1518(0.6699)	0.8445(0.0519)	1(0)

The corresponding time lags between the muscle-pairs for pathologically affected movements performed by the second subject. Muscles of interest are biceps, lateral head triceps, long head triceps, deltoideus medial and deltoideus anterior respectively.

MEAN(SD) TIME LAG CCF AFFECTED MOVEMENTS [s]					
Muscles	**Bi**	***Tri (lat)***	***Tri (long)***	**DM**	**DA**
Bi	0(0)				
Tri (lat)	-0.0033(0.0058)	0(0)			
Tri (long)	-0.67(0.6429)	-0.1417(0.1666)	0(0)		
DM	0.0267(0.0306)	0.0167(0.0208)	0.255(0.5888)	0(0)	
DA	-0.0483(0.0837)	0(0)	0.165(0.1645)	-0.0217(0.0126)	0(0)

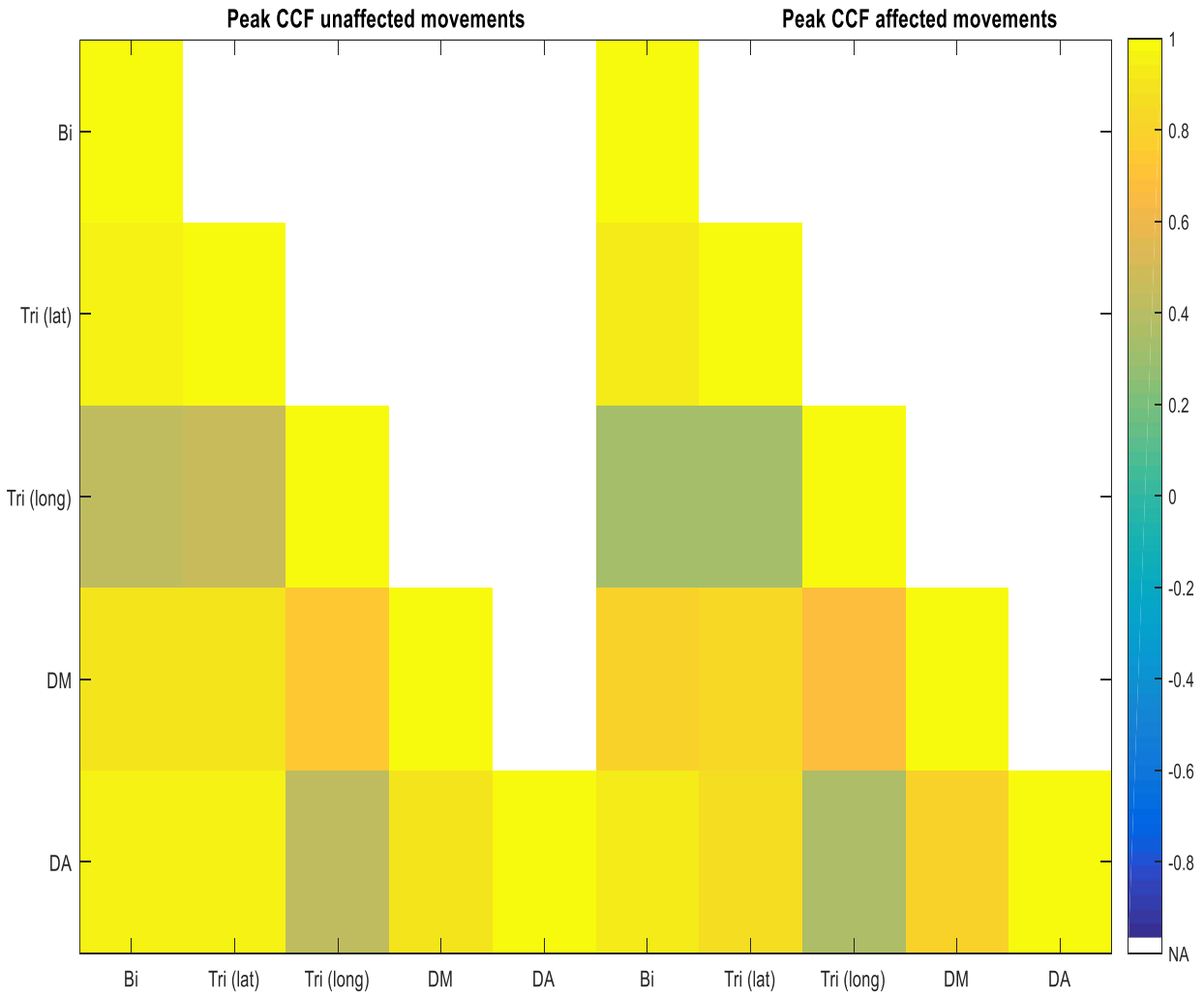

The averaged peak of each cross-correlation function (CCF) between the muscle-pairs for pathologically unaffected (left) and affected (right) movements respectively. Movements performed by the third subject.

The averaged peak values of each cross-correlation function (CCF) between the muscle-pairs for pathologically unaffected movements performed by the third subject. Muscles of interest are biceps, lateral head triceps, long head triceps, deltoideus medial and deltoideus anterior respectively. These values are the maximum Pearson correlations of the CCF.

MEAN(SD) PEAK CCF UNAFFECTED MOVEMENTS					
Muscles	**Bi**	***Tri (lat)***	***Tri (long)***	**DM**	**DA**
Bi	1(0)				
Tri (lat)	0.9648(0.0198)	1(0)			
Tri (long)	0.4367(0.8428)	0.4571(0.8439)	1(0)		
DM	0.8774(0.0574)	0.8959(0.0668)	0.7291(0.2733)	1(0)	
DA	0.9579(0.0099)	0.9545(0.0192)	0.4267(0.8409)	0.9056(0.0551)	1(0)

The corresponding time lags between the muscle-pairs for pathologically unaffected movements performed by the third subject. Muscles of interest are biceps, lateral head triceps, long head triceps, deltoideus medial and deltoideus anterior respectively.

MEAN(SD) TIME LAG CCF UNAFFECTED MOVEMENTS [s]					
Muscles	**Bi**	***Tri (lat)***	***Tri (long)***	**DM**	**DA**
Bi	0(0)				
Tri (lat)	0.015(0.01)	0(0)			
Tri (long)	-0.4583(0.9202)	-0.5900(1.0219)	0(0)		
DM	0.0683(0.0351)	0.0133(0.0189)	-0.21(0.4623)	0(0)	
DA	0.0100(0.005)	0.0033(0.0058)	0.565(0.9786)	-0.005(0.0087)	0(0)

The averaged peak values of each cross-correlation function (CCF) between the muscle-pairs for pathologically affected movements performed by the third subject. Muscles of interest are biceps, lateral head triceps, long head triceps, deltoideus medial and deltoideus anterior respectively. These values are the maximum Pearson correlations of the CCF.

MEAN(SD) PEAK CCF AFFECTED MOVEMENTS					
Muscles	**Bi**	***Tri (lat)***	***Tri (long)***	**DM**	**DA**
Bi	1(0)				
Tri (lat)	0.9223(0.0064)	1(0)			
Tri (long)	0.3264(0.7651)	0.3187(0.7898)	1(0)		
DM	0.8121(0.0163)	0.8337(0.0431)	0.6653(0.1789)	1(0)	
DA	0.9121(0.0032)	0.8622(0.0372)	0.3500(0.7722)	0.7907(0.0458)	1(0)

The corresponding time lags between the muscle-pairs for pathologically affected movements performed by the third subject. Muscles of interest are biceps, lateral head triceps, long head triceps, deltoideus medial and deltoideus anterior respectively.

MEAN(SD) TIME LAG CCF AFFECTED MOVEMENTS [s]					
Muscles	**Bi**	***Tri (lat)***	***Tri (long)***	**DM**	**DA**
Bi	0(0)				
Tri (lat)	0.0033(0.0029)	0(0)			
Tri (long)	0.1733(1.0834)	-0.02(0.9146)	0(0)		
DM	0.0083(0.0104)	0.0033(0.0104)	-0.6517(0.1318)	0(0)	
DA	0(0)	-0.1417(0.0369)	-0.1767(1.0663)	-0.0667(0.0987)	0(0)

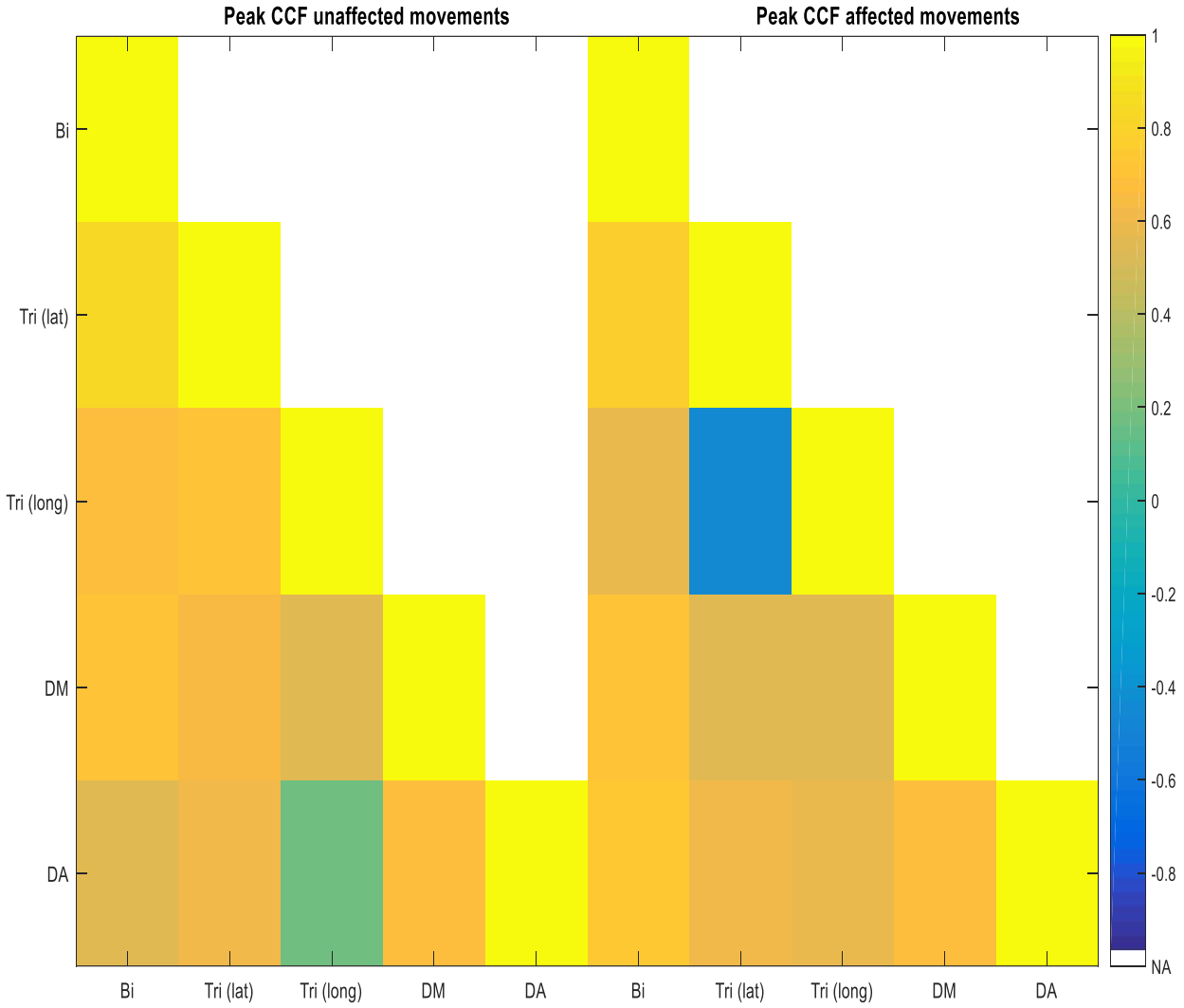

The averaged peak of each cross-correlation function (CCF) between the muscle-pairs for pathologically unaffected (left) and affected (right) movements respectively. Movements performed by the fourth subject.

The averaged peak values of each cross-correlation function (CCF) between the muscle-pairs for pathologically unaffected movements performed by the fourth subject. Muscles of interest are biceps, lateral head triceps, long head triceps, deltoideus medial and deltoideus anterior respectively. These values are the maximum Pearson correlations of the CCF.

MEAN(SD) PEAK CCF UNAFFECTED MOVEMENTS					
Muscles	**Bi**	***Tri (lat)***	***Tri (long)***	**DM**	**DA**
Bi	1(0)				
Tri (lat)	0.8133(0.0493)	1(0)			
Tri (long)	0.6874(0.0935)	0.7065(0.03)	1(0)		
DM	0.7043(0.0362)	0.632(0.0108)	0.5498(0.0282)	1(0)	
DA	0.5509(0.0295)	0.6226(0.1106)	0.1587(0.527)	0.6625(0.0756)	1(0)

The corresponding time lags between the muscle-pairs for pathologically unaffected movements performed by the fourth subject. Muscles of interest are biceps, lateral head triceps, long head triceps, deltoideus medial and deltoideus anterior respectively.

MEAN(SD) TIME LAG CCF UNAFFECTED MOVEMENTS [s]					
Muscles	**Bi**	***Tri (lat)***	***Tri (long)***	**DM**	**DA**
Bi	0(0)				
Tri (lat)	0.01(0.0173)	0(0)			
Tri (long)	-1.3617(1.1882)	0.0033(0.0058)	0(0)		
DM	1(0.1879)	0.7933(0.0701)	2.2567(1.3364)	0(0)	
DA	0.37(0.3218)	0.0067(0.0058)	2.3267(0.7595)	-0.4633(0.395)	0(0)

The averaged peak values of each cross-correlation function (CCF) between the muscle-pairs for pathologically affected movements performed by the fourth subject. Muscles of interest are biceps, lateral head triceps, long head triceps, deltoideus medial and deltoideus anterior respectively. These values are the maximum Pearson correlations of the CCF.

MEAN(SD) PEAK CCF AFFECTED MOVEMENTS					
Muscles	**Bi**	***Tri (lat)***	***Tri (long)***	**DM**	**DA**
Bi	1(0)				
Tri (lat)	0.7596(0.0625)	1(0)			
Tri (long)	0.5738(0.0533)	-0.4657(0.0488)	1(0)		
DM	0.7147(0.0926)	0.5346(0.0856)	0.554(0.0202)	1(0)	
DA	0.7496(0.0526)	0.6188(0.1034)	0.5889(0.0616)	0.6829(0.0072)	1(0)

The corresponding time lags between the muscle-pairs for pathologically affected movements performed by the fourth subject. Muscles of interest are biceps, lateral head triceps, long head triceps, deltoideus medial and deltoideus anterior respectively.

MEAN(SD) TIME LAG CCF AFFECTED MOVEMENTS [s]					
Muscles	**Bi**	***Tri (lat)***	***Tri (long)***	**DM**	**DA**
Bi	0(0)				
Tri (lat)	-0.0067(0.0029)	0(0)			
Tri (long)	-2.225(0.1958)	-1.4917(1.749)	0(0)		
DM	0.0433(0.0751)	0.1117(0.1848)	2.5017(0.4565)	0(0)	
DA	-0.1617(0.1625)	0.0017(0.0029)	2.1383(0.1397)	-0.1133(0.1793)	0(0)

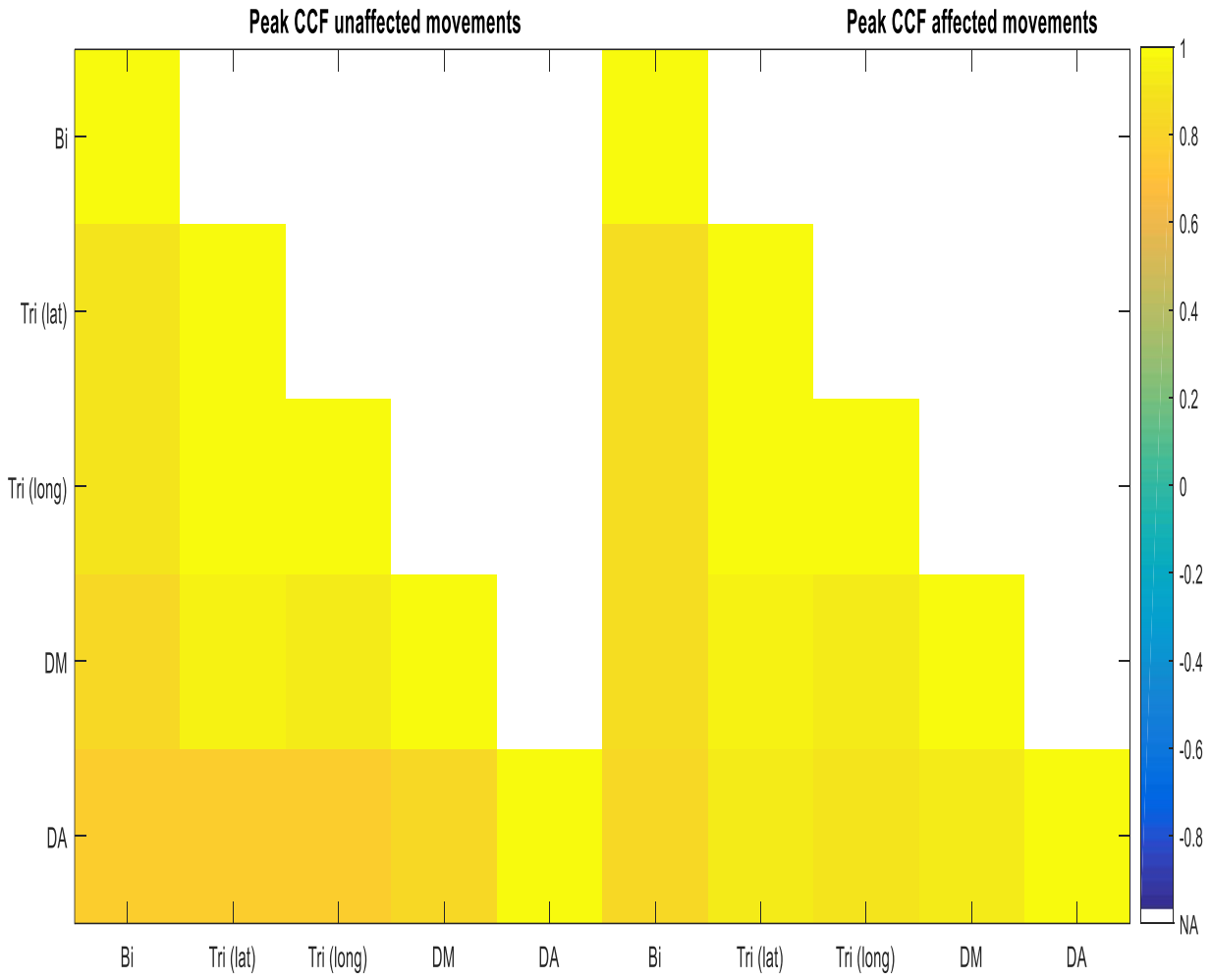

Figure D.1: The averaged peak of each cross-correlation function (CCF) between the muscle-pairs for pathologically unaffected (left) and affected (right) movements respectively. Movements performed by the fifth subject.

Table D.1: The averaged peak values of each cross-correlation function (CCF) between the muscle-pairs for pathologically unaffected movements performed by the fifth subject. Muscles of interest are biceps, lateral head triceps, long head triceps, deltoideus medial and deltoideus anterior respectively. These values are the maximum Pearson correlations of the CCF.

MEAN(SD) PEAK CCF UNAFFECTED MOVEMENTS					
Muscles	**Bi**	***Tri (lat)***	***Tri (long)***	**DM**	**DA**
Bi	1(0)				
Tri (lat)	0.8806(0.0565)	1(0)			
Tri (long)	0.8766(0.0446)	0.9855(0.0015)	1(0)		
DM	0.8156(0.1098)	0.9487(0.0274)	0.933(0.0398)	1(0)	
DA	0.7639(0.0559)	0.7681(0.0913)	0.7505(0.1051)	0.8311(0.0356)	1(0)

Table D.2: The corresponding time lags between the muscle-pairs for pathologically unaffected movements performed by the fifth subject. Muscles of interest are biceps, lateral head triceps, long head triceps, deltoideus medial and deltoideus anterior respectively.

MEAN(SD) TIME LAG CCF UNAFFECTED MOVEMENTS [s]					
Muscles	**Bi**	***Tri (lat)***	***Tri (long)***	**DM**	**DA**
Bi	0(0)				
Tri (lat)	0.0417(0.0558)	0(0)			
Tri (long)	-0.0383(0.1871)	0.0017(0.0029)	0(0)		
DM	0.3667(0.3559)	0.005(0.005)	0.0067(0.0076)	0(0)	
DA	0.895(0.6934)	0.5033(0.4216)	0.5583(0.4783)	0.3267(0.2747)	0(0)

Table D.3: The averaged peak values of each cross-correlation function (CCF) between the muscle-pairs for pathologically affected movements performed by the fifth subject. Muscles of interest are biceps, lateral head triceps, long head triceps, deltoideus medial and deltoideus anterior respectively. These values are the maximum Pearson correlations of the CCF.

MEAN(SD) PEAK CCF AFFECTED MOVEMENTS					
Muscles	**Bi**	***Tri (lat)***	***Tri (long)***	**DM**	**DA**
Bi	1(0)				
Tri (lat)	0.8645(0.0189)	1(0)			
Tri (long)	0.8713(0.0128)	0.9792(0.0045)	1(0)		
DM	0.8632(0.0322)	0.938(0.0364)	0.9211(0.0407)	1(0)	
DA	0.8349(0.0385)	0.9092(0.0424)	0.901(0.0442)	0.932(0.0234)	1(0)

Table D.4: The corresponding time lags between the muscle-pairs for pathologically affected movements performed by the fifth subject. Muscles of interest are biceps, lateral head triceps, long head triceps, deltoideus medial and deltoideus anterior respectively.

MEAN(SD) TIME LAG CCF AFFECTED MOVEMENTS [s]					
Muscles	**Bi**	***Tri (lat)***	***Tri (long)***	**DM**	**DA**
Bi	0(0)				
Tri (lat)	0(0)	0(0)			
Tri (long)	0(0)	0(0)	0(0)		
DM	0.0233(0.0493)	0(0)	0(0)	0(0)	
DA	0(0)	0.02(0.0132)	0.0167(0.0161)	0.0067(0.0115)	0(0)

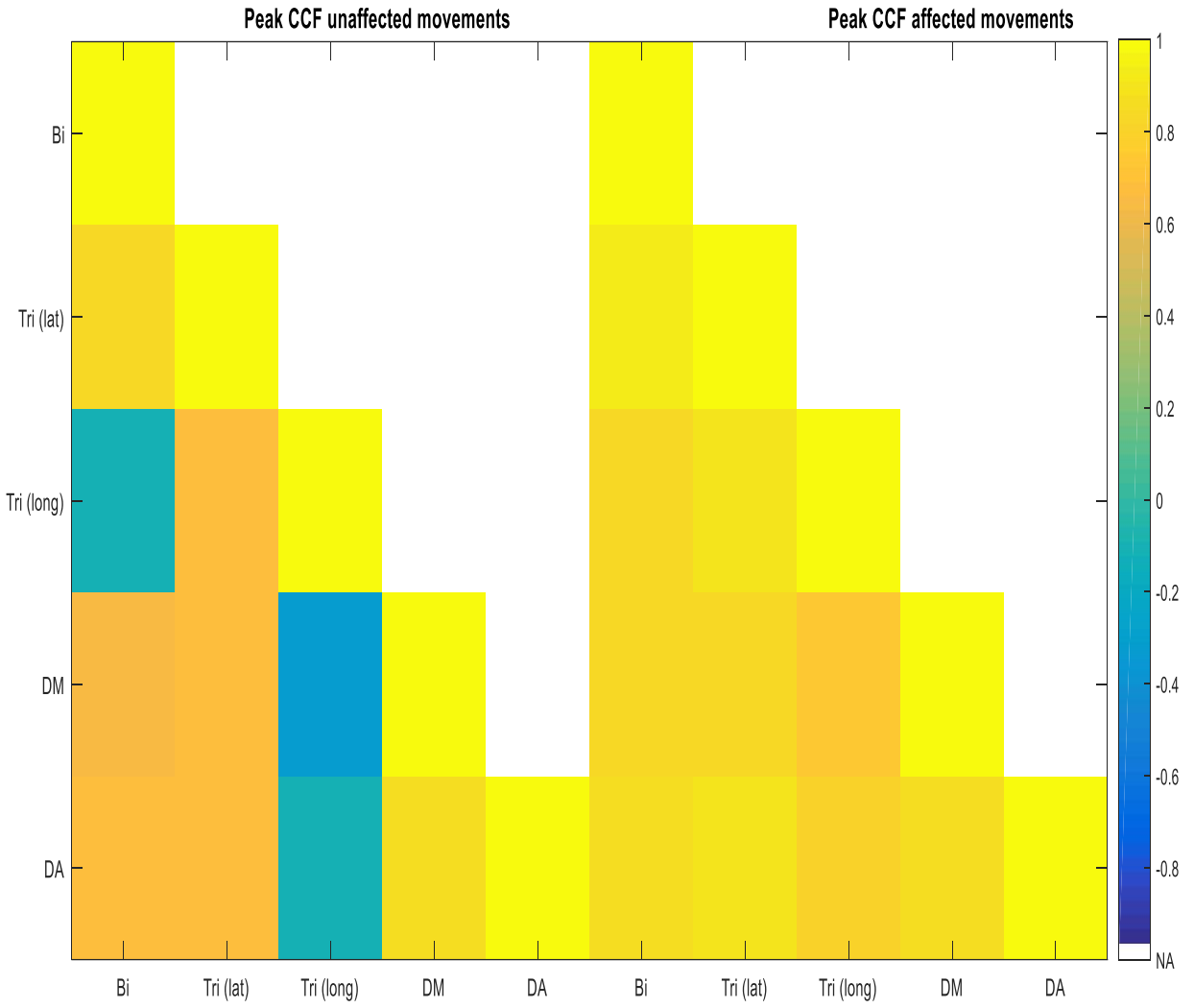

Figure D.2: The averaged peak of each cross-correlation function (CCF) between the muscle-pairs for pathologically unaffected (left) and affected (right) movements respectively. Movements performed by the sixth subject.

Table D.5: The averaged peak values of each cross-correlation function (CCF) between the muscle-pairs for pathologically unaffected movements performed by the sixth subject. Muscles of interest are biceps, lateral head triceps, long head triceps, deltoideus medial and deltoideus anterior respectively. These values are the maximum Pearson correlations of the CCF.

MEAN(SD) PEAK CCF UNAFFECTED MOVEMENTS					
Muscles	**Bi**	***Tri (lat)***	***Tri (long)***	**DM**	**DA**
Bi	1(0)				
Tri (lat)	0.8253(0.0316)	1(0)			
Tri (long)	-0.1218(0.7167)	0.6677(0.1532)	1(0)		
DM	0.6452(0.0534)	0.6837(0.0984)	-0.3396(0.0645)	1(0)	
DA	0.6859(0.0615)	0.6785(0.0955)	-0.1199(0.486)	0.8681(0.0282)	1(0)

Table D.6: The corresponding time lags between the muscle-pairs for pathologically unaffected movements performed by the sixth subject. Muscles of interest are biceps, lateral head triceps, long head triceps, deltoideus medial and deltoideus anterior respectively.

MEAN(SD) TIME LAG CCF UNAFFECTED MOVEMENTS [s]					
Muscles	**Bi**	***Tri (lat)***	***Tri (long)***	**DM**	**DA**
Bi	0(0)				
Tri (lat)	0.0883(0.153)	0(0)			
Tri (long)	-0.6283(0.6107)	0(0)	0(0)		
DM	0.3517(0.09)	0.0917(0.1097)	0.4233(2.1723)	0(0)	
DA	0.4183(0.2155)	0.0633(0.1054)	1.2233(0.5318)	0(0)	0(0)

Table D.7: The averaged peak values of each cross-correlation function (CCF) between the muscle-pairs for pathologically affected movements performed by the sixth subject. Muscles of interest are biceps, lateral head triceps, long head triceps, deltoideus medial and deltoideus anterior respectively. These values are the maximum Pearson correlations of the CCF.

MEAN(SD) PEAK CCF AFFECTED MOVEMENTS					
Muscles	**Bi**	***Tri (lat)***	***Tri (long)***	**DM**	**DA**
Bi	1(0)				
Tri (lat)	0.9358(0.0271)	1(0)			
Tri (long)	0.8289(0.0878)	0.905(0.0578)	1(0)		
DM	0.8317(0.0091)	0.8346(0.0141)	0.7371(0.0747)	1(0)	
DA	0.8673(0.0332)	0.8854(0.0179)	0.7927(0.0589)	0.8701(0.0114)	1(0)

Table D.8: The corresponding time lags between the muscle-pairs for pathologically affected movements performed by the sixth subject. Muscles of interest are biceps, lateral head triceps, long head triceps, deltoideus medial and deltoideus anterior respectively.

MEAN(SD) TIME LAG CCF AFFECTED MOVEMENTS [s]					
Muscles	**Bi**	***Tri (lat)***	***Tri (long)***	**DM**	**DA**
Bi	0(0)				
Tri (lat)	0(0)	0(0)			
Tri (long)	0(0)	0(0)	0(0)		
DM	0.0833(0.1115)	0.0967(0.1285)	0.0767(0.1114)	0(0)	
DA	0.055(0.091)	0.005(0)	0.005(0.005)	0(0)	0(0)

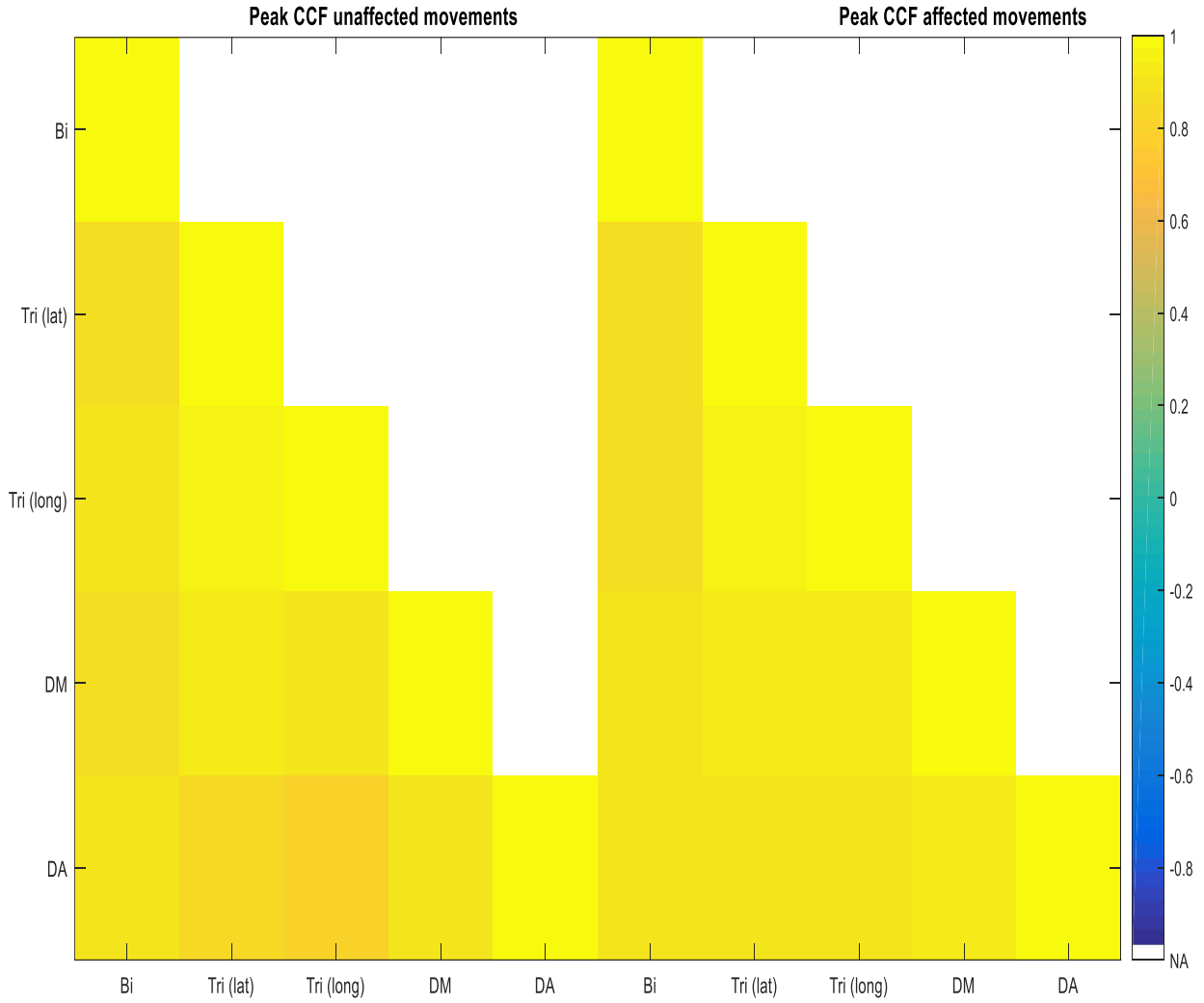

Figure D.3: The averaged peak of each cross-correlation function (CCF) between the muscle-pairs for pathologically unaffected (left) and affected (right) movements respectively. Movements performed by the seventh subject.

Table D.9: The averaged peak values of each cross-correlation function (CCF) between the muscle-pairs for pathologically unaffected movements performed by the seventh subject. Muscles of interest are biceps, lateral head triceps, long head triceps, deltoideus medial and deltoideus anterior respectively. These values are the maximum Pearson correlations of the CCF.

MEAN(SD) PEAK CCF UNAFFECTED MOVEMENTS					
Muscles	**Bi**	***Tri (lat)***	***Tri (long)***	**DM**	**DA**
Bi	1(0)				
Tri (lat)	0.868(0.0244)	1(0)			
Tri (long)	0.8816(0.0234)	0.9651(0.018)	1(0)		
DM	0.8748(0.0411)	0.9124(0.0279)	0.8895(0.0407)	1(0)	
DA	0.8785(0.0394)	0.8158(0.0779)	0.8106(0.072)	0.889(0.0627)	1(0)

Table D.10: The corresponding time lags between the muscle-pairs for pathologically unaffected movements performed by the seventh subject. Muscles of interest are biceps, lateral head triceps, long head triceps, deltoideus medial and deltoideus anterior respectively.

MEAN(SD) TIME LAG CCF UNAFFECTED MOVEMENTS [s]					
Muscles	**Bi**	***Tri (lat)***	***Tri (long)***	**DM**	**DA**
Bi	0(0)				
Tri (lat)	-0.085(0.0757)	0(0)			
Tri (long)	-0.045(0.0427)	0.0017(0.0029)	0(0)		
DM	-0.0183(0.0202)	0.005(0.0087)	0.0183(0.0318)	0(0)	
DA	0.045(0.0779)	0.2433(0.1589)	0.2533(0.125)	0.075(0.0507)	0(0)

Table D.11: The averaged peak values of each cross-correlation function (CCF) between the muscle-pairs for pathologically affected movements performed by the seventh subject. Muscles of interest are biceps, lateral head triceps, long head triceps, deltoideus medial and deltoideus anterior respectively. These values are the maximum Pearson correlations of the CCF.

MEAN(SD) PEAK CCF AFFECTED MOVEMENTS					
Muscles	**Bi**	***Tri (lat)***	***Tri (long)***	**DM**	**DA**
Bi	1(0)				
Tri (lat)	0.8687(0.0376)	1(0)			
Tri (long)	0.8657(0.0283)	0.9641(0.0215)	1(0)		
DM	0.8933(0.0588)	0.9193(0.0184)	0.9156(0.0037)	1(0)	
DA	0.8951(0.0613)	0.9041(0.0323)	0.8909(0.0333)	0.9248(0.0083)	1(0)

Table D.12: The corresponding time lags between the muscle-pairs for pathologically affected movements performed by the seventh subject. Muscles of interest are biceps, lateral head triceps, long head triceps, deltoideus medial and deltoideus anterior respectively.

MEAN(SD) TIME LAG CCF AFFECTED MOVEMENTS [s]					
Muscles	**Bi**	***Tri (lat)***	***Tri (long)***	**DM**	**DA**
Bi	0(0)				
Tri (lat)	-0.0417(0.0551)	0(0)			
Tri (long)	-0.0283(0.0448)	0(0)	0(0)		
DM	0(0)	0.005(0.005)	0.0033(0.0029)	0(0)	
DA	0(0.0087)	0.02(0.005)	0.005(0.005)	0(0)	0(0)

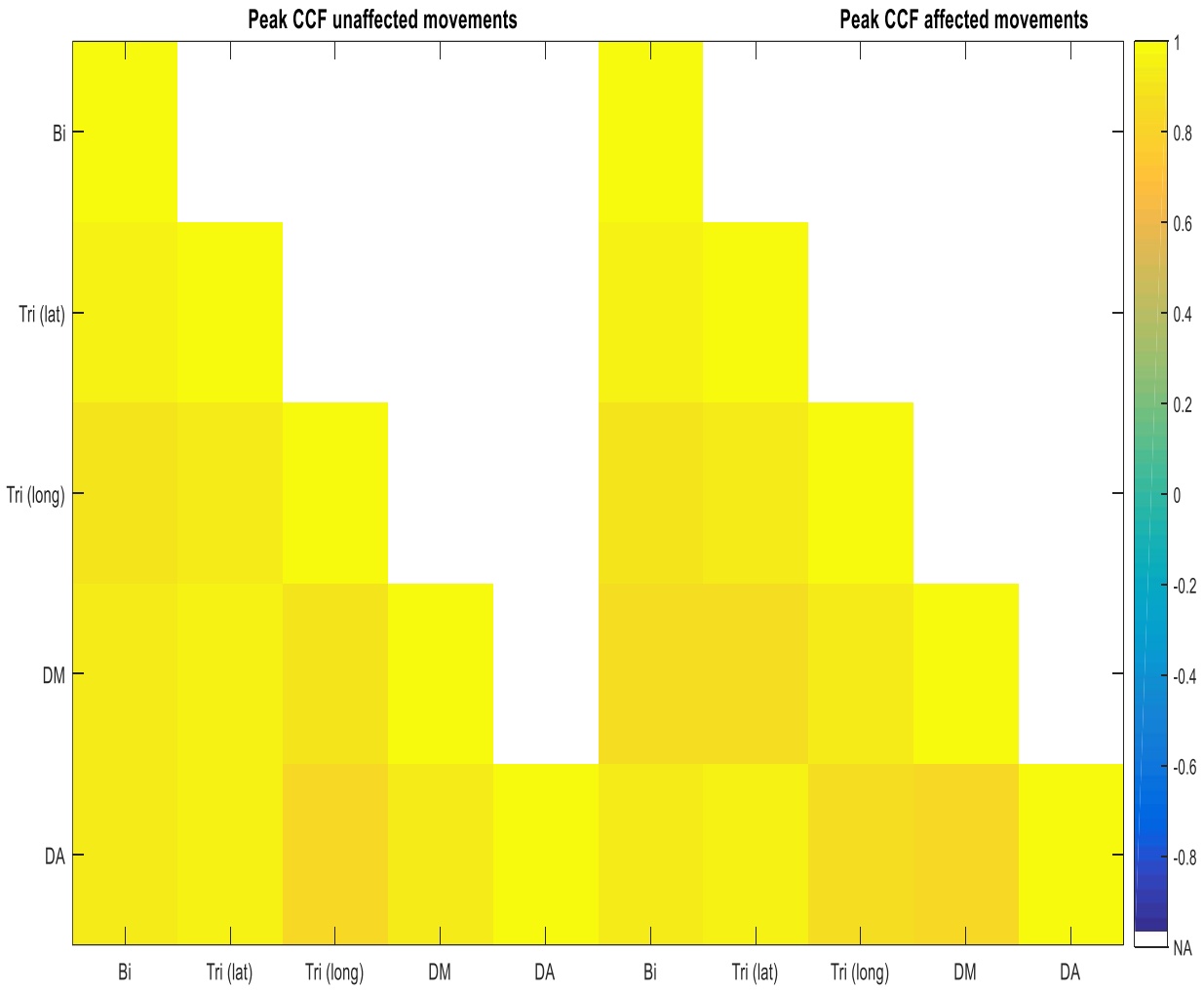

Figure D.4: The averaged peak of each cross-correlation function (CCF) between the muscle-pairs for pathologically unaffected (left) and affected (right) movements respectively. Movements performed by the eighth subject.

Table D.13: The averaged peak values of each cross-correlation function (CCF) between the muscle-pairs for pathologically unaffected movements performed by the eighth subject. Muscles of interest are biceps, lateral head triceps, long head triceps, deltoideus medial and deltoideus anterior respectively. These values are the maximum Pearson correlations of the CCF.

MEAN(SD) PEAK CCF UNAFFECTED MOVEMENTS					
Muscles	**Bi**	***Tri (lat)***	***Tri (long)***	**DM**	**DA**
Bi	1(0)				
Tri (lat)	0.9611(0.0122)	1(0)			
Tri (long)	0.8918(0.0061)	0.9149(0.0286)	1(0)		
DM	0.9327(0.0155)	0.9482(0.0041)	0.8778(0.0302)	1(0)	
DA	0.9243(0.0392)	0.9477(0.0034)	0.8346(0.0411)	0.9132(0.0158)	1(0)

Table D.14: The corresponding time lags between the muscle-pairs for pathologically unaffected movements performed by the eighth subject. Muscles of interest are biceps, lateral head triceps, long head triceps, deltoideus medial and deltoideus anterior respectively.

MEAN(SD) TIME LAG CCF UNAFFECTED MOVEMENTS [s]					
Muscles	**Bi**	***Tri (lat)***	***Tri (long)***	**DM**	**DA**
Bi	0(0)				
Tri (lat)	-0.005(0.005)	0(0)			
Tri (long)	-0.0017(0.0029)	0.0033(0.0058)	0(0)		
DM	0(0)	0.0017(0.0029)	-0.04(0.0608)	0(0)	
DA	-0.01(0.0087)	0(0)	-0.0683(0.0874)	-0.005(0.0087)	0(0)

Table D.15: The averaged peak values of each cross-correlation function (CCF) between the muscle-pairs for pathologically affected movements performed by the eighth subject. Muscles of interest are biceps, lateral head triceps, long head triceps, deltoideus medial and deltoideus anterior respectively. These values are the maximum Pearson correlations of the CCF.

MEAN(SD) PEAK CCF AFFECTED MOVEMENTS					
Muscles	**Bi**	***Tri (lat)***	***Tri (long)***	**DM**	**DA**
Bi	1(0)				
Tri (lat)	0.9408(0.0583)	1(0)			
Tri (long)	0.8974(0.0548)	0.9322(0.0165)	1(0)		
DM	0.8512(0.087)	0.8642(0.0828)	0.9228(0.0286)	1(0)	
DA	0.9114(0.0693)	0.9517(0.0173)	0.8693(0.0384)	0.8204(0.0678)	1(0)

Table D.16: The corresponding time lags between the muscle-pairs for pathologically affected movements performed by the eighth subject. Muscles of interest are biceps, lateral head triceps, long head triceps, deltoideus medial and deltoideus anterior respectively.

MEAN(SD) TIME LAG CCF AFFECTED MOVEMENTS [s]					
Muscles	**Bi**	***Tri (lat)***	***Tri (long)***	**DM**	**DA**
Bi	0(0)				
Tri (lat)	0(0)	0(0)			
Tri (long)	0.0233(0.0362)	0.0033(0.0058)	0(0)		
DM	0.0817(0.0742)	0.045(0.0737)	0(0)	0(0)	
DA	-0.0183(0.0318)	-0.0067(0.0115)	-0.08(0.0608)	-0.0833(0.0737)	0(0)

APPENDIX C MOVEMENTS MIXING SYNERGIES

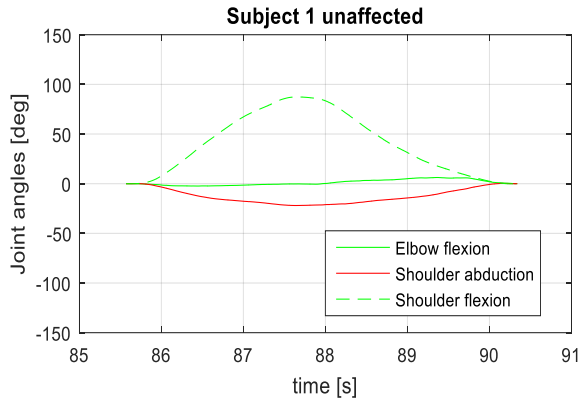

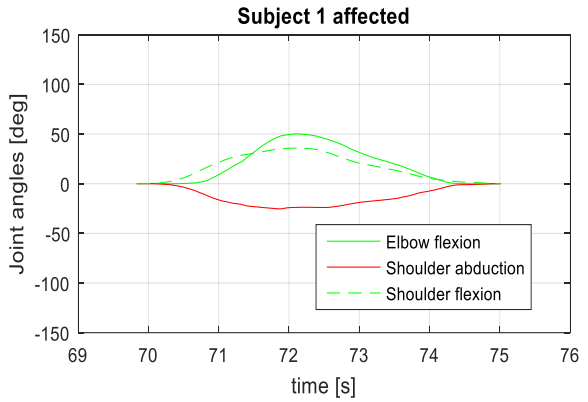

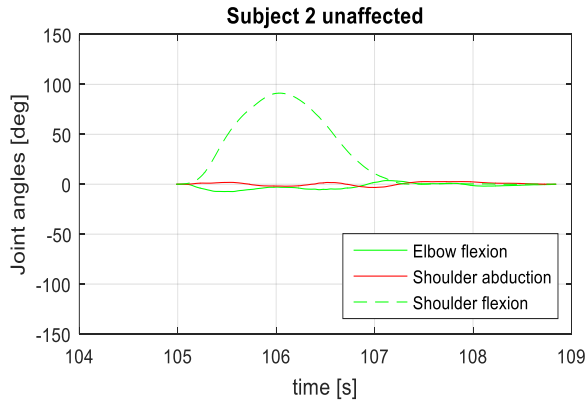

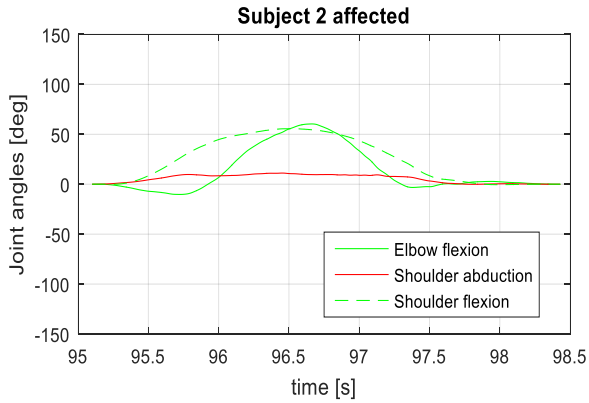

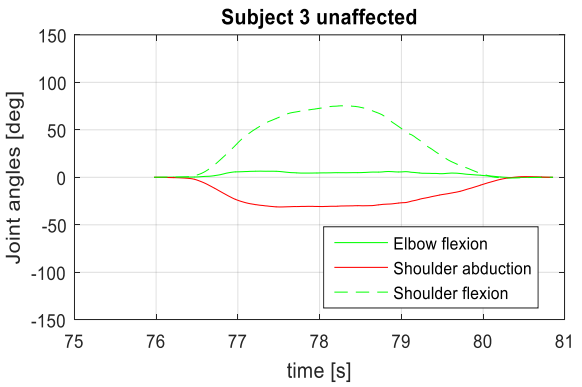
Subject 3 unaffected
Joint angles [deg]
time [s]
Elbow flexion
Shoulder abduction
Shoulder flexion

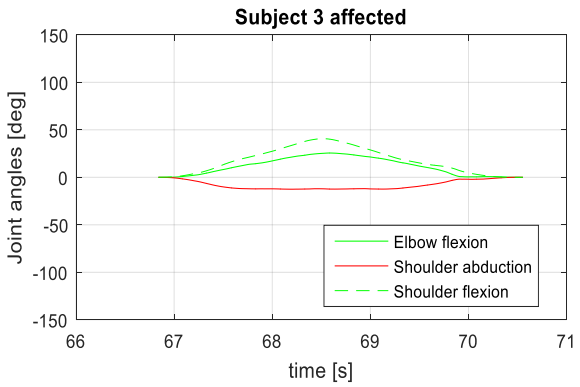
Subject 3 affected
Joint angles [deg]
time [s]
Elbow flexion
Shoulder abduction
Shoulder flexion

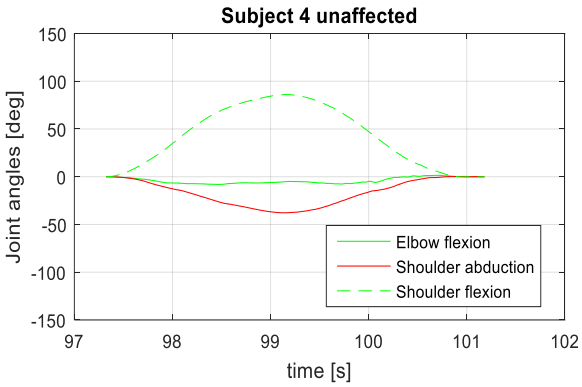
Subject 4 unaffected
Joint angles [deg]
time [s]
Elbow flexion
Shoulder abduction
Shoulder flexion

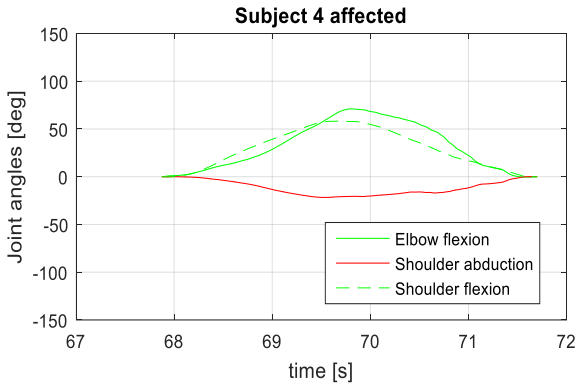
Subject 4 affected
Joint angles [deg]
time [s]
Elbow flexion
Shoulder abduction
Shoulder flexion

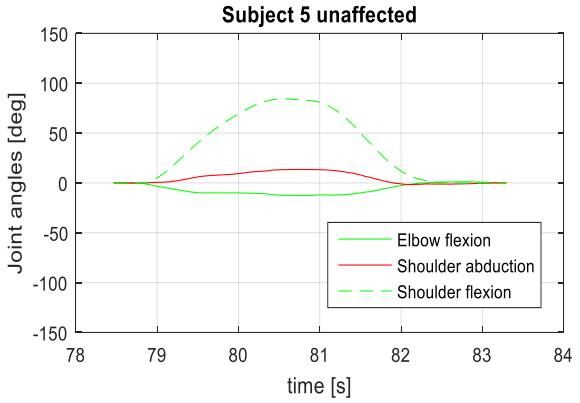
Subject 5 unaffected
Joint angles [deg]
time [s]
Elbow flexion
Shoulder abduction
Shoulder flexion

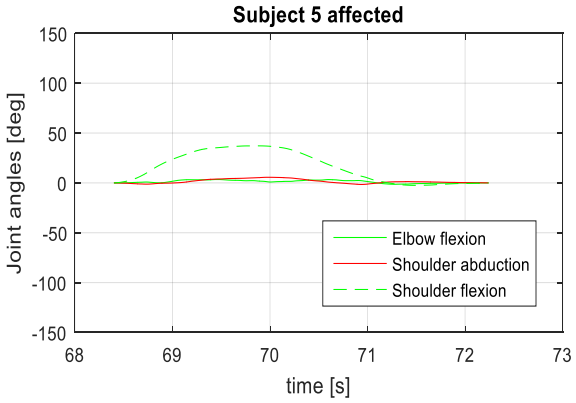
Subject 5 affected
Joint angles [deg]
time [s]
Elbow flexion
Shoulder abduction
Shoulder flexion

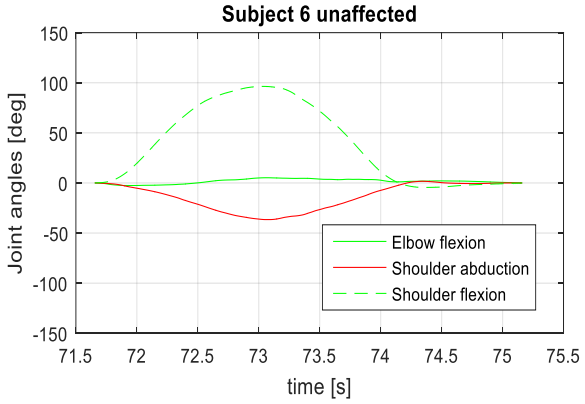
Subject 6 unaffected
Joint angles [deg]
time [s]
Elbow flexion
Shoulder abduction
Shoulder flexion

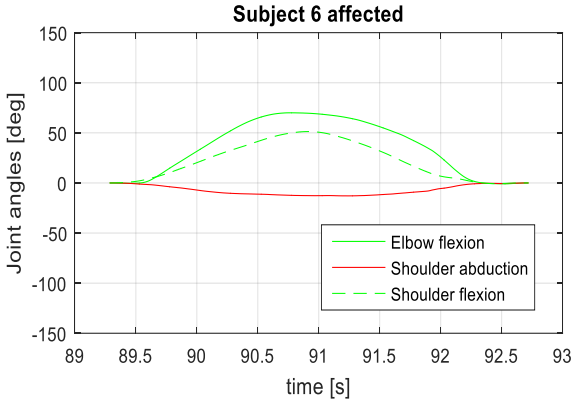
Subject 6 affected
Joint angles [deg]
time [s]
Elbow flexion
Shoulder abduction
Shoulder flexion

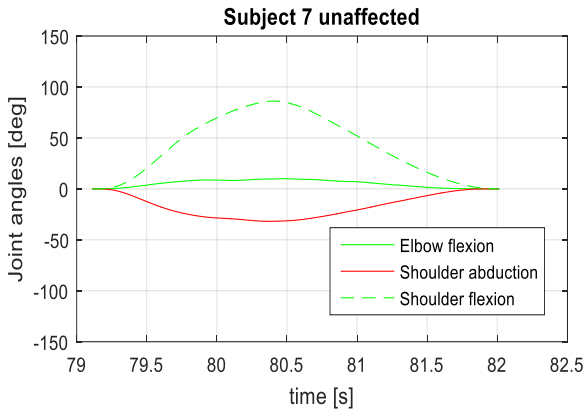
Subject 7 unaffected
Joint angles [deg]
time [s]
Elbow flexion
Shoulder abduction
Shoulder flexion

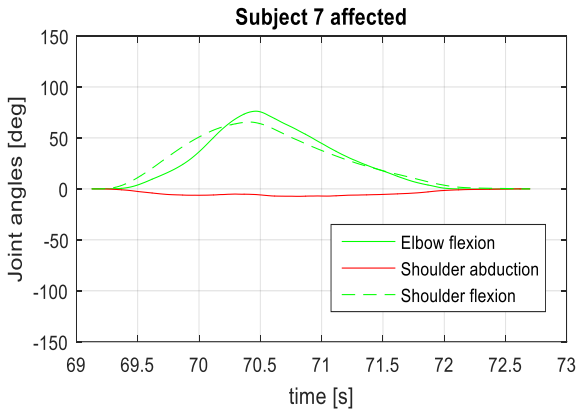
Subject 7 affected
Joint angles [deg]
time [s]
Elbow flexion
Shoulder abduction
Shoulder flexion

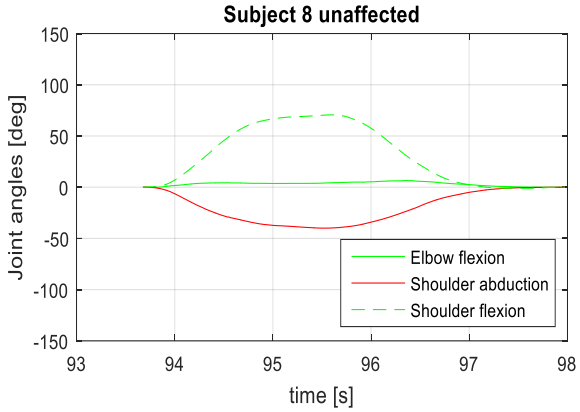
Subject 8 unaffected
Joint angles [deg]
time [s]
Elbow flexion
Shoulder abduction
Shoulder flexion

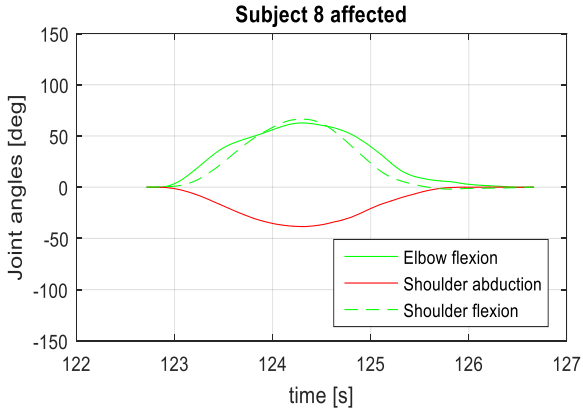
Subject 8 affected
Joint angles [deg]
time [s]
Elbow flexion
Shoulder abduction
Shoulder flexion

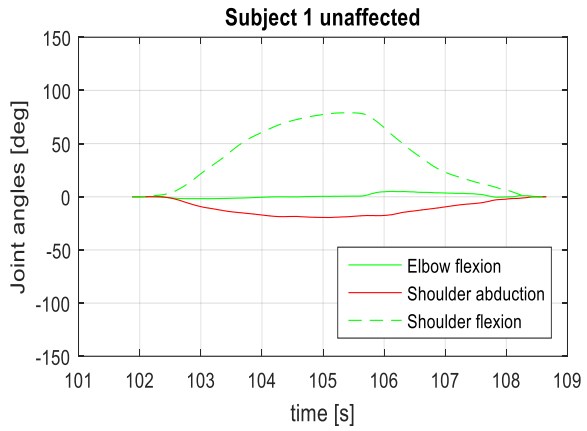
Subject 1 unaffected
Joint angles [deg]
time [s]
Elbow flexion
Shoulder abduction
Shoulder flexion

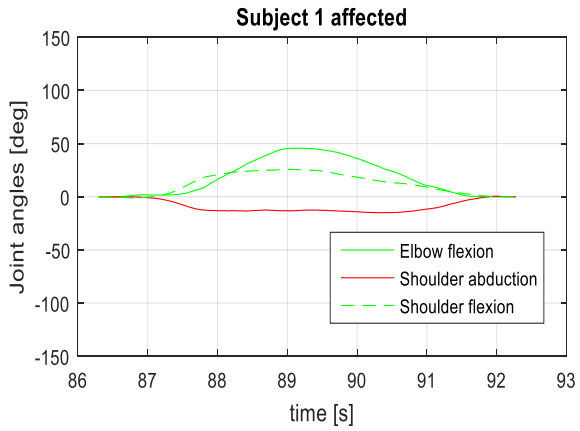
Subject 1 affected
Joint angles [deg]
time [s]
Elbow flexion
Shoulder abduction
Shoulder flexion

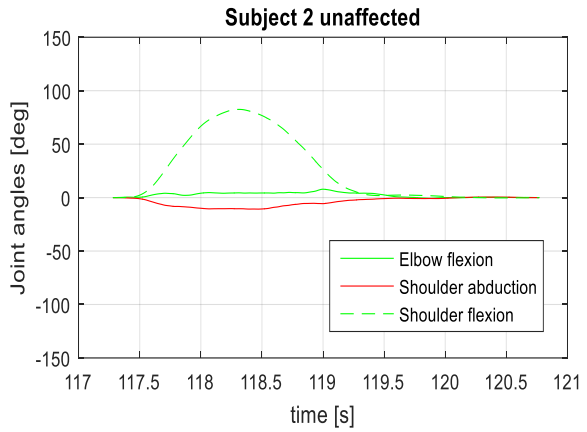
Subject 2 unaffected
Joint angles [deg]
time [s]
Elbow flexion
Shoulder abduction
Shoulder flexion

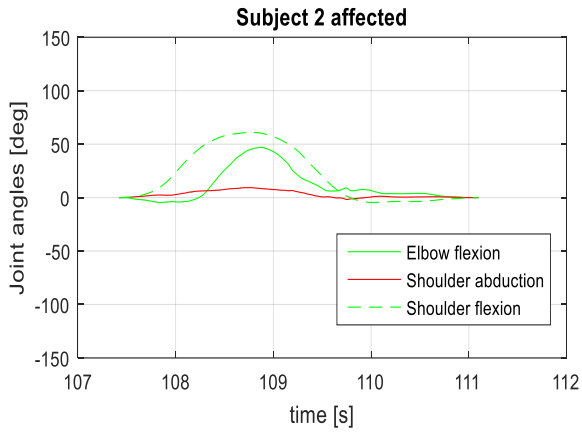
Subject 2 affected
Joint angles [deg]
time [s]
Elbow flexion
Shoulder abduction
Shoulder flexion

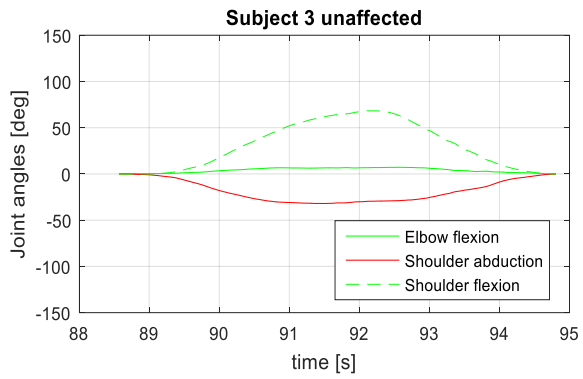
Subject 3 unaffected
Joint angles [deg]
time [s]
Elbow flexion
Shoulder abduction
Shoulder flexion

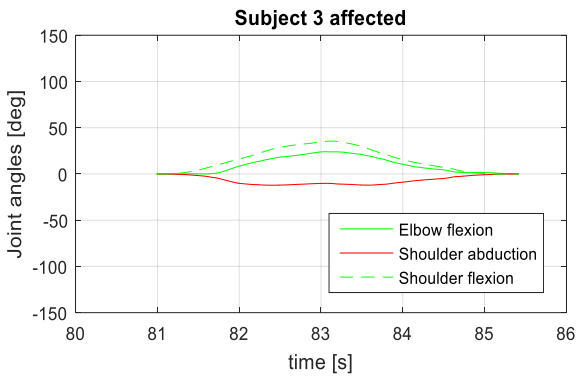
Subject 3 affected
Joint angles [deg]
time [s]
Elbow flexion
Shoulder abduction
Shoulder flexion

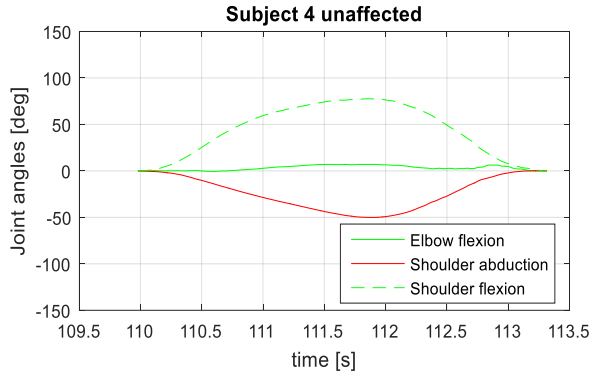
Subject 4 unaffected
Joint angles [deg]
time [s]
Elbow flexion
Shoulder abduction
Shoulder flexion

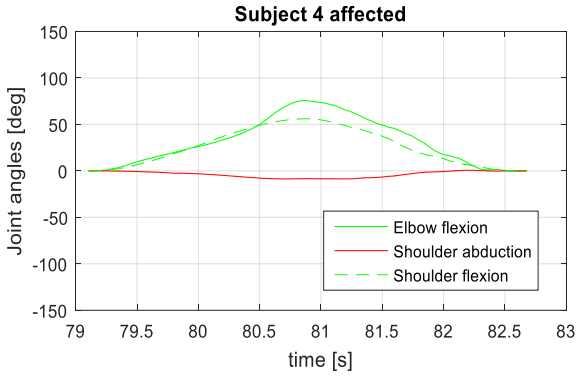
Subject 4 affected
Joint angles [deg]
time [s]
Elbow flexion
Shoulder abduction
Shoulder flexion

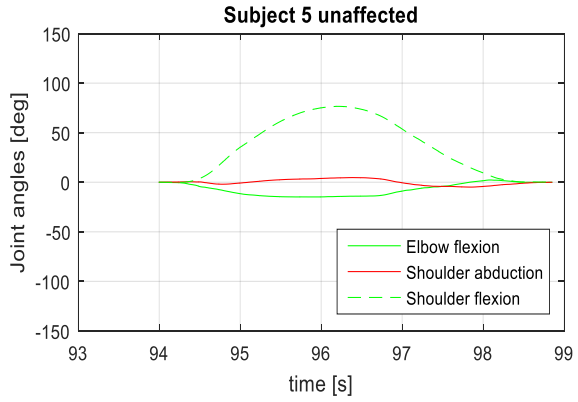
Subject 5 unaffected
Joint angles [deg]
time [s]
Elbow flexion
Shoulder abduction
Shoulder flexion

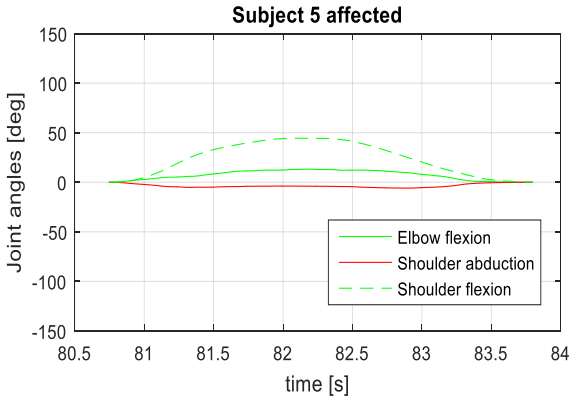
Subject 5 affected
Joint angles [deg]
time [s]
Elbow flexion
Shoulder abduction
Shoulder flexion

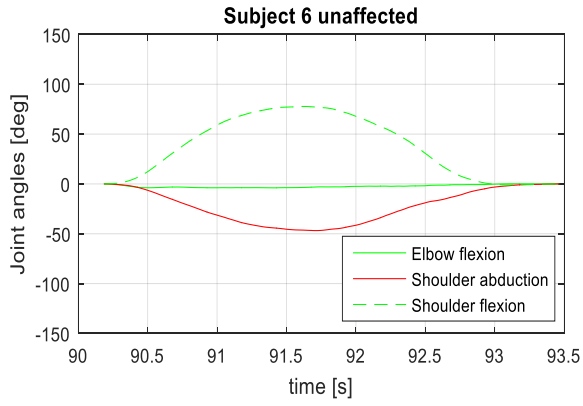
Subject 6 unaffected
Joint angles [deg]
time [s]
Elbow flexion
Shoulder abduction
Shoulder flexion

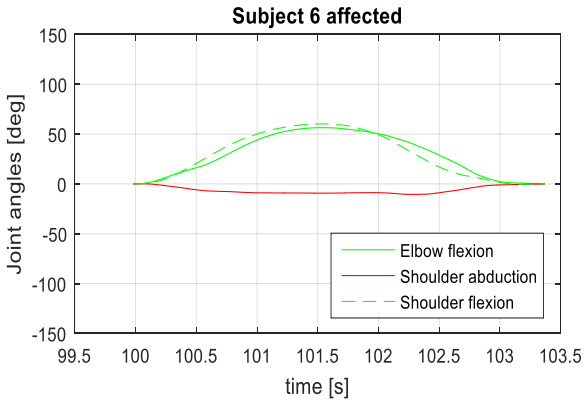
Subject 6 affected
Joint angles [deg]
time [s]
Elbow flexion
Shoulder abduction
Shoulder flexion

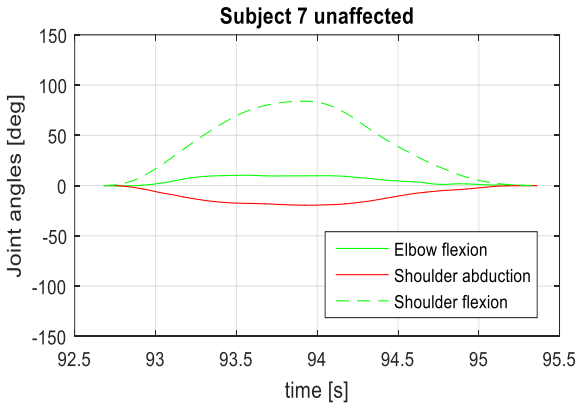
Subject 7 unaffected
Joint angles [deg]
time [s]
Elbow flexion
Shoulder abduction
Shoulder flexion

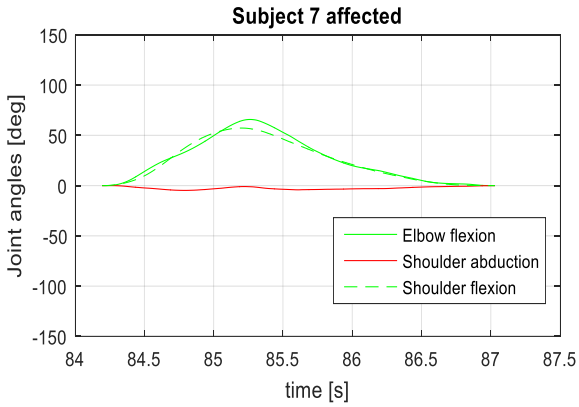
Subject 7 affected
Joint angles [deg]
time [s]
Elbow flexion
Shoulder abduction
Shoulder flexion

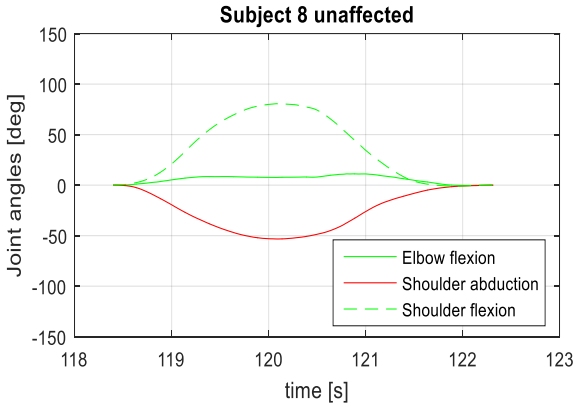
Subject 8 unaffected
Joint angles [deg]
time [s]
Elbow flexion
Shoulder abduction
Shoulder flexion

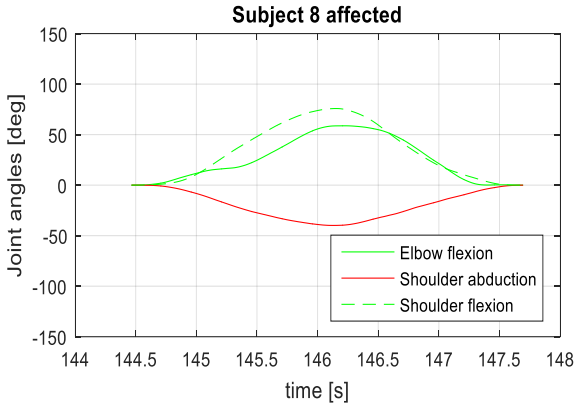
Subject 8 affected
Joint angles [deg]
time [s]
Elbow flexion
Shoulder abduction
Shoulder flexion

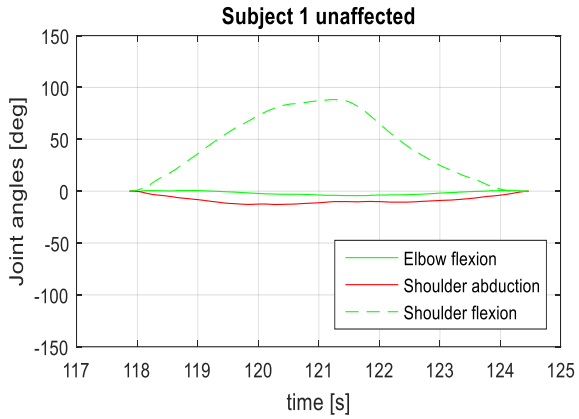
Subject 1 unaffected
Joint angles [deg]
time [s]
Elbow flexion
Shoulder abduction
Shoulder flexion

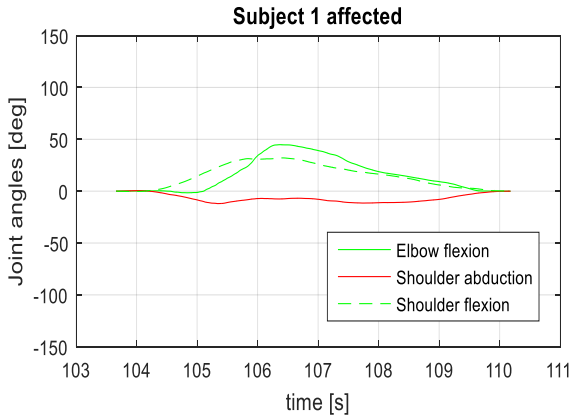
Subject 1 affected
Joint angles [deg]
time [s]
Elbow flexion
Shoulder abduction
Shoulder flexion

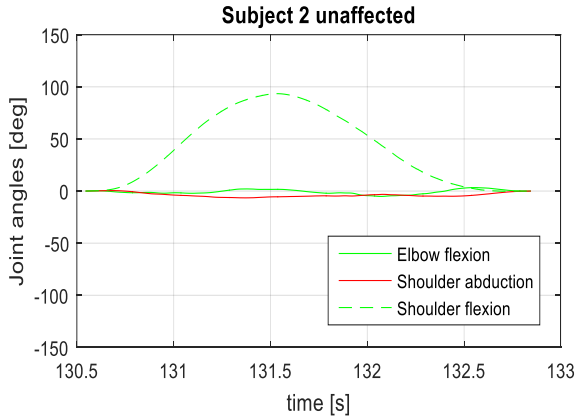
Subject 2 unaffected
Joint angles [deg]
time [s]
Elbow flexion
Shoulder abduction
Shoulder flexion

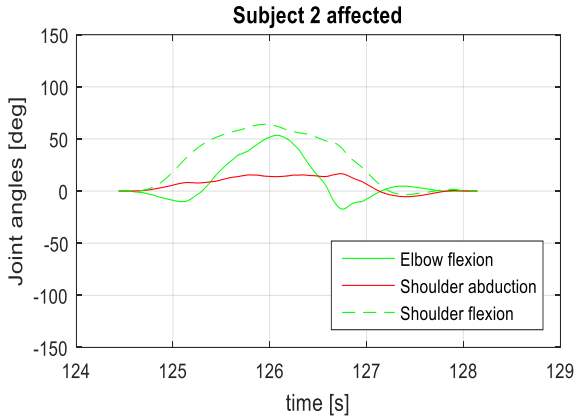
Subject 2 affected
Joint angles [deg]
time [s]
Elbow flexion
Shoulder abduction
Shoulder flexion

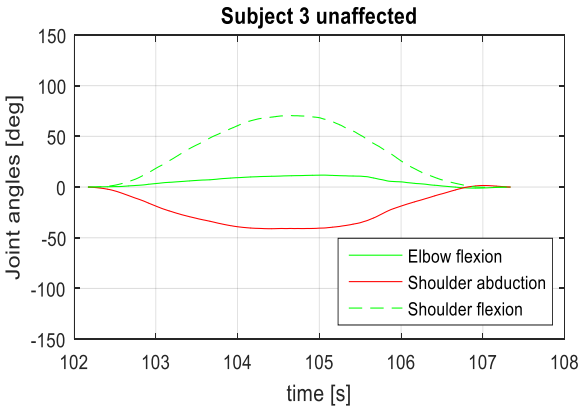
Subject 3 unaffected
Joint angles [deg]
time [s]
Elbow flexion
Shoulder abduction
Shoulder flexion

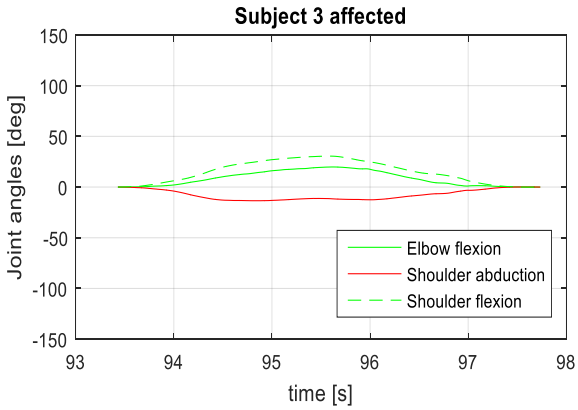
Subject 3 affected
Joint angles [deg]
time [s]
Elbow flexion
Shoulder abduction
Shoulder flexion

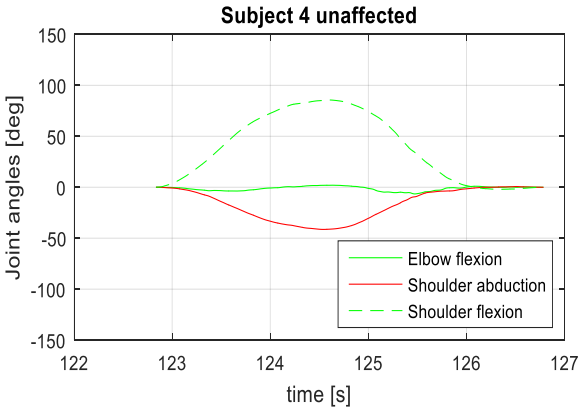
Subject 4 unaffected
Joint angles [deg]
time [s]
Elbow flexion
Shoulder abduction
Shoulder flexion

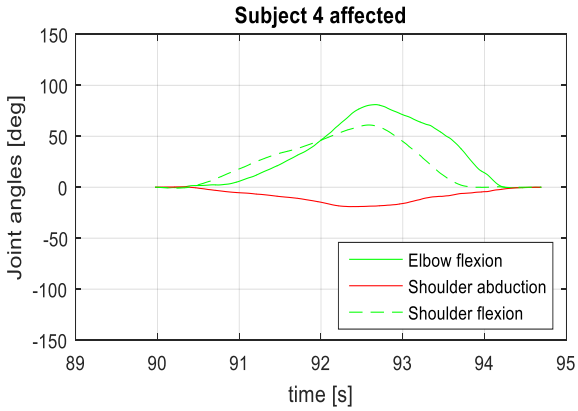
Subject 4 affected
Joint angles [deg]
time [s]
Elbow flexion
Shoulder abduction
Shoulder flexion

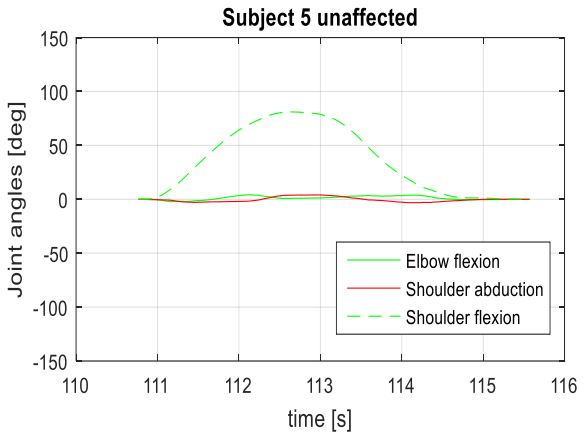
Subject 5 unaffected
Joint angles [deg]
time [s]
Elbow flexion
Shoulder abduction
Shoulder flexion

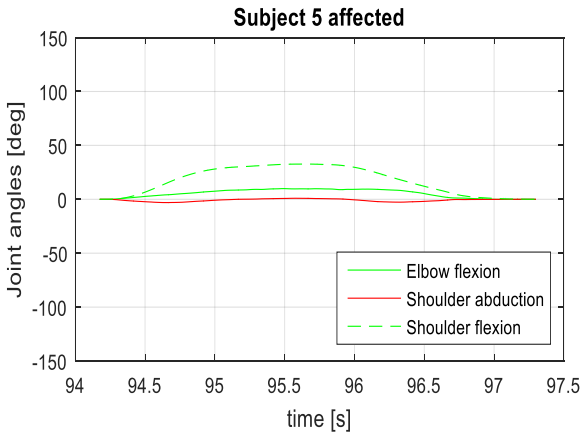
Subject 5 affected
Joint angles [deg]
time [s]
Elbow flexion
Shoulder abduction
Shoulder flexion

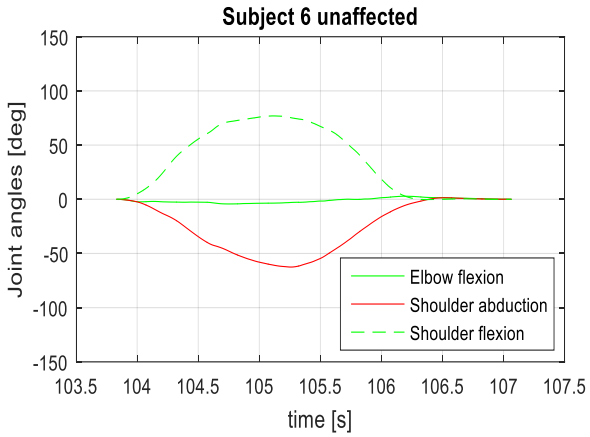
Subject 6 unaffected
Joint angles [deg]
time [s]
Elbow flexion
Shoulder abduction
Shoulder flexion

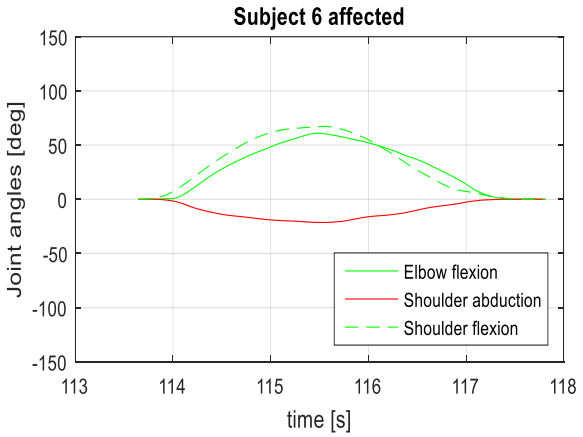
Subject 6 affected
Joint angles [deg]
time [s]
Elbow flexion
Shoulder abduction
Shoulder flexion

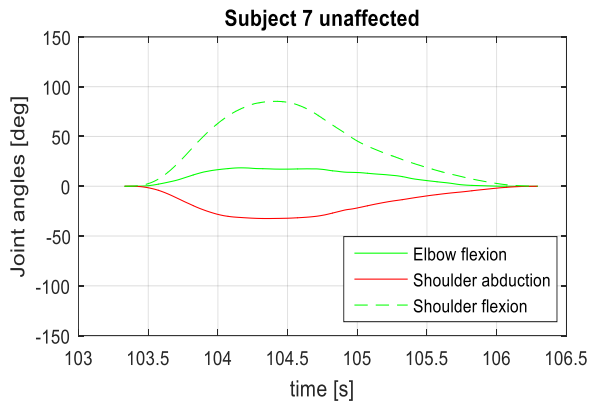

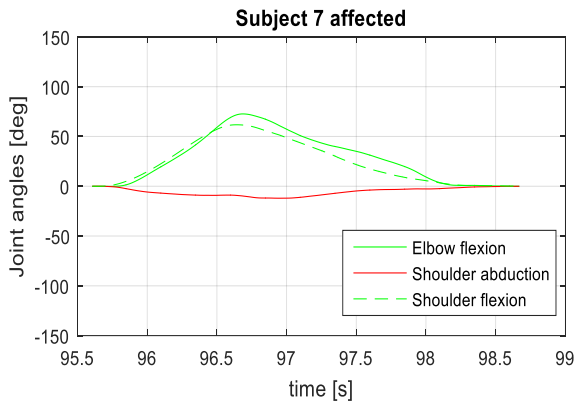

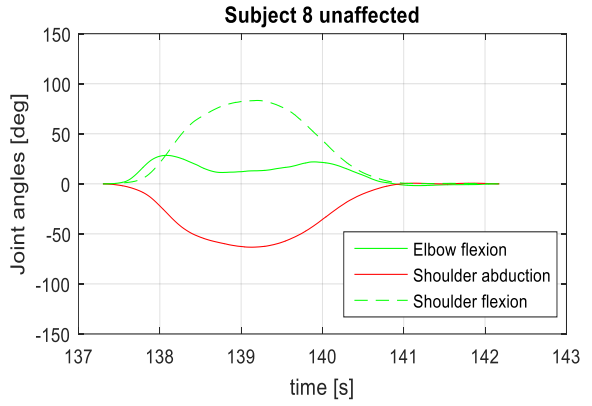

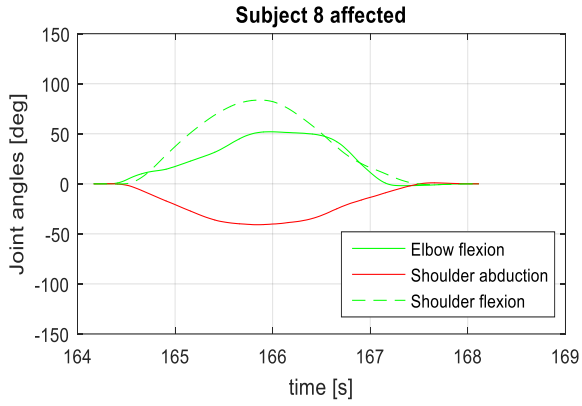

	Averaged joint angles and corresponding standard deviation (SD)					
	Shoulder abduction (SD)		Elbow flexion (SD)		Shoulder flexion (SD)	
Subject	**Unaffected**	**Affected**	**Unaffected**	**Affected**	**Unaffected**	**Affected**
1	18.1(4.7)	17.4(7.0)	5.2(1)	46.8(2.9)	84.9(5.2)	31.2(5.1)
2	6.8(3.8)	12.4(3.8)	6.8(1.4)	53.6(6.7)	89.1(5.8)	60.2(4.2)
3	34.8(5.5)	12.7(0.7)	8.5(2.9)	23.1(3)	71.3(3.6)	35.6(5.1)
4	43.1(6.3)	16.4(6.9)	7.2(0.8)	75.9(5)	83.1(4.8)	58.4(2.5)
5	7.5(5.3)	4.9(1.6)	10.5(5.6)	8.8(5)	80.7(3.9)	38.1(5.9)
6	48.6(13.1)	14.9(5.7)	4.5(0.7)	62.5(6.9)	83.7(11)	59.6(8)
7	27.9(7.3)	8(3.7)	12.9(4.8)	71.5(5.3)	85.1(1.1)	61.5(4.2)
8	52.2(11.7)	39.7(1.2)	15.3(11.6)	57.8(5.4)	78.2(6.7)	75.3(8.6)

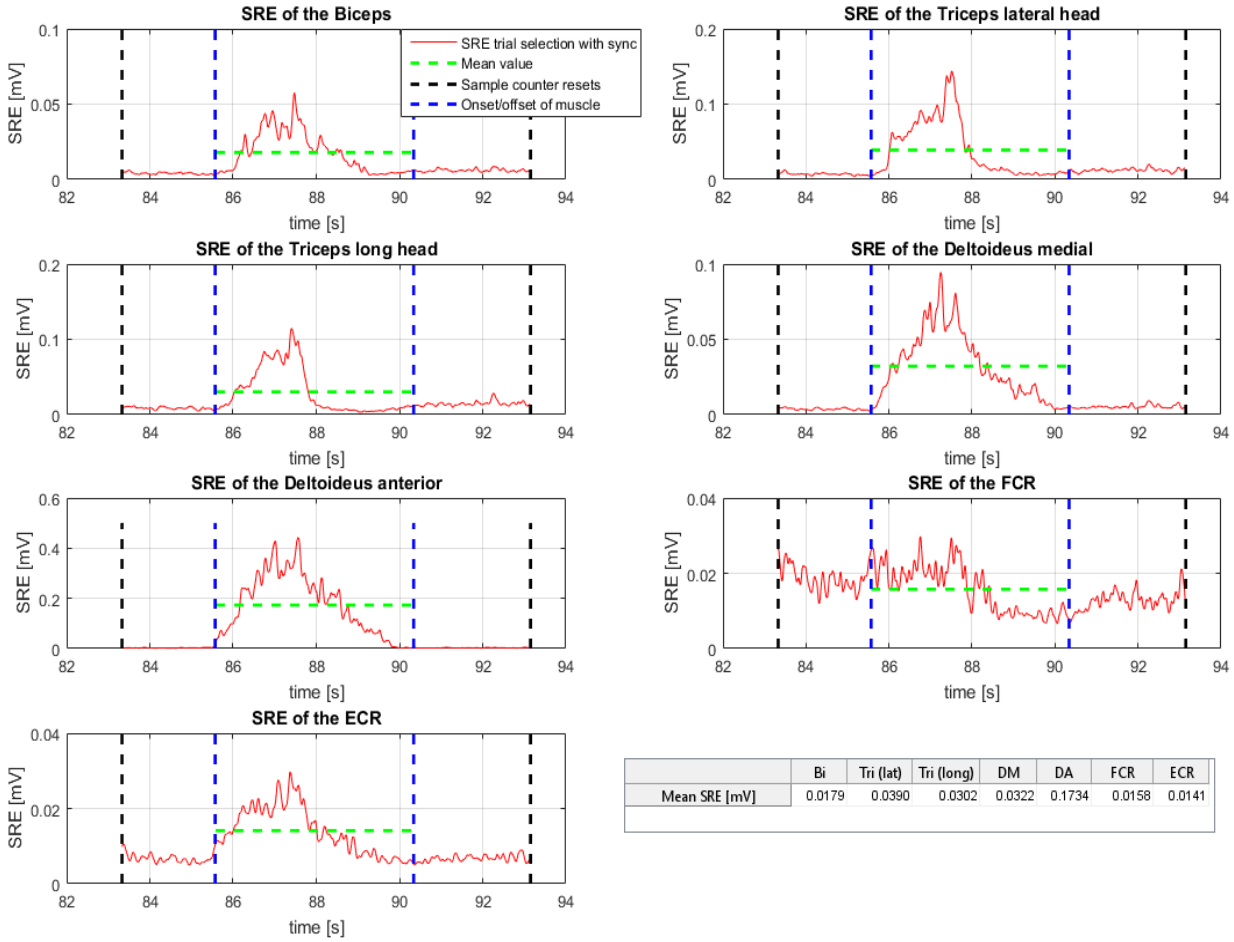

	Bi	Tri (lat)	Tri (long)	DM	DA	FCR	ECR
Mean SRE [mV]	0.0179	0.0390	0.0302	0.0322	0.1734	0.0158	0.0141

Figure 4.4.4: Smoothed rectified EMG of the biceps, triceps lateral head, triceps long head, deltoideus medial, deltoideus anterior, flexor carpi radialis (FCR), extensor carpi radialis (ECR) during the first trial concerning pathologically unaffected movements mixing synergies. The figure-table (bottom right) gives an overview of the mean values of the SREs regarding the first trial.

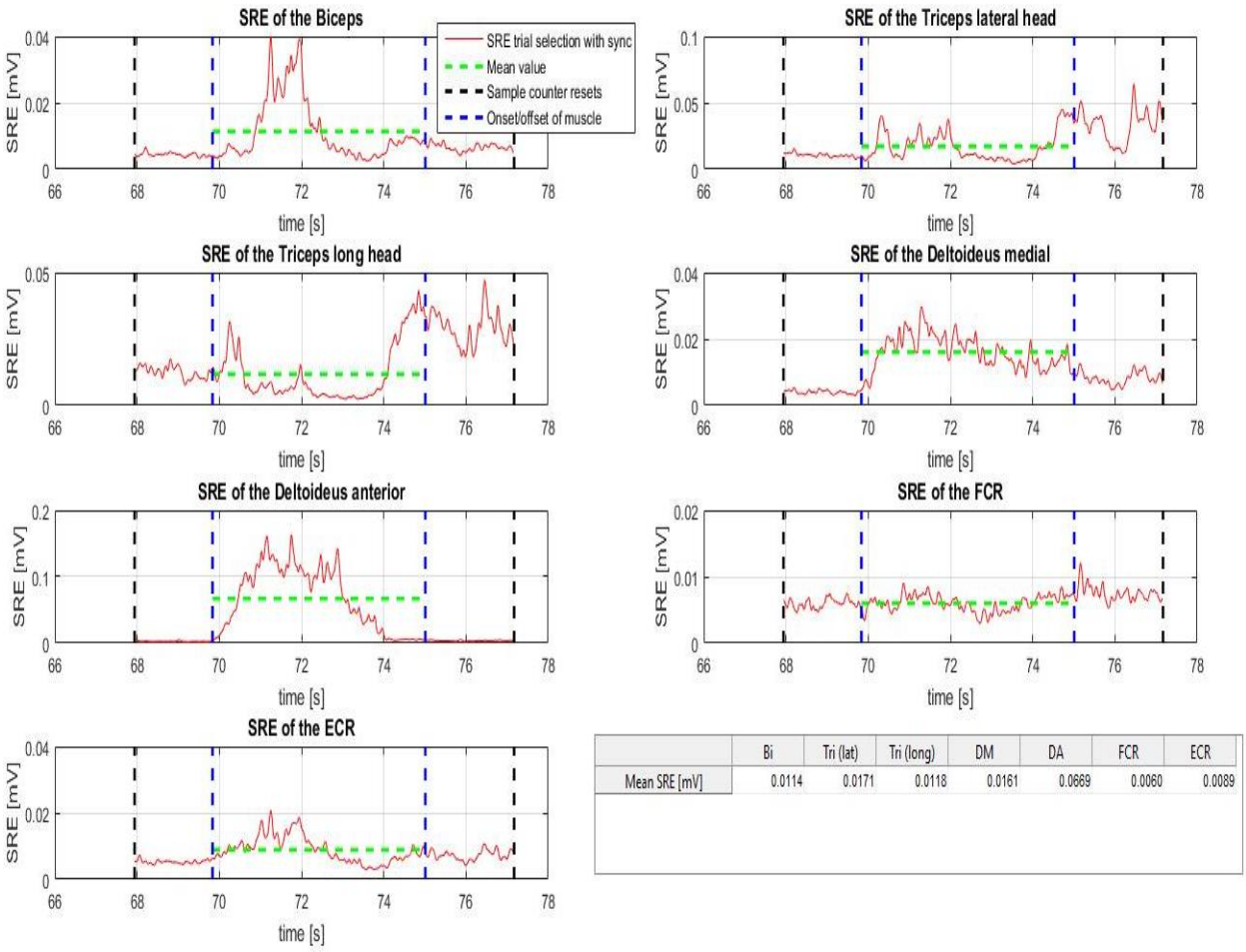

Figure 4.4.5: Smoothed rectified EMG of the biceps, triceps lateral head, triceps long head, deltoideus medial, deltoideus anterior, flexor carpi radialis (FCR), extensor carpi radialis (ECR) during the first trial concerning pathologically affected movements mixing synergies. The figure-table (bottom right) gives an overview of the mean values of the SREs regarding the first trial.

MUSCLE ACTIVITY (SD) [mV]						
	Bi		Tri (lat)		Tri (long)	
	Unaffected	Affected	Unaffected	Affected	Unaffected	Affected
Subject 1	0.0416(0.0319)	0.0248(0.0138)	0.0668(0.0319)	0.0216(0.0039)	0.0544(0.0277)	0.0139(0.0019)
Subject 2	0.0225(0.0026)	0.0183(0.0011)	0.0331(0.0043)	0.0254(0.0018)	0.0193(0.0093)	0.0178(0.0055)
Subject 3	0.0148(0.0021)	0.007(0.0004)	0.0167(0.0028)	0.0063(0.0002)	0.011(0.0016)	0.0046(0.0007)
Subject 4	0.0388(0.0041)	0.0466(0.0039)	0.0324(0.0068)	0.0285(0.005)	0.0322(0.0077)	0.0201(0.0038)
Subject 5	0.0134(0.0016)	0.02(0.0012)	0.0261(0.0049)	0.0079(0.0004)	0.0156(0.0058)	0.0035(0.0004)
Subject 6	0.0261(0.0041)	0.0174(0.0023)	0.0199(0.0026)	0.0096(0.0006)	0.0193(0.0018)	0.0063(0.0003)
Subject 7	0.0222(0.0027)	0.0172(0.0021)	0.0155(0.001)	0.0132(0.0041)	0.007(0.0002)	0.0054(0.0009)
Subject 8	0.0253(0.0043)	0.0205(0.003)	0.0219(0.0039)	0.0122(0.0006)	0.0157(0.0058)	0.0048(0.0002)

MUSCLE ACTIVITY (SD) [mV]				
	DM		DA	
	Unaffected	Affected	Unaffected	Affected
Subject 1	0.0344(0.0058)	0.0149(0.0016)	0.1471(0.0244)	0.0624(0.0062)
Subject 2	0.0346(0.0053)	0.0338(0.0005)	0.0775(0.0059)	0.0674(0.0036)
Subject 3	0.0186(0.0014)	0.0055(0.0008)	0.0313(0.0039)	0.0078(0.0015)
Subject 4	0.0748(0.0147)	0.0435(0.0048)	0.1845(0.0326)	0.0564(0.0036)
Subject 5	0.0377(0.0015)	0.0082(0.0019)	0.0572(0.0014)	0.0253(0.0044)
Subject 6	0.0221(0.0028)	0.0132(0.0019)	0.0863(0.0069)	0.0402(0.0069)
Subject 7	0.0292(0.0003)	0.016(0.0012)	0.0555(0.001)	0.0283(0.0017)
Subject 8	0.0422(0.0009)	0.0381(0.002)	0.0486(0.0013)	0.0395(0.0062)

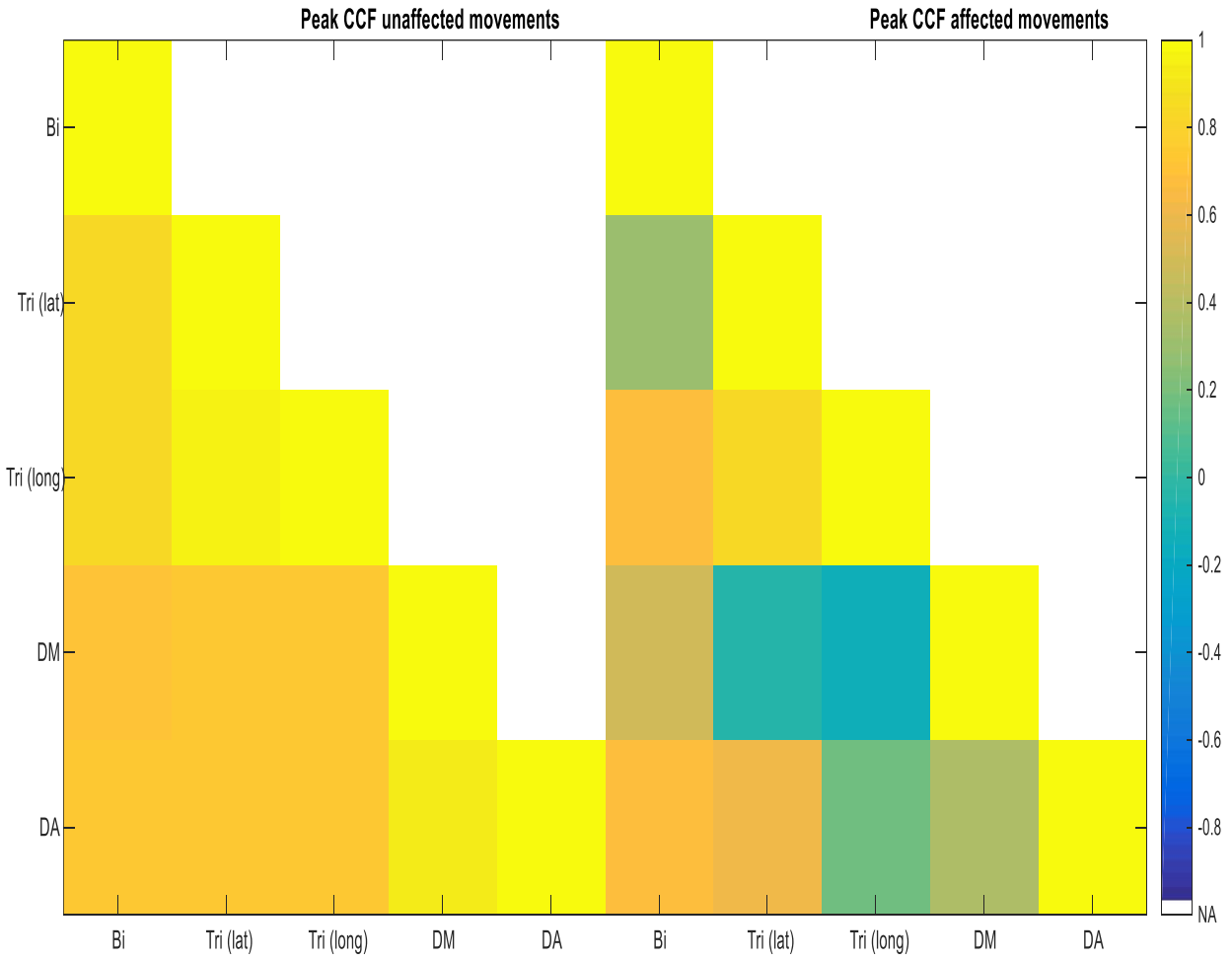

MEAN(SD) PEAK CCF UNAFFECTED MOVEMENTS					
Muscles	**Bi**	***Tri (lat)***	***Tri (long)***	**DM**	**DA**

Bi	1(0)				
Tri (lat)	0.8353(0.1214)	1(0)			
Tri (long)	0.8411(0.0911)	0.9571(0.0246)	1(0)		
DM	0.7071(0.2475)	0.7213(0.1976)	0.7256(0.1507)	1(0)	
DA	0.7275(0.272)	0.7427(0.1582)	0.7365(0.1061)	0.9088(0.0411)	1(0)

Table 2

MEAN(SD) TIME LAG CCF UNAFFECTED MOVEMENTS [s]					
Muscles	**Bi**	***Tri (lat)***	***Tri (long)***	**DM**	**DA**
Bi	0(0)				
Tri (lat)	0.0817(0.0605)	0(0)			
Tri (long)	0.0483(0.0388)	0.0033(0.0058)	0(0)		
DM	0(0)	-0.145(0.1899)	-0.98(0.7701)	0(0)	
DA	-0.415(0.5667)	-0.5517(0.6084)	-0.7317(0.789)	0(0)	0(0)

Table 3

MEAN(SD) PEAK CCF AFFECTED MOVEMENTS					
Muscles	**Bi**	***Tri (lat)***	***Tri (long)***	**DM**	**DA**
Bi	1(0)				
Tri (lat)	0.2914(0.7251)	1(0)			
Tri (long)	0.6644(0.0613)	0.827(0.0922)	1(0)		
DM	0.497(0.1868)	-0.0604(0.6048)	-0.1379(0.5182)	1(0)	
DA	0.6754(0.0605)	0.5984(0.1083)	0.1677(0.7507)	0.3454(0.5867)	1(0)

Table 4

MEAN(SD) TIME LAG CCF AFFECTED MOVEMENTS [s]					
Muscles	**Bi**	***Tri (lat)***	***Tri (long)***	**DM**	**DA**
Bi	0(0)				
Tri (lat)	-0.0617(1.2128)	0(0)			
Tri (long)	-0.3783(2.2544)	-0.0017(0.0104)	0(0)		
DM	0.7667(0.864)	-1.0533(3.5831)	-1.8417(2.8695)	0(0)	
DA	-0.12(0.1513)	-0.8783(0.2708)	-0.4433(0.7038)	1.2267(2.34)	0(0)

Table 5:

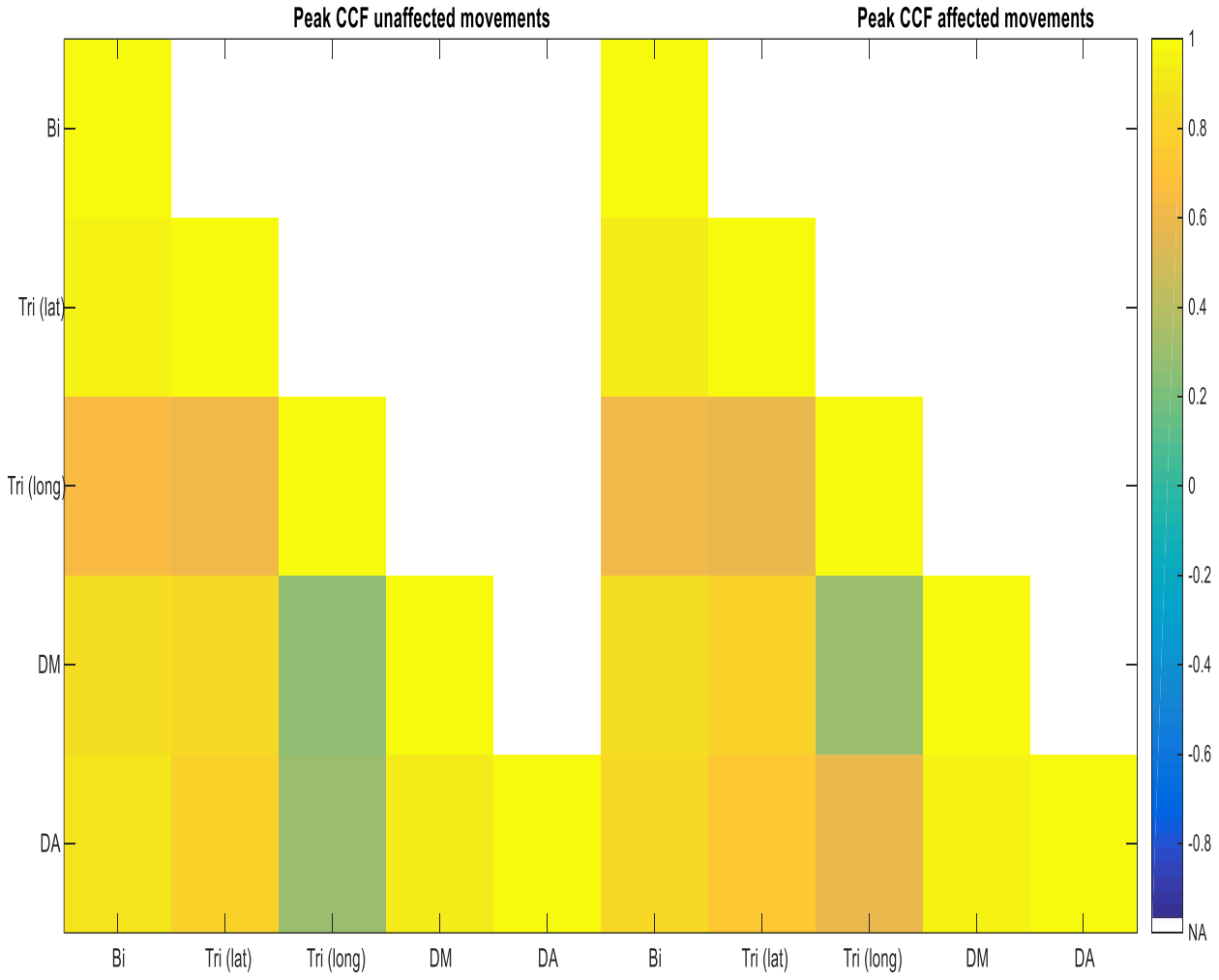

MEAN(SD) PEAK CCF UNAFFECTED MOVEMENTS					
Muscles	**Bi**	***Tri (lat)***	***Tri (long)***	**DM**	**DA**
Bi	1(0)				
Tri (lat)	0.9528(0.0241)	1(0)			
Tri (long)	0.6293(0.1518)	0.6199(0.1521)	1(0)		
DM	0.8542(0.0639)	0.8313(0.0957)	0.28(0.6002)	1(0)	
DA	0.9061(0.071)	0.8114(0.1513)	0.2976(0.6121)	0.9134(0.0488)	1(0)

Table 2

MEAN(SD) TIME LAG CCF UNAFFECTED MOVEMENTS [s]					
Muscles	**Bi**	***Tri (lat)***	***Tri (long)***	**DM**	**DA**
Bi	0(0)				
Tri (lat)	-0.0033(0.0029)	0(0)			
Tri (long)	-0.7717(1.3193)	-0.7783(1.3438)	0(0)		
DM	0.015(0.0132)	0.015(0.018)	1.0717(1.2114)	0(0)	
DA	0.005(0.0087)	0.0067(0.0115)	1.0567(1.196)	-0.0067(0.0115)	0(0)

Table 3

MEAN(SD) PEAK CCF AFFECTED MOVEMENTS					
Muscles	**Bi**	***Tri (lat)***	***Tri (long)***	**DM**	**DA**
Bi	1(0)				
Tri (lat)	0.9347(0.033)	1(0)			
Tri (long)	0.621(0.1057)	0.5917(0.0845)	1(0)		
DM	0.8638(0.0361)	0.8036(0.0791)	0.2939(0.6512)	1(0)	
DA	0.8307(0.0753)	0.7378(0.1256)	0.586(0.071)	0.9517(0.0059)	1(0)

Table 4

MEAN(SD) TIME LAG CCF AFFECTED MOVEMENTS [s]					
Muscles	**Bi**	***Tri (lat)***	***Tri (long)***	**DM**	**DA**
Bi	0(0)				
Tri (lat)	-0.005(0.005)	0(0)			
Tri (long)	-0.9633(1.6484)	-0.9083(1.6313)	0(0)		
DM	0.005(0.0132)	0.0183(0.0202)	1.2867(1.264)	0(0)	
DA	0(0)	0.0083(0.0144)	1.0067(1.739)	-0.0017(0.0029)	0(0)

Table 5:

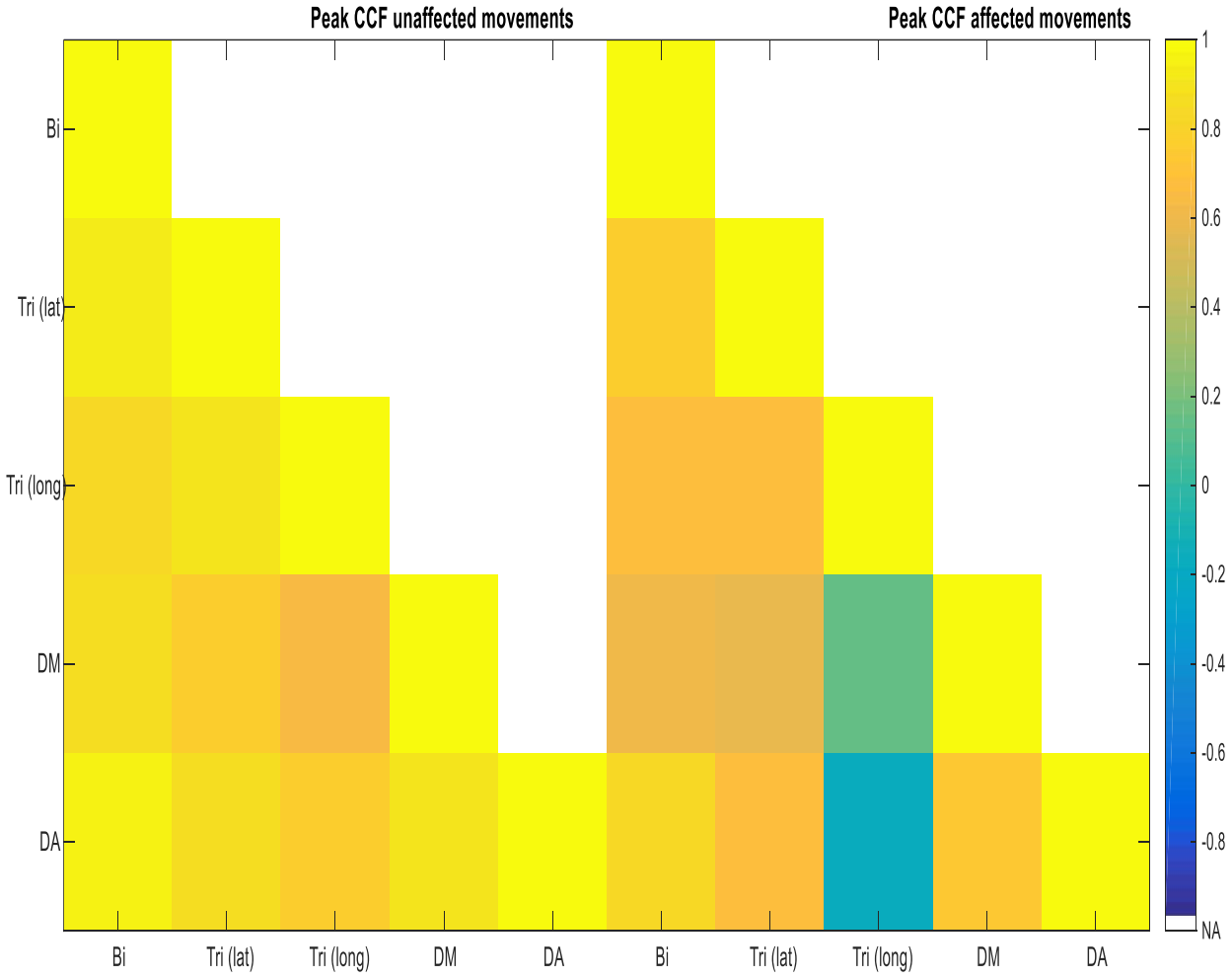

MEAN(SD) PEAK CCF UNAFFECTED MOVEMENTS					
Muscles	**Bi**	***Tri (lat)***	***Tri (long)***	**DM**	**DA**
Bi	1(0)				
Tri (lat)	0.9247(0.0301)	1(0)			
Tri (long)	0.8383(0.0249)	0.9053(0.01)	1(0)		
DM	0.8553(0.0176)	0.7783(0.048)	0.64(0.0508)	1(0)	
DA	0.9495(0.0032)	0.8644(0.0566)	0.7545(0.0243)	0.9036(0.0211)	1(0)

Table 2

MEAN(SD) TIME LAG CCF UNAFFECTED MOVEMENTS [s]					
Muscles	**Bi**	***Tri (lat)***	***Tri (long)***	**DM**	**DA**
Bi	0(0)				
Tri (lat)	0.0017(0.0029)	0(0)			
Tri (long)	-0.045(0.0444)	-0.0367(0.0208)	0(0)		
DM	0.01(0.0087)	0.0783(0.1188)	0.2083(0.1674)	0(0)	
DA	0.0117(0.0104)	0.0167(0.0289)	0.1217(0.0558)	0(0)	0(0)

Table 3

MEAN(SD) PEAK CCF AFFECTED MOVEMENTS					
Muscles	**Bi**	***Tri (lat)***	***Tri (long)***	**DM**	**DA**
Bi	1(0)				
Tri (lat)	0.7752(0.0774)	1(0)			
Tri (long)	0.6642(0.1318)	0.6589(0.0325)	1(0)		
DM	0.6249(0.026)	0.5886(0.064)	0.146(0.6565)	1(0)	
DA	0.8281(0.0601)	0.6703(0.1275)	-0.1792(0.7279)	0.719(0.0765)	1(0)

Table 4

MEAN(SD) TIME LAG CCF AFFECTED MOVEMENTS [s]					
Muscles	**Bi**	***Tri (lat)***	***Tri (long)***	**DM**	**DA**
Bi	0(0)				
Tri (lat)	0.0367(0.0293)	0(0)			
Tri (long)	0.19(2.1009)	0.2183(2.0857)	0(0)		
DM	0.285(0.286)	-0.0017(0.7119)	-0.2583(0.4876)	0(0)	
DA	-0.005(0.0087)	-0.5667(0.3676)	-0.1617(0.9848)	-0.1683(0.2872)	0(0)

Table 5:

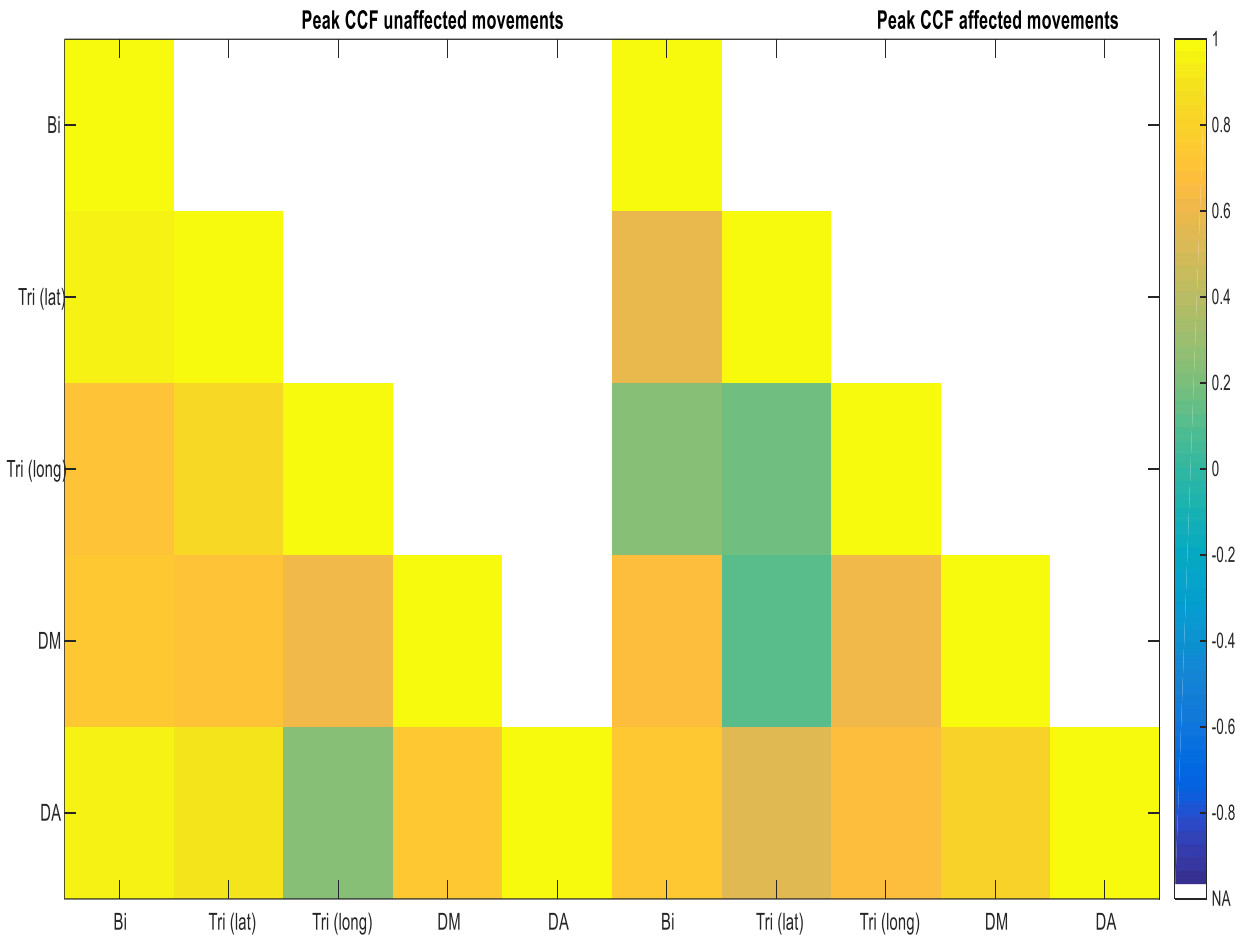

MEAN(SD) PEAK CCF UNAFFECTED MOVEMENTS					
Muscles	**Bi**	***Tri (lat)***	***Tri (long)***	**DM**	**DA**
Bi	1(0)				
Tri (lat)	0.9444(0.0147)	1(0)			
Tri (long)	0.6974(0.1301)	0.8213(0.1215)	1(0)		
DM	0.7312(0.1065)	0.7176(0.0764)	0.622(0.0722)	1(0)	
DA	0.9394(0.0074)	0.8857(0.054)	0.2323(0.7484)	0.7349(0.0936)	1(0)

Table 2

MEAN(SD) TIME LAG CCF UNAFFECTED MOVEMENTS [s]					
Muscles	**Bi**	***Tri (lat)***	***Tri (long)***	**DM**	**DA**
Bi	0(0)				
Tri (lat)	0(0)	0(0)			
Tri (long)	-0.0033(0.0153)	0.0033(0.0208)	0(0)		
DM	0.2133(0.1772)	0.4367(0.1079)	0.3583(0.345)	0(0)	
DA	0.895(0.6934)	0.5033(0.4216)	0.5583(0.4783)	0.3267(0.2747)	0(0)

Table 3

MEAN(SD) PEAK CCF AFFECTED MOVEMENTS					
Muscles	**Bi**	***Tri (lat)***	***Tri (long)***	**DM**	**DA**
Bi	1(0)				
Tri (lat)	0.5922(0.1201)	1(0)			
Tri (long)	0.2391(0.6071)	0.1603(0.6131)	1(0)		
DM	0.6802(0.1021)	0.0967(0.651)	0.6142(0.0787)	1(0)	
DA	0.7233(0.0105)	0.5593(0.1359)	0.6626(0.0106)	0.808(0.0625)	1(0)

Table 4

MEAN(SD) TIME LAG CCF AFFECTED MOVEMENTS [s]					
Muscles	**Bi**	***Tri (lat)***	***Tri (long)***	**DM**	**DA**
Bi	0(0)				
Tri (lat)	0.1233(0.218)	0(0)			
Tri (long)	-1.82(0.8487)	-0.28(0.4893)	0(0)		
DM	-0.0083(0.0076)	0.1583(0.8536)	2.1333(0.0946)	0(0)	
DA	-0.3517(0.3058)	-0.5433(0.0548)	2.0133(0.0831)	-0.0083(0.0058)	0(0)

Table 5:

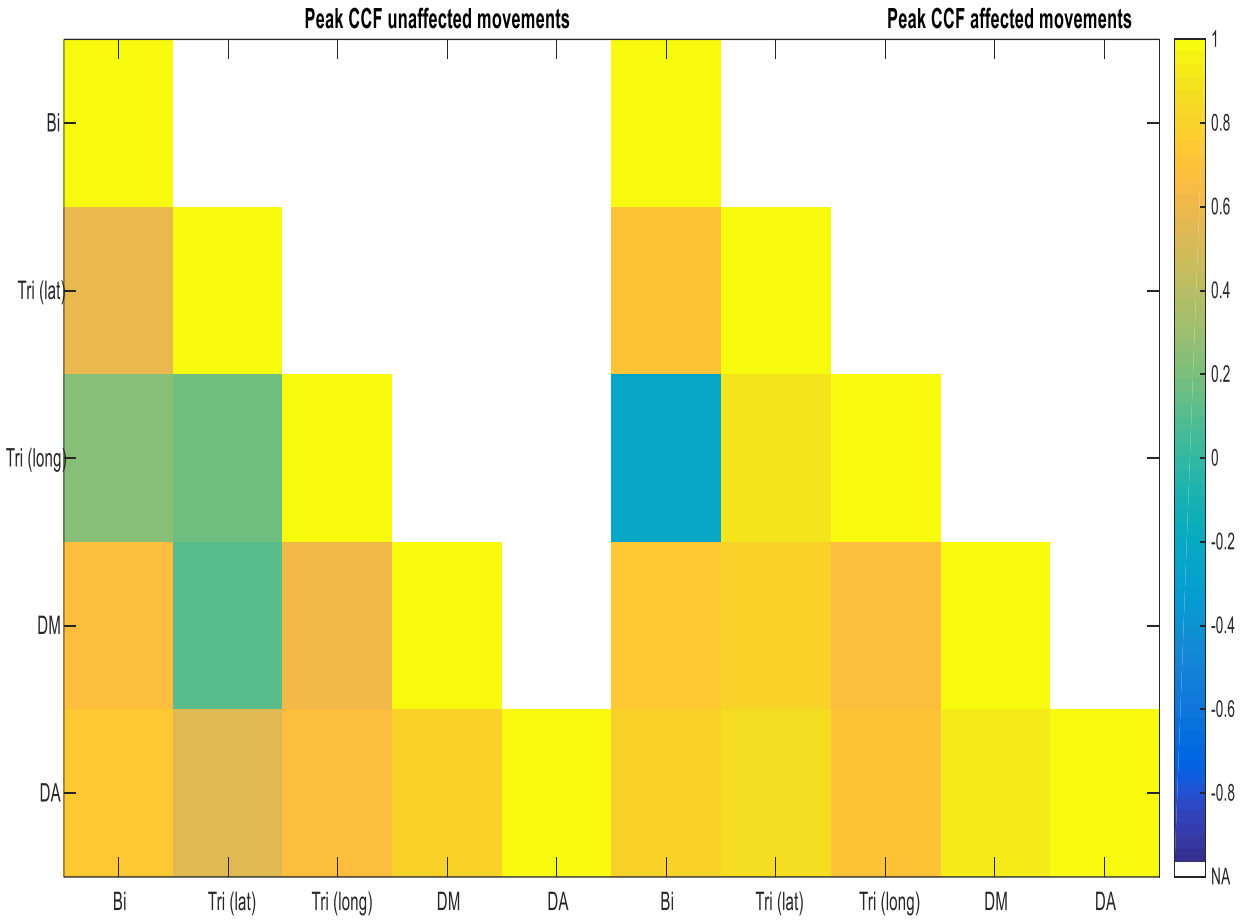

MEAN(SD) PEAK CCF UNAFFECTED MOVEMENTS					
Muscles	**Bi**	***Tri (lat)***	***Tri (long)***	**DM**	**DA**
Bi	1(0)				
Tri (lat)	0.5922(0.1201)	1(0)			
Tri (long)	0.2391(0.6071)	0.1603(0.6131)	1(0)		
DM	0.6802(0.1021)	0.0967(0.651)	0.6142(0.0787)	1(0)	
DA	0.7233(0.0105)	0.5593(0.1359)	0.6626(0.0106)	0.808(0.0625)	1(0)

Table 2

MEAN(SD) TIME LAG CCF UNAFFECTED MOVEMENTS [s]					
Muscles	**Bi**	***Tri (lat)***	***Tri (long)***	**DM**	**DA**
Bi	0(0)				
Tri (lat)	0.1233(0.218)	0(0)			
Tri (long)	-1.82(0.8487)	-0.28(0.4893)	0(0)		
DM	-0.0083(0.0076)	0.1583(0.8536)	2.1333(0.0946)	0(0)	
DA	-0.3517(0.3058)	-0.5433(0.0548)	2.0133(0.0831)	-0.0083(0.0058)	0(0)

Table 3

MEAN(SD) PEAK CCF AFFECTED MOVEMENTS					
Muscles	**Bi**	***Tri (lat)***	***Tri (long)***	**DM**	**DA**
Bi	1(0)				
Tri (lat)	0.7052(0.0301)	1(0)			
Tri (long)	-0.2461(0.5807)	0.8768(0.0584)	1(0)		
DM	0.7389(0.0371)	0.7925(0.0228)	0.668(0.1)	1(0)	
DA	0.8023(0.0825)	0.8538(0.022)	0.6998(0.1088)	0.9136(0.0172)	1(0)

Table 4

MEAN(SD) TIME LAG CCF AFFECTED MOVEMENTS [s]					
Muscles	**Bi**	***Tri (lat)***	***Tri (long)***	**DM**	**DA**
Bi	0(0)				
Tri (lat)	0.005(0.018)	0(0)			
Tri (long)	1.1867(0.9076)	0(0)	0(0)		
DM	0.0017(0.0325)	0.005(0.0087)	-0.0017(0.0029)	0(0)	
DA	0.0133(0.0231)	-0.0183(0.0236)	-0.0267(0.0104)	0.0183(0.0275)	0(0)

Table 5:

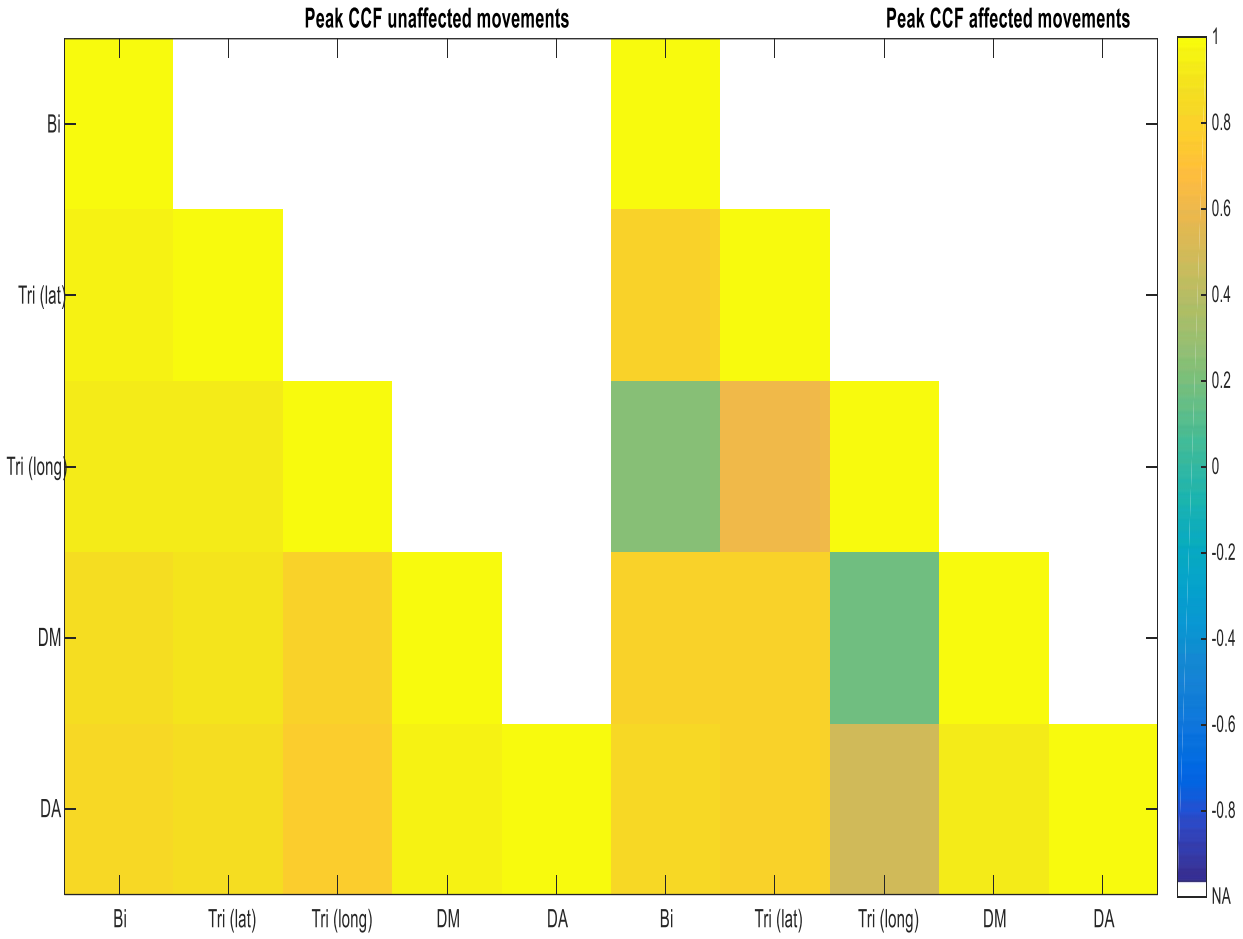

MEAN(SD) PEAK CCF UNAFFECTED MOVEMENTS					
Muscles	**Bi**	***Tri (lat)***	***Tri (long)***	**DM**	**DA**
Bi	1(0)				
Tri (lat)	0.9545(0.0212)	1(0)			
Tri (long)	0.914(0.034)	0.9142(0.0404)	1(0)		
DM	0.8693(0.0537)	0.8777(0.0387)	0.8058(0.0595)	1(0)	
DA	0.833(0.033)	0.8438(0.0231)	0.7725(0.0534)	0.943(0.0022)	1(0)

Table 2

MEAN(SD) TIME LAG CCF UNAFFECTED MOVEMENTS [s]					
Muscles	**Bi**	***Tri (lat)***	***Tri (long)***	**DM**	**DA**
Bi	0(0)				
Tri (lat)	0.01(0.0132)	0(0)			
Tri (long)	0.005(0.0087)	0(0.005)	0(0)		
DM	0.0383(0.058)	0.0067(0.0058)	0.0217(0.0189)	0(0)	
DA	0.105(0.105)	0.0267(0.0208)	0.0467(0.0161)	0.0083(0.0104)	0(0)

Table 3

MEAN(SD) PEAK CCF AFFECTED MOVEMENTS					
Muscles	**Bi**	***Tri (lat)***	***Tri (long)***	**DM**	**DA**
Bi	1(0)				
Tri (lat)	0.8079(0.0415)	1(0)			
Tri (long)	0.2307(0.4857)	0.6152(0.0296)	1(0)		
DM	0.7873(0.0415)	0.7927(0.0509)	0.1713(0.63)	1(0)	
DA	0.8231(0.0354)	0.8032(0.0167)	0.4887(0.1056)	0.9155(0.0108)	1(0)

Table 4

MEAN(SD) TIME LAG CCF AFFECTED MOVEMENTS [s]					
Muscles	**Bi**	***Tri (lat)***	***Tri (long)***	**DM**	**DA**
Bi	0(0)				
Tri (lat)	0.0117(0.0126)	0(0)			
Tri (long)	-0.9133(1.4216)	-0.72(1.2384)	0(0)		
DM	-0.1867(0.1741)	-0.22(0.22)	0.96(1.1521)	0(0)	
DA	-0.1367(0.121)	-0.2117(0.0797)	0.2917(1.2606)	0.005(0.0087)	0(0)

Table 5:

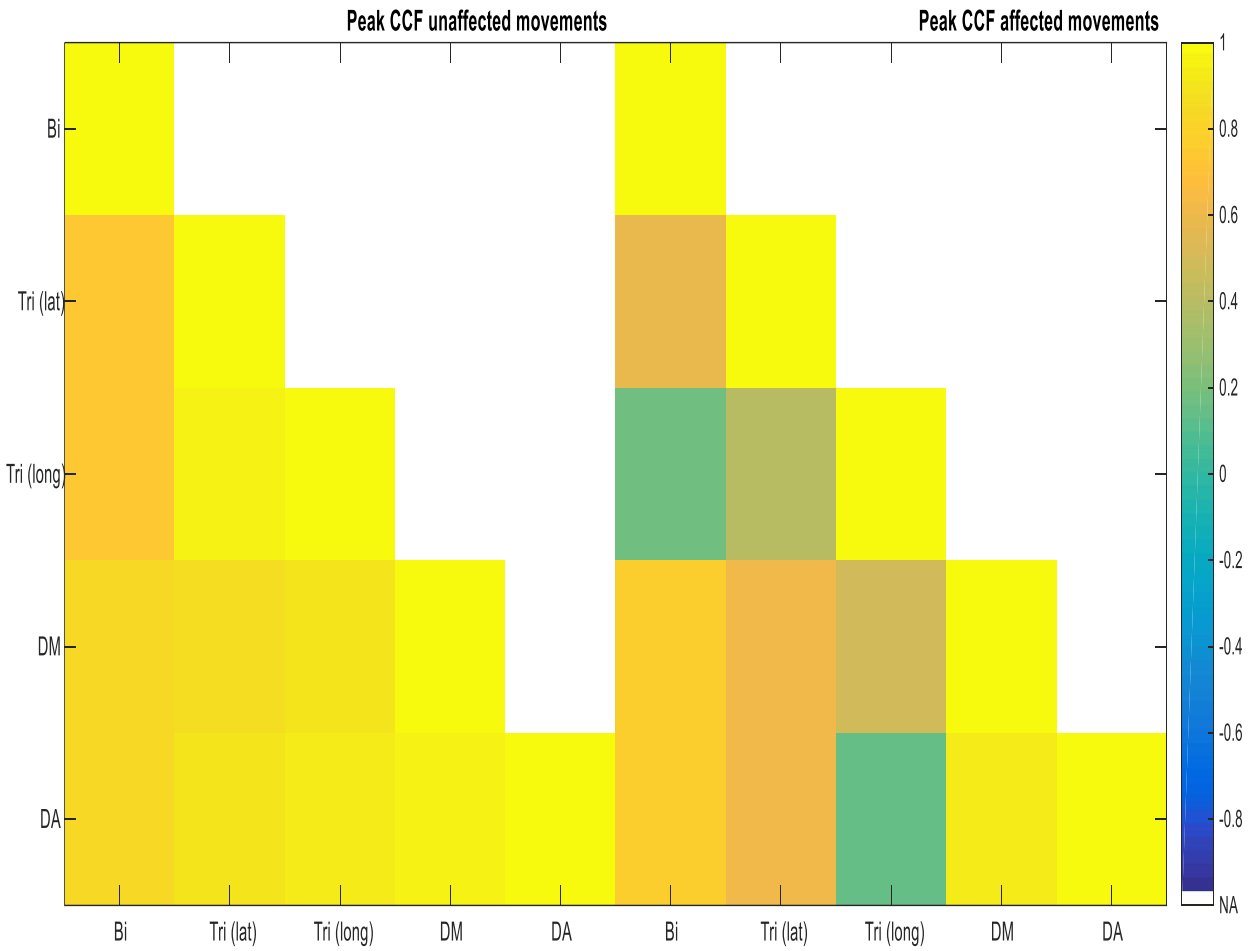

MEAN(SD) PEAK CCF UNAFFECTED MOVEMENTS					
Muscles	**Bi**	***Tri (lat)***	***Tri (long)***	**DM**	**DA**
Bi	1(0)				
Tri (lat)	0.7313(0.0615)	1(0)			
Tri (long)	0.7323(0.0479)	0.9403(0.0237)	1(0)		
DM	0.8385(0.0471)	0.856(0.0642)	0.8825(0.0326)	1(0)	
DA	0.8261(0.0249)	0.8829(0.0198)	0.9089(0.0328)	0.9451(0.0186)	1(0)

Table 2

MEAN(SD) TIME LAG CCF UNAFFECTED MOVEMENTS [s]					
Muscles	**Bi**	***Tri (lat)***	***Tri (long)***	**DM**	**DA**
Bi	0(0)				
Tri (lat)	-0.0333(0.0321)	0(0)			
Tri (long)	-0.02(0.0409)	0.0017(0.0029)	0(0)		
DM	-0.0067(0.0115)	0.0167(0.0058)	0.0233(0.0144)	0(0)	
DA	-0.0083(0.0076)	0.01(0.0132)	0.005(0.005)	-0.0017(0.0029)	0(0)

Table 3

MEAN(SD) PEAK CCF AFFECTED MOVEMENTS					
Muscles	**Bi**	***Tri (lat)***	***Tri (long)***	**DM**	**DA**
Bi	1(0)				
Tri (lat)	0.5875(0.1458)	1(0)			
Tri (long)	0.1822(0.553)	0.3782(0.8472)	1(0)		
DM	0.7551(0.0336)	0.6057(0.1018)	0.4738(0.0129)	1(0)	
DA	0.7782(0.0343)	0.6078(0.0883)	0.1439(0.5322)	0.927(0.0252)	1(0)

Table 4

MEAN(SD) TIME LAG CCF AFFECTED MOVEMENTS [s]					
Muscles	**Bi**	***Tri (lat)***	***Tri (long)***	**DM**	**DA**
Bi	0(0)				
Tri (lat)	-0.37(1.3531)	0(0)			
Tri (long)	-0.7433(1.0348)	-0.355(0.6107)	0(0)		
DM	0.0517(0.0451)	0.525(1.4522)	1.3983(1.3083)	0(0)	
DA	0.0967(0.0928)	0.6133(1.3128)	1.0433(1.0575)	0.0133(0.0153)	0(0)

Table 5:

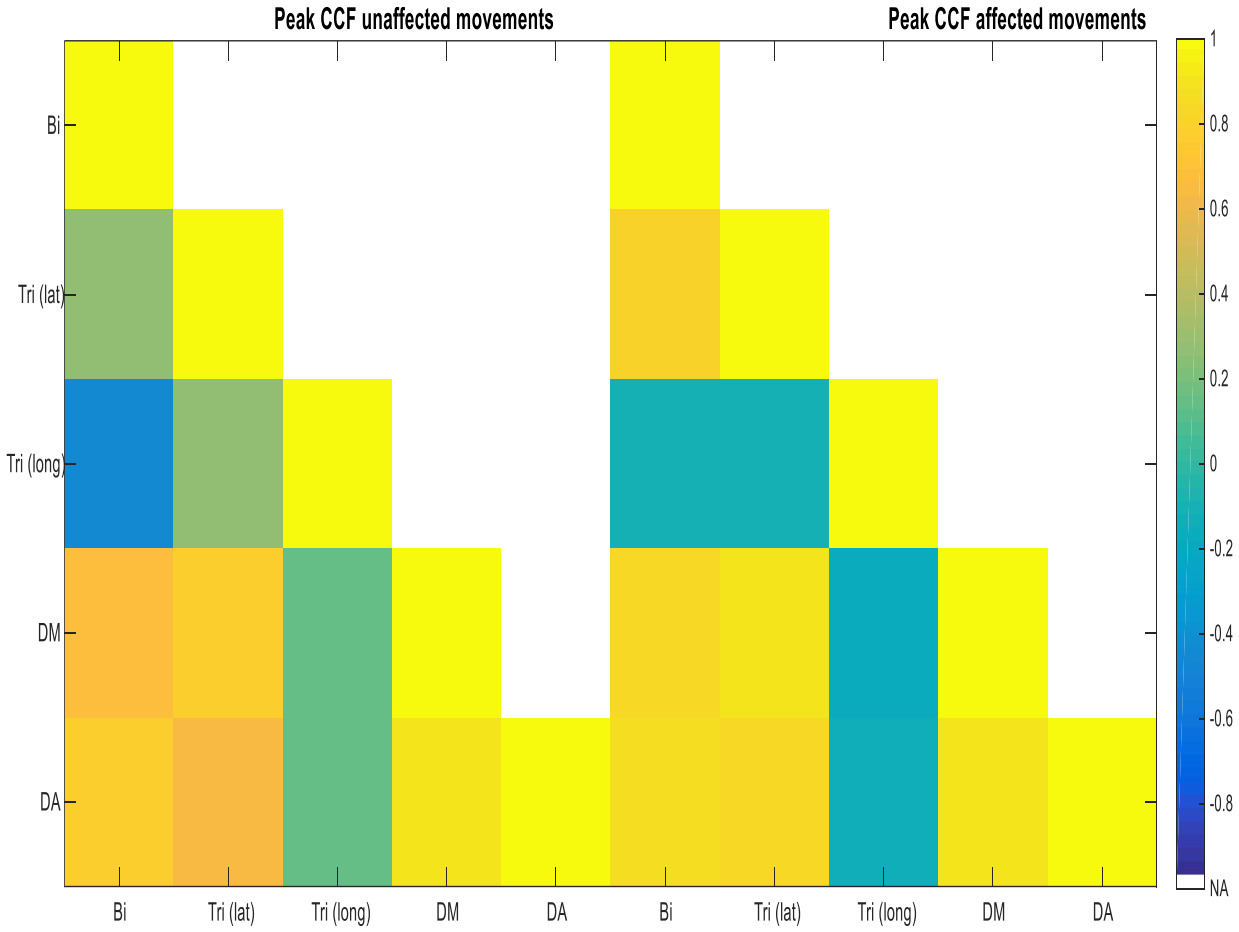

MEAN(SD) PEAK CCF UNAFFECTED MOVEMENTS					
Muscles	**Bi**	***Tri (lat)***	***Tri (long)***	**DM**	**DA**
Bi	1(0)				
Tri (lat)	0.2603(0.6239)	1(0)			
Tri (long)	-0.4378(0.0987)	0.2737(0.7361)	1(0)		
DM	0.6813(0.0578)	0.7716(0.1331)	0.1284(0.5774)	1(0)	
DA	0.7517(0.0344)	0.6504(0.2644)	0.1547(0.5218)	0.897(0.0533)	1(0)

Table 2

MEAN(SD) TIME LAG CCF UNAFFECTED MOVEMENTS [s]					
Muscles	**Bi**	***Tri (lat)***	***Tri (long)***	**DM**	**DA**
Bi	0(0)				
Tri (lat)	0.7867(1.3756)	0(0)			
Tri (long)	1.0367(1.1953)	-0.3183(0.5427)	0(0)		
DM	-0.0833(0.0907)	0.0017(0.0029)	0.5117(1.8499)	0(0)	
DA	-0.0267(0.0275)	0.175(0.1262)	0.6767(1.7262)	0.015(0.0132)	0(0)

Table 3

MEAN(SD) PEAK CCF AFFECTED MOVEMENTS					
Muscles	**Bi**	***Tri (lat)***	***Tri (long)***	**DM**	**DA**
Bi	1(0)				
Tri (lat)	0.7949(0.0476)	1(0)			
Tri (long)	-0.1047(0.6195)	-0.0988(0.7353)	1(0)		
DM	0.8198(0.0482)	0.8853(0.017)	-0.1724(0.6917)	1(0)	
DA	0.8692(0.058)	0.8178(0.0631)	-0.1468(0.6442)	0.9022(0.0292)	1(0)

Table 4

MEAN(SD) TIME LAG CCF AFFECTED MOVEMENTS [s]					
Muscles	**Bi**	***Tri (lat)***	***Tri (long)***	**DM**	**DA**
Bi	0(0)				
Tri (lat)	-0.0433(0.0375)	0(0)			
Tri (long)	-0.75(0.6235)	-0.6617(0.58)	0(0)		
DM	-0.11(0.1011)	-0.005(0.005)	0.505(0.4701)	0(0)	
DA	-0.1767(0.0794)	-0.005(0.0087)	0.555(0.5027)	0.0183(0.0362)	0(0)

Table 5:

Table 4.4.4: Maximum averaged Pearson correlation coefficients and corresponding averaged time lags regarding the pathologically unaffected and affected shoulder flexion performed by all subjects. The muscle-pair of interest is formed by the biceps brachii and the deltoideus medial.

	BICEPS — DELTOIDEUS MEDIAL			
	Maximum averaged Pearson correlation (SD)		**Corresponding Time lag (s)**	
	Unaffected	**Affected**	**Unaffected**	**Affected**
Subject 1	0.71(0.25)	0.50(0.19)	0.00(0.00)	0.77(0.86)
Subject 2	0.85(0.06)	0.86(0.04)	0.02(0.01)	0.01(0.01)
Subject 3	0.86(0.02)	0.62(0.03)	0.01(0.01)	0.29(0.29)
Subject 4	0.73(0.11)	0.68(0.10)	0.21(0.18)	-0.01(0.01)
Subject 5	0.68(0.10)	0.74(0.04)	-0.01(0.01)	0.00(0.03)
Subject 6	0.87(0.05)	0.79(0.04)	0.04(0.06)	-0.19(0.17)
Subject 7	0.84(0.05)	0.76(0.03)	-0.01(0.01)	0.05(0.05)
Subject 8	0.68(0.06)	0.82(0.05)	-0.08(0.09)	-0.11(0.10)

Table 4.4.5: Maximum averaged Pearson correlation coefficients and corresponding averaged time lags regarding the pathologically unaffected and affected shoulder flexion performed by all subjects. The muscle-pair of interest is formed by the biceps brachii and the deltoideus anterior.

	BICEPS — DELTOIDEUS ANTERIOR	
	Maximum averaged Pearson correlation (SD)	**Corresponding Time lag (s)**

	Unaffected	Affected	Unaffected	Affected
Subject 1	0.73(0.27)	0.68(0.06)	-0.42(0.57)	-0.12(0.15)
Subject 2	0.91(0.07)	0.83(0.08)	0.01(0.01)	0.00(0.00)
Subject 3	0.95(0.00)	0.83(0.06)	0.01(0.01)	-0.01(0.01)
Subject 4	0.94(0.01)	0.72(0.01)	0.90(0.69)	-0.35(0.31)
Subject 5	0.72(0.01)	0.80(0.08)	-0.35(0.31)	0.01(0.02)
Subject 6	0.83(0.03)	0.82(0.04)	0.11(0.11)	-0.14(0.12)
Subject 7	0.83(0.02)	0.78(0.03)	-0.01(0.01)	0.10(0.09)
Subject 8	0.75(0.03)	0.87(0.06)	-0.03(0.03)	-0.18(0.08)

Table 4.4.6: Maximum averaged Pearson correlation coefficients and corresponding averaged time lags regarding the pathologically unaffected and affected shoulder flexion performed by all subjects. The muscle-pair of interest is formed by the deltoideus medial and the deltoideus anterior.

DELTOIDEUS MEDIAL — DELTOIDEUS ANTERIOR				
	Maximum averaged Pearson correlation (SD)		Corresponding Time lag (s)	
	Unaffected	Affected	Unaffected	Affected
Subject 1	0.91(0.04)	0.35(0.59)	0.00(0.00)	1.23(2.34)
Subject 2	0.91(0.05)	0.95(0.01)	-0.01(0.01)	-0.00(0.00)
Subject 3	0.90(0.02)	0.72(0.08)	0.00(0.00)	-0.17(0.29)
Subject 4	0.73(0.09)	0.81(0.06)	0.33(0.27)	-0.01(0.01)
Subject 5	0.81(0.06)	0.91(0.02)	-0.01(0.01)	0.02(0.03)
Subject 6	0.94(0.00)	0.92(0.01)	0.01(0.01)	0.01(0.01)
Subject 7	0.95(0.02)	0.93(0.03)	-0.00(0.00)	0.01(0.02)
Subject 8	0.90(0.05)	0.90 (0.03)	0.02(0.01)	0.02(0.04)

APPENDIX D MOVEMENTS OUT OF SYNERGIES

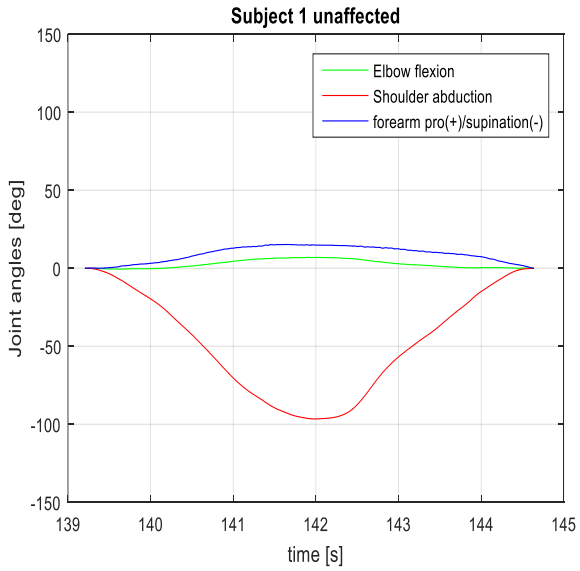

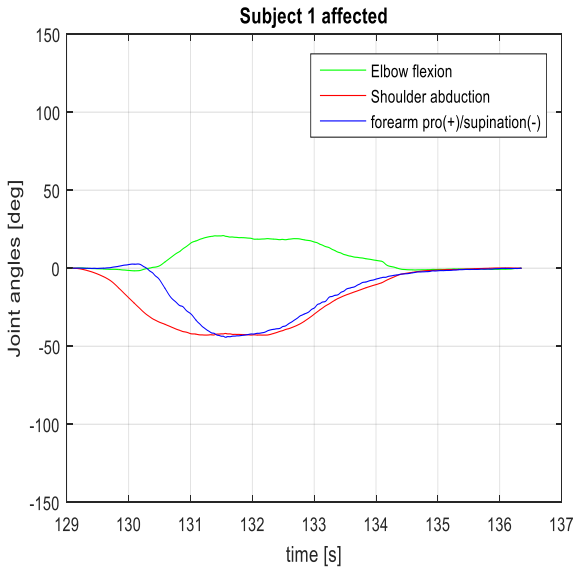

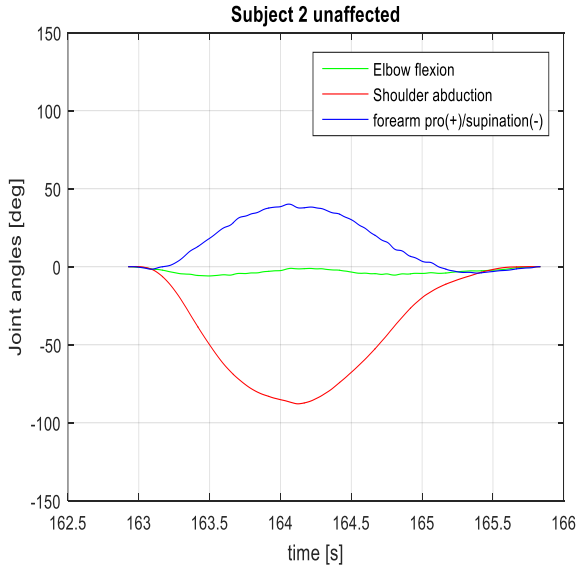

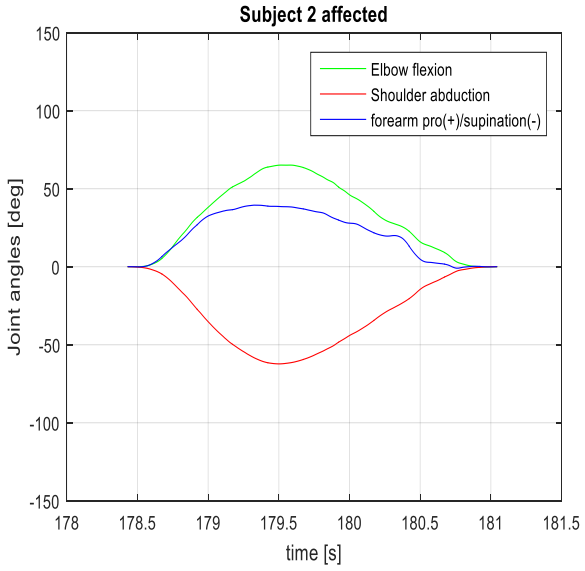

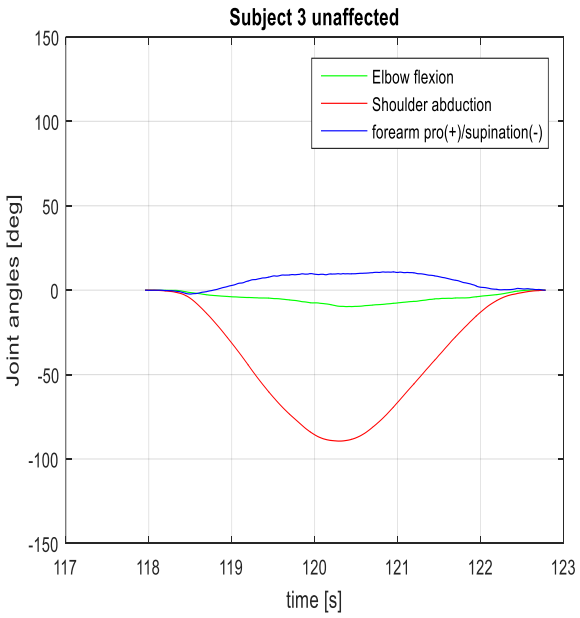
Subject 3 unaffected
Elbow flexion
Shoulder abduction
forearm pro(+)/supination(-)
Joint angles [deg]
time [s]

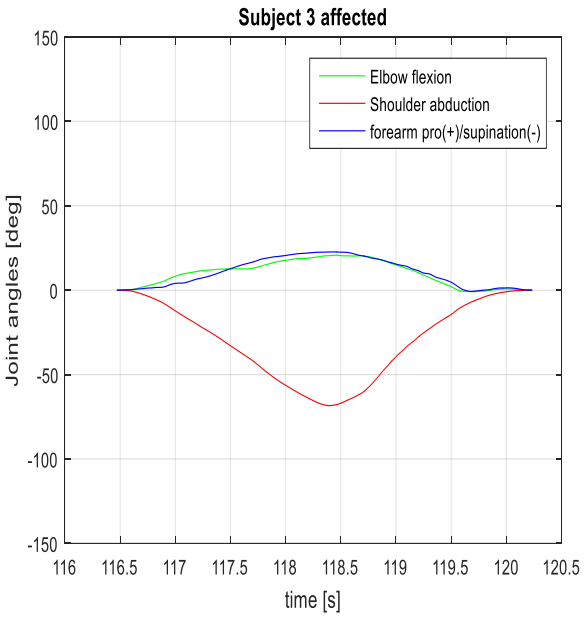
Subject 3 affected
Elbow flexion
Shoulder abduction
forearm pro(+)/supination(-)
Joint angles [deg]
time [s]

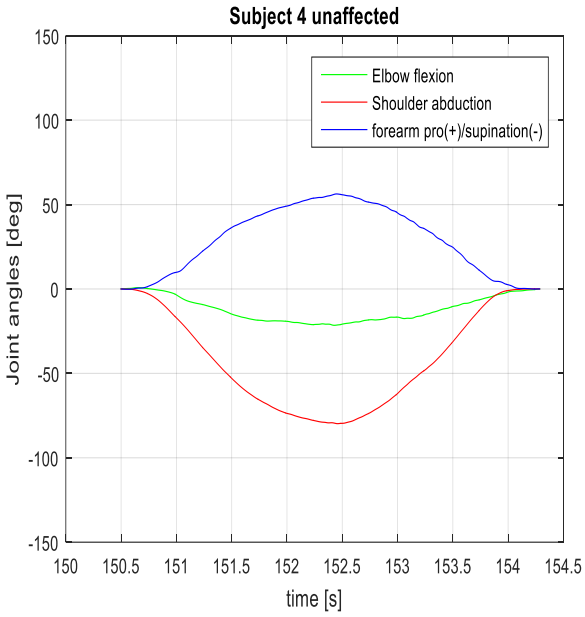
Subject 4 unaffected
Elbow flexion
Shoulder abduction
forearm pro(+)/supination(-)
Joint angles [deg]
time [s]

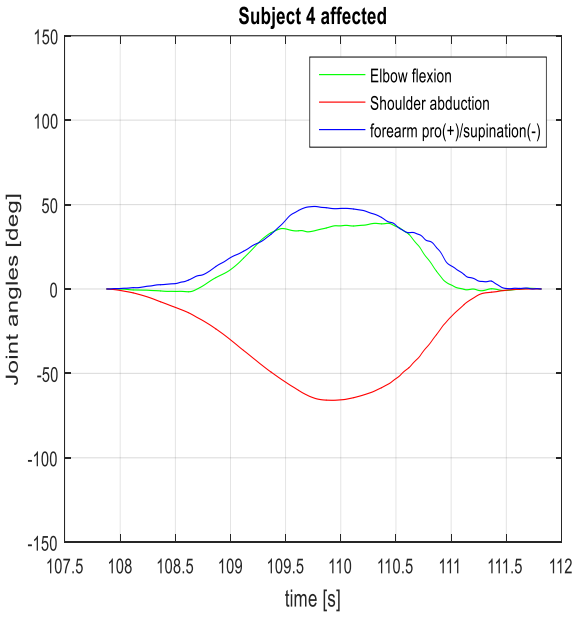
Subject 4 affected
Elbow flexion
Shoulder abduction
forearm pro(+)/supination(-)
Joint angles [deg]
time [s]

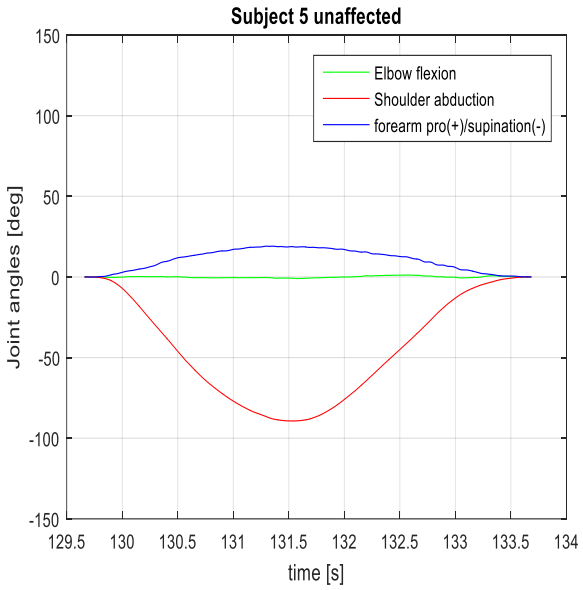
Subject 5 unaffected
Elbow flexion
Shoulder abduction
forearm pro(+)/supination(-)
Joint angles [deg]
time [s]

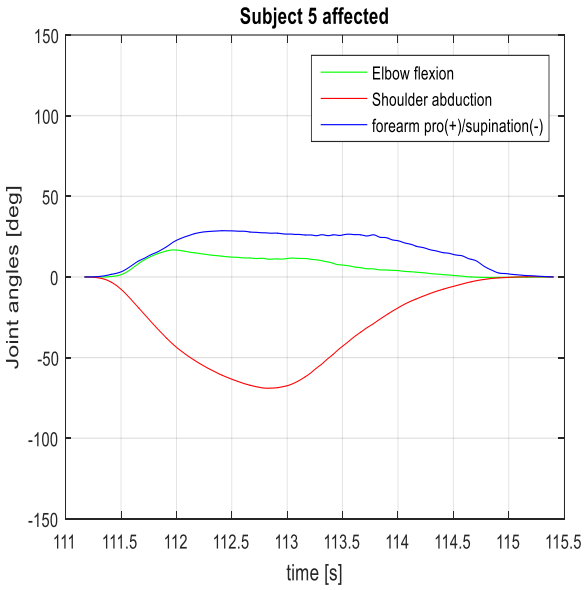
Subject 5 affected
Elbow flexion
Shoulder abduction
forearm pro(+)/supination(-)
Joint angles [deg]
time [s]

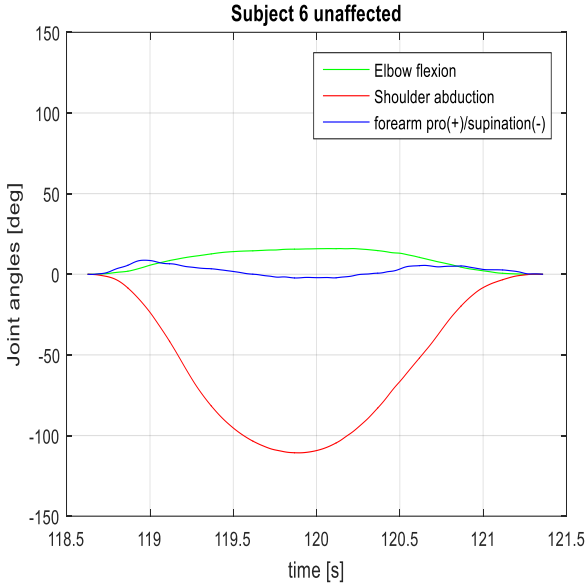
Subject 6 unaffected
Elbow flexion
Shoulder abduction
forearm pro(+)/supination(-)
Joint angles [deg]
time [s]

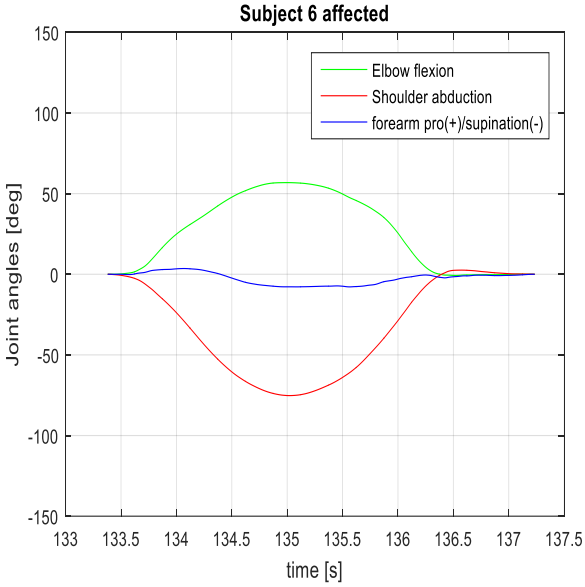
Subject 6 affected
Elbow flexion
Shoulder abduction
forearm pro(+)/supination(-)
Joint angles [deg]
time [s]

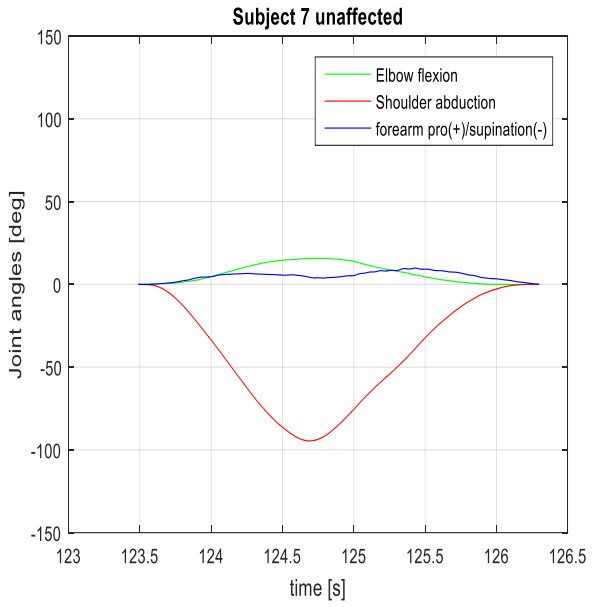
Subject 7 unaffected
Elbow flexion
Shoulder abduction
forearm pro(+)/supination(-)
Joint angles [deg]
time [s]

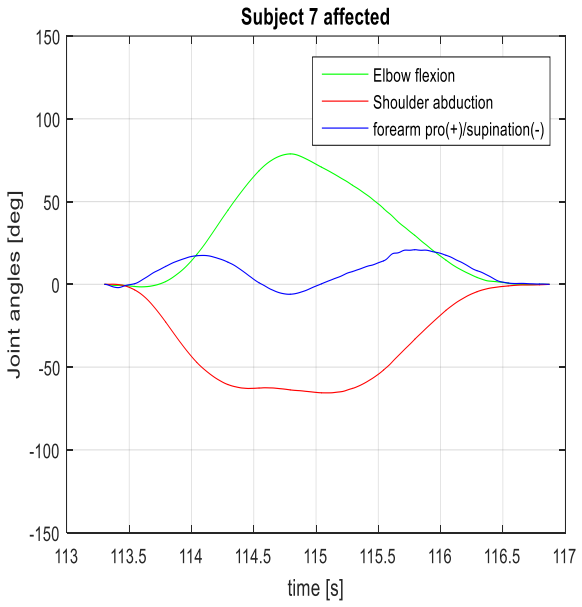
Subject 7 affected
Elbow flexion
Shoulder abduction
forearm pro(+)/supination(-)
Joint angles [deg]
time [s]

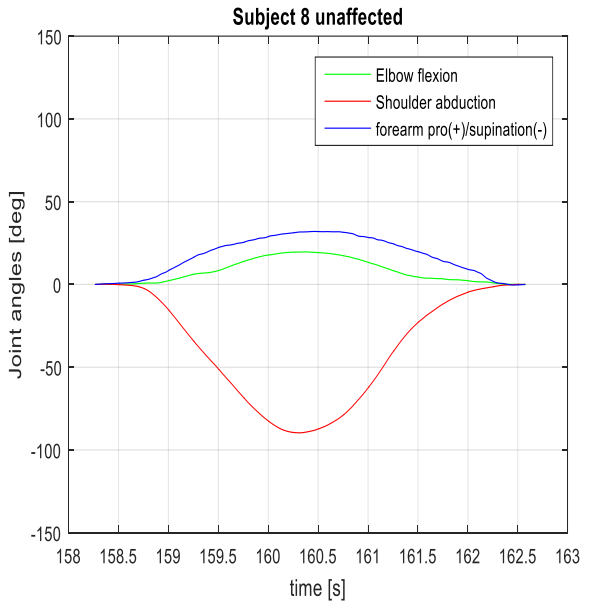
Subject 8 unaffected
Elbow flexion
Shoulder abduction
forearm pro(+)/supination(-)
Joint angles [deg]
time [s]

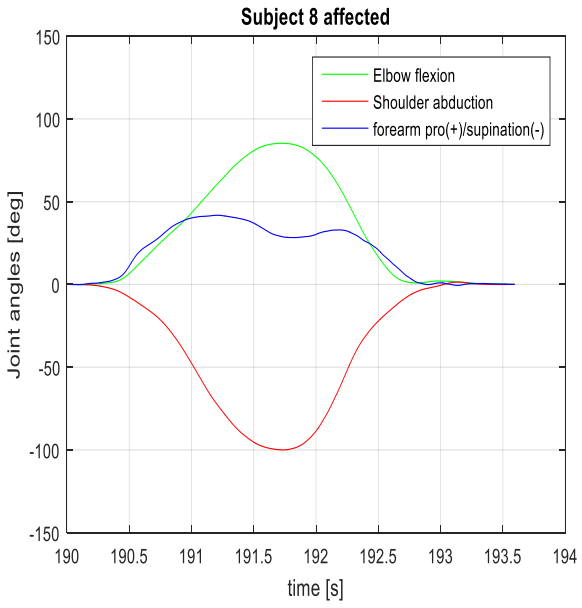
Subject 8 affected
Elbow flexion
Shoulder abduction
forearm pro(+)/supination(-)
Joint angles [deg]
time [s]

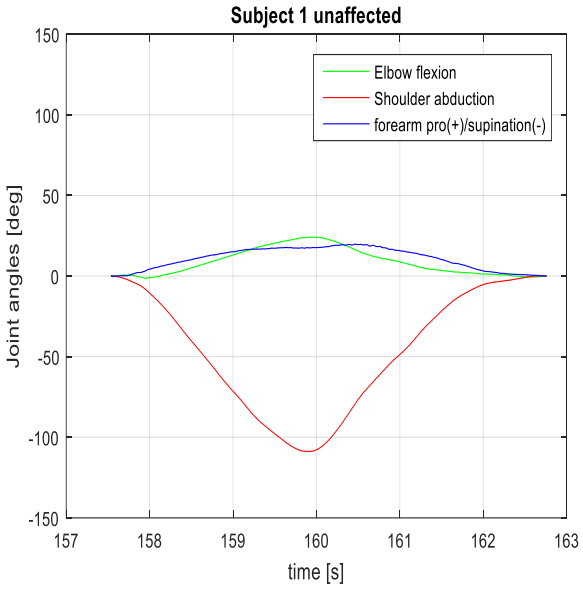
Subject 1 unaffected
Elbow flexion
Shoulder abduction
forearm pro(+)/supination(-)
Joint angles [deg]
time [s]
150
100
50
0
-50
-100
-150
157
158
159
160
161
162
163

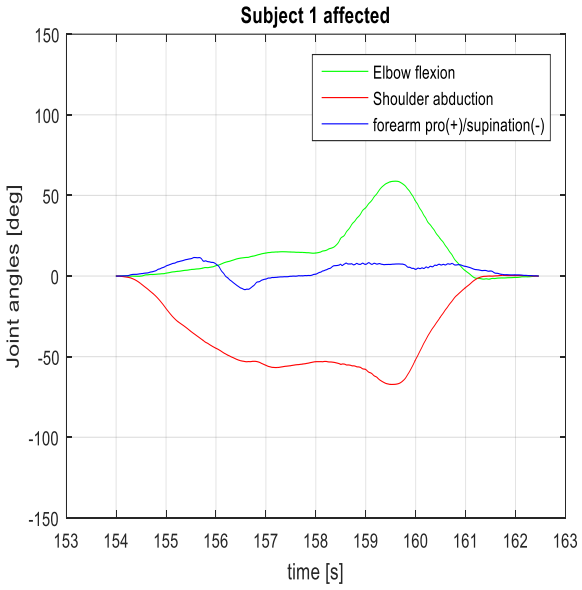
Subject 1 affected
Elbow flexion
Shoulder abduction
forearm pro(+)/supination(-)
Joint angles [deg]
time [s]
150
100
50
0
-50
-100
-150
153
154
155
156
157
158
159
160
161
162
163

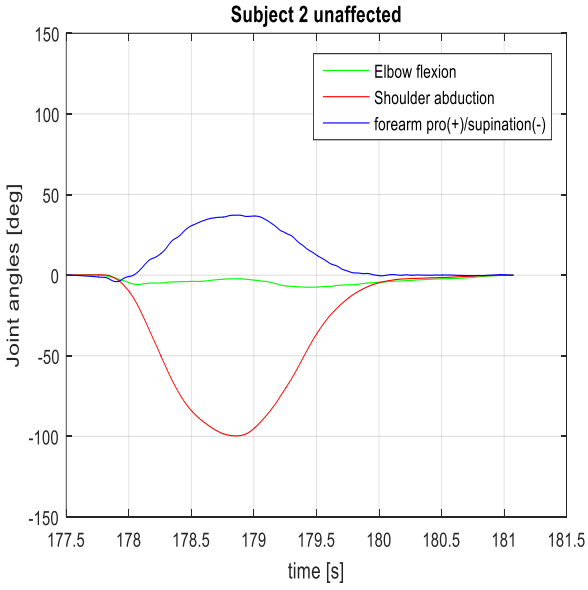
Subject 2 unaffected
Elbow flexion
Shoulder abduction
forearm pro(+)/supination(-)
Joint angles [deg]
time [s]
150
100
50
0
-50
-100
-150
177.5
178
178.5
179
179.5
180
180.5
181
181.5

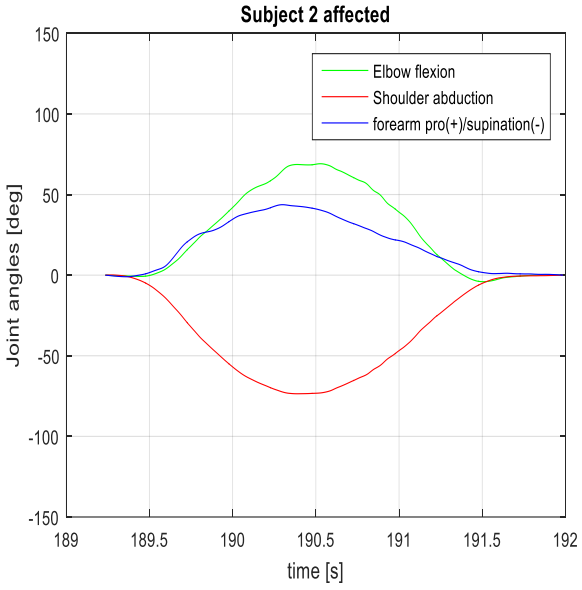
Subject 2 affected
Elbow flexion
Shoulder abduction
forearm pro(+)/supination(-)
Joint angles [deg]
time [s]
150
100
50
0
-50
-100
-150
189
189.5
190
190.5
191
191.5
192

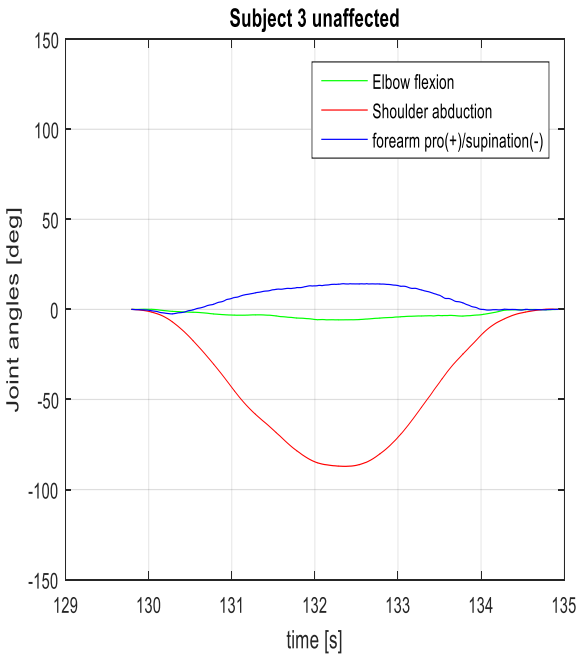
Subject 3 unaffected
Elbow flexion
Shoulder abduction
forearm pro(+)/supination(-)
Joint angles [deg]
time [s]

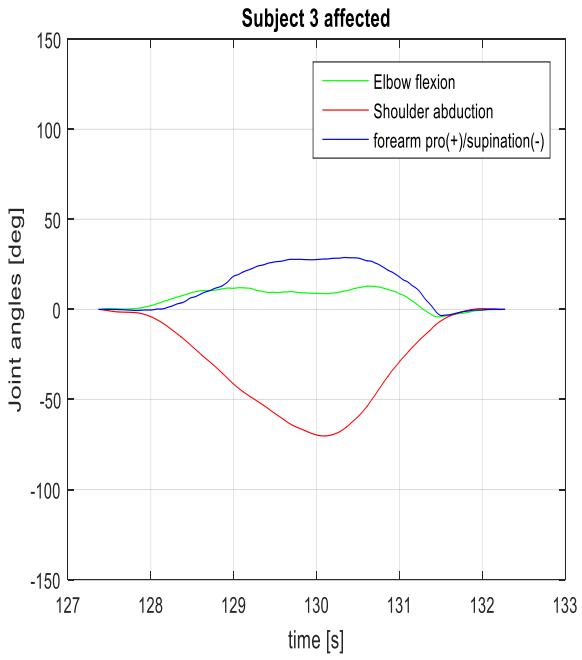
Subject 3 affected
Elbow flexion
Shoulder abduction
forearm pro(+)/supination(-)
Joint angles [deg]
time [s]

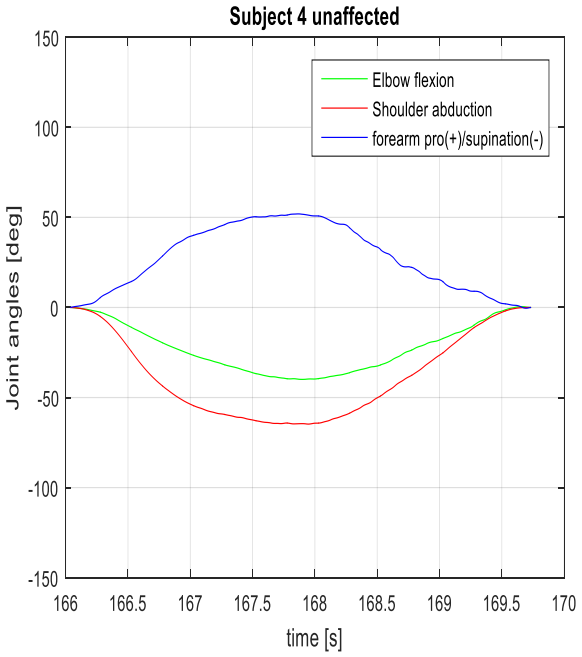
Subject 4 unaffected
Elbow flexion
Shoulder abduction
forearm pro(+)/supination(-)
Joint angles [deg]
time [s]

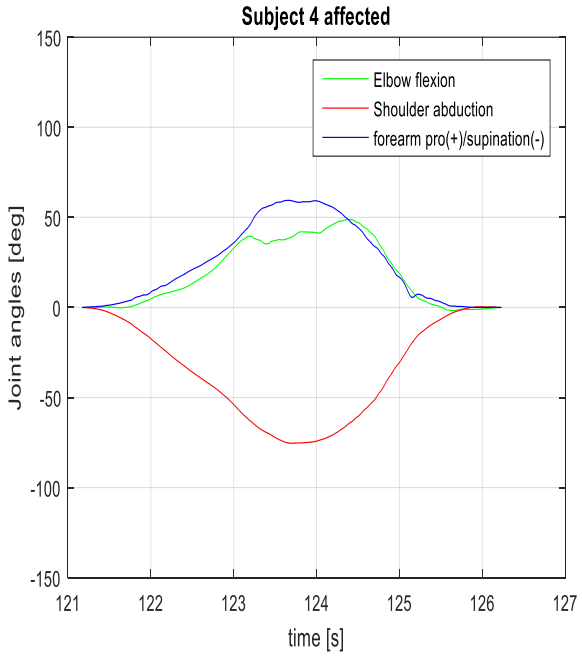
Subject 4 affected
Elbow flexion
Shoulder abduction
forearm pro(+)/supination(-)
Joint angles [deg]
time [s]

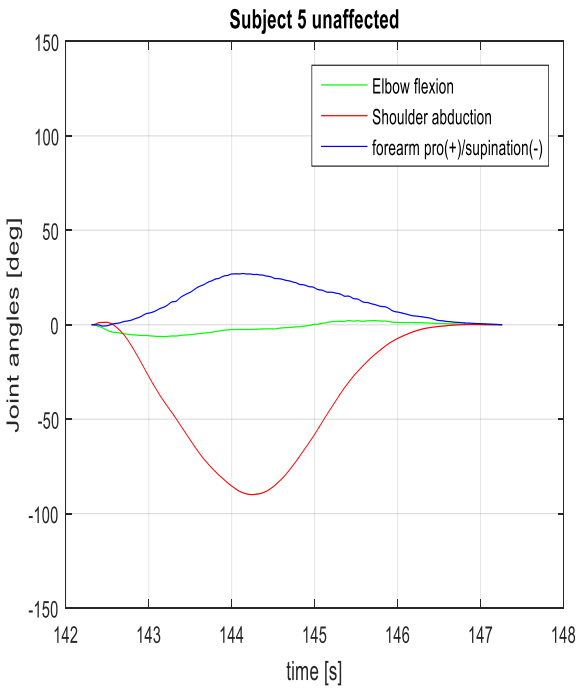
Subject 5 unaffected
Elbow flexion
Shoulder abduction
forearm pro(+)/supination(-)
Joint angles [deg]
time [s]
150
100
50
0
-50
-100
-150
142
143
144
145
146
147
148

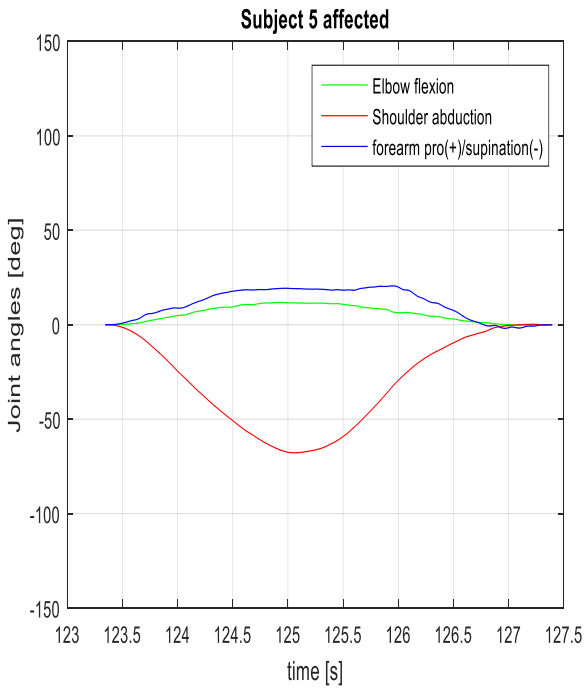
Subject 5 affected
Elbow flexion
Shoulder abduction
forearm pro(+)/supination(-)
Joint angles [deg]
time [s]
150
100
50
0
-50
-100
-150
123
123.5
124
124.5
125
125.5
126
126.5
127
127.5

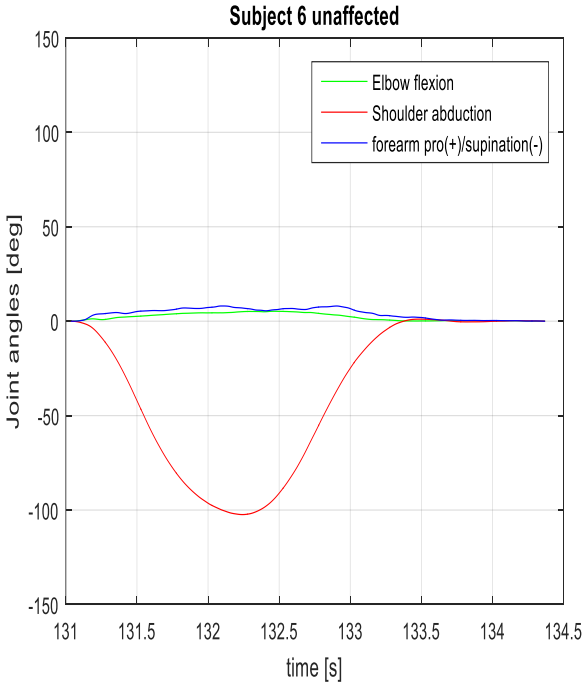
Subject 6 unaffected
Elbow flexion
Shoulder abduction
forearm pro(+)/supination(-)
Joint angles [deg]
time [s]
150
100
50
0
-50
-100
-150
131
131.5
132
132.5
133
133.5
134
134.5

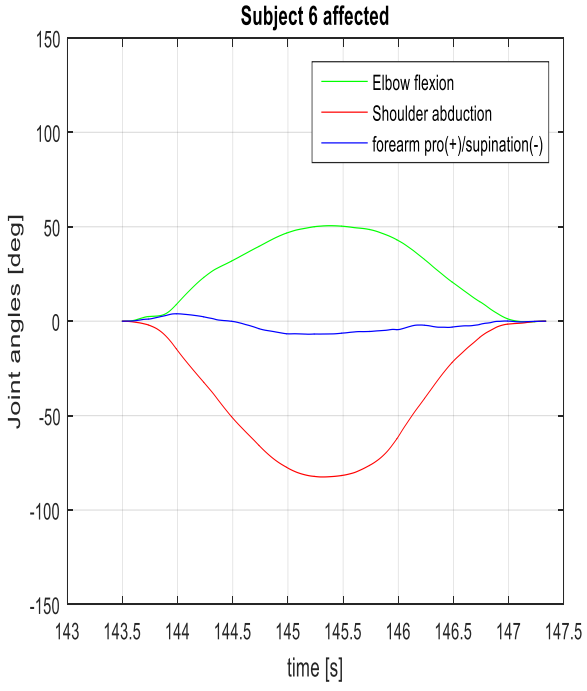
Subject 6 affected
Elbow flexion
Shoulder abduction
forearm pro(+)/supination(-)
Joint angles [deg]
time [s]
150
100
50
0
-50
-100
-150
143
143.5
144
144.5
145
145.5
146
146.5
147
147.5

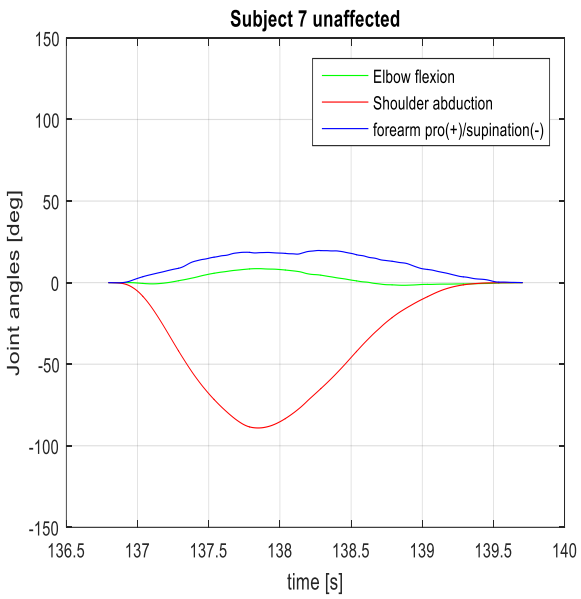
Subject 7 unaffected
Elbow flexion
Shoulder abduction
forearm pro(+)/supination(-)
Joint angles [deg]
time [s]
150
100
50
0
-50
-100
-150
136.5
137
137.5
138
138.5
139
139.5
140

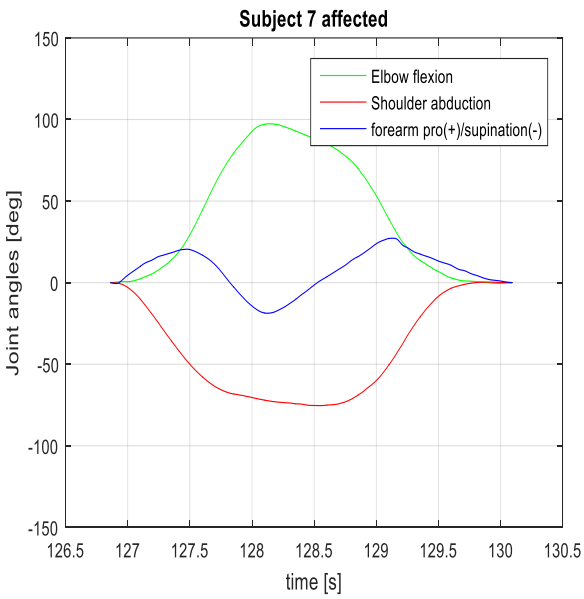
Subject 7 affected
Elbow flexion
Shoulder abduction
forearm pro(+)/supination(-)
Joint angles [deg]
time [s]
150
100
50
0
-50
-100
-150
126.5
127
127.5
128
128.5
129
129.5
130
130.5

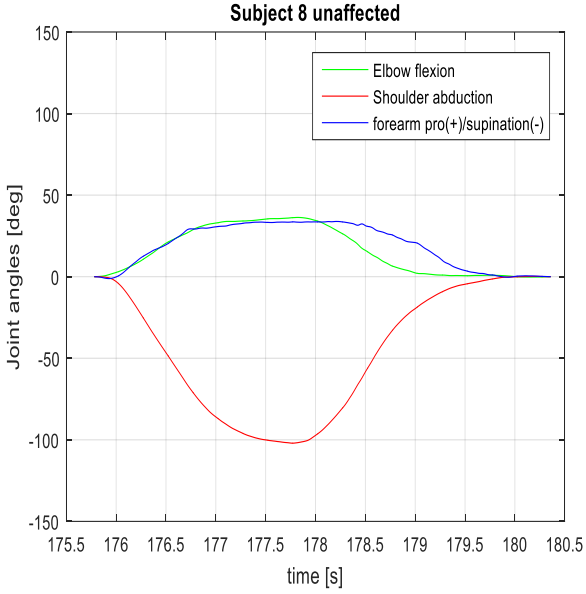
Subject 8 unaffected
Elbow flexion
Shoulder abduction
forearm pro(+)/supination(-)
Joint angles [deg]
time [s]
150
100
50
0
-50
-100
-150
175.5
176
176.5
177
177.5
178
178.5
179
179.5
180
180.5

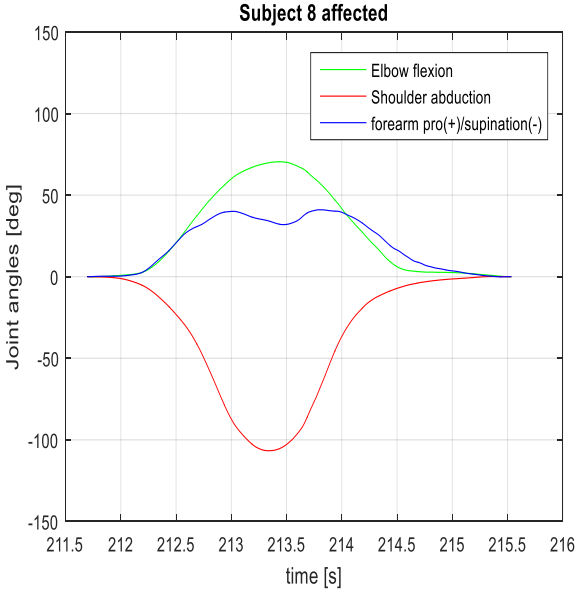
Subject 8 affected
Elbow flexion
Shoulder abduction
forearm pro(+)/supination(-)
Joint angles [deg]
time [s]
150
100
50
0
-50
-100
-150
211.5
212
212.5
213
213.5
214
214.5
215
215.5
216

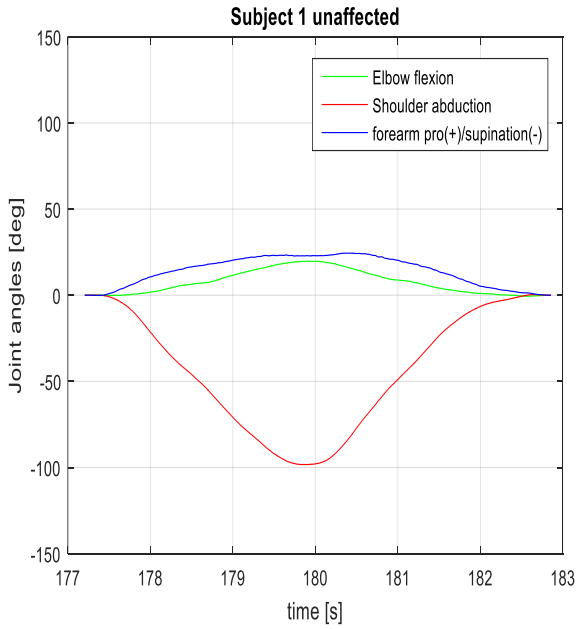
Subject 1 unaffected
Elbow flexion
Shoulder abduction
forearm pro(+)/supination(-)
Joint angles [deg]
time [s]
150
100
50
0
-50
-100
-150
177
178
179
180
181
182
183

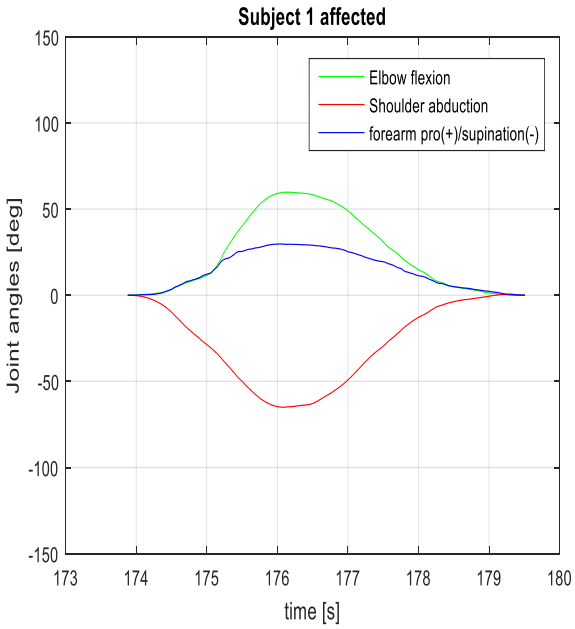
Subject 1 affected
Elbow flexion
Shoulder abduction
forearm pro(+)/supination(-)
Joint angles [deg]
time [s]
150
100
50
0
-50
-100
-150
173
174
175
176
177
178
179
180

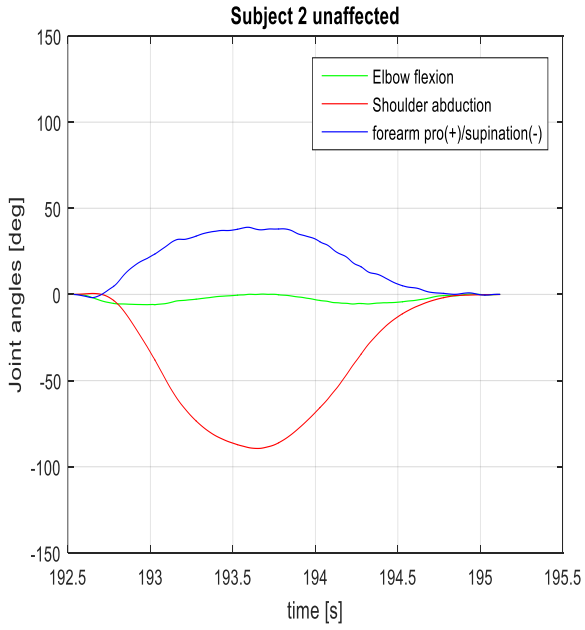
Subject 2 unaffected
Elbow flexion
Shoulder abduction
forearm pro(+)/supination(-)
Joint angles [deg]
time [s]
150
100
50
0
-50
-100
-150
192.5
193
193.5
194
194.5
195
195.5


Subject 2 affected
Elbow flexion
Shoulder abduction
forearm pro(+)/supination(-)
Joint angles [deg]
time [s]
150
100
50
0
-50
-100
-150
203
203.5
204
204.5
205
205.5
206
206.5
207

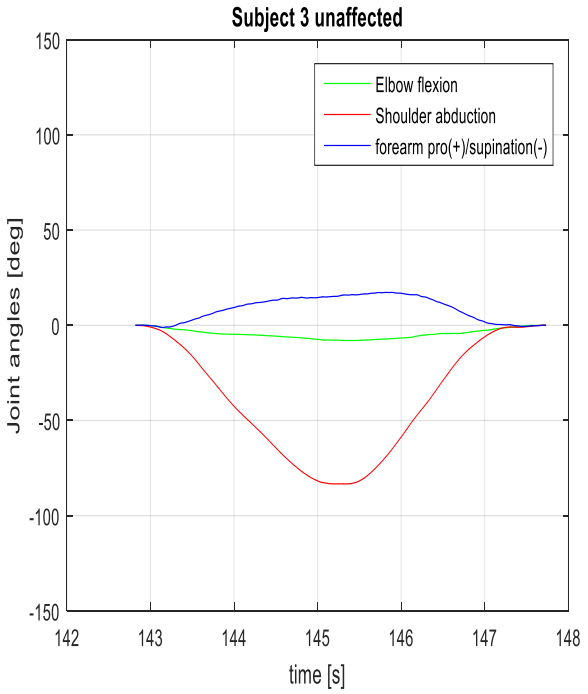
Subject 3 unaffected
Elbow flexion
Shoulder abduction
forearm pro(+)/supination(-)
Joint angles [deg]
time [s]
150
100
50
0
-50
-100
-150
142
143
144
145
146
147
148

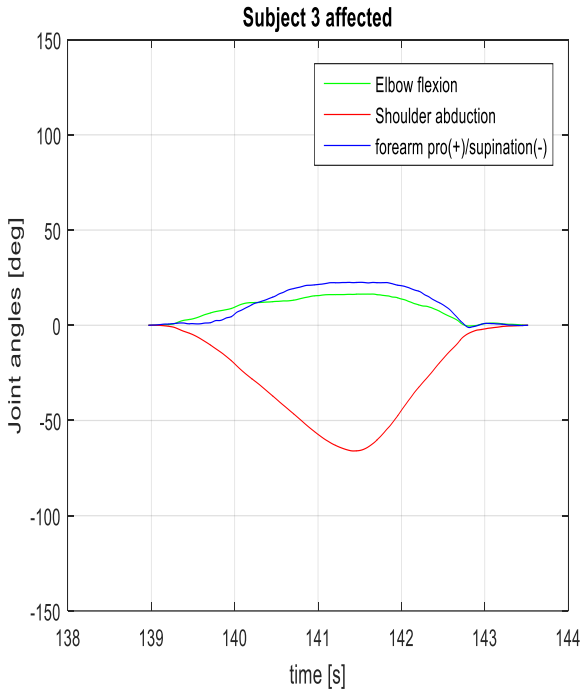
Subject 3 affected
Elbow flexion
Shoulder abduction
forearm pro(+)/supination(-)
Joint angles [deg]
time [s]
150
100
50
0
-50
-100
-150
138
139
140
141
142
143
144

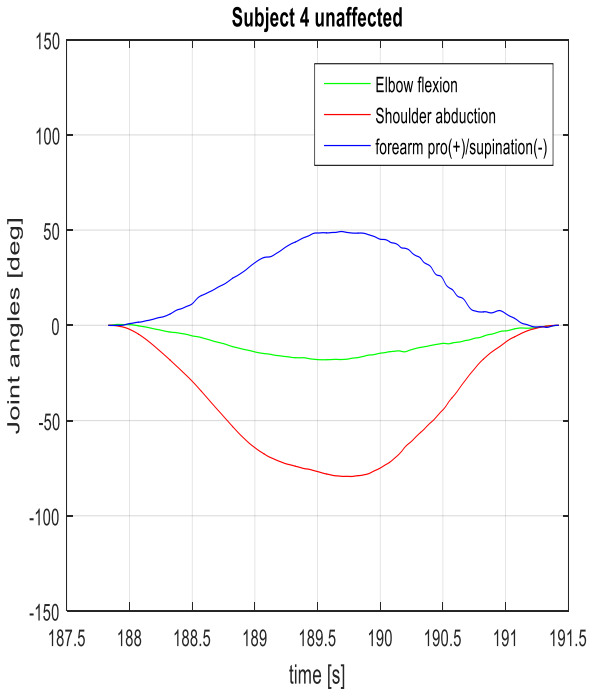
Subject 4 unaffected
Elbow flexion
Shoulder abduction
forearm pro(+)/supination(-)
Joint angles [deg]
time [s]
150
100
50
0
-50
-100
-150
187.5
188
188.5
189
189.5
190
190.5
191
191.5

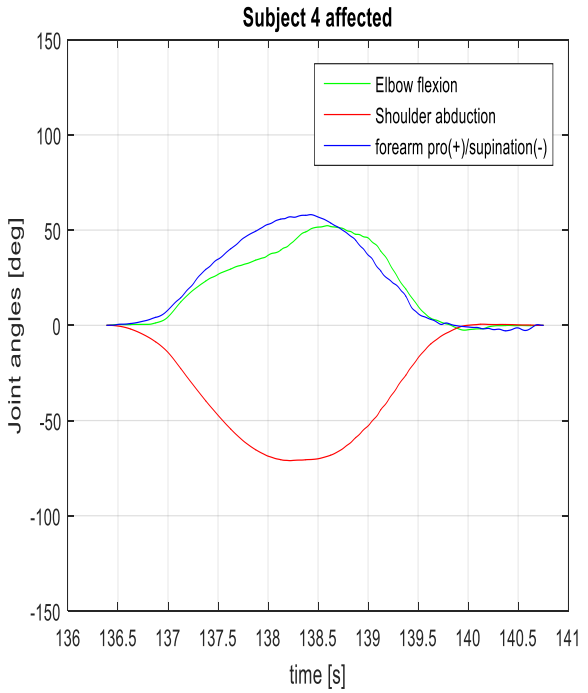
Subject 4 affected
Elbow flexion
Shoulder abduction
forearm pro(+)/supination(-)
Joint angles [deg]
time [s]
150
100
50
0
-50
-100
-150
136
136.5
137
137.5
138
138.5
139
139.5
140
140.5
141

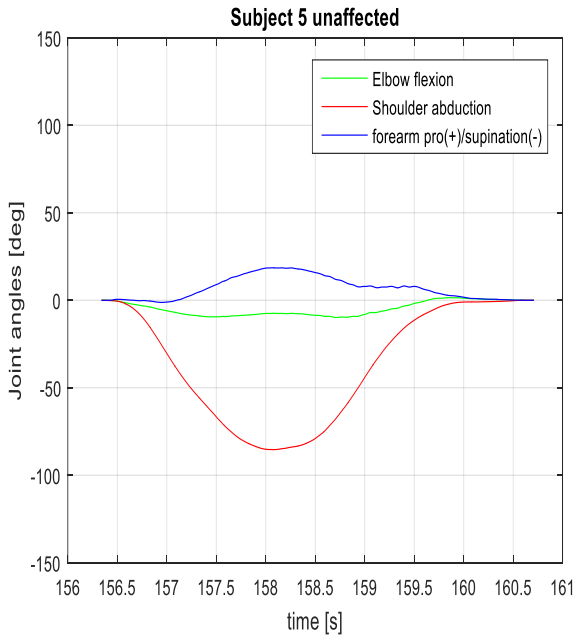
Subject 5 unaffected
Elbow flexion
Shoulder abduction
forearm pro(+)/supination(-)
Joint angles [deg]
time [s]

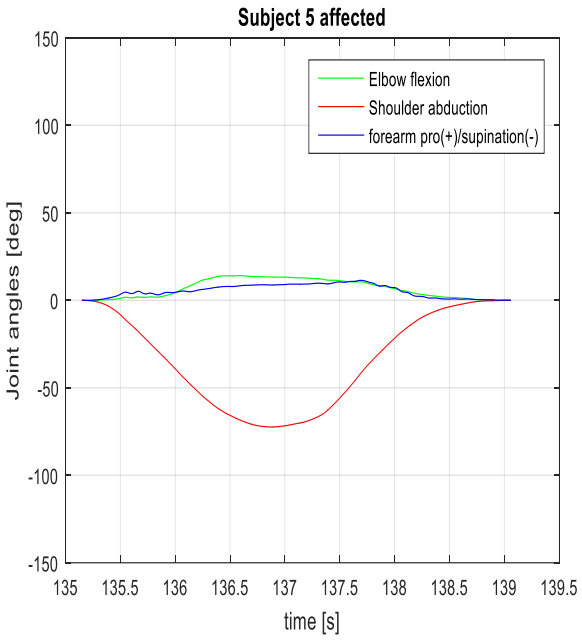
Subject 5 affected
Elbow flexion
Shoulder abduction
forearm pro(+)/supination(-)
Joint angles [deg]
time [s]

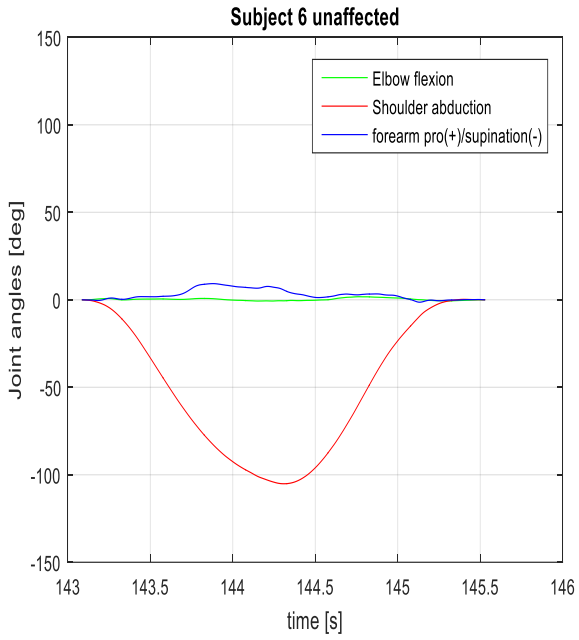
Subject 6 unaffected
Elbow flexion
Shoulder abduction
forearm pro(+)/supination(-)
Joint angles [deg]
time [s]

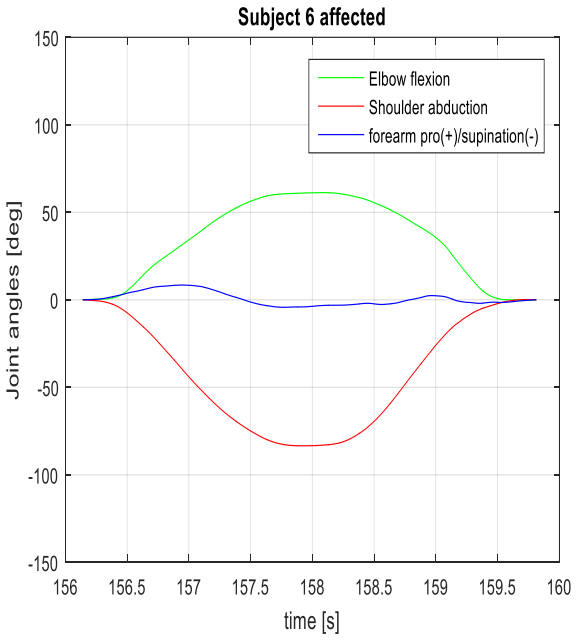
Subject 6 affected
Elbow flexion
Shoulder abduction
forearm pro(+)/supination(-)
Joint angles [deg]
time [s]

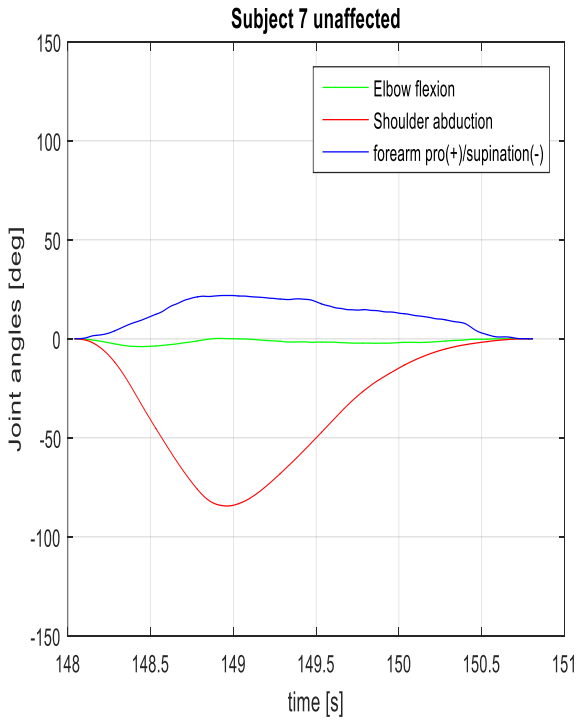
Subject 7 unaffected
Elbow flexion
Shoulder abduction
forearm pro(+)/supination(-)
Joint angles [deg]
time [s]
150
100
50
0
-50
-100
-150
148
148.5
149
149.5
150
150.5
151

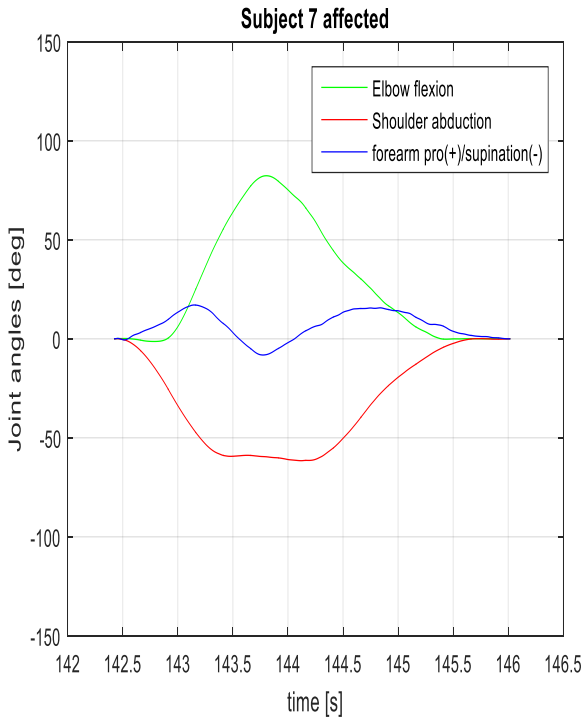
Subject 7 affected
Elbow flexion
Shoulder abduction
forearm pro(+)/supination(-)
Joint angles [deg]
time [s]
150
100
50
0
-50
-100
-150
142
142.5
143
143.5
144
144.5
145
145.5
146
146.5

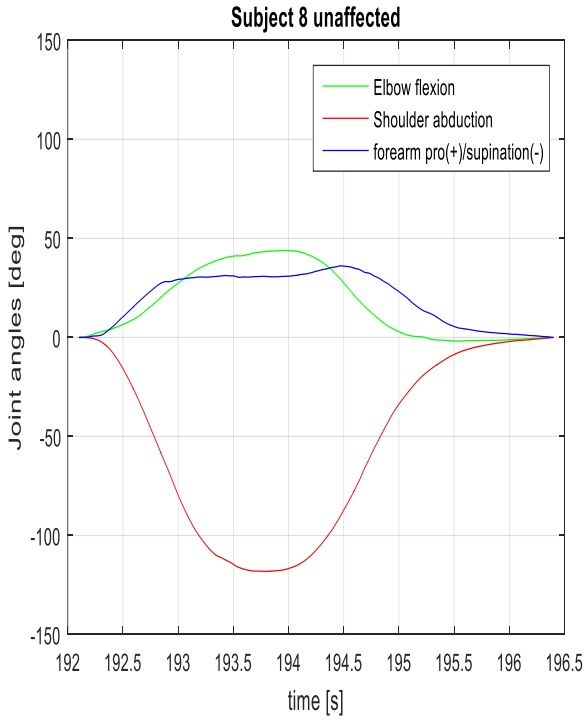
Subject 8 unaffected
Elbow flexion
Shoulder abduction
forearm pro(+)/supination(-)
Joint angles [deg]
time [s]
150
100
50
0
-50
-100
-150
192
192.5
193
193.5
194
194.5
195
195.5
196
196.5

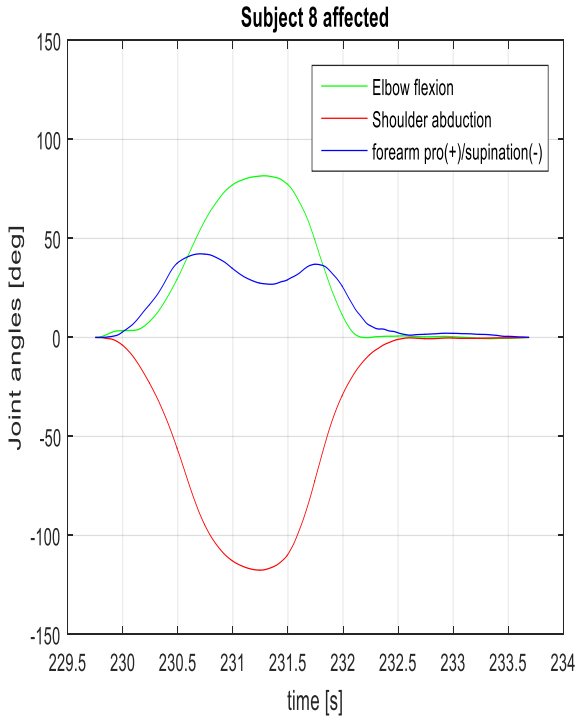
Subject 8 affected
Elbow flexion
Shoulder abduction
forearm pro(+)/supination(-)
Joint angles [deg]
time [s]
150
100
50
0
-50
-100
-150
229.5
230
230.5
231
231.5
232
232.5
233
233.5
234

	Averaged joint angles and corresponding standard deviation (SD)					
	Shoulder abduction (SD)		Elbow flexion (SD)		Forearm pro/supination (SD)	
Subject	**Unaffected**	**Affected**	**Unaffected**	**Affected**	**Unaffected**	**Affected**
1	101.2(6.6)	58.4(13.5)	17(8.9)	46.5(22.2)	19.8(4.6)	28.5(16.4)
2	92.3(6.4)	71.7(8.6)	6.5(0.9)	66.4(2.3)	38.8(1.5)	41.1(2.3)
3	86.6(3.1)	68.2(2.1)	7.8(2)	16.7(3.9)	14.1(3.2)	24.7(3.6)
4	74.6(8.6)	70.8(4.7)	26.5(11.7)	46.7(7)	52.5(3.5)	55.5(5.8)
5	88.2(2.5)	69.7(2.4)	5.8(4.3)	14.2(2.4)	21.6(4.8)	20.2(8.6)
6	106.1(4.2)	80.4(4.5)	7.6(7.4)	56.2(5.4)	8.7(0.6)	7.7(0.8)
7	89.4(5.1)	67.5(7.1)	9.4(5.9)	86.2(9.9)	17.1(6.4)	21.7(5.1)
8	103.3(14.3)	108.1(8.9)	33.3(12.4)	79.1(7.7)	34(2.1)	41.7(0.6)

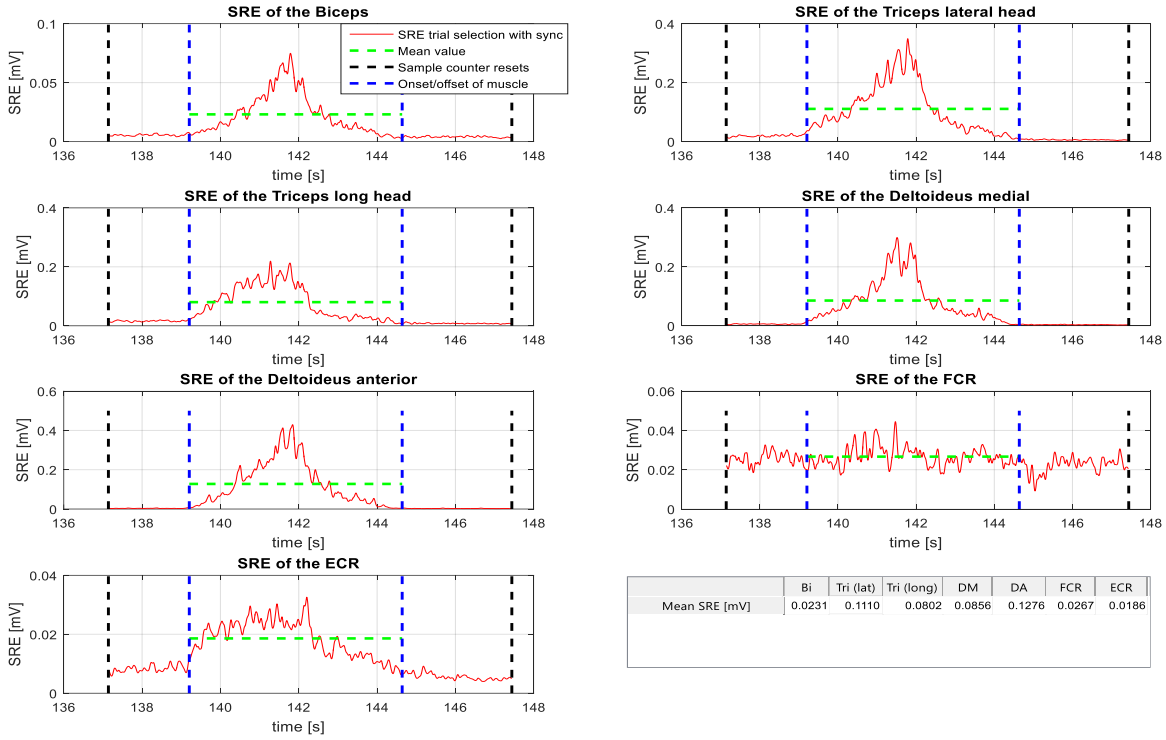

Figure 4.5.1: Smoothed rectified EMG of the biceps, triceps lateral head, triceps long head, deltoideus medial, deltoideus anterior, flexor carpi radialis (FCR), extensor carpi radialis (ECR) during the first trial concerning pathologically unaffected movements out of synergies. The figure-table (bottom right) gives an overview of the mean values of the SREs regarding the first trial.

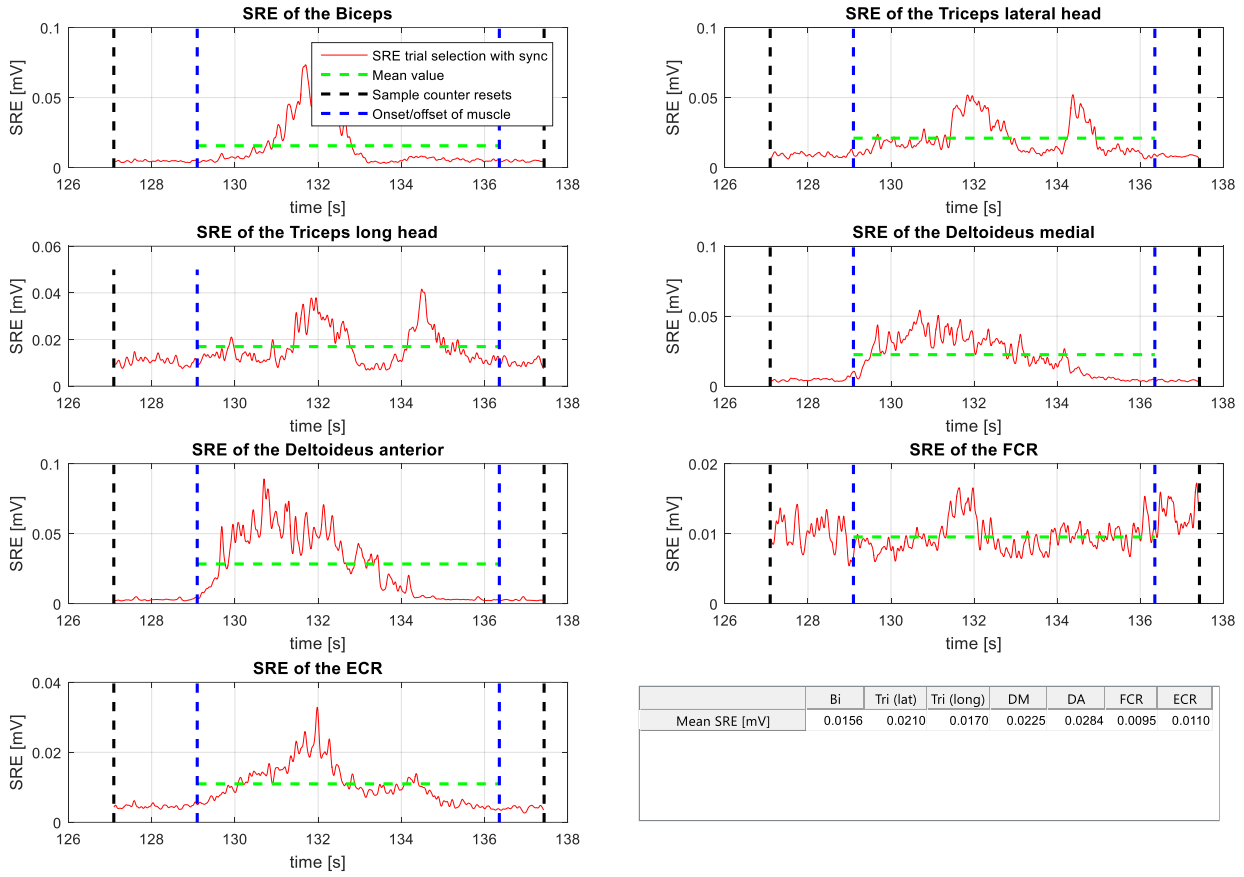

Figure 4.5.2: Smoothed rectified EMG of the biceps, triceps lateral head, triceps long head, deltoideus medial, deltoideus anterior, flexor carpi radialis (FCR), extensor carpi radialis (ECR) during the first trial concerning pathologically affected movements out of synergies. The figure-table (bottom right) gives an overview of the mean values of the SREs regarding the first trial.

MUSCLE ACTIVITY (SD) [mV]						
	Bi		Tri (lat)		Tri (long)	
	Unaffected	Affected	Unaffected	Affected	Unaffected	Affected
Subject 1	0.0207(0.0024)	0.0139(0.0033)	0.0965(0.0174)	0.0314(0.0119)	0.0657(0.0168)	0.0186(0.006)
Subject 2	0.0324(0.0039)	0.0176(0.0014)	0.0713(0.0086)	0.0482(0.0071)	0.0265(0.0034)	0.0127(0.0032)
Subject 3	0.037(0.0002)	0.0136(0.0009)	0.0591(0.0014)	0.0184(0.0018)	0.028(0.001)	0.0125(0.0006)
Subject 4	0.0375(0.0064)	0.0202(0.0024)	0.0545(0.0099)	0.0274(0.0032)	0.0478(0.0037)	0.0304(0.0037)
Subject 5	0.0109(0.0003)	0.0086(0.0006)	0.0523(0.0068)	0.0251(0.0082)	0.0232(0.0027)	0.0153(0.0037)
Subject 6	0.0406(0.0076)	0.0249(0.0037)	0.0384(0.0063)	0.0205(0.0018)	0.0273(0.0039)	0.015(0.0007)
Subject 7	0.0229(0.0035)	0.0201(0.0027)	0.0591(0.0189)	0.027(0.0018)	0.0269(0.0075)	0.0135(0.0012)
Subject 8	0.0198(0.0046)	0.0086(0.0007)	0.0782(0.0083)	0.0295(0.0021)	0.0372(0.0092)	0.0109(0.002)

MUSCLE ACTIVITY (SD) [mV]				
	DM		DA	
	Unaffected	Affected	Unaffected	Affected

Subject 1	0.0816(0.0035)	0.0397(0.0157)	0.1223(0.008)	0.0598(0.0277)
Subject 2	0.055(0.0066)	0.0418(0.0026)	0.1082(0.0163)	0.0619(0.0072)
Subject 3	0.0468(0.0017)	0.0262(0.0022)	0.0822(0.0019)	0.0338(0.0008)
Subject 4	0.1236(0.0212)	0.0868(0.0106)	0.0986(0.0237)	0.0352(0.0072)
Subject 5	0.0839(0.0108)	0.0406(0.0124)	0.0374(0.0041)	0.0168(0.005)
Subject 6	0.0547(0.0075)	0.0333(0.0036)	0.0832(0.0079)	0.0488(0.0047)
Subject 7	0.0667(0.012)	0.0386(0.0015)	0.1011(0.0098)	0.0504(0.0023)
Subject 8	0.109(0.0105)	0.0531(0.0037)	0.1277(0.0136)	0.0333(0.006)

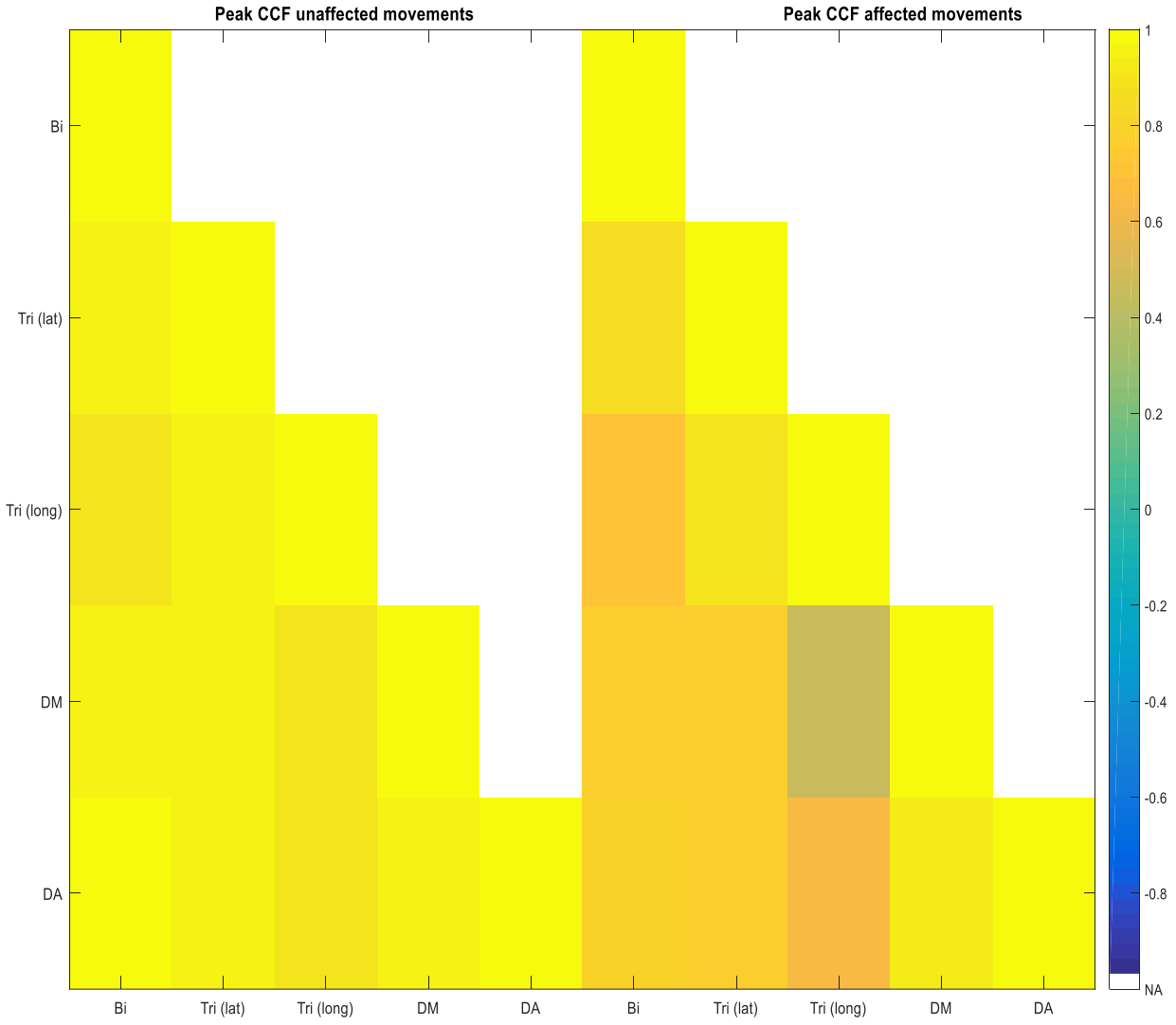

MEAN(SD) PEAK CCF UNAFFECTED MOVEMENTS					
Muscles	**Bi**	***Tri (lat)***	***Tri (long)***	**DM**	**DA**
Bi	1(0)				
Tri (lat)	0.9654(0.0196)	1(0)			
Tri (long)	0.8856(0.0611)	0.9384(0.0234)	1(0)		
DM	0.9465(0.0056)	0.9577(0.0028)	0.9018(0.0507)	1(0)	
DA	0.9705(0.0163)	0.9553(0.0202)	0.8844(0.0515)	0.9522(0.0188)	1(0)

Table 2

MEAN(SD) TIME LAG CCF UNAFFECTED MOVEMENTS [s]					
Muscles	**Bi**	***Tri (lat)***	***Tri (long)***	**DM**	**DA**
Bi	0(0)				
Tri (lat)	0.0067(0.0115)	0(0)			
Tri (long)	0.0417(0.0289)	0.0133(0.0126)	0(0)		
DM	0.0217(0.0189)	0.0067(0.0115)	-0.025(0.0391)	0(0)	
DA	0.0017(0.0029)	-0.0017(0.0029)	-0.0667(0.0584)	-0.0233(0.0161)	0(0)

Table 3

MEAN(SD) PEAK CCF AFFECTED MOVEMENTS					
Muscles	**Bi**	***Tri (lat)***	***Tri (long)***	**DM**	**DA**
Bi	1(0)				
Tri (lat)	0.8479(0.1198)	1(0)			
Tri (long)	0.7157(0.0952)	0.8826(0.033)	1(0)		
DM	0.7723(0.1527)	0.7541(0.2834)	0.4542(0.6412)	1(0)	
DA	0.7857(0.1392)	0.7759(0.2729)	0.6411(0.279)	0.92(0.0216)	1(0)

Table 4

MEAN(SD) TIME LAG CCF AFFECTED MOVEMENTS [s]					
Muscles	**Bi**	***Tri (lat)***	***Tri (long)***	**DM**	**DA**
Bi	0(0)				
Tri (lat)	-0.075(0.1258)	0(0)			
Tri (long)	-0.0617(0.1112)	0.0017(0.0029)	0(0)		
DM	0.1200(0.2078)	0.38(0.6582)	-1.1583(2.0063)	0(0)	
DA	0.2683(0.4476)	0.365(0.6322)	0.4083(0.7159)	-0.0033(0.0058)	0(0)

Table 5:

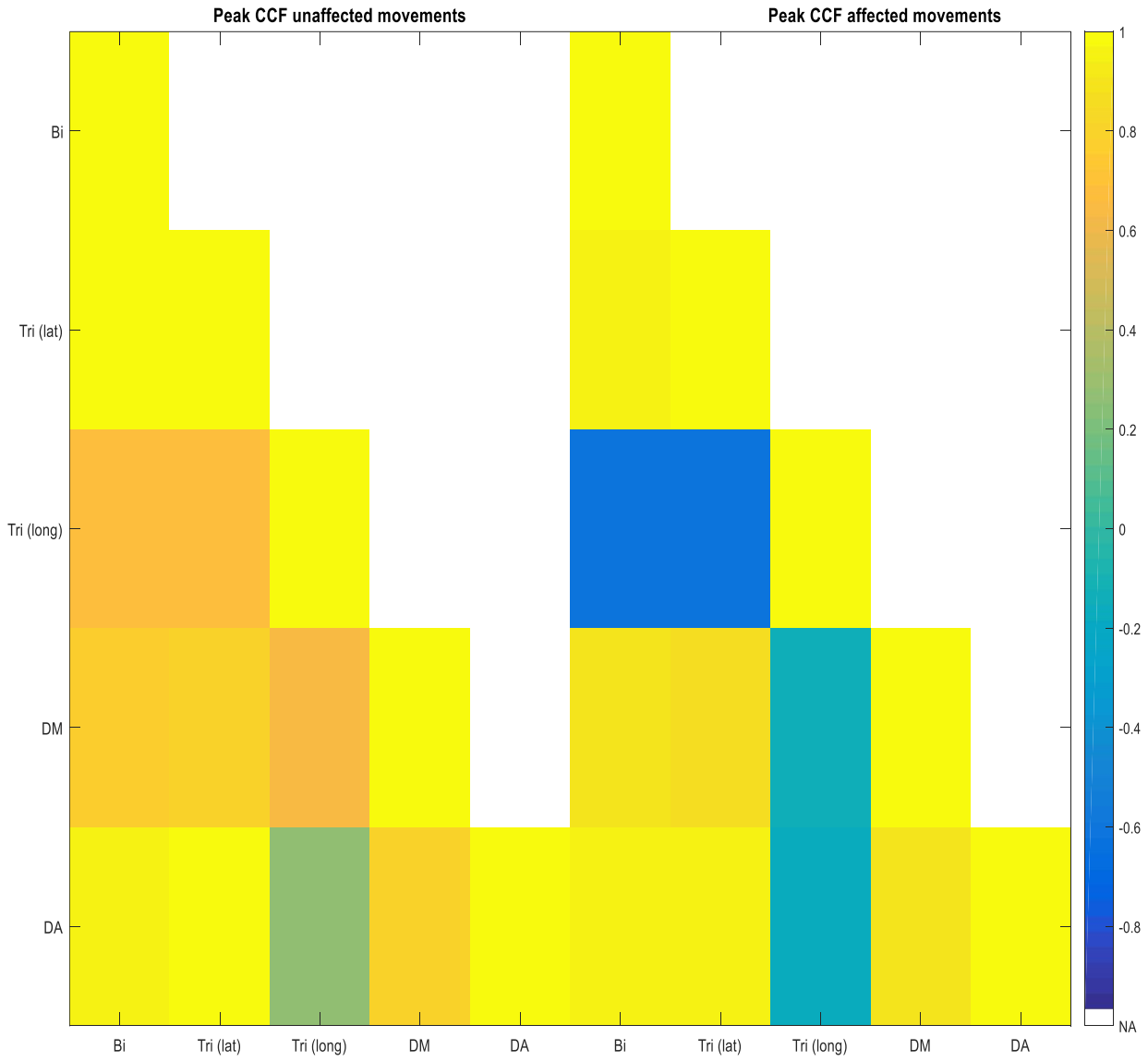

MEAN(SD) PEAK CCF UNAFFECTED MOVEMENTS					
Muscles	**Bi**	***Tri (lat)***	***Tri (long)***	**DM**	**DA**
Bi	1(0)				
Tri (lat)	0.9799(0.0016)	1(0)			
Tri (long)	0.6653(0.1284)	0.6657(0.1243)	1(0)		
DM	0.7646(0.026)	0.8049(0.0102)	0.6526(0.0218)	1(0)	
DA	0.9629(0.0208)	0.9735(0.0092)	0.2663(0.6841)	0.799(0.0335)	1(0)

Table 2

MEAN(SD) TIME LAG CCF UNAFFECTED MOVEMENTS [s]					
Muscles	**Bi**	***Tri (lat)***	***Tri (long)***	**DM**	**DA**
Bi	0(0)				

Tri (lat)	0.0017(0.0029)	0(0)			
Tri (long)	0.2067(0.171)	0.2417(0.2126)	0(0)		
DM	0.2117(0.0785)	0.1317(0.11)	-0.1433(0.2483)	0(0)	
DA	0(0)	0(0)	0.345(0.7629)	-0.1133(0.0729)	0(0)

Table 3

MEAN(SD) PEAK CCF AFFECTED MOVEMENTS					
Muscles	**Bi**	***Tri (lat)***	***Tri (long)***	**DM**	**DA**
Bi	1(0)				
Tri (lat)	0.9686(0.0122)	1(0)			
Tri (long)	-0.6095(0.0675)	-0.6179(0.0928)	1(0)		
DM	0.8917(0.0269)	0.8598(0.04)	-0.1547(0.5851)	1(0)	
DA	0.9538(0.0158)	0.9412(0.0274)	-0.169(0.7051)	0.8836(0.0382)	1(0)

Table 4

MEAN(SD) TIME LAG CCF AFFECTED MOVEMENTS [s]					
Muscles	**Bi**	***Tri (lat)***	***Tri (long)***	**DM**	**DA**
Bi	0(0)				
Tri (lat)	0(0)	0(0)			
Tri (long)	-0.755(0.0397)	-0.7317(0.0683)	0(0)		
DM	0.0267(0.0104)	0.055(0.0436)	0.325(0.9579)	0(0)	
DA	0(0)	0(0)	0.33(0.711)	-0.0167(0.0176)	0(0)

Table 5:

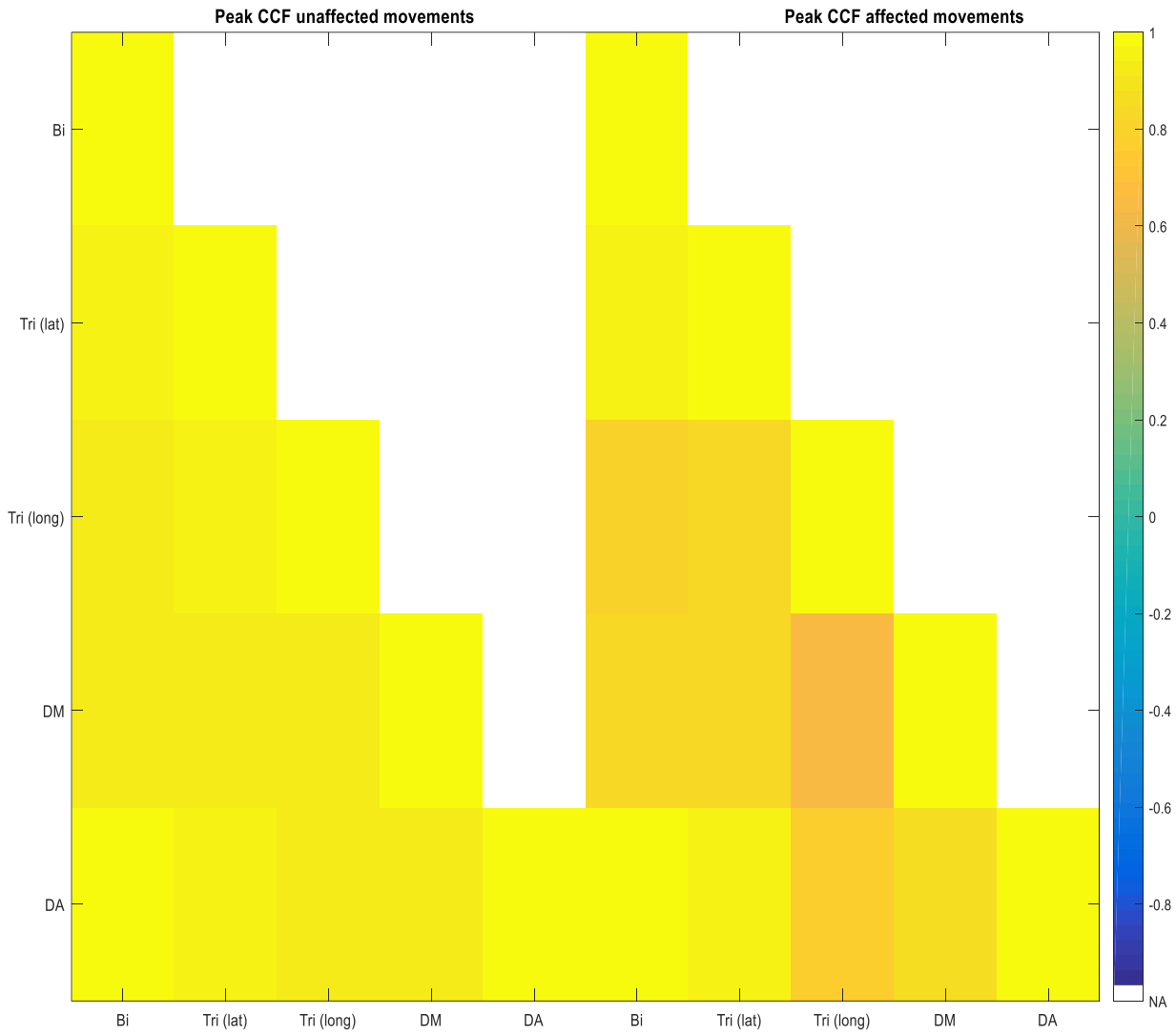

MEAN(SD) PEAK CCF UNAFFECTED MOVEMENTS					
Muscles	**Bi**	***Tri (lat)***	***Tri (long)***	**DM**	**DA**
Bi	1(0)				
Tri (lat)	0.9512(0.0207)	1(0)			
Tri (long)	0.9243(0.0274)	0.9437(0.0211)	1(0)		
DM	0.9085(0.0162)	0.9371(0.0171)	0.9099(0.0173)	1(0)	
DA	0.9847(0.0044)	0.9536(0.0226)	0.9301(0.0332)	0.9215(0.0202)	1(0)

Table 2

MEAN(SD) TIME LAG CCF UNAFFECTED MOVEMENTS [s]					
Muscles	**Bi**	***Tri (lat)***	***Tri (long)***	**DM**	**DA**
Bi	0(0)				
Tri (lat)	0.01(0.0132)	0(0)			
Tri (long)	0.025(0.0229)	0.0033(0.0104)	0(0)		

DM	0.03(0.0361)	0.0067(0.0058)	0(0)	0(0)	
DA	0(0)	-0.0017(0.0029)	-0.0133(0.0231)	-0.0033(0.0058)	0(0)

Table 3

MEAN(SD) PEAK CCF AFFECTED MOVEMENTS					
Muscles	**Bi**	***Tri (lat)***	***Tri (long)***	**DM**	**DA**
Bi	1(0)				
Tri (lat)	0.967(0.0136)	1(0)			
Tri (long)	0.7855(0.0464)	0.8337(0.0281)	1(0)		
DM	0.8248(0.0403)	0.8245(0.0347)	0.6556(0.0452)	1(0)	
DA	0.9704(0.0074)	0.9529(0.0083)	0.7808(0.0762)	0.8556(0.0435)	1(0)

Table 4

MEAN(SD) TIME LAG CCF AFFECTED MOVEMENTS [s]					
Muscles	**Bi**	***Tri (lat)***	***Tri (long)***	**DM**	**DA**
Bi	0(0)				
Tri (lat)	0(0)	0(0)			
Tri (long)	0.085(0.1472)	0.0583(0.0967)	0(0)		
DM	0.02(0.0173)	0.0567(0.1025)	-0.005(0.0132)	0(0)	
DA	0.0017(0.0029)	0.0017(0.0029)	-0.1017(0.1549)	-0.0467(0.0569)	0(0)

Table 5:

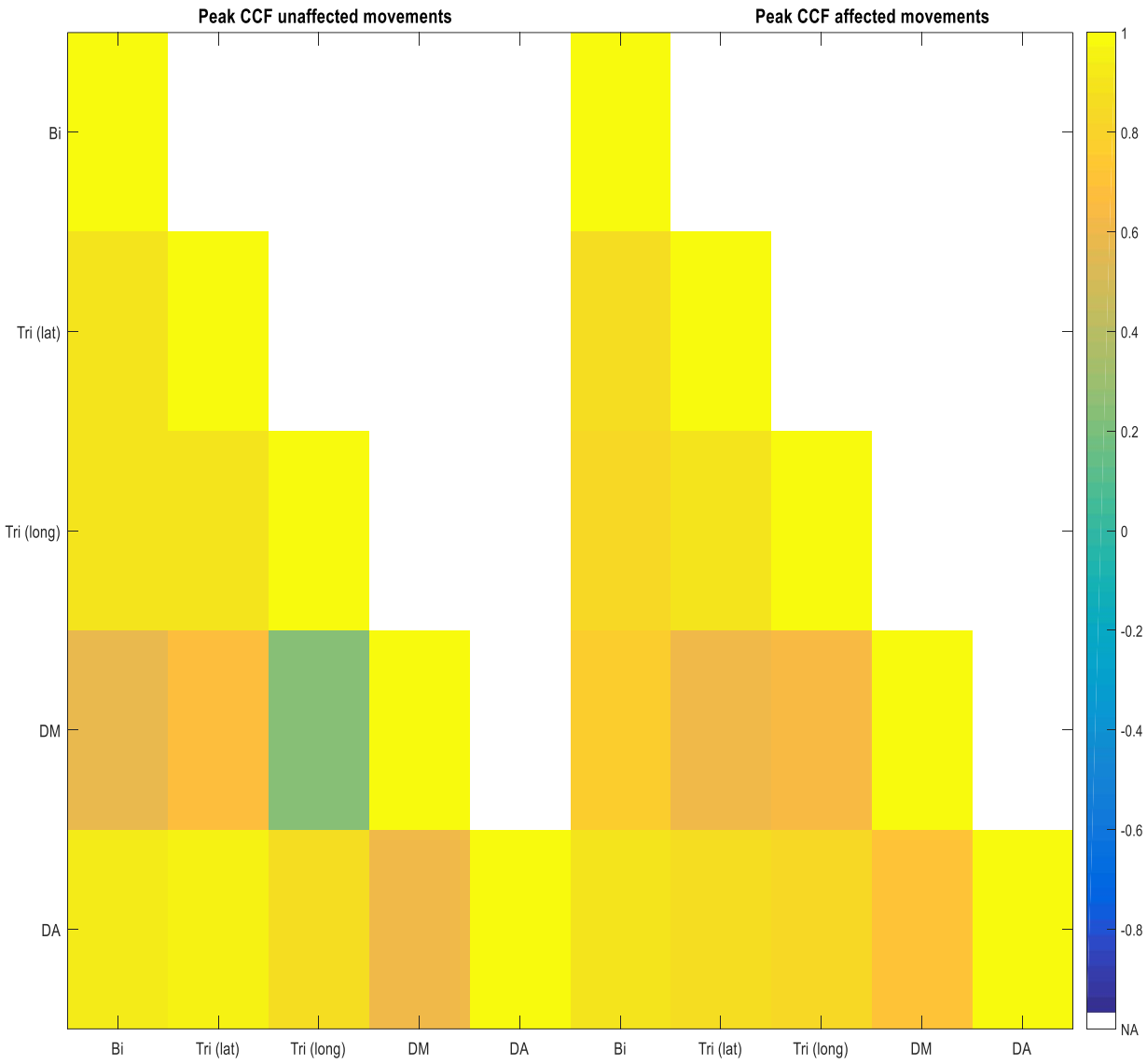

MEAN(SD) PEAK CCF UNAFFECTED MOVEMENTS					
Muscles	**Bi**	***Tri (lat)***	***Tri (long)***	**DM**	**DA**
Bi	1(0)				
Tri (lat)	0.8959(0.0358)	1(0)			
Tri (long)	0.8943(0.0244)	0.8827(0.0382)	1(0)		
DM	0.5676(0.0785)	0.6613(0.0882)	0.2411(0.6768)	1(0)	
DA	0.9137(0.023)	0.9383(0.0258)	0.8663(0.0321)	0.6227(0.0983)	1(0)

Table 2

MEAN(SD) TIME LAG CCF UNAFFECTED MOVEMENTS [s]					
Muscles	**Bi**	***Tri (lat)***	***Tri (long)***	**DM**	**DA**
Bi	0(0)				

Tri (lat)	-0.0033(0.0058)	0(0)			
Tri (long)	0(0)	0.0133(0.0076)	0(0)		
DM	0.535(0.466)	0.88(0.104)	0.2733(0.8762)	0(0)	
DA	0(0)	0.01(0.0132)	0(0)	-0.7983(0.1179)	0(0)

Table 3

MEAN(SD) PEAK CCF AFFECTED MOVEMENTS					
Muscles	**Bi**	***Tri (lat)***	***Tri (long)***	**DM**	**DA**
Bi	1(0)				
Tri (lat)	0.8583(0.0417)	1(0)			
Tri (long)	0.8347(0.0053)	0.8853(0.0376)	1(0)		
DM	0.7696(0.068)	0.6193(0.0796)	0.6379(0.1257)	1(0)	
DA	0.8952(0.0283)	0.8734(0.0208)	0.8201(0.0236)	0.6995(0.07)	1(0)

Table 4

MEAN(SD) TIME LAG CCF AFFECTED MOVEMENTS [s]					
Muscles	**Bi**	***Tri (lat)***	***Tri (long)***	**DM**	**DA**
Bi	0(0)				
Tri (lat)	-0.0117(0.0076)	0(0)			
Tri (long)	-0.005(0.0087)	0.0067(0.0029)	0(0)		
DM	0.0083(0.0076)	0.35(0.3003)	0.2783(0.2362)	0(0)	
DA	-0.0017(0.0176)	0.01(0.0173)	0(0)	-0.0283(0.0058)	0(0)

Table 5:

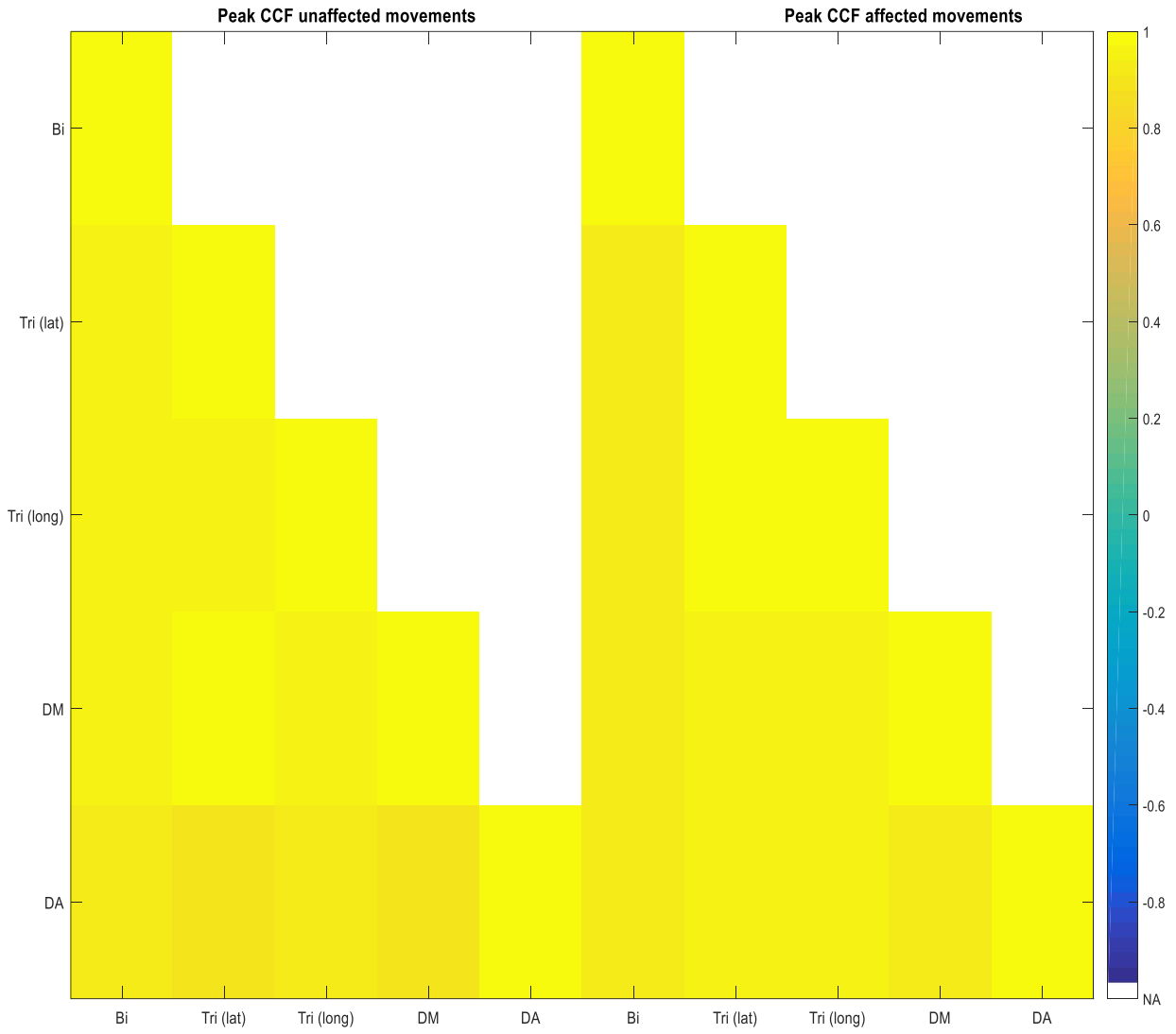

MEAN(SD) PEAK CCF UNAFFECTED MOVEMENTS					
Muscles	**Bi**	***Tri (lat)***	***Tri (long)***	**DM**	**DA**
Bi	1(0)				
Tri (lat)	0.9514(0.0331)	1(0)			
Tri (long)	0.9488(0.0424)	0.9646(0.0036)	1(0)		
DM	0.9432(0.031)	0.9841(0.0028)	0.946(0.0146)	1(0)	
DA	0.9175(0.0559)	0.9043(0.0263)	0.913(0.0144)	0.9055(0.0183)	1(0)

Table 2

MEAN(SD) TIME LAG CCF UNAFFECTED MOVEMENTS [s]					
Muscles	**Bi**	***Tri (lat)***	***Tri (long)***	**DM**	**DA**
Bi	0(0)				

Tri (lat)	0(0)	0(0)			
Tri (long)	0.0117(0.0126)	0.015(0.01)	0(0)		
DM	-0.0017(0.0029)	-0.0017(0.0029)	-0.0217(0.0189)	0(0)	
DA	0(0)	-0.0017(0.0029)	-0.0167(0.0208)	-0.0017(0.0029)	0(0)

Table 3

MEAN(SD) PEAK CCF AFFECTED MOVEMENTS					
Muscles	**Bi**	***Tri (lat)***	***Tri (long)***	**DM**	**DA**
Bi	1(0)				
Tri (lat)	0.9335(0.0318)	1(0)			
Tri (long)	0.9294(0.0252)	0.9746(0.0148)	1(0)		
DM	0.9282(0.0206)	0.9571(0.016)	0.9406(0.0104)	1(0)	
DA	0.9196(0.0179)	0.956(0.01)	0.9478(0.011)	0.9369(0.0157)	1(0)

Table 4

MEAN(SD) TIME LAG CCF AFFECTED MOVEMENTS [s]					
Muscles	**Bi**	***Tri (lat)***	***Tri (long)***	**DM**	**DA**
Bi	0(0)				
Tri (lat)	0.0033(0.0058)	0(0)			
Tri (long)	0.005(0.0132)	0.0017(0.0029)	0(0)		
DM	0.005(0.005)	0(0)	-0.0033(0.0058)	0(0)	
DA	-0.0017(0.0176)	-0.0017(0.0029)	-0.0033(0.0029)	-0.0033(0.0104)	0(0)

Table 5:

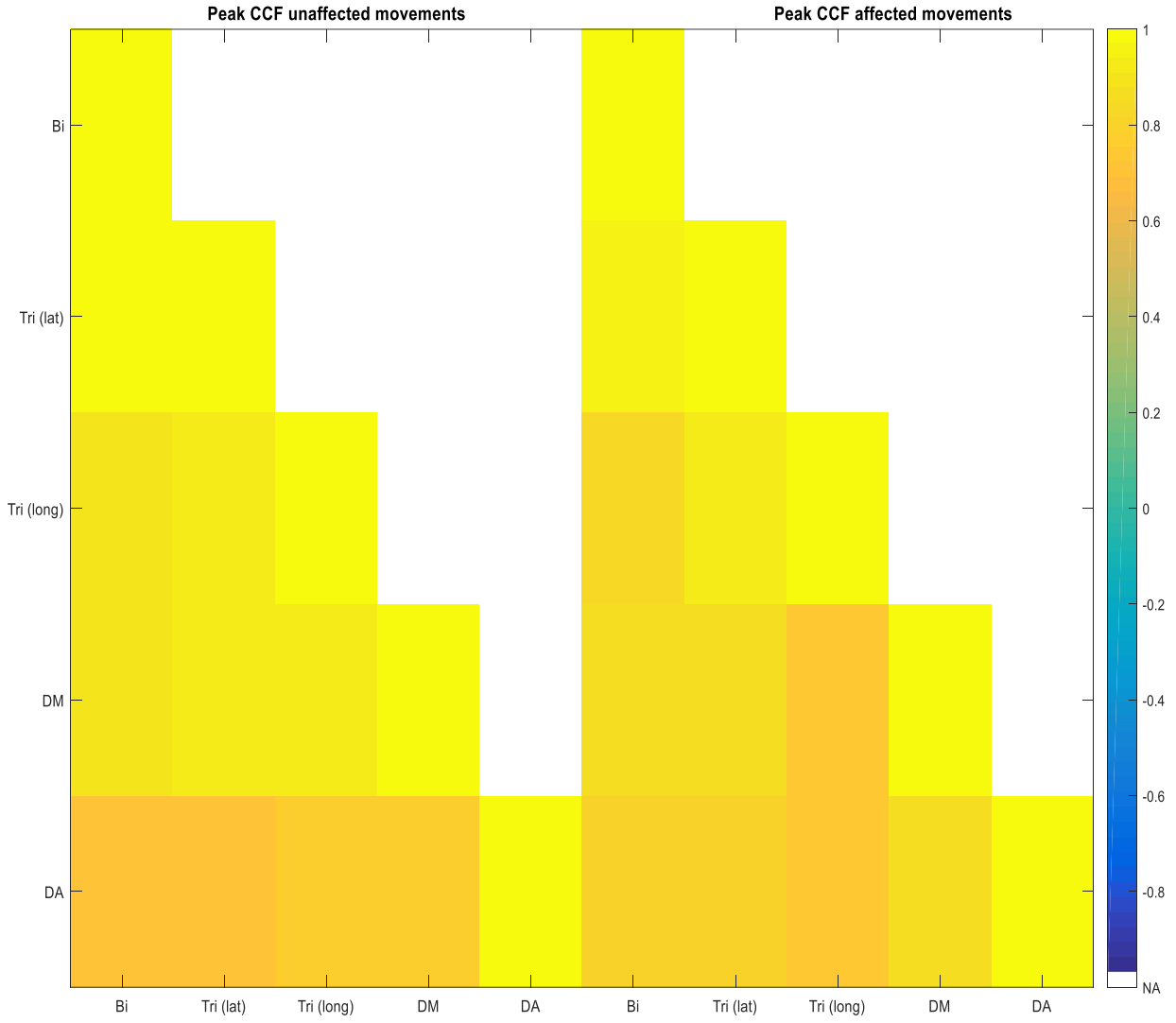

MEAN(SD) PEAK CCF UNAFFECTED MOVEMENTS					
Muscles	**Bi**	***Tri (lat)***	***Tri (long)***	**DM**	**DA**
Bi	1(0)				
Tri (lat)	0.9735(0.0059)	1(0)			
Tri (long)	0.9044(0.0328)	0.9152(0.0115)	1(0)		
DM	0.9039(0.0312)	0.9107(0.014)	0.9171(0.007)	1(0)	
DA	0.6917(0.1522)	0.7048(0.1208)	0.7755(0.0854)	0.7645(0.126)	1(0)

Table 2

MEAN(SD) TIME LAG CCF UNAFFECTED MOVEMENTS [s]					
Muscles	**Bi**	***Tri (lat)***	***Tri (long)***	**DM**	**DA**
Bi	0(0)				

Tri (lat)	0(0.005)	0(0)			
Tri (long)	-0.0017(0.0126)	0(0.005)	0(0)		
DM	0(0)	-0.005(0.0087)	0(0)	0(0)	
DA	0.1667(0.1474)	0.0083(0.0076)	0.0367(0.0473)	0.0017(0.0029)	0(0)

Table 3

MEAN(SD) PEAK CCF AFFECTED MOVEMENTS					
Muscles	**Bi**	***Tri (lat)***	***Tri (long)***	**DM**	**DA**
Bi	1(0)				
Tri (lat)	0.9575(0.0183)	1(0)			
Tri (long)	0.8277(0.0611)	0.9109(0.031)	1(0)		
DM	0.8634(0.0314)	0.8508(0.0161)	0.7295(0.0728)	1(0)	
DA	0.8009(0.0522)	0.7991(0.0292)	0.7303(0.0515)	0.8684(0.063)	1(0)

Table 4

MEAN(SD) TIME LAG CCF AFFECTED MOVEMENTS [s]					
Muscles	**Bi**	***Tri (lat)***	***Tri (long)***	**DM**	**DA**
Bi	0(0)				
Tri (lat)	0(0)	0(0)			
Tri (long)	-0.0017(0.0029)	0(0)	0(0)		
DM	0(0)	0(0)	0.0033(0.0058)	0(0)	
DA	0.0133(0.0126)	0.0067(0.0029)	0.005(0.005)	0.0017(0.0029)	0(0)

Table 5:

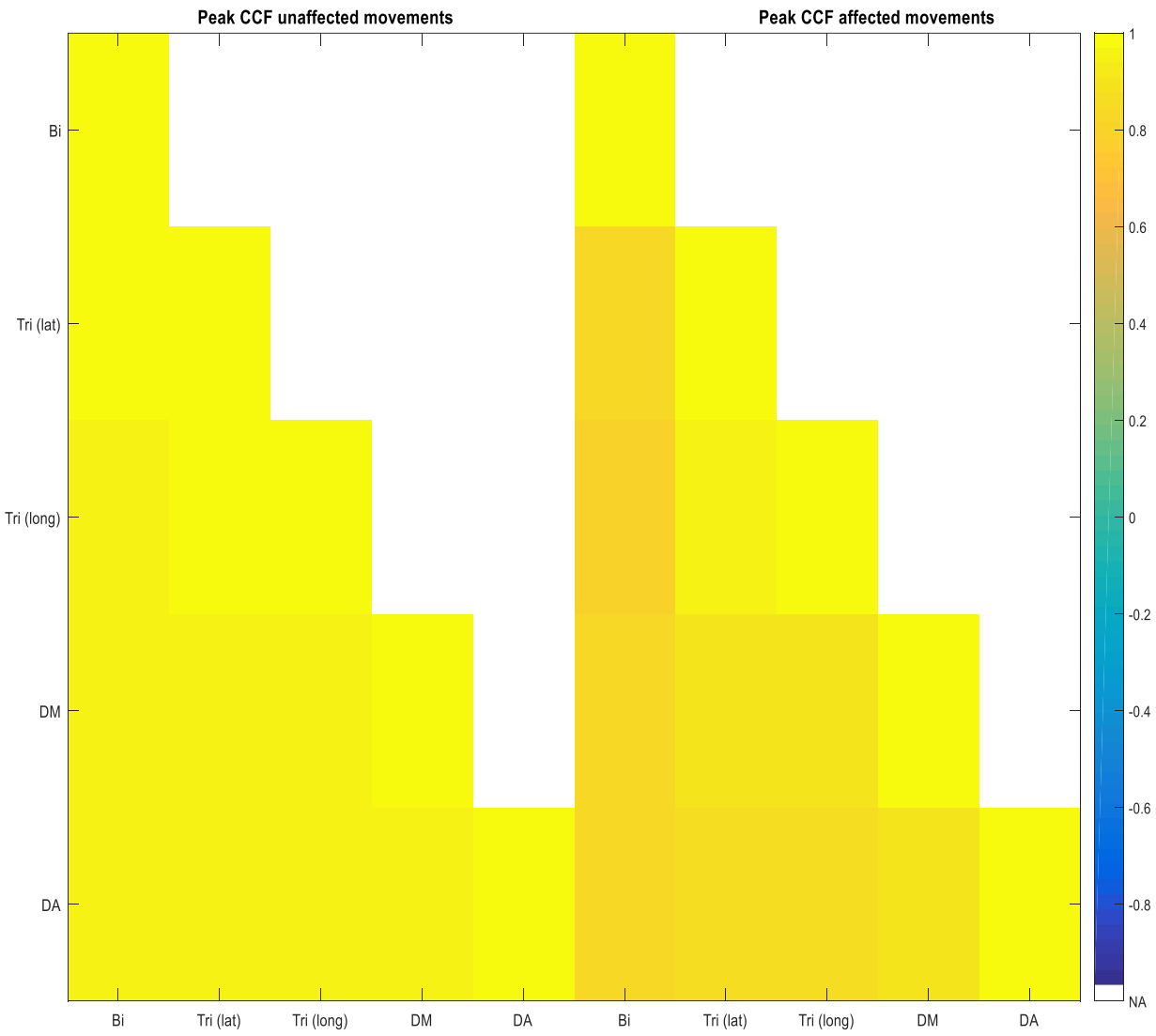

MEAN(SD) PEAK CCF UNAFFECTED MOVEMENTS					
Muscles	**Bi**	***Tri (lat)***	***Tri (long)***	**DM**	**DA**
Bi	1(0)				
Tri (lat)	0.978(0.0151)	1(0)			
Tri (long)	0.9664(0.0134)	0.9849(0.0053)	1(0)		
DM	0.9405(0.0287)	0.9404(0.0372)	0.9498(0.0356)	1(0)	
DA	0.9637(0.0111)	0.9553(0.0076)	0.944(0.0191)	0.9575(0.0052)	1(0)

Table 2

MEAN(SD) TIME LAG CCF UNAFFECTED MOVEMENTS [s]					
Muscles	**Bi**	***Tri (lat)***	***Tri (long)***	**DM**	**DA**

Bi	0(0)				
Tri (lat)	-0.0033(0.0058)	0(0)			
Tri (long)	0(0)	0.0017(0.0029)	0(0)		
DM	0.02(0.01)	0.0283(0.0247)	0.045(0.0541)	0(0)	
DA	0.0017(0.0202)	0.0017(0.0369)	-0.0083(0.0189)	-0.0133(0.0231)	0(0)

Table 3

MEAN(SD) PEAK CCF AFFECTED MOVEMENTS					
Muscles	**Bi**	***Tri (lat)***	***Tri (long)***	**DM**	**DA**
Bi	1(0)				
Tri (lat)	0.8151(0.0765)	1(0)			
Tri (long)	0.7876(0.0857)	0.948(0.0253)	1(0)		
DM	0.8137(0.0319)	0.878(0.0482)	0.8885(0.0277)	1(0)	
DA	0.8251(0.0795)	0.8712(0.0739)	0.8607(0.087)	0.8898(0.0292)	1(0)

Table 4

MEAN(SD) TIME LAG CCF AFFECTED MOVEMENTS [s]					
Muscles	**Bi**	***Tri (lat)***	***Tri (long)***	**DM**	**DA**
Bi	0(0)				
Tri (lat)	0.0267(0.0462)	0(0)			
Tri (long)	0.0383(0.0664)	0(0)	0(0)		
DM	0.0233(0.0404)	0(0)	0(0)	0(0)	
DA	0.07(0.0312)	0.0417(0.0722)	0.005(0.0087)	0.0033(0.0058)	0(0)

Table 5:

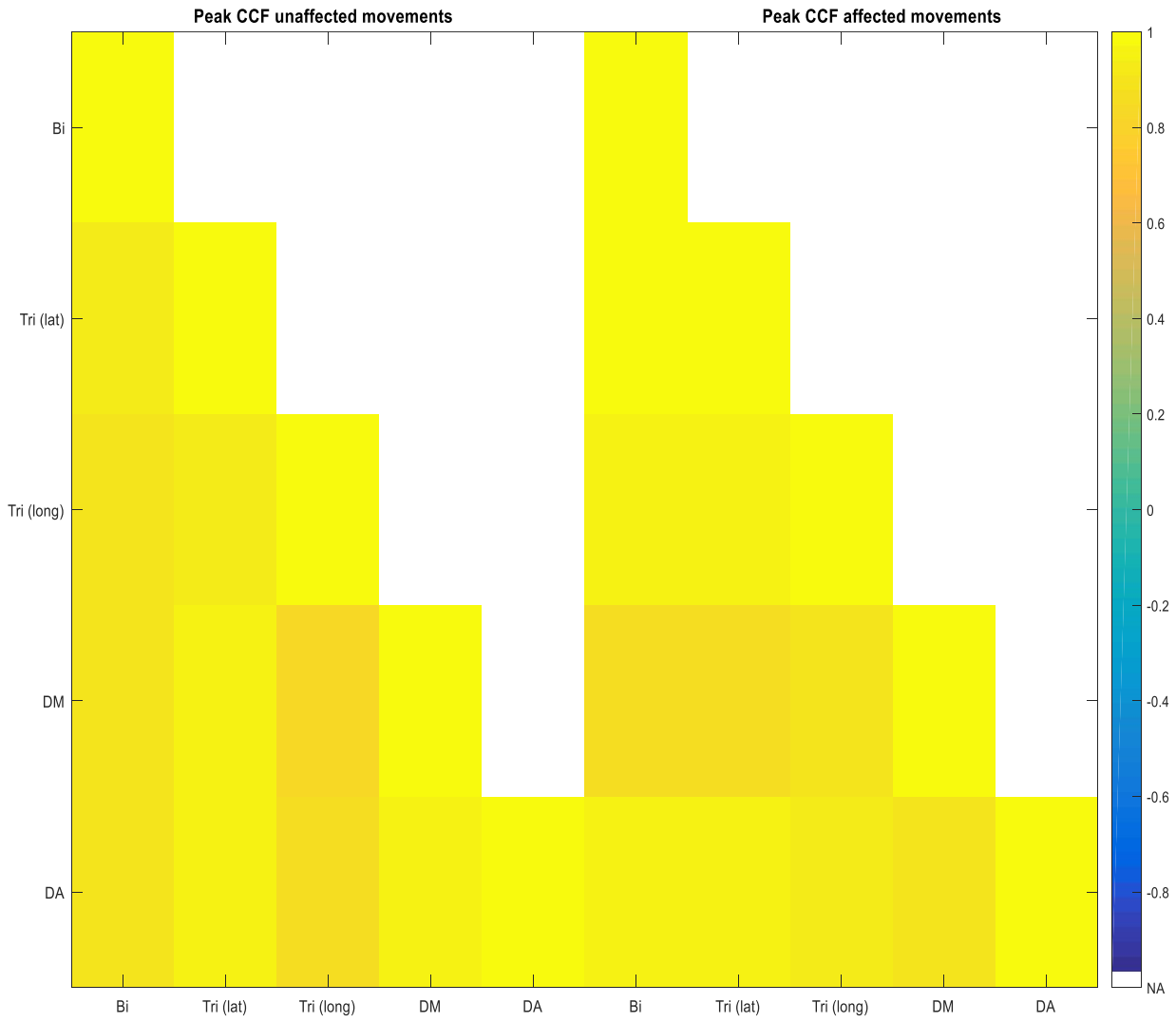

MEAN(SD) PEAK CCF UNAFFECTED MOVEMENTS					
Muscles	**Bi**	***Tri (lat)***	***Tri (long)***	**DM**	**DA**
Bi	1(0)				
Tri (lat)	0.9277(0.0928)	1(0)			
Tri (long)	0.8927(0.0634)	0.9173(0.044)	1(0)		
DM	0.8756(0.1088)	0.9466(0.0179)	0.8421(0.0845)	1(0)	
DA	0.8885(0.1346)	0.9674(0.0092)	0.8599(0.0753)	0.9433(0.0112)	1(0)

Table 2

MEAN(SD) TIME LAG CCF UNAFFECTED MOVEMENTS [s]					
Muscles	**Bi**	***Tri (lat)***	***Tri (long)***	**DM**	**DA**
Bi	0(0)				
Tri (lat)	0.0017(0.0029)	0(0)			
Tri (long)	0.0017(0.0029)	0(0)	0(0)		

DM	0(0)	0(0)	-0.0567(0.0981)	0(0)	
DA	0(0)	0(0)	0(0)	-0.0017(0.0029)	0(0)

Table 3

MEAN(SD) PEAK CCF AFFECTED MOVEMENTS					
Muscles	**Bi**	***Tri (lat)***	***Tri (long)***	**DM**	**DA**
Bi	1(0)				
Tri (lat)	0.9855(0.0029)	1(0)			
Tri (long)	0.952(0.0145)	0.9608(0.0173)	1(0)		
DM	0.8659(0.0497)	0.8736(0.0442)	0.8942(0.0604)	1(0)	
DA	0.9511(0.0182)	0.9488(0.0188)	0.9335(0.027)	0.8843(0.0403)	1(0)

Table 4

MEAN(SD) TIME LAG CCF AFFECTED MOVEMENTS [s]					
Muscles	**Bi**	***Tri (lat)***	***Tri (long)***	**DM**	**DA**
Bi	0(0)				
Tri (lat)	0(0)	0(0)			
Tri (long)	0.0017(0.0029)	0.0067(0.0058)	0(0)		
DM	0.0367(0.0351)	0.0683(0.0621)	0.005(0.0087)	0(0)	
DA	0.025(0.0278)	0.02(0.0265)	0(0)	-0.0033(0.0058)	0(0)

Table 5:

Table 4.5.1: Maximum averaged Pearson correlation coefficients and corresponding averaged time lags regarding the pathologically unaffected and affected shoulder abduction performed by all subjects. The muscle-pair of interest is formed by the biceps brachii and the deltoideus medial.

	BICEPS — DELTOIDEUS MEDIAL			
	Maximum averaged Pearson correlation (SD)		**Corresponding Time lag [s]**	
	Unaffected	**Affected**	**Unaffected**	**Affected**
Subject 1	0.9465(0.0056)	0.7723(0.1527)	0.0217(0.0189)	0.1200(0.2078)
Subject 2	-1.1583(2.0063)	0.8917(0.0269)	0.2117(0.0785)	0.0267(0.0104)
Subject 3	0.9085(0.0162)	0.8248(0.0403)	0.03(0.0361)	0.02(0.0173)
Subject 4	0.5676(0.0785)	0.7696(0.068)	0.535(0.466)	0.0083(0.0076)
Subject 5	0.9432(0.031)	0.9282(0.0206)	-0.0017(0.0029)	0.005(0.005)
Subject 6	0.9039(0.0312)	0.8634(0.0314)	0(0)	0(0)
Subject 7	0.9405(0.0287)	0.8137(0.0319)	0.02(0.01)	0.0233(0.0404)
Subject 8	0.8756(0.1088)	0.8659(0.0497)	0(0)	0.0367(0.0351)

Table 4.5.2: Maximum averaged Pearson correlation coefficients and corresponding averaged time lags regarding the pathologically unaffected and affected shoulder abduction performed by all subjects. The muscle-pair of interest is formed by the triceps lateral head and the deltoideus medial.

TRICEPS LATERAL HEAD — DELTOIDEUS MEDIAL				
	Maximum averaged Pearson correlation (SD)		Corresponding Time lag [s]	
	Unaffected	Affected	Unaffected	Affected
Subject 1	0.9577(0.0028)	0.7541(0.2834)	0.0067(0.0115)	0.38(0.6582)
Subject 2	0.8049(0.0102)	0.8598(0.04)	0.1317(0.11)	0.055(0.0436)
Subject 3	0.9371(0.0171)	0.8245(0.0347)	0.0067(0.0058)	0.0567(0.1025)
Subject 4	0.6613(0.0882)	0.6193(0.0796)	0.88(0.104)	0.35(0.3003)
Subject 5	0.9841(0.0028)	0.9571(0.016)	-0.0017(0.0029)	0(0)
Subject 6	0.9107(0.014)	0.8508(0.0161)	-0.005(0.0087)	0(0)
Subject 7	0.9404(0.0372)	0.878(0.0482)	0.0283(0.0247)	0(0)
Subject 8	0.9466(0.0179)	0.8736(0.0442)	0(0)	0.0683(0.0621)

Table 4.5.3: Maximum averaged Pearson correlation coefficients and corresponding averaged time lags regarding the pathologically unaffected and affected shoulder abduction performed by all subjects. The muscle-pair of interest is formed by the triceps long head and the deltoideus medial.

TRICEPS LONG HEAD — DELTOIDEUS MEDIAL				
	Maximum averaged Pearson correlation (SD)		Corresponding Time lag [s]	
	Unaffected	Affected	Unaffected	Affected
Subject 1	0.9018(0.0507)	0.4542(0.6412)	-0.025(0.0391)	-1.1583(2.0063)
Subject 2	0.6526(0.0218)	-0.1547(0.5851)	-0.1433(0.2483)	0.325(0.9579)
Subject 3	0.9099(0.0173)	0.6556(0.0452)	0(0)	-0.005(0.0132)
Subject 4	0.2411(0.6768)	0.6379(0.1257)	0.2733(0.8762)	0.2783(0.2362)
Subject 5	0.946(0.0146)	0.9406(0.0104)	-0.0217(0.0189)	-0.0033(0.0058)
Subject 6	0.9171(0.007)	0.7295(0.0728)	0(0)	0.0033(0.0058)
Subject 7	0.9498(0.0356)	0.8885(0.0277)	0.045(0.0541)	0(0)
Subject 8	0.8421(0.0845)	0.8942(0.0604)	-0.0567(0.0981)	0.005(0.0087)